

Department of Chemical and Process Engineering

Understanding and mitigating agglomeration and attrition during the drying of Paracetamol

Mariam Siddique

Thesis submitted at the University of Strathclyde in accordance with
the requirements for the Degree of Philosophy

2022

Declaration of Author's Rights

This thesis is the result of the author's original research. It has been composed by the author and has not been previously submitted for examination, which has led to the award of a degree.

The copyright of this thesis belongs to the author under the terms of the United Kingdom Copyright Acts as qualified by the University of Strathclyde Regulation 3.50. Due acknowledgement must always be made of the use of any material contained in, or derived from, this thesis.

Signed: *Mariam Siddique*

Date: 09/10/2023

Pandemic impact statement

I started my PhD on 1st October 2018. After completing all the inductions, I started my lab work in January 2019. By March 2020, when the pandemic began, I had completed all the work for Chapter 3 and almost 60% for Chapter 4. On 11th March 2020, before the lockdown, I went back to Pakistan to get married and could not return to the UK for nearly three and a half months due to the lockdown. During this period, I had limited access to the internet, and despite taking a copy of my research work with me on a portable hard drive as I planned to be back after four weeks. I worked there on a borrowed laptop which was considerably challenging to work productively in a very crowded household due to wedding guests being trapped there.

I returned to the UK on 22nd June 2020 when the United Kingdom resumed flights for residents, but the labs were still closed and opened by the end of August 2020. My PhD was almost entirely experimental, and during Covid restrictions which prevented access to the lab, I focused on writing up work conducted to that point and completing the literature review. As the labs were opened by the end of August 2020, there was still limited access until January 2023.

Furthermore, my placement project was planned with ROCHE in Basel, Switzerland, which was also constrained due to the pandemic as I could not go there, so it was decided to plan a virtual placement. However, the placement didn't work successfully due to some organizational complexities for virtual placement.

Signed by the Supervisor: 

Signed by the researcher: *Mariam Siddique*

Acknowledgement

First, I would like to thank ALLAH Almighty for giving me the strength to complete my thesis.

I express my sincere gratitude to my supervisor, Dr Chris Price, for his enthusiasm for the project and his encouragement and patience throughout my project. His endless support and advice have been invaluable on both an academic and a personal level, for which I am truly grateful. This thesis would not have been possible without his timely advice and guidance. I would also like to thank my secondary supervisor Dr Paul Mulheran for his guidance and support in data analysis throughout my project. I would also like to thank the whole Chris Price team: Dr Muhid Shahid, Georgia Sanxaridou, and William Eales for their valuable guidance and encouragement.

From the bottom of my heart, I would like to say a big thank you to my sister Dr. Humera Siddique. Without her support, the completion of my research would not have been possible.

Everyone in the Department of Chemical and Process Engineering and the EPSRC Centre for Continuous Manufacturing and Advanced Crystallization (CMAC) deserves gratitude and appreciation for their academic and technical support during my PhD project. I would like to thank Dr. Thomas McGlone, Dr. Deborah Bowering, Dr. Vishal Rawal, Dr Carlota Mendez and Mark McGowan for their training and assistance in using many pieces of equipment.

Thank you to all the people I have collaborated with over the time of this PhD. I would like to acknowledge Dr. Sara Ottoboni's tremendous support, helpful discussions, guidance, and kind offer to proofread my thesis. Audrey Laux, for her hard work in the lab during her internship, helped me provide data for my 3rd and 4th chapters. I would like to acknowledge the Chemical and Process Engineering Department for providing me with a Scholarship for this project and EPSRC, AWL and Dr Chris Price for financial support.

I am indebted to my mother, sisters and parents-in-law for their patience and emotional and spiritual support. I am incredibly grateful to my husband, Ali Tariq, for being a brilliant support and encouragement through the tough times of my PhD.

Finally, I would like to dedicate my thesis to my late father, Muhammad Siddique Tariq, who aimed to get his daughters the best education. His aim was the main reason for taking up this PhD and kept me motivated throughout my journey.

Abstract

Oral dose formulation is quite common for most commercial pharmaceutical products. The performance of a drug product is mainly dependent on the physical properties of the active pharmaceutical ingredient (API). As such, great care is taken during the production of the API to achieve a target particle size distribution. Control of the API particle-size distribution is traditionally achieved via the crystallization process. A significant amount of effort goes into designing crystallization processes that consistently produce the desired API properties on scale-up. The isolation (filtration, washing, and drying) process is needed to separate the pure product crystals from the impure mother liquor to produce dry, free-flowing particles while preserving the particle size distribution achieved by crystallization.

Drying is the last and critical processing step in the isolation and purification of API crystals which is performed to remove the residual solvent remaining after filtration and washing. The effectiveness of the drying process affects the quality attributes of the final drug product. Traces of residual solvent may also affect the stability of the formulated product. Any API dissolved in the residual solvent left during drying tends to create "sticky" points at the contacts between particles, promoting solid bridges and being responsible for particle agglomeration. The residual moisture content and composition, solvent polarity, surface tension, and viscosity significantly impact agglomeration. The drying process can also impact the particle-size distribution of the API, which affects the stability, bioavailability, dissolution rate and content uniformity of the drug product and the reproducibility of the manufacturing process.

The main aim of this work was to explore the role of residual solvent during drying by quantifying the threshold limit of the residual moisture content and the dissolved material to form a robust agglomerate. Based on using a model API, paracetamol, the results indicating the minimum API mass that can cause agglomeration is helpful information to support the design of filter cake-washing processes to avoid agglomeration. This research also addresses the work done for developing a convenient method for quantifying agglomerate brittleness based on experimental validation.

Further objectives include the work done to analyze the interaction and transport of residual solvent with API during drying by evaluating the role of contact angles and capillary forces to

understand the transport of residual moisture and the dissolved material during drying. The final component was the development of a semi-empirical approach based on the correlation of material properties and breakage assessment tests to provide a corresponding scale-down concept/apparatus for mimicking particle breakage in agitated dryers at various scales.

Contents

Declaration of Author's Rights.....	ii
Pandemic impact statement.....	iii
Acknowledgement	iv
Abstract	v
Conference Proceedings and Presentations	xx
Chapter 1: Introduction.....	21
1.1 Aims and objectives	27
1.2 Thesis outline	29
1.3 References	31
Chapter 2: Literature Review: Drying basics, kinetics and transport mechanisms	34
2.1 Drying basics.....	34
2.1.1 Drying types classified by the heat transfer mechanism	36
2.1.2 Drying Kinetics	37
2.1 Transport Mechanism During drying.....	38
2.1.3 Classification of evaporation during the drying mechanism.....	39
2.1.4 Mechanism of internal moisture transport.....	40
2.1.5 Properties of a porous media	45
2.1.6 Properties of wet granular media	46
2.2 Classification of dryers and their applications	47
2.3 Summary	50
2.4 References	51
Chapter 3: Agitated filter dryer & inter particle phenomenon: Agitation and attrition.....	56
3.1 Agitated Filter dryer.....	56
3.2 Agglomeration.....	59
3.2.1 Factors affecting agglomeration.....	59
3.2.2 Characterization of agglomerates	69
3.3 Attrition.....	71
3.3.1 Particle attrition due to shear deformation	72
3.3.2 Particle attrition due to impact breakage	73
3.3.3 Mode's particle breakage	74
3.3.4 Parameters affecting particle attrition.....	75
3.3.5 Models for analyzing attrition of particles	77
3.4 Effect of Drying on Physical properties	81

3.4.1 PCM solid forms.....	82
3.5 Summary	83
3.6 References	86
Chapter 4: Materials and Methodology	92
4.1 Raw Materials	92
4.1.1 Substrates	92
4.1.2 Solvent	97
4.1.3 Binding agent (solute).....	98
4.1.4 DYE.....	100
4.2 Methodology	100
4.2.1 Sample preparation (lump formation)	100
4.2.2 Characterization of dried samples.....	101
4.3 References	103
Chapter 5: Quantification of granule formation as a function of solubility in residual solvents	104
5.1 Introduction	104
5.2 Materials and Methodology	104
5.2.1 Materials.....	104
5.2.2 Methodology	105
5.3 Results and discussion.....	109
5.3.1 Experiments for Method Development	109
5.3.2 Experiments with API	119
5.3.3 Filling fraction calculation.....	127
5.4 Conclusion.....	130
5.5 References	131
Chapter 6: Transport of residual moisture during drying	132
6.1 Aims and Objectives	132
6.2 Materials and Methodology	132
6.2.1 Materials.....	132
6.2.2 Methodology	133
6.3 Results and discussions	136
6.3.1 Investigation of relative transport of PCM and dye during drying.....	136
6.3.2 HPLC analysis	139
6.3.3 UV-Vis Spectroscopy.....	142
6.3.4 Investigation of the wetting behaviour of water	146

6.3.5 Washburn Method	152
6.4 Conclusion.....	157
6.5 References	158
Chapter 7: Quantification of granule formation as a function of solubility in Residual solvent (part b).....	159
7.1 Aims and objectives	159
7.2 Materials and Methodology	159
7.2.1 Materials.....	159
7.2.2 Methodology	160
5.3. Results and discussion.....	165
5.3.1. Experiments with PCM.....	165
7.2.3 Experiments with spherical agglomerates of benzoic acid	175
7.3 Conclusion.....	179
7.4 References	180
Chapter 8: Refining Agglomeration brittleness Index Method.....	181
8.1 Introduction	181
8.2 Previous work in the group	182
8.2.1 Friability Analyser	182
8.2.2 Compression tester	183
8.2.3 Exponential Decay fitting.....	186
8.3 Aims and objectives.	186
8.4 Materials and Methodology	186
8.4.1 Material	187
Glass beads (GB1-GB5), from VWR International Limited, were selected as a substrate.	187
8.4.2 Methodology	187
8.5 Results and discussion.....	188
8.5.1 Linear fitting.....	189
8.5.2 Breakage analysis	193
8.5.3 Hardness testing	195
8.6 Conclusion.....	197
8.7 References	198
Chapter 9: Investigation of lab scale equipment for particle breakage.....	199
9.1 Aims and objectives	199
9.2 Materials and Methodology	201
9.2.1 Material	201

9.2.2 Methodology	201
9.3 Results and discussion.....	210
9.3.1 Tap bulk density.....	210
9.3.2 FT4 shear cell test.....	216
9.3.3 vacuum agitated dryer experiments	218
9.4 Conclusion.....	220
9.5 References	222
Chapter 10: Overall conclusion and future work	223
10.1 Overall conclusion.....	223
10.2 Future work	226
Appendix A.....	227
Appendix B	231
Appendix C	234

Table of Figures

<i>Figure 1-1 Schematic of API manufacturing</i>	21
<i>Figure 1-2 Components of the optimum drying process for API manufacturing. (Edward W Conder et al., 2017)</i>	23
<i>Figure 1-3 Modes of heat transfer (Heat transfer _ introduction to chemical and biological engineering)</i>	24
<i>Figure 1-4 Illustrative route map of thesis chapters</i>	30
Figure 2-1 Types of moisture involves in drying (Majumdar & Marchertas, 1997)	35
Figure 2-2 The modes of heat transport in porous materials. Heat transfer by a) convection, b) radiation, c) gas conduction, including the coupling (Apostolopoulou-kalkavoura, Munier and Bergström, 2021)	36
Figure 2-3: Characteristic drying curve. (T. and Ocone, 2011).....	38
<i>Figure 2-4 Microscopic cross-section image of a porous medium (Kantzas, Apostolos; Bryan Jonathan; Taheri, 2015)</i>	45
<i>Figure 2-5 Comparison of wetting and non-wetting fluid (E. Heinemann, 2005)</i>	46
<i>Figure 2-6 Illustration of the liquid bridge and principal radii of curvature (E. Heinemann, 2005)</i>	47
Figure 3-1 Schematic of Agitated Filter Dryer process. (Tamrakar, Gunadi, Patrick M. Piccione, et al., 2016).....	57
Figure 3-2 Different levels of liquid saturation (a) Slurry state (b) Capillary state (c) Funicular state (d) Pendular state (e) Dry state (Mitarai and Nori, 2007)	63
Figure 3-3 Techniques for characterising the mechanical properties of agglomerates (A) Compression Tester (Instron) (B) Ring Shear Tester (Faulhaber) (C) Friabilator(Charles Ischi AG).	70
Figure 3-4 ABI calculation of a model compound. (Simurda, 2017)	70
<i>Figure 3-5 Cumulative distribution of undersize particles as a function of normal size particles for chipping, fragmentation, and disintegration (Goh, 2019)</i>	75
<i>Figure 3-6 Parameters affecting particle attrition</i>	76
Figure 3-7 Paracetamol phase transitions. Tc is the temperature of crystallization, Tm is the temperature of melting, Tg is the temperature of glass transition, and Ttr is the temperature of polymorphic transition. (Cruz, Rocha and Ferreira, 2019).....	83
Figure 4-1 SEM of Glass beads (a) 40-70 um (b) 90-150 um (c) 150-250 um (d) 300-400 um (e) 400-500 um.....	94

Figure 4-2 SEM of different grades of Paracetamol (a) granular PCM (b) Powdered PCM...	95
Figure 4-3 SEM of Spherical agglomerates (a) J (b) N2 (c) N15 (Raval et al., 2022)	96
Figure 4-4 Experimental sequence and equipment to create and characterize agglomerates.	101
Figure 4-5 Sieving Assembly for glass beads.....	102
Figure 5-1 Fructose/water system (a) Sample after manual tapping (b) sample after four cycles of sieving.....	111
Figure 5-2 Fructose/Methanol system (a) sample after manual tapping (b) sample after four cycles of sieving.....	111
Figure 5-3 Lactose/water system (a) sample after manual tapping (b) sample after four cycles of sieving.....	111
Figure 5-4 Extent of agglomeration and ABI index for Fructose/Methanol system	112
Figure 5-5 Extent of agglomeration for Lactose/water and Fructose/water solutions with glass bead.....	112
Figure 5-6 ABI index for Lactose/water and Fructose/water solutions with glass beads.....	113
Figure 5-7 Lactose/Methanol system (a) sample after manual tapping (b) sample after two cycles of sieving.....	115
Figure 5-8 DOE factors affect plots on ABI index ($R^2 = 0.59$)	117
Figure 5-9 DOE factors affect the plot on the extent of agglomeration ($R^2 = 0.28$)	118
Figure 5-10 Response contour Plot for ABI index	119
Figure 5-11 Response contour plot for the extent of agglomeration.	119
Figure 5-12 Extent of agglomeration and ABI index for PCM/water system.	121
Figure 5-13 Extent of agglomeration and ABI index for PCM/Methanol system.....	122
Figure 5-14 ABI index and Extent of agglomeration for decreasing concentration of PCM/water system.....	123
Figure 5-15 ABI index and Extent of agglomeration for decreasing concentration of PCM/methanol system.....	123
Figure 5-16 Comparison of ABI index for decreasing amount of PCM with Methanol with and without dye.....	124
Figure 5-17 Comparison of Extent of agglomeration for decreasing amount of PCM with Methanol with and without dye	125
Figure 5-18 Mass of Paracetamol per sphere plotted against the mass of a single sphere	128
Figure 5-19 Mass of Paracetamol per sphere against the size of the beads.....	128
Figure 5-20 Glass Bead Agglomerate.....	129

Figure 6-1 Simplified setup for Washburn capillary rise method (Meng et al., 2017).....	135
Figure 6-2 Washburn capillary rise setup utilizing Sartorius balance and density measurement kit (Pedussaut, 2018).....	136
Figure 6-3 (a) PCM/Methanol system (PCM and Dye confined within the lump) (b) PCM/water system (Dye spread out in the loose beads towards the wall).....	137
Figure 6-4 Dried sample PCM/Water system (a) dye dispersed in the loose beads transporting towards the wall (b) agglomerate formed free from dye	137
Figure 6-5 (a) Fructose/Water system (b) Lactose/water system	138
Figure 6-6 (a) Fructose/Methanol system (b) Lactose/Methanol system	138
Figure 6-7 Calibration curve of paracetamol	139
Figure 6-8 Concentration of Paracetamol in sieved fractions of PCM/Methanol Sample	141
Figure 6-9 Concentration of Paracetamol in sieved fractions of PCM/Water Sample	142
Figure 6-10 Calibration curve for blue dye.....	143
Figure 6-11 Relative amount of paracetamol plotted against the relative amount of dye for the Methanol system.....	145
Figure 6-12 Relative amount of paracetamol plotted against the relative amount of dye for the Water system.....	145
Figure 6-13 Dried samples (90-150 um glass beads) wetted with 0.0025g/ml PCM/Water solution (a) side view (b) top view	146
Figure 6-14 Lump created after first wetting (a) the top side of the lump (b) the bottom side of the lump	147
Figure 6-15 Vial with loose beads after removing the lump created by first wetting (a) top view (b) side view with half of the material removed	147
Figure 6-16 Dried samples (90-150 um glass beads) rewetted with 0.0025 g/ml PCM/water solution (a) side view (b) top view	147
Figure 6-17 Lump created after rewetting (a) top side of lump (b) side view of the lump (c) bottom side of the lump	148
Figure 6-18 (a) Single large crystal of PCM (b) Crystal habit of PCM form 1 (Heng et al., 2006)	148
Figure 6-19 Glass beads wetted with different compositions of water & methanol solution (at the start of the Experiment).....	150
Figure 6-20 Dry samples of glass beads wetted with different compositions of water & methanol solution (after completion of the experiment).....	150
Figure 6-21 (a) Decreasing concentration of PHL-t (b) Decreasing Concentration of PCM	151

Figure 6-22 Paracetamol powder wetted with water (a) bottom side of the slide (b) top side of the slide	152
Figure 6-23 PHL-T powder wetted with water (a) bottom side of the slide (b) top side of the slide	152
Figure 6-24 The mass vs time interparticle capillary rise of water and dye solution in PCM-coated glass beads compacted by tapping for 100 - 300 seconds	154
Figure 6-25 Washburn analysis for powdered PCM (a) start of experiment (b) end of experiment (c) top view of wetted sample (d) side view of the wetted sample.....	156
Figure 7-1 Sieve shaker assembly with sieve nest.....	161
Figure 7-2 QICPIC setup	162
Figure 7-3 Optical setup of QICPIC	163
Figure 7-4 Crystalline PV	164
Figure 7-5 Dry sample after wetting the granular PCM with heptane.....	165
Figure 7-6 Dry sample after transferring to sieving assembly of 1mm sieve and bottom pan	166
Figure 7-7 Sieved fractions of PCM with 20 cm diameter (a) 500 um sieve (b) 212um Sieve (c) 75 um sieve (d) bottom pan	167
Figure 7-8 Sieved fractions of PCM with 10 cm diameter sieves	168
Figure 7-9 Microscopic images of the sieved fractions (a) 250 um (b) 150 um (c) 75 um (d) bottom pan with 10x objective lens	169
Figure 7-10 75 μ m sieved fraction dried sample after transferring to the sieving assembly (a) 1mm sieve (b) bottom pan.	171
Figure 7-11 Sieving assembly after the first cycle of sieving of 75 μ m fraction sample	171
Figure 7-12 Dried sample of granular PCM (a) experiment with heptane/PCM solution (b) experiment with 90:10 heptane: Ethanol/PCM solution.....	172
Figure 7-13 Granular PCM (a) experiment with heptane/PCM solution after manual tapping(b) experiment with 90:10 heptane: Ethanol/PCM solution after manual tapping.....	172
Figure 7-14 GB1 (40-70 um) glass beads (a) experiment with heptane/PCM solution after manual tapping(b) experiment with 90:10 heptane: Ethanol/PCM solution after manual tapping	173
Figure 7-15 Sieved fraction of glass beads sample with 90:10 heptane: Ethanol/PCM solution	174
Figure 7-16 Granular PCM sample with 90:10 heptane: Ethanol/PCM solution after manual tapping.....	175

Figure 7-17 Dried sample J (a) after transferring from the vial (b) after first cycle of sieving	177
Figure 7-18 Dried sample N2 (a) after manual tapping (b) after second cycle of sieving. ...	177
Figure 7-19 Dried sample N15 (a) after manual tapping (b) after second cycle of sieving. .	178
Figure 7-20 Glass beads (GB1) dried sample with the benzoic acid solution in binary mixture of heptane and ethanol (95:05)	178
Figure 7-21 Dried sample of glass beads (GB1) (a) after transferring the material from the vial (b) after manual tapping.....	178
Figure 8-1 0.01 g/ml PCM/Methanol dried sample (a) after manual tapping (b) after 1st sieving cycle (c) after 2nd sieving cycle (d) after 3rd cycle of sieving (e) after 4th cycle of sieving	182
Figure 8-2 Friability tester or Friabilator (Charles Ischi AG – Testing Technology)	183
Figure 8-3 Compression Tester (Instron : Materials Testing Machines for Tensile, Fatigue, Impact, Rheology and Structural Testing).....	184
Figure 8-4 Fragmentation of particle agglomerate during compression test (Simurda, 2017)	184
Figure 8-5 Breakage point of model agglomerate using Instron (Simurda, 2017)	185
Figure 8-6 Distribution of force on smooth-edged particles.....	185
Figure 8-7 Distribution of force on sharp-edged particles.....	186
Figure 8-8 Hardness tester	188
Figure 8-9 Percentage of mass retained on top sieve V/s Frequency*no of cycles for 1 g PCM/100ml methanol 40-70 μ m beads.....	191
Figure 8-10 Percentage of mass retained on top sieve V/s Frequency*no of cycles for 0.2 g PCM/100ml methanol 40-70 μ m beads.....	191
Figure 8-11 Percentage of mass retained on top sieve V/s Frequency*no of cycles/solution concentration for 1 g PCM/100ml methanol 40-70 μ m beads.....	192
Figure 8-12 Percentage of mass retained on top sieve V/s Frequency*no of cycles/solution concentration for 1 g PCM/100ml methanol 40-70 μ m beads.....	192
Figure 8-13 0.01g/ml PCM methanol 40-70 μ m beads agglomerate sieved at 500 rpm (a) Agglomerate after manual tapping (b) and (c) agglomerate after 8 cycles of sieving.....	193
Figure 8-14 0.01g/ml PCM methanol 400 – 600 μ m beads agglomerate sieved at 500 rpm (a) agglomerate after manual tapping (b) agglomerate after 8 cycles of sieving	193
Figure 8-15 0.01g/ml PCM methanol 400 – 600 μ m beads agglomerate sieved at 500 rpm with the top side towards sieve (a) agglomerate after manual tapping (b) after 4 cycles of sieving (c) after 8 cycles of sieving	194

Figure 8-16 0.01g/ml PCM methanol 400 – 600 μ m beads agglomerate sieved at 500 rpm with the bottom side towards sieve (a) agglomerate after manual tapping (b) after 4 cycles of sieving (c) after 8 cycles of sieving.....	194
Figure 8-17 0.01g/ml PCM methanol 400 – 600 μ m beads agglomerate sieved at 2800 rpm (a) agglomerate after manual tapping (b) agglomerate after 4 cycles of sieving	195
Figure 8-18 0.01g/ml PCM methanol 40 – 70 μ m beads agglomerate sieved at 2800 rpm (a) agglomerate after manual tapping (b) agglomerate after 8 cycles of sieving	195
Figure 8-19 Pointed oval-shaped agglomerate.	196
Figure 8-20 (a) agglomerate completely crushed after applying force on hardness tester (b) agglomerate chipped off from one side due to unequal force distribution from hardness tester	196
Figure 9-1 Overview of potential approaches to characterizing particle breakage behaviors	200
Figure 9-2 Quanta chrome Auto tap Tapped Density Instrument (quantachrome instruments)	202
Figure 9-3 Freeman FT4 setup.....	204
Figure 9-4 FT4 shear cell method (Tsupporting documents)	205
Figure 9-5 25mm x 10ml split vessel with bottom assembly (FT4 support document – 25mm Vessel Assemblies – W7021)	205
Figure 9-6 Shear cell test sequence (FT4 support document – Shear cell – W7018).....	206
Figure 9-7 AWL agitated vacuum dryer.....	207
Figure 9-8 Components of Morphology G3 (Malvern instruments)	209
Figure 9-9 Consolidated and Unconsolidated particle bed after tap bulk density experiment with weight loads	213
Figure 9-10 Comparison of the particle size distribution of raw material with sample 1 (analysis was performed without adding weight loadson particle bed) using tap bulk density by using Morphology G3.....	214
Figure 9-11 Comparison of the particle size distribution of raw material with sample 1 (analysis performed by adding two weight loads on powder bed,) using tap bulk density by using Morphology G3.....	214
Figure 9-12 Comparison of the particle size distribution of raw material with sample 1 (analysis was performed by adding three weight loads on particle bed) using tap bulk density by using Morphology G3.....	215
Figure 9-13 Incipient shear stress versus incipient applied normal stress values collected from	

shear cell test at 3, 5, 9, and 15 kPa217
Figure 9-14 Comparison of Raw material and the samples obtained from shear cell test at 3, 5,
9, and 15 kPa.....217
Figure 9-15 Current Speed and torque curve for the motor used to provide rotational motion of
agitator used in dryer provided by the supplier.220

Table of Tables

Table 3-1 Binding mechanisms of agglomeration (Pietsch, 1997).....	60
Table 3-2 Effect of different operating parameters on agglomeration.	66
Table 3-3 Effect of different material properties on agglomeration	68
Table 4-1 List of sizes of glass beads	93
Table 4-2 Size analysis of Powdered and Granular Paracetamol	95
Table 4-3 Size analysis of spherical agglomerates (performed with Morphology G3) (Raval et al., 2022)	96
Table 4-4 Solubility of carbohydrates in water and methanol (Granberg, Ke and Rasmuson, 1999)	98
Table 4-5 Solubility of PCM in water and methanol (Montañ, Olano and Ibáñez, 2007).....	99
Table 4-6 Solubility of PCM in pure solvents and binary mixtures of heptane and ethanol (Shahid et al., 2021)	99
Table 5-1 Summary of Experiments performed for Chapter 5	106
Table 5-2 Summary of parameters and procedure for experiments performed for method development.....	110
Table 5-3 Summary of parameters of lactose decreasing concentration experiments.....	114
Table 5-4 ABI index and extent of agglomeration for Lactose decreasing concentration experiments.....	115
Table 5-5 Factors and responses of DOE for Lactose concentration.....	116
Table 5-6 Summary of Parameters of DOE experiments	116
Table 5-7 Parameters and results of die dilution experiments	126
Table 6-1 Particle size distribution of PCM and PHL-t.....	133
Table 6-2 Quantity of water used for HPLC Sample preparation.	139
Table 6-3 Results of the HPLC analysis for Methanol/PCM samples.....	140
Table 6-4 Results of the HPLC analysis for Water/PCM Samples	142
Table 6-5 Results of UV-VIs Spectroscopy for water and methanol	144
Table 6-6 Advancing and Receding angle of PCM form I with water	149
Table 6-7 K- value Results	155
Table 6-8 Contact angles of different solutes with water/dye solution	156
Table 7-1 Sieve diameters and mesh sizes.....	161
Table 7-2 Particle size analysis of Granular and powdered PCM and sieved fractions of powdered PCM by QICPIC	168

Table 7-3 Parameters of PCM agglomeration experiment with binary mixtures	170
Table 7-4 Solubility of benzoic acid in pure solvents and binary mixtures of heptane and ethanol.....	176
Table 7-5 Parameters of agglomeration experiment with spherical agglomerates using binary mixtures.....	177
Table 8-1 Experimental parameters for refining of ABI index method.....	187
Table 8-2 Results for the extent of agglomeration for minimum and maximum concentration solution samples with smallest and largest bead size	189
Table 9-1 Dimensions of measuring cylinder and disks used in modified tap bulk density experiment.....	202
Table 9-2 Parameters of experiments with tapped bulk density equipment	203
Table 9-3 Parameters of experiments with Vacuum agitated dryer.....	208
Table 9-4 Particle size analysis and breakability index of preliminary experiment with powdered PCM by QICPIC	210
Table 9-5 Particle size analysis and breakability index of 2nd experiment by using 25 ml cylinder with 150 and 250 taps performed by QICPIC	211
Table 9-6 Particle size analysis and breakability index of consolidated and unconsolidated material by using 25 ml cylinder with 150 and 250 taps performed by QICPIC	212
Table 9-7 Breakability index of FT4 shear cell experiments at 3, 5, 9, and 15 kPa	218
Table 9-9 Applied normal stress calculated for tungsten washers used in Vacuum agitated dryer experiment.....	219

s

Conference Proceedings and Presentations

Conference proceeding

- Quantification of granule formation as a function of solubility in residual solvents.
Mariam Siddique, Audrey Laux, Sara Ottoboni, Chris Price, Paul Mulheran FILTECH
2020, 8th - 10th March, 2020, Cologne, Germany

Conference Presentation

- Quantification of granule formation as a function of solubility in residual solvents.
Mariam Siddique, Audrey Laux, Sara Ottoboni, Chris Price, Paul Mulheran. FILTECH
2022, 8th - 10th March, 2022, Cologne, Germany. (presented by Dr. Sara Ottoboni)

Conference Poster

- Quantification of granule formation as a function of solubility in residual solvents. Mariam Siddique, Audrey Laux, Sara Ottoboni, Chris Price, Paul Mulheran. CMAC virtual open day, 21st -22nd October, 2020, Glasgow, United Kingdom.
- Understanding drying effects on active pharmaceutical ingredient particle properties. Mariam Siddique, Audrey Laux, Sara Ottoboni, Chris Price, Paul Mulheran. CMAC annual open day, 16th-18th May, 2022, Glasgow, United Kingdom.
- Transport of impurities and residual solvent during static drying. Mariam Siddique, Audrey Laux, Sara Ottoboni, Chris Price, Paul Mulheran. World Filtration Congress (WFC 13) 2022, 5th – 9th October, 2022, San Diego, California, USA. (presented by Dr. Sara Ottoboni)

Chapter 1: Introduction

One of the most widely used processes in the pharmaceutical industry is crystallization, which produces highly purified Active Pharmaceutical Ingredients (APIs). Generally, pharmaceutical manufacturing has two stages: primary and secondary. Primary manufacturing involves synthesizing and isolating the active pharmaceutical ingredient (API), while secondary manufacturing implies formulating the API into the desired drug product (Kemp, 2017). Typically, primary manufacturing activities end with the isolation of the API with the required physical properties for formulation. Figure 1-1 shows this as a schematic diagram of pharmaceutical manufacturing.

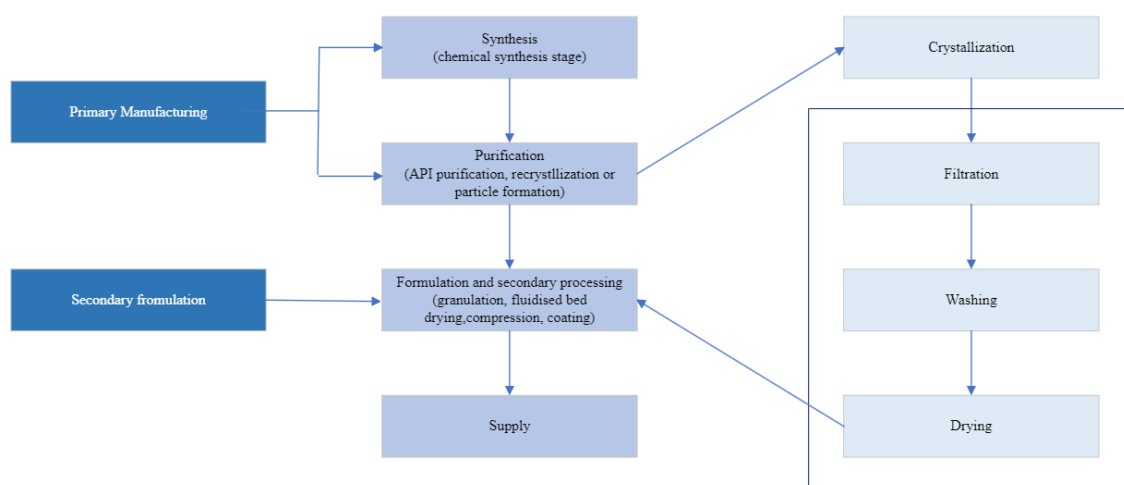


Figure 1-1 Schematic of API manufacturing

Ideally, the crystallization process generates particles of the required physical properties and purity of the suspended crystals (Lee, Lin and Lee, 2013). The isolation process separates the pure product crystals from the impure mother liquor and produces dry, free-flowing particles. Considerable efforts have been made to optimize crystallization processes to generate products with specified physical properties and chemical purity (MacLeod and Muller, 2012). However, these desired particle properties, achieved by carefully designed upstream processes, are often compromised during isolation which involves filtration, washing, and drying steps (MacLeod and Muller, 2012). In addition, these isolation processes pose significant challenges in avoiding granulating or breaking of the crystals or precipitating dissolved impurities (Lamberto *et al.*, 2011). Therefore, the isolation processes must be optimized to ensure the required properties.

After crystallization, the filtration process removes the mother liquor from the suspension

(often termed slurry) by forcing the liquid component of slurry through a filter medium whose pore size is smaller than the product's particle size. Typically, a pressure difference is applied across the filter medium to provide a driving force for filtration (Hamilton, 2011). After filtration, a washing process removes residual mother liquor (Sharma, Murugesan and Tabora, 2019). The selection of wash solvent depends upon several factors; including the solubility of the desired product and the impurities within that solvent, and the ability of the wash solvent to displace the mother liquor. Drying is the last step in isolating and purifying API crystals to remove the residual solvent after filtration and washing (Ottoboni *et al.*, 2019).

Drying refers to the process of removing moisture or liquid from a substance, typically through evaporation or other means. Drying of pharmaceuticals refers to the process of removing moisture or solvent from pharmaceutical substances, products, or components to achieve specific characteristics, stability, and quality standards. This process is crucial in pharmaceutical manufacturing to ensure the preservation of active ingredients, prevent degradation, enhance shelf life, and create suitable forms for administration (such as powders, tablets, or capsules). Various drying methods, such as vacuum drying, spray drying, freeze drying (lyophilization), and tray drying, are employed based on the nature of the pharmaceutical material and the desired product attributes. The goal of pharmaceutical drying is to achieve consistent and reproducible products that meet regulatory requirements and maintain therapeutic efficacy.

Drying is a critical processing step in the pharmaceutical industry, and it has a high impact on the characteristics of the final drug product (Parikh and Group, 2015). Although drying is the last step of the isolation process, it is often somewhat neglected during process development. An optimum drying process of API manufacturing can be developed by understanding all the parameters linked with the chemical and physical product properties and their interaction with drying kinetics (Edward W Conder *et al.*, 2017), as shown in Figure 1-2.

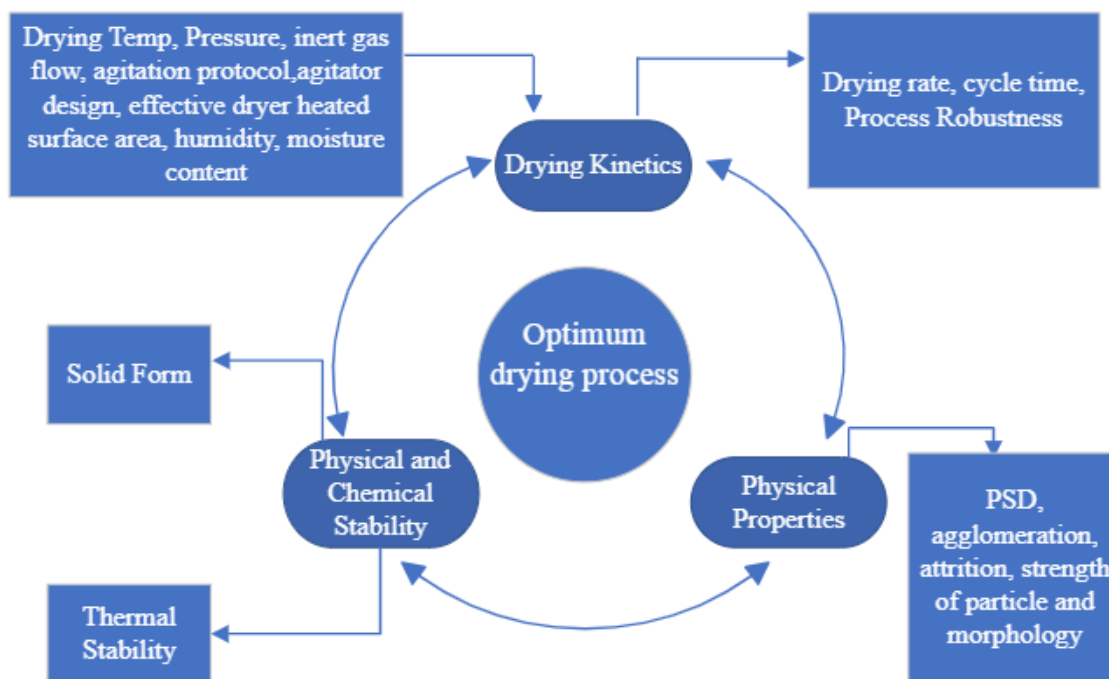


Figure 1-2 Components of the optimum drying process for API manufacturing. (Edward W Conder *et al.*, 2017)

Drying is a complex process involving both heat and mass transfer, co-occurring (Parikh and Group, 2015) with physical and chemical changes in the crystals, which must be understood while developing drying process to ensure purity and right form criteria has met. Chemical stability mostly impacted by drying temperature, so thermal stability of a compound is assessed to understand its degradation with temperature. For physical stability typically a solid form phase map as a function of solvent composition and temperature is generated which provides guides for crystallization, filtration and drying design space. Phase maps may become more complicated when the API exists in more than one physical form.

After defining thermodynamics conditions to maintain chemical stability with the right form drying process further needs to be optimized within the defined boundaries to improve process robustness, reduce process time and to increase drying rate. To achieve an optimized drying process a detailed understanding of drying kinetics is required. Therefore, it is imperative to properly define the drying process parameters i.e. drying temperature, pressure, inlet gas flow rate, agitation protocol, agitator design etc., which greatly influence drying kinetics. In addition, particle properties like size distribution and morphology are also vulnerable to changes caused by drying.

During drying, heat can be transferred by convection, in which heat transfer occurs through the stream of hot gas passing through the wet material, by conduction, in which heat transfer occurs

through a hot surface, by radiation or by freeze-drying (Mujumdar, 2007).

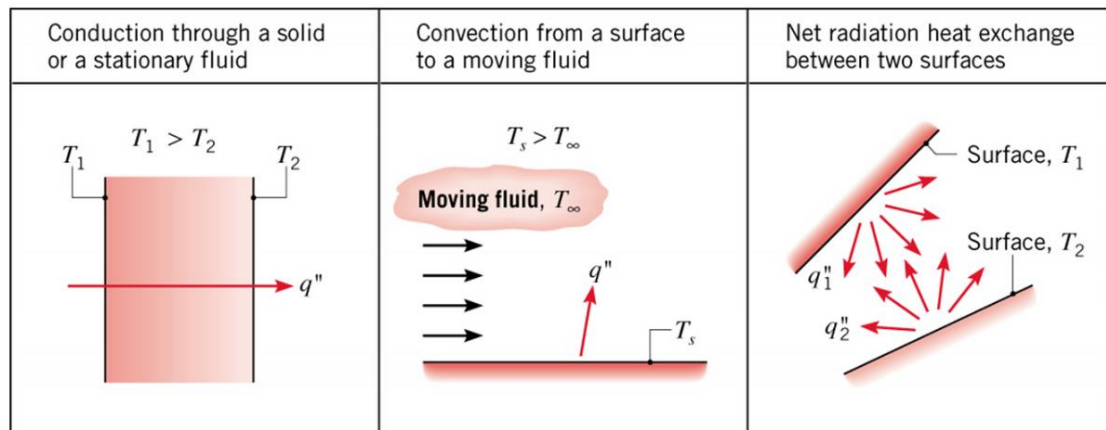


Figure 1-3 Modes of heat transfer (*Heat transfer _ introduction to chemical and biological engineering*)

The use of one or another drying mechanism can be dictated by the chemo-physical characteristics of the API or the residual solvent left in the wet filter cake. Sometimes a mixed drying mode is utilized by combining conductive and convective heat transfer. In mixed drying, the material is dried by passing a hot gas through the material, which is also heated by the walls of the dryer. This combined mode of heat transfer gives a more efficient performance than a single mode of heat transfer (Keey, 1992).

In pharmaceutical manufacturing selection of dryers depends upon product specification and safety requirements (Sharma, Murugesan and Tabora, 2019). Commonly used dryer types include fluidized bed dryers, tray dryers, conical dryers, tumble dryers, filter dryers etc. (Kudra and Mujumdar, 2009). The most widely used dryer in pharmaceutical industries is the agitated filter dryer (AFD). AFDs combine different unit operations, i.e., filtration, washing, and drying (that drying includes contact or even a combination of contact and convective drying mechanism) in one piece of equipment. Several advantages of AFDs include excellent containment, which is highly desirable when handling highly potent drug substances. Its closed design makes it able to operate under a vacuum allowing AFDs to be used for thermally sensitive materials as it can be operated at lower pressure, significantly reducing solvents' vaporization temperature and allowing drying to be done at a lower temperature. The most common problem encountered in AFD is agglomeration and attrition of the particles (Lim, Hapgood and Haig, 2016).

During drying, the moisture vaporizes and moves towards the surface of the bulk powder by

diffusion (Pietsch, 2004). As this process continues, the remaining moisture content forms liquid bridges between crystals, which can cause agglomeration. If the liquid in agglomerates contains any dissolved material, it can cause recrystallization, creating a crust layer on the surface of the agglomerates. This phenomenon occurs when drying is performed at low temperatures under a vacuum. In this case, the crust becomes hard by the end of drying, while the agglomerate under the crust can still be wet, thus producing a dry granule with high moisture inside. These granules are problematic to store as there is a chance of moisture transfer from core to crust hence reducing the stability of stored product.

API solubility in wash solvent cause solid bridges, leading to agglomeration (Tamrakar, Gunadi, Patrick M. Piccione, *et al.*, 2016). Wash solvent selection also influences agglomeration during drying. Factors like wash solvent viscosity, evaporation tendency, surface tension, and API solubility play an essential role in agglomeration during drying (Tamrakar, Gunadi, Patrick M. Piccione, *et al.*, 2016). Birch and Marziano (2013) also studied the effect of API solubility with different solvent mixtures. According to their study, the more solubility of API in wash solvent, and the greater the chance of forming solid bridges. In their study they showed that the solubility of their API was more in pure solvent as compared to a binary mixture with water (i.e. solubility in pure 2-MeTHF was 15.4 g/L and in 2-MeTHF/water 99:1 v/v was 6.4 g/L) hence resulting in greater extent and hard agglomerates. In their work, Lim, Hapgood and Haig (2016) found that solid bridges formed due to the crystallization of dissolved API, which leads to severe agglomeration. If the solubility of API is very high in the solvent system, then it is impossible to mitigate agglomeration (Am Ende *et al.*, 2013). So, selecting a wash solvent and removing residual moisture during washing can help reduce aggregation during drying.

Previous studies in this field have primarily focused on API solubility in the wash solvent, overlooking the significance of API solubility in the residual mother liquor retained within the cake after washing, and its potential impact on agglomeration. As residual solvent properties have been identified as a crucial factor influencing particle agglomeration during drying, this research aims to address this gap by investigating the minimum amount of dissolved material in the residual solvent that can trigger lump formation during the drying process. By determining the critical threshold of dissolved API required for lump formation, we can effectively modify the washing strategy to prevent agglomeration during drying. This approach holds the promise of mitigating agglomeration-related issues and optimizing the drying process

for improved pharmaceutical product quality.

Another major issue encountered during agitated drying is preserving the particle's initial shape and size by preventing its damage from attrition. Many factors can cause attrition, like the mechanical effect of the blades of the stirrer, particle-particle collision, and collision of particles with other parts of the dryer (Ghadiri and Zhang, 2002). Lekhal *et al.* (2004) suggested that attrition can be minimized by varying the agitation speed according to the moisture level present in the cake. Another commonly applied method is intermittent agitation with alternating periods of agitation and no agitation. In this research, we try to find different techniques by which the attrition of the particles can be estimated at the lab scale.

In addition, the attrition and agglomeration that occur with extreme drying conditions (very high temperature to reduce drying time or continuous agitation to fragile crystals) can have unpredictable effects on the function and quality of the dried material. It is also important to realize that many API powders are shear-sensitive, so agitating such materials while wet can cause agglomeration. The best way to dry API is to minimize the effects of agitation to maintain particle integrity without creating lumps or fines. Therefore, detailed studies of the effects of drying processes on powder properties are required due to the lack of appropriate tools to predict agitated dryer design and operation from both particle behavior and scaling perspectives.

In the pharmaceutical industry, the major challenge during crystal materials drying is the preservation of the initial grain size and shape during the process by preventing the agglomeration and attrition phenomena. It is clear from the preceding discussion that many tools, practices and studies tried to develop a robust drying process there are still many knowledge and technology gaps that inhibit the creation of standardized workflows which incorporate agglomeration and attrition problem during drying process like:

- Limited real time drying process understanding causing agglomeration and attrition due to limitation of PAT tools to single point assessments to avoid contact with mechanical agitators.
- Lack of effective and efficient universal models which incorporate agglomeration and attrition problem along with drying kinetics and thermodynamics.
- Lack of standardized, commercially available scale-down equipment

The absence of standardized and commercially available scale-down equipment poses a significant challenge in the pharmaceutical industry. Scale-down equipment is essential for conducting small-scale experiments that accurately mimic larger production processes. However, the lack of standardized options hampers the reproducibility and comparability of research findings across different laboratories and organizations. Currently, custom-made scale-down equipment, leading to inconsistencies in experimental setups and data interpretation. Such variability can result in difficulties when attempting to scale-up processes from the laboratory to commercial production.

The need for standardized, commercially available scale-down equipment is crucial for several reasons:

- Standardized equipment ensures that experiments can be replicated with precision across different laboratories, enhancing the reliability and robustness of research outcomes.
- By having access to uniform scale-down equipment, pharmaceutical companies can more effectively optimize their processes during early development stages, leading to improved efficiency and cost-effectiveness.
- Standardized equipment can facilitate compliance with regulatory requirements, as consistent and validated experimental setups are easier to document and demonstrate to regulatory authorities.
- A lack of standardized scale-down equipment can impede technology transfer between research and manufacturing facilities, leading to delays and inefficiencies.

To address this issue, in this research several different small-scale equipment have been tested in order to develop a standard scale down equipment which can mimic attrition occurring at large scale industrial dryers. By providing a standardized and reliable scale-down apparatus, this research aims to bridge the gap between small-scale laboratory investigations and large-scale production processes. Ultimately, it will contribute to the development of safer, more effective pharmaceutical manufacturing.

1.1 Aims and objectives

This research program focuses on understanding and mitigating the issues during API drying, mainly predicting the potential aggregation and attrition during agitated drying. Although the

drying operating conditions are complex, it is essential to investigate current industrial concerns, which give rise to the following research questions:

1. How can the amount of residual solution be optimized after washing to reduce agglomeration?
2. Does the transport of moisture content during drying effects agglomeration?
3. How to reduce attrition during agitated drying by correlating material properties with processing parameters?

This work tries to resolve the questions mentioned above by setting the following objectives:

- Before drying, the final product composition is critical in determining the flow properties and quality of the end-dried product. Therefore, addressing some vital factors at the filtration and washing stages is essential to avoid issues during drying. One of these factors is quantifying granule formation as a function of solubility in residual solvents. Therefore, the aim is to establish a correlation between the residual solvent amount and its effects on granule formation.
- Based on the outcomes of the experiments, quantify the minimum amount of residual solvent which can cause lump formation and modify deliquoring and washing protocols to remove mother liquor (residual solvent) below the threshold of lump formation.
- After quantifying the threshold limit of the residual moisture content, the next step will be to analyze the interaction and transport of residual solvent with API during drying.
- Investigate the effect of solvent composition and initial solvent concentrations on drying behavior and product particle properties.
- Explore different approaches to develop convenient methods for quantifying agglomerates brittleness based on experimental validation.
- Evaluate contact angles to understand how residual moisture influences drying.
- After investigating the agglomeration factors, the next step will be to design an

optimum drying process that minimizes lump formation (or gets friable/soft agglomerates). This work will focus on finding the roles of the factors responsible for agglomeration during filtration and drying.

- The next aim of the project is to develop a semi-empirical approach based on the correlation of material properties and breakage assessment tests to provide a corresponding scale-down concept/apparatus for mimicking particle breakage in agitated dryers at various scales.

- A specifically small-scale agitated dryer (Figure 9-7), designed by Alconbury Weston Ltd, was used to investigate attrition as a function of drier loading. This dryer is a novel piece of equipment, and its performance characterization has not been tested yet. After detailed commissioning of the agitated drying rig, process parameters such as rate of agitation and bed height will be investigated. Different materials respond differently to the shear rate (crystal mechanical properties), so there is a need to explore the relationship between agitation rate and particle properties. In addition, bed height and crystal interaction are essential factors affecting final product attributes. I will investigate these factors in detail.

1.2 Thesis outline

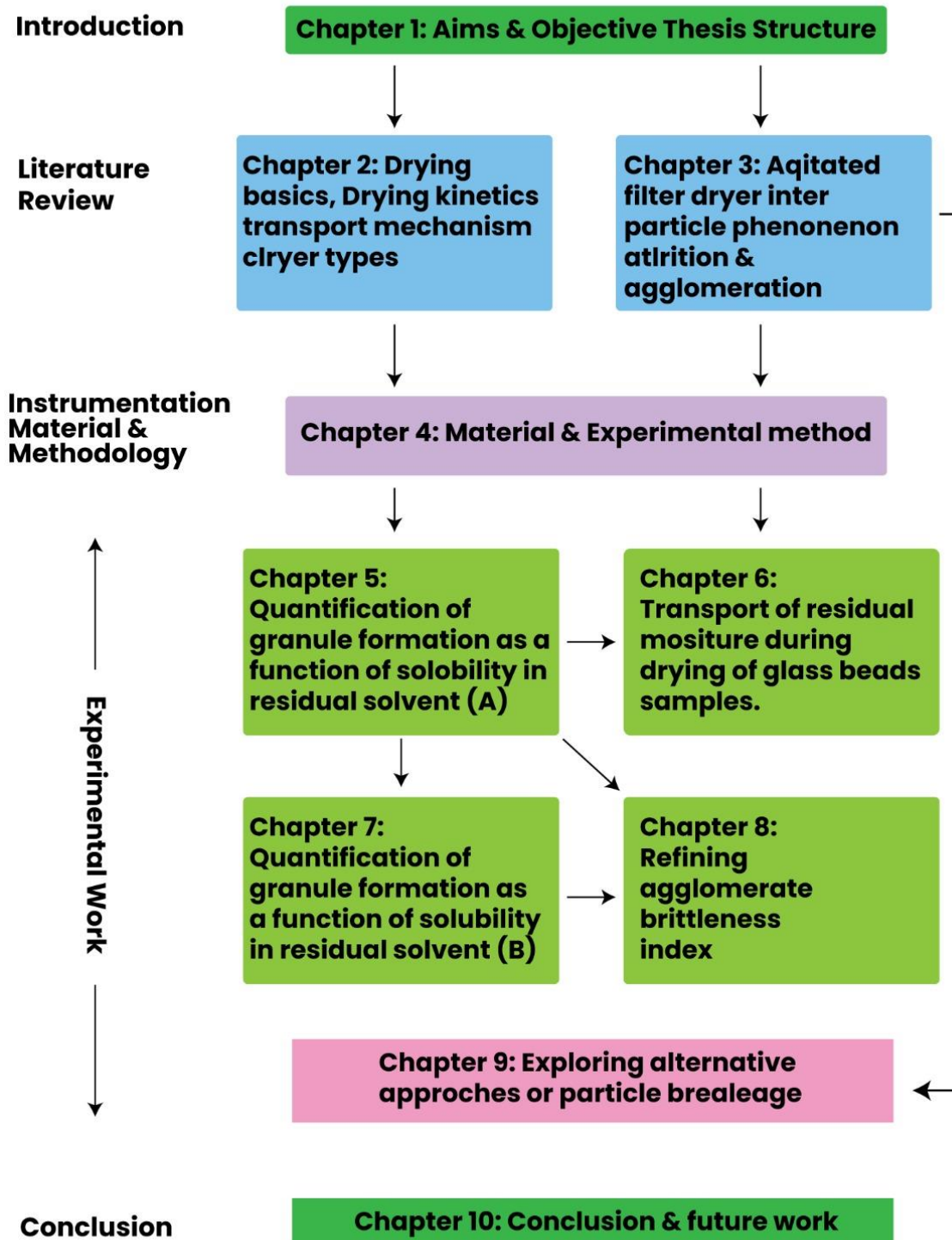


Figure 1-4 Illustrative route map of thesis chapters

1.3 References

Am Ende, D. *et al.* (2013) ‘Development and Application of Laboratory Tools To Predict Particle Properties upon Scale-Up in Agitated Filter-Dryers’, *Organic Process Research & Development*, 17(10), pp. 1345–1358. doi: 10.1021/op400080x.

Birch, M. and Marziano, I. (2013) ‘Understanding and Avoidance of Agglomeration During Drying Processes: A Case Study’. doi: 10.1021/op4000972.

Conder, E. W. *et al.* (2017) ‘The Pharmaceutical Drying Unit Operation: An Industry Perspective on Advancing the Science and Development Approach for Scale-Up and Technology Transfer’. doi: 10.1021/acs.oprd.6b00406.

Ghadiri, M. and Zhang, Z. (2002) ‘Impact attrition of particulate solids. Part 1: A theoretical model of chipping’, *Chemical Engineering Science*, 57(17), pp. 3659–3669. doi: 10.1016/S0009-2509(02)00240-3.

Hamilton, P. (2011) ‘Investigation of a drying process of needle-shaped particles using particle size analysis techniques and non-invasive Raman spectrometry’. doi: 10.48730/ZVV6-A488.

Keey, R. B. (1992) ‘Drying of Loose and Particulate Materials’, *Drying Technology*, 10(4). doi: 10.1080/07373939208916507.

Kemp, I. C. (2017) ‘Drying of pharmaceuticals in theory and practice’, *Drying Technology*. Taylor & Francis, 35(8), pp. 918–924. doi: 10.1080/07373937.2016.1222539.

Kudra, T. and Mujumdar, A. S. (2009) *Advanced drying technologies*. CRC Press/Taylor & Francis. Available at: https://www.academia.edu/25013702/Advanced_Drying_Technologies (Accessed: 9 May 2019).

Lamberto, D. J. *et al.* (2011) ‘Laboratory methods for assessing API sensitivity to mechanical stress during agitated drying’, *Chemical Engineering Science*. Elsevier, 66(17), pp. 3868–3875. doi: 10.1016/j.ces.2011.05.016.

Lee, T., Lin, H. Y. and Lee, H. L. (2013) ‘Engineering Reaction and Crystallization and the

Impact on Filtration, Drying, and Dissolution Behaviors: The Study of Acetaminophen (Paracetamol) by In-Process Controls’.

Lekhal, A. *et al.* (2004) ‘The effect of agitated drying on the morphology of l -threonine (needle-like) crystals’, 270, pp. 263–277. doi: 10.1016/j.ijpharm.2003.10.022.

Lim, H. L., Hapgood, K. P. and Haig, B. (2016) ‘Understanding and preventing agglomeration in a filter drying process’, *Powder Technology*. Elsevier B.V., 300, pp. 146–156. doi: 10.1016/j.powtec.2016.03.003.

Macleod, C. S. and Muller, F. L. (2012) ‘On the Fracture of Pharmaceutical Needle-Shaped Crystals during Pressure Filtration: Case Studies and Mechanistic Understanding’. doi: 10.1021/op200279m.

MacLeod, C. S. and Muller, F. L. (2012) ‘On the Fracture of Pharmaceutical Needle-Shaped Crystals during Pressure Filtration: Case Studies and Mechanistic Understanding’, *Organic Process Research & Development*. American Chemical Society, 16(3), pp. 425–434. doi: 10.1021/op200279m.

Mujumdar, A. S. (2007) *Handbook of industrial drying*. CRC/Taylor & Francis. Available at: <https://www.crcpress.com/Handbook-of-Industrial-Drying/Mujumdar/p/book/9781466596658> (Accessed: 24 April 2019).

Ottoboni, S. *et al.* (2019) ‘Development of a Novel Continuous Filtration Unit for Pharmaceutical Process Development and Manufacturing’, *Journal of Pharmaceutical Sciences*, 108(1). doi: 10.1016/j.xphs.2018.07.005.

Parikh, B. D. M. and Group, D. (2015) ‘Pdf Solids Drying: Basics and Applications’, (October), pp. 1–11.

Pietsch, W. (2004) *Agglomeration in Industry, Agglomeration in Industry: Occurrence and Applications*. Wiley. doi: 10.1002/9783527619795.

Sharma, P. K., Murugesan, S. and Tabora, J. E. (2019) ‘DESIGN OF FILTRATION AND

DRYING OPERATIONS’, in *Chemical Engineering in the Pharmaceutical Industry*. Hoboken, NJ, USA: John Wiley & Sons, Inc., pp. 799–831. doi: 10.1002/9781119600800.ch35.

Tamrakar, A. *et al.* (2016) ‘Dynamic agglomeration profiling during the drying phase in an agitated filter dryer: Parametric investigation and regime map studies’, *Powder Technology*. Elsevier B.V., 303, pp. 109–123. doi: 10.1016/j.powtec.2016.09.012.

https://www.engr.colostate.edu/CBE101/topics/heat_transfer.html

Chapter 2: Literature Review: Drying basics, kinetics and transport mechanisms

This chapter explains the basic theory and concepts concerning the drying process, including dryer types and kinetics. Drying removes solvent by evaporation of solvent from wet products; solutions, suspensions, slurries, and pastes. The process is termed vaporisation when it occurs at the solvent boiling point. Therefore, understanding the thermodynamics and heat & mass transfer mechanisms involved is essential to predict drying curves and temperature profile variations with time. This chapter also gives a general overview of the classification of dryers used in the pharmaceutical industry.

2.1 Drying basics

During pharmaceutical manufacturing, the main process involving drying is the isolation and recovery of API crystals from mother liquor after crystallisation and filtration. An alternative approach to modify the shape and size of particles is spray drying which can produce free-flowing particles. Another approach to manage particle size and shape is fluidised bed drying. (Kemp, 2017)

Drying involves removing volatile liquids from solutions, slurries, or suspensions by applying thermal energy (Jerger, 1951). Drying is a necessary final step of API isolation, as the mechanical separation achieved by solid-liquid separation is never complete. One of the complicated factors for drying is the heterogeneous aspect involving solids, liquids, and vapors and the requirement for heat to be supplied to evaporate the solvent.

The drying process significantly impacts the characteristics of the end drug product. Therefore, it is necessary to understand several drying processing requirements like complete removal of residual solvent, agglomeration prevention, cake cracking, and uniform distribution of impurities. In addition, residual solvent levels must meet ICH guidelines (ICH Q3C(R8) Guideline on Impurities, 2021) to safeguard patients. Also, traces of residual solvent may affect the stability of the formulated product. Therefore, one of the most appropriate ways to understand and communicate drying parameters is to plot a graph of moisture content against time (Jerger, 1951).

Moisture concentration (X), the moisture content in wet material, is defined as the mass of

moisture present per unit of dry material.

$$\text{Moisture concentration } (X) = \frac{m_A}{m_C} \quad \text{Equation 2-1}$$

Where m_A is the mass of wet material and m_C is the mass of dried material.

The drying rate (\dot{m}) (g/min) is the rate of change of moisture content (Simurda, 2017).

$$\dot{m} = \frac{m_C}{A} \frac{dX}{dt} \quad \text{Equation 2-2}$$

Where m_C is the mass of dried material, and A is the surface area exposed to the drying conditions and dX/dt is the rate of change of moisture with time. Another convenient approach to present weight loss during drying is to express moisture content as a Loss of solvent drying (LOD) (Ottoboni *et al.*, 2020).

$$LOD = \frac{\text{initial wet sample weight} - \text{weight of the sample after drying}}{\text{initial wet sample weight}} * 100 \quad \text{Equation 2-3}$$

There are different types of residual moisture content depending on the moisture level and how the moisture is retained in the sample (see Figure 2-1). For example, the residual moisture content can be the bound solvent in the form of a solvate. In contrast, the excess moisture in wet samples of such materials is an unbound solvent. Because of its structural role in the crystal lattice, the vapor pressure of bound moisture is lower than that of the unbound solvent at the same temperature. Solvent retained in the pores of a porous material is intermediate between free and bound moisture.

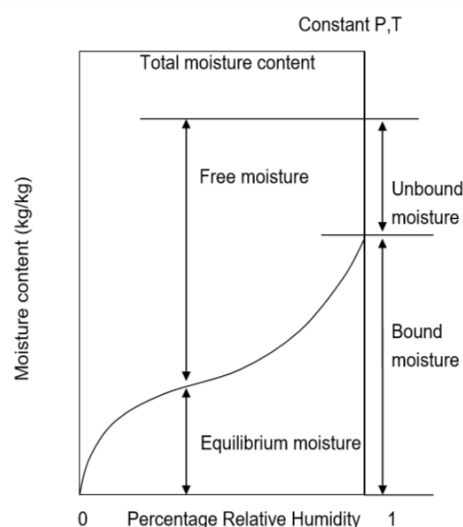


Figure 2-1 Types of moisture involves in drying (Majumdar & Marchertas, 1997)

Free moisture, which consists of the unbound, and some part of the bound moisture, can be evaporated during drying. Figure 2-1 illustrates a key concept in drying, the equilibrium moisture content, which depends on the sample temperature and pressure. The moisture content will never reduce below this point, even if the duration of drying is extended (Hall, 1988). Therefore, this value is the lowest moisture content for the specific material (substrate and solvent), which can be achieved by drying under the defined temperature and humidity conditions (Jerger, 1951).

Thermal evaporation is usually used to dry materials that can resist thermal decomposition at a standard boiling point, where the vapour pressure of moisture equals atmospheric pressure. Correspondingly, vacuum evaporation occurs at lower pressures where reduced pressure has been applied to lower the solvent boiling point. In vaporisation, hot air or heated nitrogen passes through the wet solids and directly supplies the heat for moisture removal (Hall, 1988).

2.1.1 Drying types classified by the heat transfer mechanism

There are three drying modes of heat transfer in porous media: convection, conduction, and radiation. According to the moisture's heat transfer mechanism, dryers can be classified as direct-heat (convection) dryers, indirect-heat (conduction) dryers, and those driven by radiation from a hot surface.

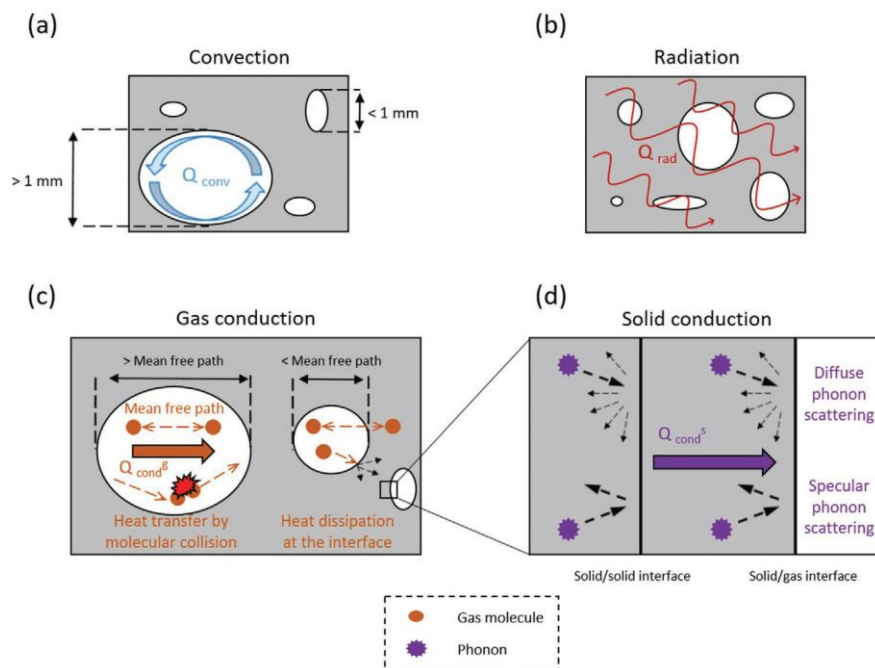


Figure 2-2 The modes of heat transport in porous materials. Heat transfer by a) convection, b) radiation, c) gas conduction, including the coupling (Apostolopoulou-kalkavoura, Munier and Bergström, 2021)

During direct drying, heat is transferred from hot gases passing through a bed of particles, and indirect heat transfer occurs from hot walls. The hot gas can be air, steam, nitrogen, or any other non-reactive gas. Conductive drying occurs due to the evaporation of liquids by applying heat to the wet material. Especially under vacuum conditions, contact drying is used for heat and oxygen-sensitive drugs to avoid thermal degradation. The extreme case of vacuum drying is freeze drying, where the moisture in the starting material has been frozen. The ice sublimates into a gaseous state by contact, convective, or radiative heating. The advantage of freeze drying is that during the sublimation process, the structure and properties of the dried material remain unchanged.

Contact drying is an indirect process that removes the liquid phase from a solid by heating it, converting the liquid from the surface of the solid to an unsaturated vapour phase. It is a standard process in industries dealing with chemicals, catalysts, food, pharmaceuticals, and other products. The driving force for contact drying is temperature difference; therefore, higher contact surface temperatures approaching the solvent's boiling point exhibit faster drying performance. The evaporation temperature for contact drying is the saturation temperature at the prevalent vapour pressure; it can be calculated from Antoine's equation (Green & Perry, 2008).

2.1.2 Drying Kinetics

A typical pair of drying curves, as shown in Figure 2-3, can illustrate drying kinetics, the curve on the left shows the drying rate against time, and the curve on the right shows the drying rate against residual moisture content therefore, the trajectory over time in the righthand curve is from top right to bottom left. Together the curves show the different stages of drying, and each drying curve has three distinct drying periods: the induction / initial adjustment period, the constant rate period, and the falling rate period,

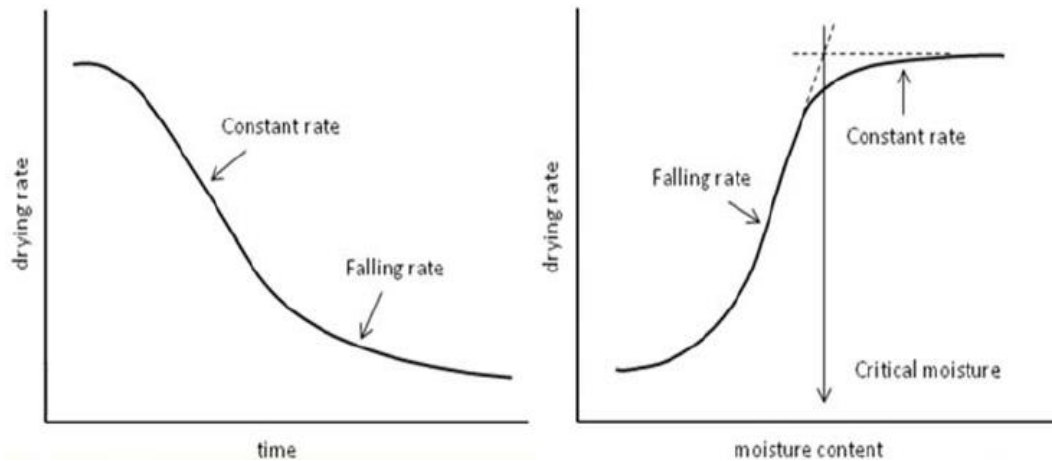


Figure 2-3: Characteristic drying curve. (T. and Ocone, 2011)

The first stage of the drying stage starts when the material is heated or until the solvent evaporates rapidly by reducing the pressure as the boiling point approaches. As soon as moisture evaporates, the drying rate increases. However, this period is brief and abrupt, so not very noticeable in the drying curve. The second drying stage is the constant rate period, in which the temperature and pressure are maintained at the boiling point. The heat transfer rate controls the evaporation of unbound (free) moisture content from the saturated surface. During this stage, the slope and drying rate depends upon dryer agitation, the inlet gas temperature and humidity, and operating pressure (Edward W. Conder *et al.*, 2017).

Once the sample surface becomes mainly dry, and the solvent diffusion from the bulk to the surface is insufficient to maintain vapour saturation at the evaporative surface, the drying rate decreases; this stage is the falling rate period. This phase of drying is linked to the evaporation of more tightly bound moisture from within the particle bed, especially if the particles are agglomerates as presented as granules. The temperature of the solid bulk material rises during this period due to lower vapour pressure and the correspondingly higher boiling point (Pakowski & Mujumdar, 2014). At the end of the falling rate period, there is a point when no further moisture removal takes place. This point is the equilibrium moisture content, the lowest possible moisture to which the material needs to be dry at this temperature and pressure (Jerger, 1951).

2.1 Transport Mechanism During drying

The moisture transport during drying can be controlled either internally (by diffusion) or externally (by providing heat). External conditions dominate the drying mechanism when the

resistance of the boundary layer to the mass transfer is greater than the internal resistance and vice versa. When external conditions dominate, drying mainly depends on the delivery of heat energy, while for internal conditions, drying is more dependent on wet material properties (Freire, da Silveira, and Carmo Ferreira, 2012).

During drying, evaporation occurs by transporting moisture from the interior to the exterior surface of the wet material. Moisture present in the wet cake can be of two types (section 2.12.1.2) bonded moisture is chemically attached to the material or trapped within its microstructure, while the moisture in excess of the bonded moisture is termed unbonded or free moisture (Figure 2-1). Bonded moisture exerts lower vapour pressures and has apparent values of latent heat of vaporization due to the additional resistance associated with the interactions with the substrate material (Freire, Freire, and Perazzini, 2014).

For drying to take place, the wet solid materials' moisture must migrate from the wet cake's interior to the external surface (Whitaker, 1985). Sherwood (1929) discussed for the first time the mechanism of movement of moisture. He concludes that liquid or vapour diffusion causes moisture transport from the interior to the external surface. However, Jerger (1951) discussed that gravitational flow and vaporization condensation process also affect the moisture transport at the pore level. Similarly, Shi and Wang (2004) mentioned that possible mechanisms of moisture transport during drying include moisture transport due to the difference in total pressure, shrinkage, and by surface diffusion. Even though several transport mechanisms have been suggested for internal moisture transfer there is still no generalized theory (Khraisheh, Cooper and Magee, 1997).

Important issues to be addressed in solid drying are how exactly liquid or solvent is transported through the solids to the surface, how and where evaporation occurs and how these factors affect the distribution of moisture through the solids; the temperature of the material, and evaporation rate under different drying conditions, i.e., dryer temperature, air humidity and air velocity (Sherwood, 1929a).

2.1.3 Classification of evaporation during the drying mechanism

During drying, evaporation may occur at the surface of the solid material or within the solid structure. Evaporation at each point is then further classified into two categories, depending upon the comparison of the resistance of the diffusion of internal moisture to the total resistance of the vapour removal (Sherwood, 1929a).

- I. Evaporation of the moisture at the surface of the solid due to lower internal diffusion resistance of the moisture compared to the total resistance of vapour removal.
- II. Evaporation of the moisture at the surface of the solid due to greater internal diffusion resistance of the moisture compared to the total resistance of vapour removal.
- III. Evaporation of the moisture within the solid structure due to lower internal diffusion resistance of the moisture compared to the total resistance of vapour removal.
- IV. Evaporation of the moisture within the solid structure due to greater internal diffusion resistance of the moisture compared to the total resistance of vapour removal.

However, Sherwood (1929b) suggested that the evaporation within the solid due to lower resistance of internal diffusion to the overall resistance of vapour removal is not possible, as the evaporation within the wet material occurs because of higher internal diffusion resistance. The drying is not restricted to one case; as drying proceeds, the mechanism of moisture transport may vary from one case to another. For example, evaporation occurs from the surface (case I) while drying a very wet surface at a constant drying rate. When the moisture content starts to decline, the drying rate falls as evaporation proceeds. The falling drying rate is then divided into two zones: the first zone, in which the decrease in the rate of drying is due to reduced wetted surface available for evaporation, and the second zone, which is the final zone and is controlled by the diffusion of moisture from internal to the external surface of the material (Sherwood, 1929a, 1929b). Smith (1959) reported that the moisture removal rate from the material's interior depends not only on the resistance of the material's cell structure but also on the size and distribution of capillary passages. Similarly, Vu and Tsotsas (2018) also reported that moisture transport in solid material during drying is also caused by gravity, external pressure, convection, vaporization, and condensation.

2.1.4 Mechanism of internal moisture transport

During the drying of the material, which contains internal moisture, a point comes when the evaporation of moisture from the surface occurs after replenishment from the interior. If the material contains connecting pore spaces, moisture may be transported in the liquid phase under surface tension or capillarity. As drying proceeds, the remaining internal moisture must be transported to the surface by diffusion due to the breakage of interior surfaces. Hence, moisture transport is a complex process, which also depends on the material's nature and has not been completely acknowledged yet (Smith, 1959).

2.1.1.1 Moisture transport by capillarity

Capillary flow occurs through voids and on solid surfaces due to molecular attraction between liquid and solid. Porous solids exhibit capillary action when saturated with solvent and are known to be in a capillary state. A typical example of capillary flow is the rise of kerosene in a wick. Moisture movement in capillary flow is due to the surface tension of the liquid. The material in a powder bed can contain a bundle of capillaries which allow moisture movement during drying. The drying rate depends on the size of the pores or voids and their distribution within the material.

The moisture held between the crevices of solid material is transported by gravity and capillary action. These phenomena transport the moisture that is above equilibrium moisture content. As the material dries, the moisture meniscus formed between the pores of the particles successively becomes narrow and then collapses. If appropriate pore sizes are available, then the moisture flow continues from the area of high concentration to the lower concentration. Slichter C. (1905) first indicated the influence of pathways on the transport of moisture due to the pore sizes. Later Ceaglske and Hougen (1937) used capillary theory and suggested that a similar mechanism occurs in granular material drying.

Haines (1925) also studied the meniscus formation on the bed of solid spheres and developed an expression for its surface potential. Later Newitt and Conway-Jones (1958) proposed a method of measuring the surface potentials of menisci with particles of mixed sizes. However, there are still no valuable predictions of drying rates related to capillarity. These models have been influential in understanding and describing the kinetics of drying.

Haines Model (1925):

Haines developed a model to describe the drying of porous materials, particularly during the constant-rate period of drying. This model is often referred to as the "Haines drying equation." It assumes that the rate of drying is proportional to the difference between the moisture content of the material and the equilibrium moisture content at the drying temperature. The Haines model helps explain the initial rapid drying period when moisture is readily available at the material's surface.

Newitt Model (1958):

Newitt extended the work of Haines by considering the falling-rate period of drying. The falling-rate period occurs when the drying process becomes limited by the rate at which moisture can move from the interior of the material to the surface. Newitt's model incorporates both diffusion of moisture within the material and the resistance offered by the external layer of dried material. This model is particularly relevant for cases where the drying process is no longer controlled solely by external conditions.

Both models are foundational in the study of drying kinetics and have contributed to the understanding of moisture migration within porous materials during the drying process. They provide valuable insights into how different factors such as temperature, humidity, and material properties affect drying rates and the overall drying behavior. Keep in mind that subsequent research might have refined or expanded upon these models, so it's a good idea to explore more recent literature for the latest advancements in the field.

2.1.1.2 Moisture transport by diffusion

When porous particles dry, moisture diffuses through the solids. Diffusion is a molecular process, primarily the random motion of individual solvent molecules. It is assumed that the solvent molecules in the material can move freely. In this case, they tend to spread from areas with high moisture concentrations to areas with lower moisture concentrations to counteract the reduced moisture gradient and balance the moisture concentration. Moisture diffusion occurs when there is a concentration difference between the core of the particle and the surface. Moisture diffusivity generally decreases with decreasing moisture content. Therefore, the diffusion level is usually an average value over the concentration range used.

As drying proceeds, the capillary action ceases as described above, and then the remaining moisture must reach the external surface of the material by diffusion. Diffusion is the random mixing of molecules and causes moisture transfer from regions of high concentration to regions of low concentration. Diffusion often controls drying rates at low moisture levels.

Sherwood (1929) and Lewis *et al.* (1979) developed a mathematical model for drying by using the Fourier heat equation. To develop a simple diffusion model during drying, they replace temperature and thermal diffusivity with moisture and moisture diffusivity, respectively. This model can calculate the moisture distribution in solid material during drying by considering the

diffusivity of the liquid constant.

$$\frac{\partial X}{\partial t} = \delta_{eff} \nabla^2 X \quad \text{Equation 2-4}$$

Where,

X = moisture content,

t = time,

δ_{eff} = effective diffusion coefficient, and

∇ is a gradient, three-dimensional differential operator and gives the direction of diffusion of moisture content vector.

Extensive work has been carried out to determine the effective diffusion coefficient in the past (Koponen (1984), Raouzeos and Saravacos (1986), Jaros *et al.* (1992), Pel *et al.* (1993), Mourad, Hemati, and Laguerie (1996), Pel, Brocken and Kopinga (1996) and Srikiatden and Roberts (2006). Blackband and Mansfield (1986), McDonald, Pritchard, and Roberts (1996), and Schrader and Litchfield (2007) used magnetic resonance imaging (MRI) to study moisture transport during drying. They then directly used these measured moisture profiles to calculate the effective distribution coefficient. Their studies show that MRI is an effective technique as it can measure moisture at any point. Moreover, this technique provides a rapid, precise, and non-destructive procedure to measure moisture profiles and consequently allows the analysis of several models for drying.

Diffusion models are considered the simplest way to describe the drying process. However, diffusion theory is an oversimplified technique to explain the mass transfer during drying because of its single-phase modelling. Despite diffusion theory, the capillary theory is more elaborated; still, it does not provide sufficient information for mass transfer. Capillary flow theory provides good predictions of moisture transport for coarse granular material, but for fine particles, the surface energy of the pores between particles, which considerably affects moisture transport, is not covered by both diffusion or capillary theory (Bažant, 1970). In their work, Huang, Siang and Best (1979) showed that moisture transport through porous media strongly depends on the structure of porous material.

2.1.1.3 Gravitational flow

Gravity tends to pull liquid towards the bottom of a bed of wet solid. Gravity only works in the vertical direction. In contrast, diffusion works in all directions with decreasing concentration, and capillary flow depends on the size and interstitial pore distribution.

2.1.1.4 Convection

Convection is based on the movement of liquids in porous materials driven by heat flow and is the driving force associated with the temperature difference created by energy transfer. This process is often referred to as thermal diffusion. The direction of moisture flow is in the direction of a decrease in temperature - the more significant the temperature difference, the faster the heat transfer. Conversely, at lower temperature differences, the heat transfer rate is slower.

2.1.1.5 Vaporisation and condensation process

In this theory, it is assumed that the temperature difference causes a vapour pressure gradient within the solid, resulting in liquid evaporation and its subsequent condensation on cooler surfaces. Therefore, when the wet solid is heated at its bottom surface, and dry air circulates at the top, moisture vaporises at the bottom, where the temperature is at the highest point, and the upwardly diffusing vapours repeatedly condense and evaporate before finally escaping into the vapour space. If the moisture is heated to the boiling point, then the whole column of the liquid moves upward.

Shi and Wang (2004) also mentioned other possible drying mechanisms at the pore level.

- Moisture vapour diffusion due to the difference in partial pressures within air-filled pores.
- Moisture flow due to difference in total pressure
- Moisture flow caused by shrinkage
- Surface diffusion

These mechanisms exist in different drying stages; their relative importance depends on drying conditions, pore geometry, and composition of the porous medium (Segura, 2007).

2.1.5 Properties of a porous media

Fluid flow through porous media has attracted many engineers and scientists from various fields, including chemical and environmental engineering, the food industry, and geothermal physics. It is generally accepted that every material is porous to some extent. The physical and chemical properties of porous materials depend upon the pore structure. The diversity of porous materials has led to various studies on transport mechanisms through porous materials (Coutelieris and Delgado, 2012).

2.1.1.6 Porous media and porosity

According to Kantzas, Apostolos; Bryan Jonathan; Taheri (2015), a solid material or system could be categorized as porous if:

- It contains pores, spaces, or voids free from solids and may be filled with air, water, or other liquids.
- It is permeable, allowing fluid penetration from one face and emerging from the other.

Regarding mechanical properties, porous material could be classified as consolidated, in which any cementing material holds particles, and unconsolidated, in which particles are loose (Morita, 2020).

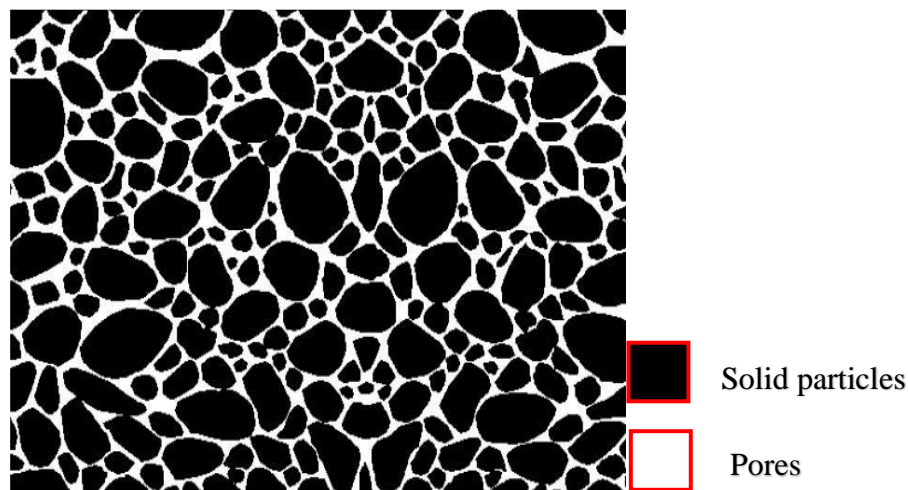


Figure 2-4 Microscopic cross-section image of a porous medium (Kantzas, Apostolos; Bryan Jonathan; Taheri, 2015)

Porosity

Porosity is one of the essential properties of porous material and is defined as the ratio of pore volume to bulk volume. The bulk volume is the sum of the volume of particles and pores.

$$\phi = \frac{\text{Pore volume}}{\text{bulk volume}} = 1 - \frac{\text{particle volume}}{\text{bulk volume}} \quad \text{Equation 2-5}$$

$$\text{bulk volume} = \text{particle volume} + \text{pore volume} \quad \text{Equation 2-6}$$

Where,

ϕ = Porosity

However, from a moisture transport point of view, interconnected pores are of greater interest, leading to the concept of effective porosity. Effective porosity is the ratio of interconnected pore volume to bulk volume. There is a significant difference in total and effective porosity values for consolidated material, while for unconsolidated materials, both are approximately the same (Kantzas, Apostolos; Bryan Jonathan; Taheri, 2015).

Wettability

The wettability of porous media plays an essential role in studying moisture transport. The contact angle usually determines the extent of wetting of a solid by a liquid. If the contact angle is less than 90° , the fluid is wetting the solid particle; if the contact angle is greater than 90° , then the fluid is non-wetting (Morita, 2020).

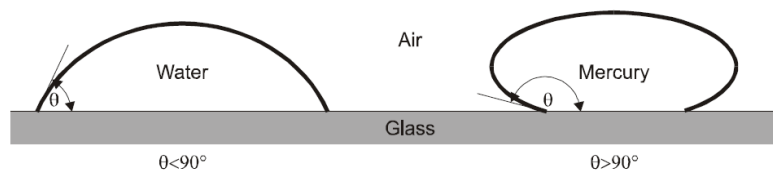


Figure 2-5 Comparison of wetting and non-wetting fluid (E. Heinemann, 2005)

2.1.6 Properties of wet granular media

Menisci and Capillary forces

The attractive forces caused by the liquid menisci between two particles are called capillary forces. Two main reasons for meniscus formation are capillary condensation and deposition of adsorbed liquid on a solid surface (Butt and Kappl, 2009). Capillary forces and surface tension give rise to cohesive forces within the wet granular material (Mitarai and Nori, 2007).

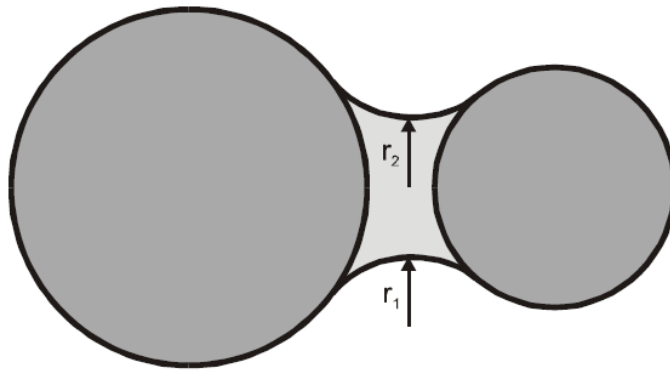


Figure 2-6 Illustration of the liquid bridge and principal radii of curvature (E. Heinemann, 2005)

The pressure difference ΔP between both sides of the fluid, i.e., liquid and air with menisci of radii r_1 and r_2 , can be calculated by the Laplace equation and is given as:

$$\Delta P = P_a - P_b = \gamma \left[\frac{1}{r_1} + \frac{1}{r_2} \right] \quad \text{Equation 2-7}$$

Where,

γ = surface tension

P_a = air pressure

P_b = liquid pressure

If the curvature is positive, that is, menisci drawn back to the liquid phase, then ΔP is positive, also known as suction.

Liquid bridges between particles

Liquid bridges (Figure 2-6) also induce attraction forces between particles due to surface tension and suction. The presence of liquid between particles reduces the surface area resulting in suction and cohesive forces between particles.

2.2 Classification of dryers and their applications

Dryers can be classified on several different bases. Depending upon the heat transfer mechanism, dryers can be classified as direct (convection), indirect (conduction), radiant, and microwave / dielectric dryers. Convective or adiabatic dryers use the latent heat of hot gases to evaporate the moisture, while heat transfer in conductive dryers occurs through heated surfaces

in the dryers (indirect drying). Generally, contact dryers operating under vacuum conditions are suitable for heat and oxygen-sensitive pharmaceutical products.

Dryers can also be classified based on material handling in the dryers. The essential criteria in this type of Classification are the presence or absence of agitation, i.e., static or dynamic drying. In static drying, there is no imposed movement of the material to be dried, for example, in a vacuum tray drier. Similarly, hot gas can flow gently through a static bed of wet material, inducing the solvent's evaporation. However, in a dynamic dryer, movement of the material in the bed can be achieved typically by using agitators, e.g. in an agitated filter drier (Parikh & Group, 2015) or in a fluidised bed drier where the hot gas flow is sufficient to suspend the particles during drying

Different drying technologies are used in the pharmaceutical industry to address APIs with different properties and to achieve different outcomes. For example, for API recovery after crystallisation, filter or contact dryers are used, after wet granulation, fluidised bed dryers are used, and spray dryers can be used to produce free-flowing particles. Another particular use of dryers is to isolate sterile products, such as freeze-drying antibiotics directly in vials for reconstitution at the point of use (Kemp, 2017). Hence, selecting the best dryer for the scope of the work needs to be carefully determined. Some commonly used dryers in pharmaceutical manufacturing are listed below:

Laboratory vacuum ovens are suitable for drying very small batches of pharmaceuticals in early development. Material can be presented as a thin layer on a glass dish. Although a small nitrogen flow (nitrogen bleed) is frequently provided, the heat energy needed to dry the product is supplied through the oven's walls (Pakowski & Mujumdar, 2014).

Tray dryers, a scaled-up version of the vacuum oven, consist of trays inside a vacuum chamber. A modest flow of heated nitrogen provides a carrier to displace solvent vapour. The trays, typically stainless steel, are placed on heated shelves. Tray dryers are suitable for relatively small amounts of material to avoid attrition. However, tray driers have many disadvantages, including inhomogeneous drying and the distribution of impurities.

Furthermore, the formation of hard lumps frequently accompanies tray drying. For these reasons, tray-dried material often requires milling to remove lumps and ensure a uniform distribution of residual impurities. In addition, these involve quite an extended drying time, usually 12-24 hours (Guerrero *et al.*, 2003). Many organisations do not use tray dryers due to

onerous PPE requirements needed to manage the risk of operator exposure to the drug substance and the potential for product contamination during these manual operations.

Filter dryers perform both filtration and drying. These dryers are the most widely used dryer in the pharmaceutical industry. Effectively they are a filter equipped with an agitator and jacketed walls to supply heat. In some larger units, an internally heated agitator also delivers heat to the material. Filter dryers can also function as convective dryers. A key advantage is enhanced containment, as transfer of the solvent wet API cake from, for example, a filter to a tray drier is avoided. The accompanying disadvantage is that the process sequence is extended as the same equipment is used for filtration, washing, and drying, potentially becoming a bottleneck. (Pakowski and Mujumdar, 2014).

Spray dryers involve the drying of solutions and slurries. In a spray dryer, either a solution of the API or a suspension of very fine particles of API is dispersed as fine droplets in a moving stream of hot nitrogen to facilitate the evaporation of the solvent. Spray driers can be useful when drying temperature-sensitive materials. One of the main advantages of spray dryers is that if the end product is very fine, usually spherical particles, it can be used directly for tableting after mixing with other components. In addition, the maximum attainable size is the drop diameter volume which evaporates during the time of flight through the drying chamber (Pakowski & Mujumdar, 2014).

Fluidised bed dryers are the most widely used in secondary processing (formulation). They are frequently associated with wet granulators, where they are used to remove the water used in the granulation process. Wet granulation is one of the most common formulation routes to ensure content uniformity. The feed rates for these dryers can vary from a few grams to tons per hour, though the units employed in the pharmaceutical sector are usually at the lower end of the scale. Heated air or nitrogen passes through a bed of product granules to create a fluidised bed. Typically pharmaceutical fluidised bed driers are operated batch-wise based on the manufacturing scale. However, these dryers achieve uniform drying in other industry sectors for continuous large-scale production. The main disadvantage of fluidised bed dryers is that they are not suitable for friable products and with large sizes, where particles show poor fluidisation (Guerrero *et al.*, 2003).

In addition to the dryers, as mentioned earlier, other dryers include centrifugal filter dryers, tumble dryers, radiation-based dryers like microwave ovens, etc. (Mujumdar, 2007)

Traditionally, filtration and drying unit operations were carried out with different equipment. Consequently, material transfer losses added to cleaning conditions and other issues that come with product transfer, like increased production time. A single unit capable of carrying out both operations can avoid all the downsides mentioned. This idea leads to the migration toward Agitated Filter Dryers (AFDs).

2.3 Summary

Drying is the removal of solvent either from aqueous or organic solvent solution. The basic dryers that are used for pharmaceutical drying process are introduced. Different drying periods along with drying kinetics are sketched. The distinctive drying stages with regarding to different mass and heat transfer mechanisms are described. Comprehensive interpretations of drying stages are essential to understanding experimental drying behaviours. The basic drying theory included in this chapter: two common modes include contact and convective drying usually used industrial filter dryer equipment are described. The thermophysical and transport properties porous beds that are essential to drying process are described.

2.4 References

Apostolopoulou-kalkavoura, V., Munier, P. and Bergström, L. (2021) ‘Thermally Insulating Nanocellulose-Based Materials’, 2001839. doi: 10.1002/adma.202001839.

Bažant, Z. P. (1970) ‘Constitutive equation for concrete creep and shrinkage based on thermodynamics of multiphase systems’, *Matériaux et Constructions*, 3(1). doi: 10.1007/BF02475106.

Blackband, S. and Mansfield, P. (1986) ‘Diffusion in liquid-solid systems by NMR imaging’, *Journal of Physics C: Solid State Physics*. IOP Publishing, 19(2), p. L49. doi: 10.1088/0022-3719/19/2/004.

Butt, H. J. and Kappl, M. (2009) ‘Normal capillary forces’, *Advances in Colloid and Interface Science*. Elsevier B.V., 146(1–2), pp. 48–60. doi: 10.1016/j.cis.2008.10.002.

C., S. (1905) ‘Field measurements of the rate of movement of underground waters’, *U. S. Geological Survey Water-Supply and Irrigation Paper*, 140. Available at: <https://cir.nii.ac.jp/crid/1571135649709113344> (Accessed: 2 September 2022).

Ceaglske, N. H. and Hougen, O. A. (1937) ‘Drying granular solids’, *Industrial and Engineering Chemistry*. American Chemical Society, 29(7), pp. 805–813. doi: 10.1021/IE50331A017/ASSET/IE50331A017.FP.PNG_V03.

Ceaglske, N. H., Hougen, O. A. and Loughborough, K. W. (no date) ‘DRYING GRANULAR SOLIDS Methods are described for calculating the moisture distribution and average moisture content of a granular solid for any thickness and for calculating the drying-rate curves during the first and second falling periods, provided the value at the constant-rate’. Available at: <https://pubs.acs.org/sharingguidelines> (Accessed: 2 September 2022).

Conder, E. W. *et al.* (2017) ‘The Pharmaceutical Drying Unit Operation: An Industry Perspective on Advancing the Science and Development Approach for Scale-Up and Technology Transfer’, *Organic Process Research and Development*, 21(3), pp. 420–429. doi: 10.1021/acs.oprd.6b00406.

Coutelieris, F. A. and Delgado, J. M. P. Q. (2012) ‘Fundamentals of Porous Structures’. Springer, Berlin, Heidelberg, pp. 5–21. doi: 10.1007/978-3-642-27910-2_2.

- E. Heinemann, Z. (2005) 'Text-book series in education', 2(October).
- Freire, J. T., Freire, F. B. and Perazzini, H. (2014) 'On the Influence of Particles Characteristics on Moisture Diffusivity during Drying of Granular Porous Media', 2014(January), pp. 7–16.
- Freire, J. T., da Silveira, A. M. and do Carmo Ferreira, M. (2012) 'Transport phenomena in particulate systems', *Transport Phenomena in Particulate Systems*. Bentham Science Publishers Ltd. doi: 10.2174/97816080522711120101.
- Green, D. W. and Perry, R. H. (2008) 'Perry's Chemical Engineers' Handbook, Eighth Edition'. McGraw-Hill: New York, Chicago, San Francisco, Lisbon, London, Madrid, Mexico City, Milan, New Delhi, San Juan, Seoul, Singapore, Sydney, Toronto. Available at: /content/book/9780071422949 (Accessed: 2 July 2020).
- Guerrero, M. *et al.* (2003) 'Drying in pharmaceutical and biotechnological industries', *Food Science and Technology International*, 9(3), pp. 237–243. doi: 10.1177/1082013203035567.
- Haines, W. B. (1925) 'Studies in the physical properties of soils: II. A note on the cohesion developed by capillary forces in an ideal soil', *The Journal of Agricultural Science*, 15(4). doi: 10.1017/S0021859600082460.
- Hall, C. W. (1988) 'HANDBOOK OF INDUSTRIAL DRYING', *Drying Technology*. Taylor & Francis Group , 6(3), pp. 571–573. doi: 10.1080/07373938808916399.
- ICH Q3C(R8) Guideline on Impurities (2021) *ICH Q3C (R8) Residual solvents - Scientific guideline | European Medicines Agency*. Available at: <https://www.ema.europa.eu/en/ich-q3c-r8-residual-solvents-scientific-guideline> (Accessed: 3 December 2022).
- Jaros, M. *et al.* (1992) 'A method of determination of the diffusion coefficient based on kernel moisture content and its temperature', *Drying Technology*, pp. 213–222. doi: 10.1080/07373939208916422.
- Jerger, E. W. (1951) 'Mechanism of moisture movement in the drying of organic granular solids', *Energy Conversion and Management*, 40(6), p. 551. Available at: http://www.sciencedirect.com/science/article/pii/S0196890498000934%5Cnhttp://www.arunmujumdar.com/file/Publications/books/ME5202_2011_Mujumdar.pdf%5Cnhttp://www.sciencedirect.com/science/article/pii/S0196890498000922.

Jerger, E. W. (no date) *Mechanism of moisture movement in the drying of organic granular solids Recommended Citation*. Available at: <https://lib.dr.iastate.edu/rtd/13871> (Accessed: 29 April 2019).

Kantzas, Apostolos; Bryan Jonathan; Taheri, S. (2015) 'Fundamentals of Fluid Flow in Porous Media', *Pore size distribution*.

Kemp, I. C. (2017) 'Drying of pharmaceuticals in theory and practice', *Drying Technology*. Taylor & Francis, 35(8), pp. 918–924. doi: 10.1080/07373937.2016.1222539.

Khraisheh, M. A. M., Cooper, T. J. R. and Magee, T. R. A. (1997) 'Transport mechanisms of moisture during air drying processes', *Food and Bioproducts Processing: Transactions of the Institution of Chemical Engineers, Part C*, 75(1). doi: 10.1205/096030897531342.

Koponen, H. (1984) 'Dependences of moisture diffusion coefficients of wood and wooden panels on moisture content and wood properties', *Paperi ja puu = Papper och yra = Paper and timber*. Suomen Paperi- ja Puutavaralehti Oy, 66(12), pp. 740–745.

Lewis, R. W. *et al.* (1979) 'Drying-induced stresses in porous bodies —an elastoviscoplastic model', *Computer Methods in Applied Mechanics and Engineering*. North-Holland, 20(3), pp. 291–301. doi: 10.1016/0045-7825(79)90004-5.

Majumdar, P. and Marchertas, A. (1997) 'Heat, moisture transport, and induced stresses in porous materials under rapid heating', *Numerical Heat Transfer; Part A: Applications*, 32(2), pp. 111–130. doi: 10.1080/10407789708913883.

McDonald, P. J., Pritchard, T. and Roberts, S. P. (1996) 'Diffusion of Water at Low Saturation Levels into Sandstone Rock Plugs Measured by Broad Line Magnetic Resonance Profiling', *Journal of Colloid and Interface Science*. Academic Press, 177(2), pp. 439–445. doi: 10.1006/JCIS.1996.0056.

Mitarai, N. and Nori, F. (2007) 'Wet granular materials', <https://doi.org/10.1080/00018730600626065>. Taylor & Francis Group, 55(1–2), pp. 1–45. doi: 10.1080/00018730600626065.

Morita (2020) 'Fluid flow through porous media', in *Developments in Petroleum Science*. doi: 10.1016/B978-0-12-823825-7.00016-8.

Mourad, M., Hemati, M. and Laguerie, C. (1996) 'A new correlation for the estimation of moisture diffusivity in corn kernels from drying kinetics', *Drying Technology*. Marcel Dekker Inc., 14(3–4), pp. 873–894. doi: 10.1080/07373939608917129.

Mujumdar, A. S. (2007) *Handbook of industrial drying*. CRC/Taylor & Francis. Available at: <https://www.crcpress.com/Handbook-of-Industrial-Drying/Mujumdar/p/book/9781466596658> (Accessed: 24 April 2019).

Newitt, D. M. and Conway-Jones, J. M. (1958) 'A contribution to the theory and practice of granulation', *Transactions Institute Chemical Engineers*, 36, pp. 422–441.

Ottoboni, S. *et al.* (2020) 'Understanding effect of filtration and washing on dried product: Paracetamol case study', *Powder Technology*. Elsevier, 366, pp. 305–323. doi: 10.1016/J.POWTEC.2020.02.064.

Pakowski, Z. and Mujumdar, A. (2014) 'Drying of Pharmaceutical Products', *Handbook of Industrial Drying, Fourth Edition*, (January), pp. 681–701. doi: 10.1201/b17208-37.

Parikh, B. D. M. and Group, D. (2015) 'Pdf Solids Drying: Basics and Applications', (October), pp. 1–11.

Pel, L. *et al.* (1993) 'Determination of moisture diffusivity in porous media using scanning neutron radiography', *International Journal of Heat and Mass Transfer*. Pergamon, 36(5), pp. 1261–1267. doi: 10.1016/S0017-9310(05)80095-X.

Pel, L., Brocken, H. and Kopinga, K. (1996) 'Determination of moisture diffusivity in porous media using moisture concentration profiles', *International Journal of Heat and Mass Transfer*. Elsevier Ltd, 39(6), pp. 1273–1280. doi: 10.1016/0017-9310(95)00201-4.

Raouzeos, G. S. and Saravacos, G. D. (1986) 'Solar drying of raisins', *Drying Technology*, 4(4), pp. 633–649. doi: 10.1080/07373938608916353.

Schrader, G. W. and Litchfield, J. B. (2007) 'MOISTURE PROFILES IN A MODEL FOOD GEL DURING DRYING: MEASUREMENT USING MAGNETIC RESONANCE IMAGING AND EVALUATION OF THE HCKIAN MODEL', <http://dx.doi.org/10.1080/07373939208916440>. Taylor & Francis Group, 10(2), pp. 295–332. doi: 10.1080/07373939208916440.

- Segura, L. A. (2007) 'Modeling at pore-scale isothermal drying of porous materials: Liquid and vapor diffusivity', *Drying Technology*, 25(10). doi: 10.1080/07373930701590889.
- Sherwood, T. K. (1929a) 'The Drying of Solids—I', *Industrial and Engineering Chemistry*, 21(1), pp. 12–16. doi: 10.1021/ie50229a004.
- Sherwood, T. K. (1929b) 'The Drying of Solids—II', *Industrial and Engineering Chemistry*, 21(10), pp. 976–980. doi: 10.1021/ie50238a021.
- Shi, M. and Wang, X. (2004) 'Investigation on Moisture Transfer Mechanism in Porous Media During Rapid Drying Process', *Drying Technology*, 22(1–2), pp. 111–122. doi: 10.1081/DRT-120028222.
- Simurda, M. (2017) *SOLVENT SELECTION FOR ISOLATION OF PHARMACEUTICAL PRODUCTS*. University of Chemistry and Technology Prague.
- Smith, J. C. (1959) 'The Drying of Vegetable Materials in a Stream of Air'. ProQuest Dissertations & Theses,.
- Srikiatden, J. and Roberts, J. S. (2006) 'Measuring moisture diffusivity of potato and carrot (core and cortex) during convective hot air and isothermal drying', *Journal of Food Engineering*, 74(1), pp. 143–152. doi: 10.1016/j.jfoodeng.2005.02.026.
- Vu, H. T. and Tsotsas, E. (2018) 'Mass and Heat Transport Models for Analysis of the Drying Process in Porous Media: A Review and Numerical Implementation', *International Journal of Chemical Engineering*. doi: 10.1155/2018/9456418.
- Whitaker, S. (1985) 'MOISTURE TRANSPORT MECHANISMS DURING THE DRYING OF GRANULAR POROUS MEDIA.' Hemisphere Publ Corp, pp. 21–32. doi: 10.1007/978-3-662-21830-3_3/COVER.

Chapter 3: Agitated filter dryer & inter particle phenomenon: Agitation and attrition

In this chapter, a detailed description of the Agitated Filter Dryer (AFD) is provided. The development of agitated filter dryer (AFD) equipment and techniques evolved over the last decade and are well appealed to the manufacturer once employed in the industry. The wide use of commercial AFD in pharmaceutical engineering receives great concern. Vacuum contact drying theory related to AFD either experimentally or in simulation aspects has been extensively researched. The transport and separation process takes place in a single unit involving heat transfer and mass transfer at the same time. It is also considered as one of the most suitable processes for drying thermal-sensitive and oxygen-sensitive pharmaceutical chemicals due to the specific desired characteristics of AFD. The combination of vacuum contact drying, and convective drying is considered as an efficient method to optimize the drying process, but two major issues occurring during agitated drying are agglomeration and attrition. Different parameters that affect agglomeration and attrition during agitated drying have been discussed in detail in this chapter.

3.1 Agitated Filter dryer

Appropriate dryers may be selected depending on product requirements and safety concerns. Several dryer types used in pharmaceutical manufacturing have been described briefly in Chapter 2; the agitated filter dryer is one of the most commonly used equipment items in API production. It can perform material filtration from the mother liquor, washing, and drying (Seader & Henley, 2006). The main benefit of combining all these unit operations in one piece of equipment is to reduce staff exposure during material transfers between the filter and dryer. In addition, there is an associated reduction in the risk of product contamination bringing a quality benefit. Generally, AFD is also suitable for oxygen and temperature-sensitive substances due to its enclosed design and the ability to work under a vacuum (Kudra & Mujumdar, 2009) since a vacuum reduces the vaporisation temperature of the solvent. Furthermore, AFD can provide high content uniformity due to the agitation, ensuring product quality (Sharma, Murugesan, and Tabora, 2019). Despite all these advantages and drawbacks of using AFD, one of the most evident drawbacks is lump formation occurring during drying and particle breakage due to agitation.

In agitated dryers, there is a complex interaction of agitation, agglomeration, and attrition during drying. Agitation redistributes the material being dried to improve the heat and mass transfer rate, as drying is not homogenous (dry material would accumulate at the edges and wet material remain within the core). Without agitation, drying will be nonhomogeneous, and the drying process becomes long. Still, a significant liability of using agitation during drying is the formation of agglomerates or the attrition of particles that could adversely affect the product's required properties. In the early stages of drying, the material is above or at critical moisture content, and agglomeration dominates (Wallack & King, 1988). While attrition occurs in the later drying stages when the material tends to become free-flowing, this is especially significant near the impeller and when the dryer operates with an increased bed height (Lim, Hapgood, and Haig, 2016). In addition, trapped moisture within the lumps can cause product degradation and particle size modification during storage and secondary processing (formulation of the drug product) (Lim, Hapgood, and Haig, 2016). In some cases, additional processing equipment and steps, like dry milling, may be required to control particle size and ensure content uniformity of material subjected to agitated drying (Yalkowsky & Bolton, 1990).

Practically agitated filter dryers operate in three working stages: the filtration stage, the washing stage, and the drying stage, as shown in Figure 3-1 (Tamrakar, Gunadi, Patrick M Piccione, *et al.*, 2016).

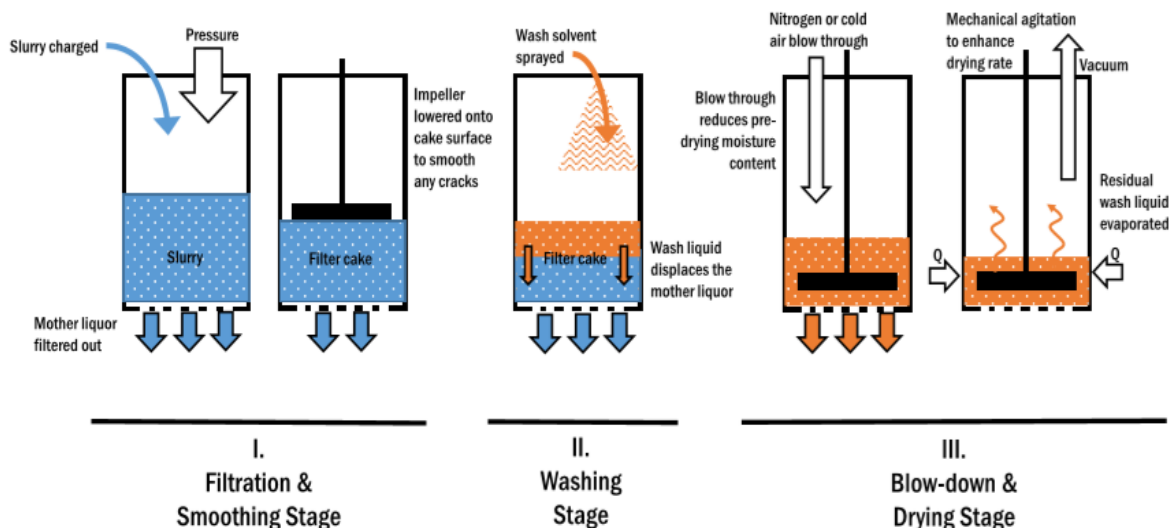


Figure 3-1 Schematic of Agitated Filter Dryer process. (Tamrakar, Gunadi, Patrick M. Piccione, *et al.*, 2016)

The process starts with charging the product suspension into the dryer. The slurry is often allowed to settle before applying pressure to drive the filtration. In some cases, the filtration stops at dry land when the filter cake surface is exposed, and then the wash is applied on top of a fully saturated cake. Alternatively, the filtration can continue until a breakthrough and the cake is deliquored. Filtration to breakthrough can cause cake cracking. Thus, consolidation or smoothing is performed using the agitator to smooth the cake surface before washing. Washing removes the residual mother liquor and impurities within the cake. Washing can be performed either by displacement or by reslurrying. In displacement washing, the solvent is sprayed carefully onto the cake surface, minimising the cake disturbance to avoid a thin spot forming through which much of the wash solvent would pass, reducing washing efficiency. The washed material is then deliquored by applying pressure.

In reslurry washing, sometimes called resuspension washing, the filter dryer is filled with sufficient wash solvent to resuspend the product particles by stirring. In this approach, impurity removal depends on the relative quantity of mother liquor left in the filter cake and the amount of wash solvent employed. Washing steps are repeated several times if necessary to attain the required purification. A blowdown step at the end of washing reduces the cake solvent content before drying (Am Ende *et al.*, 2013). Finally, drying is achieved by setting the desired jacket temperature and vacuum level. Contact drying uses conduction to heat the wet particle bed by exchanging heat from the surfaces (walls or impeller) with the wet powder. Heat sources can be hot water, steam, or heat transfer oil. In addition, there is a vapour space above. Nitrogen is the main gas used in contact drying in the pharmaceutical industry as it is relatively inexpensive and provides inertness to minimise the risk of solvent vapour ignition. The use of the impeller achieves particle mixing. Mechanical agitation prevents local overheating by improving temperature and moisture content uniformity across the particle bed. However, agitation during drying can cause both lump formation i.e. agglomeration and particle breakage i.e. attrition, contributing to particle size variation. For these reasons, selecting agitation conditions is vital to avoid the breakage of fragile particles. Contact drying can operate at ambient pressure or under a vacuum (the preferred method for thermo-sensitive materials because solvent evaporation occurs at a lower temperature than the standard solvent boiling temperature). Vacuum drying is also suggested for compounds sensitive to oxidation as reduced pressure, temperature, and nitrogen (nitrogen purge: to remove saturated flammable vapours in headspace due to evaporation during drying) use minimise oxidative degradation.

3.2 Agglomeration

During the drying phase of AFD, there is usually a risk of particle agglomeration and breakage, which can sometimes be linked to the dryer's maloperation. To understand the primary agglomeration mechanism, several studies have been done. However, there is still no widely applicable protocol to avoid this problem. Many factors, including the design of the crystallisation process, the drying operating conditions, properties of the wash solvent, the shape and size of the washed crystals, solid-liquid interactions, e.g., solubility and contact angle, the presence of impurities and residual solvent, dripping of condensed solvent from the upper surfaces of the dryer, and particle size distribution can all contribute to agglomeration. This list is probably not rigorous, and it is difficult to assign a single cause in any instance of drying.

3.2.1 Factors affecting agglomeration.

3.2.1.1 Solid-solvent binding and sticky issues

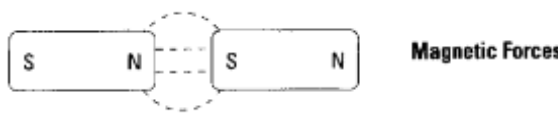

Stickiness is frequently encountered when manufacturing and drying powders (Papadakis & Bahu, 1992). Stickiness is the flow resistance or agglomeration caused by particle-particle and particle wall interactions. Cohesion and adhesion are two defined phenomena caused by stickiness. Cohesion is an internal particle property in which particles contact and stick to each other by forming an agglomerate. Therefore, it is very disadvantageous for the drying process.

In contrast, adhesion is an interfacial property that gives the measure of forces that holds the powders to other surfaces. A more significant force than adhesive force is required to break the bond between the particles and the surface. So, this usually describes the phenomenon of powders sticking to the heated drier walls as moisture reduces. The particles form a solid bridge at the inner walls, especially during contact drying (Iveson *et al.*, 2001b). During the agitation process, granules consolidate, increasing saturation in liquid pores and causing changes in mechanical properties. This shows that consolidation has a prominent effect on the behavior of granule growth. The enlargement of particle size induced by coalescence is known as balling. Various forces cause balling according to different mechanisms of binding, which can be classified into five major groups:

Table 3-1 Binding mechanisms of agglomeration (Pietsch, 1997)

<p>Solid Bridges</p>	<ul style="list-style-type: none"> • Sintering <ul style="list-style-type: none"> ○ Solid bridges developed due to diffusion of molecule from one particle to other when the temperature of the systems rises above approximately two third of melting temperature of solid. • Chemical reaction <ul style="list-style-type: none"> ○ Solid bridges formed due to chemical reaction depends upon reactivity of the material. Elevated temperature or pressure can cause a chemical reaction in presence of moisture. • Partial melting <ul style="list-style-type: none"> ○ Partial melting occurs due to heat caused by friction or pressure which results in formation of liquid bridges. These liquid bridges quickly solidify due to large heat sink provided by surrounding solids. • Hardening binders <ul style="list-style-type: none"> a) Recrystallization of dissolved substances <ul style="list-style-type: none"> ○ these are usually caused by temperature fluctuations. Most commonly happens with salts or mixtures of salts which contain some free moisture and on temperature elevations get dissolved and recrystallize on temperature drop. b) Deposition of suspended particles <ul style="list-style-type: none"> ○ When moisture evaporates during drying the dissolved material or suspended material with the moisture from solid bridges upon evaporation of moisture.
<p>Adhesion and cohesion forces</p>	<ul style="list-style-type: none"> • Adsorption layers (approximately 3-5nm thickness) <ul style="list-style-type: none"> ○ Very fine particles attract free atoms and molecules and form an immobile adsorption layer which cause a strong force high enough to cause agglomeration. • Highly viscous binders <ul style="list-style-type: none"> ○ Highly viscous binders can create an adhesion force at solid-binder interface and cohesion forces within viscous material which can cause agglomeration.
<p>Interfacial</p>	<ul style="list-style-type: none"> • Liquid bridges

<p>and capillary forces</p>	<ul style="list-style-type: none"> ○ Most commonly developed by capillary condensation. Usually considered as precondition for the formation of solid bridges. ● Capillary forces at the surface of agglomerates filled with liquid. <ul style="list-style-type: none"> ○ Mostly cause wet agglomeration when the entire pore volume between particles filled with liquid and a concave meniscus formed at the end of the pore. This phenomenon creates a negative capillary pressure which provide strength to wet agglomerate.
<p>Attraction forces between solid particles</p>	<ul style="list-style-type: none"> ● Molecular forces <ul style="list-style-type: none"> a) Van der Waals forces <div data-bbox="630 728 885 851" data-label="Diagram"> </div> <p style="text-align: right;">Molecular Forces van-der-Waals Forces</p> b) Chemical forces <div data-bbox="670 963 805 1108" data-label="Diagram"> </div> <p style="text-align: right;">Valence Forces at newly created surfaces (Recombination Bonding)</p> c) Hydrogen bridges <div data-bbox="606 1198 941 1668" data-label="Chemical-Block"> <p>1. c.</p> <p>a. <chem>C=O <-> HO-C</chem> <chem>OH <-> O-C</chem></p> <p>b. <chem>H-O-H</chem> <chem>C=O <-> HO-C</chem> <chem>OH <-> O-C</chem> <chem>H-O-H</chem></p> <p>c. <chem>C=O</chem> <chem>OH</chem> <chem>H-O-H</chem> <chem>O=C</chem> <chem>HO</chem></p> <p style="text-align: right;">Nonvalence Association e.g., Hydrogen bridges between oxygen and hydroxyl radicals</p> <p>a: Association — H interact with nonbinding electron pair of oxygen</p> <p>b: Water molecules intensify association</p> <p>c: Bridging by nonvalence association of bipolar (water) molecules</p> </div> ● Electrostatic forces <div data-bbox="638 1814 917 1937" data-label="Diagram"> </div> <p style="text-align: right;">Electrostatic Forces</p>

	<ul style="list-style-type: none"> • Magnetic forces <div style="text-align: center;">  </div>
Interlocking bonds	

For large particles, various attraction forces aggregate together and lead to agglomeration. The agglomeration tendency will be extremely high in the broad particle size distribution where fine powders fill the large voids. Recrystallization of solids in a miscible solvent can cause the formation of solid bridges as well. (Pietsch, 1997).

Solid particles can form hard agglomerates with trapped solvents (Ende, 2010). This phenomenon exists in AFD. There are several methods to lessen agglomeration. One is to control the agitation speed and period. Another approach is to change the composition of the solvent mixture during the washing step. Much research shows that the degree of agglomeration is related to the solubility of the API in the residual and wash solvents. If the solubility of the solvent is very high, the high quantity of dissolved material deposited during solvent evaporation leads to agglomeration.

Papadakis and Bahu (1992) mentioned that interparticle attraction (cohesion and adhesion) could also play a significant role in agglomeration. Cohesive forces are forces between particles which can hold them together when they come in contact with each other. Cohesion can cause caking phenomena when the powder bed is exposed to high temperature and humidity. In comparison, adhesion is an interfacial property that holds the surface of the powder to the surface of another material. These attractive forces depend on the nature of the material and the process by which the particles come in contact with each other. (Papadakis and Bahu, 1992).

The extent of cohesive forces is different at different stages of isolation depending upon the quantity of liquid present between the particles. The end product of the crystallization is a

mixture of solid crystals and solvent. Filtration separates the API crystals from solvent however typically 10-20% of residual solvent still left in the crystal bed after filtration and deliquoring (Goh, 2019). Figure 3-2 represents the schematic of different levels of liquid saturation (Newitt and Conway-Jones, 1958; Iveson *et al.*, 2001b; Mitarai and Nori, 2007). As the isolation process proceeds the saturation levels changes in different states from (a) to (e) as shown in Figure 3-2(Goh, 2019). At the end of crystallization, the product is in the form of a slurry (a). In the slurry state the liquid pressure is greater than air pressure and no cohesive forces exist between the particles (Mitarai and Nori, 2007). After filtration and draining the system is shifted to capillary state (Goh, 2019). At this stage liquid fills most of the pores between crystals and forms menisci and the liquid pressure is lower than air pressure. Cohesive forces arise in this state in result of suction (Mitarai and Nori, 2007). In order to remove the solvent by drying the wet material is heated and as solvent is evaporated the saturation level reduces from funicular state (c) via the pendular state (d) to the dry state (e). In funicular state there is the coexistence of liquid filled pores and liquid bridges around contact points and both of these phenomena cause cohesive forces between the particles (Mitarai and Nori, 2007). On further solvent evaporation the system progresses towards pendular state in which very thin layers of liquid bridges remain located at contact points, capillary forces act through these bridges (Goh, 2019).

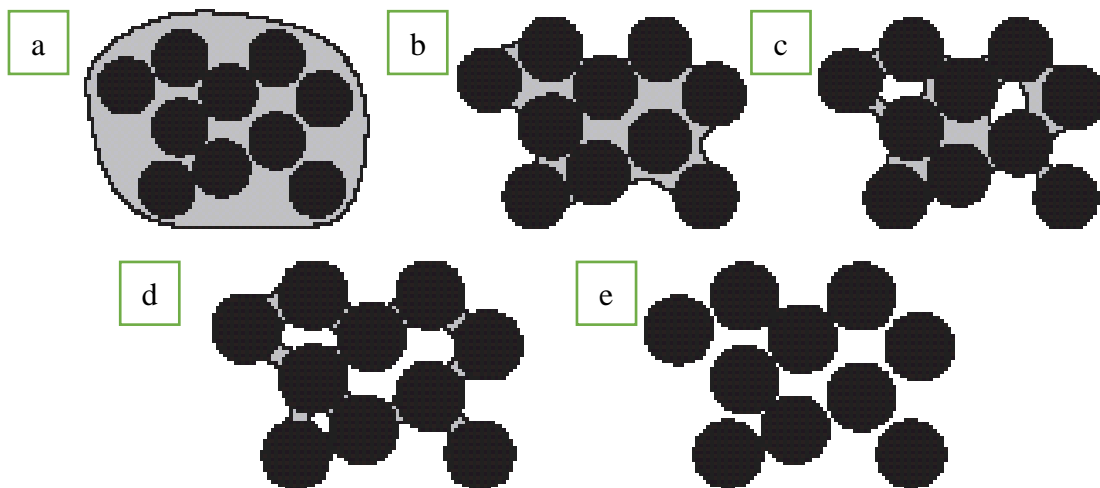


Figure 3-2 Different levels of liquid saturation (a) Slurry state (b) Capillary state (c) Funicular state (d) Pendular state (e) Dry state (Mitarai and Nori, 2007)

Agglomerates are unwanted for their low dissolution rate, undermining the drug's bioavailability and causing problems in subsequent processing. In addition, different binding

mechanisms give rise to the forces which keep the particles in agglomerates from moving apart. For example, capillary forces are dominant for low-viscosity solvents like water, while electrostatic and van der Waals forces are insignificant when particle size is more significant than 10 μ m (Rumpf, 1962).

Schæfer et al. studied how impeller speed and power input are related to agglomeration (Schæfer *et al.*, 1993), equipment variables, and the size and shape of particles (Schæfer, 1996). Higher impeller speed can cause larger agglomerates. He found that curved impeller blades in the 8-L mixer generated a high-power input and produced smooth spherical shape agglomerates; plane blades generated lower power input and irregular agglomerates. Agglomerate growth was shown to be affected by the size of the mixers (8-L and 50-L) because of differences in the movement of the particles, power input, and product temperature. Different particle sizes and shapes also affect agglomeration (Schæfer, 1996).

Some other agglomeration causes also include the solubility of the main product in the wash solvent and different properties of the wash solvent, like polarity, surface tension, and viscosity. When API dissolves in the wash solvent, it creates sticky points that increase the formation of solid bridges (Simurda, 2017). Papageorgiou *et al.* (2016) show that critical moisture content and wash solvent selection significantly impact agglomeration. They reported that polar solvent produces harder agglomerates. Likewise, Birch and Marziano (2013), Zhang and Lamberto (2014), and Tamrakar *et al.* (2016) show that agglomeration strength increases by increasing solvent polarity. Birch and Marziano used different wash solvent combinations and showed that the systems with higher solubility tend to form agglomerates more than those with lower solubility. The surface tension of wash solvent on agglomeration was investigated by Hapgood et al. (2016); high surface tension tends toward a higher risk of agglomeration. The degree of agglomeration depends on the solvent viscosity (Schæfer & Mathiesen, 1996) and product temperature (Schæfer *et al.*, 1993). Tamrakar *et al.* (2016) show that fluids with high viscosity tend to form agglomerates.

Another critical factor that may cause agglomeration is the interaction between solid and liquid particles. Water molecules form hydrogen bonds which cause the attraction of solid particles toward each other. Lim, Hapgood, and Haig (2016) used alcohol washes to show that less polar solvents have a lesser tendency to form agglomerates due to a reduction in attraction forces.

3.2.1.2 Operating conditions

During drying, agglomeration can produce big particles. Large agglomerates are undesirable because of their low dissolution, affecting a drug's bioavailability. Crystal size enlargement is primarily due to the contact of wet crystals with others. A collision between two or more crystals can cause a permanent bond depending on various factors, including morphology and their mechanical properties (size and shape) (Iveson *et al.*, 2001b). Capillary and viscous forces can cause liquid bridges between the crystals. These bridges restrict the movement of crystals. Schaefer *et al.*, 1993, and Lee, Lin, and Lee, 2014 showed that plate or needle-like crystals produce agglomerates with low strength. Schaefer also showed that combining needle or plate-like crystals with spherical crystals makes strong agglomerates. The above discussion clarifies that attrition and agglomeration depend on the drying conditions (temperature, shear rate, vacuum, moisture content) and the mechanical properties and morphology of the solid material (size, shape, hardness). Therefore, developing a fundamental understanding of these two phenomena is necessary for industrial dryer design and scale-up.

Lekhal *et al.* studied the effect of different drying conditions, like temperature, agitation speed, drying kinetics and particle size distribution, and crystal morphology. They found that attrition dominated when the drying rate was low and the shear rate was high, while agglomeration was the contrary.

Lekhal *et al.* also investigated the effect of agitation speed, drying temperature, and pressure on L-threonine and potassium chloride (KCL) crystals. They show that an increase in agitation speed decreases the average diameter of crystals, causing attrition. The rise in temperature increases the particle size due to fast drying and reduced shearing, causing agglomeration (Lekhal *et al.*, 2003, 2004). Similarly, Hsu and Chiou (2011) and Sahni, Bogner, and Chaudhuri (2013) also demonstrated that increasing drying temperature causes severe agglomeration. Sahni, Bogner, and Chaudhuri (2013) and Lim, Hapgood, and Haig (2016) studied the effect of agitation speed and filled volume on agglomeration. According to their research, increasing the agitation speed causes particle size reduces while increasing the fill volume particle size increases (lump formation) due to fewer collisions between particles and between particles and impeller blades. The duration of applied agitation also affects agglomeration. Hamilton *et al.* (2013) show that continuous agitation supports agglomeration by spreading the residual solvent throughout the bed. Thus, the agitated drying process can be optimised by introducing alternating stirring periods or without stirring or starting agitation at a certain solvent content.

Table 3-2 summarises the reported effects of different parameters on agglomeration.

Table 3-2 Effect of different operating parameters on agglomeration.

Property	The main effect on agglomeration
Temperature	An increase in temperature promotes the formation of agglomerates as by increasing the temperature, the drying time reduces, and the material experiences less shearing, which in turn reduces the opportunity of agglomerates to break (Lim, Hapgood, and Haig, 2016).
Pressure	By reducing pressure, the solvent's boiling point reduces (usually required to remove bound moisture), leading to faster drying and increasing agglomeration tendency (Lekhal <i>et al.</i> , 2004).
Bed height	The thicker the powder bed, the lower the tendency to form agglomerates, as thin beds facilitate faster heating, reducing drying time, reducing shear, and promoting agglomeration (Lim, Hapgood, and Haig, 2016).
Residual moisture content	High moisture content promotes agglomeration due to the cohesive behaviour of liquid bridges, which prevents individual particles from moving separately (Lim, Hapgood, and Haig, 2016).
Agitation	By increasing the agitation, shear forces increase, resulting in the attrition of the particles and agglomerates. Increasing agitation has a limited effect on reducing agglomeration (Tamrakar, Gunadi, Patrick M Piccione, <i>et al.</i> , 2016).
Blowdown period	An extended blowdown period before drying to reduce the initial moisture content is commonly used to minimise agglomeration (Lim,

	Hapgood, and Haig, 2016).
--	---------------------------

Some external factors, like condensate dripping, also affect the process of agglomeration. The dripping of condensate is a common phenomenon that occurs in AFD. Condensate dripping may arise in the initial drying stages when a large amount of moisture is evaporated, and the headspace of the dryer becomes saturated with vapours. Apart from hot surfaces (heated jacket and impeller), some cold surfaces like the dryer ceiling and spray bars may act as preferential sites for condensing evaporated solvent vapours, which ultimately drip back to the powder bed. Lim, Hapgood, and Haig (2016) investigated the effect of condensate drips by injecting different coloured dyes in drips at different times during drying. Their investigation reveals that drip-induced nucleation is not considered during initial drying periods with high moisture content. It mainly occurs during the latter drying stages when the paste-like material is transformed into free-flowing particles.

3.2.1.3 Material properties

Material properties like crystal morphology and size can also affect agglomeration and attrition phenomena during agitated drying (Lekhal et al., 2003, 2004). Lekhal et al. (2004) showed that long needle or plate-like crystals are more prone to attrition by chipping the edges during agitation while the small crystals form agglomerates. In their study, Bemrose and Bridgwater (1987) showed that spherical particles are less vulnerable to attrition. Similarly, Lekhal et al. (2003) showed that cubic crystals like KCl are more resistant to attrition than long needle shape crystals.

Crystallisation and wash solvent properties include the solubility of API in solvents, solvent polarity, surface tension, and viscosity. Papageorgiou et al. (2016) showed that residual moisture content and wash solvent selection have a more significant impact on agglomeration than different API size distributions (micronised, fine, and granular). They also reported that polar solvents produce harder agglomerates. Likewise (Birch & Marziano (2013), Tamrakar, Gunadi, Piccione, & Ramachandran (2016), and Zhang & Lamberto (2014) report that agglomeration strength increases with increasing solvent polarity. Birch and Marziano employed different combinations of wash solvents to demonstrate that systems with higher solubility have a higher tendency to form agglomerates than systems with lower solubility. If

API has any solubility in the residual solvent, then during drying, it creates "sticky" points at the contacts between particles, increasing the formation of solid bridges (Simurda, 2017). Lim, Hapgood, & Haig investigated the effect of wash solvent surface tension on agglomeration. They conclude that high surface tension enhances the risk of agglomeration. Tamrakar et al. (2016) showed that fluids with high viscosity have a greater tendency to form agglomerates.

Am Ende et al. (2013) and Birch and Marziano (2013) investigated the agglomeration process in AFDs and suggested different approaches to overcome agglomeration during agitated drying. They examined the solubility effect of wash solvent on agglomeration by screening various wash solvent systems to have the best solid-solvent system with the lowest agglomeration potential. According to their research, either a blow down period or avoiding agitation until critical moisture content level passes could help to reduce agglomeration. Critical moisture content is the moisture level at which wet powder has the maximum tendency to form agglomerates. They also suggested using a wash solvent, in which the API has low particle solubility. However, these recommendations could not be applied to every material as the minimum achievable moisture content for each material depends upon particle shape, size distribution, the exposed functional group and the molecular characteristics of the solvent.

Moreover, each material's pore network structure is different, which plays a significant role in trapping the solvent within the pores. Therefore, their studies showed that each powder type led to its own recommendation for agglomeration prevention. More systematic approaches are required to eliminate agglomeration.

Another factor known to cause agglomeration is the deposition of previously dissolved material at the contact points between particles when the solvent evaporates on drying. Birch and Marziano (2013) showed in their investigation that higher solubility in wash solvent mixtures leads to agglomeration as the dissolved API can be deposited to form solid bridges between particles upon drying.

Table 3-3 Effect of different material properties on agglomeration

Property	The main effect on agglomeration
-----------------	---

Crystal Morphology and size	Long needle shape particle prone to attrition instead of agglomeration, and if the particle size distribution is wide then there are more chances to get strong agglomerates as smaller particles fills in the pores in between large particle hence causing hard agglomerates. (Lekhal <i>et al.</i> , 2003, 2004)
Crystallization and wash solvent polarity	By increasing solvent polarity agglomerate strength increases.(Zhang and Lamberto, 2014b; Papageorgiou <i>et al.</i> , 2016; Tamrakar, Gunadi, Patrick M Piccione, <i>et al.</i> , 2016)
API Solubility in residual solvent	API solubility in residual moisture leads to the formation of agglomerates. Higher the solubility harder the agglomerate. (Simurda, 2017)
Wash solvent surface tension	High surface tension of wash solvent higher the risk of agglomeration (Lim, Hapgood, and Haig, 2016).
Fluid viscosity	Fluid with high viscosity have a greater tendency to form agglomerates. (Tamrakar, Gunadi, Patrick M Piccione, <i>et al.</i> , 2016)

3.2.2 Characterization of agglomerates

Agglomeration is a frequently observed phenomenon that occurs during drying. Different factors and processing parameters of filtration, washing, and drying contribute to this process (Ottoboni, 2018). Therefore, to minimize/avoid agglomerate formation, understanding particle agglomeration during drying is a fundamental step. Unfortunately, limited literature describes generalised methodologies to determine agglomerates' properties (hardness/brittleness). However, some techniques have been developed by modifying previous methods to test the tablets' hardness (see Figure 3-3) (Simurda, 2017).

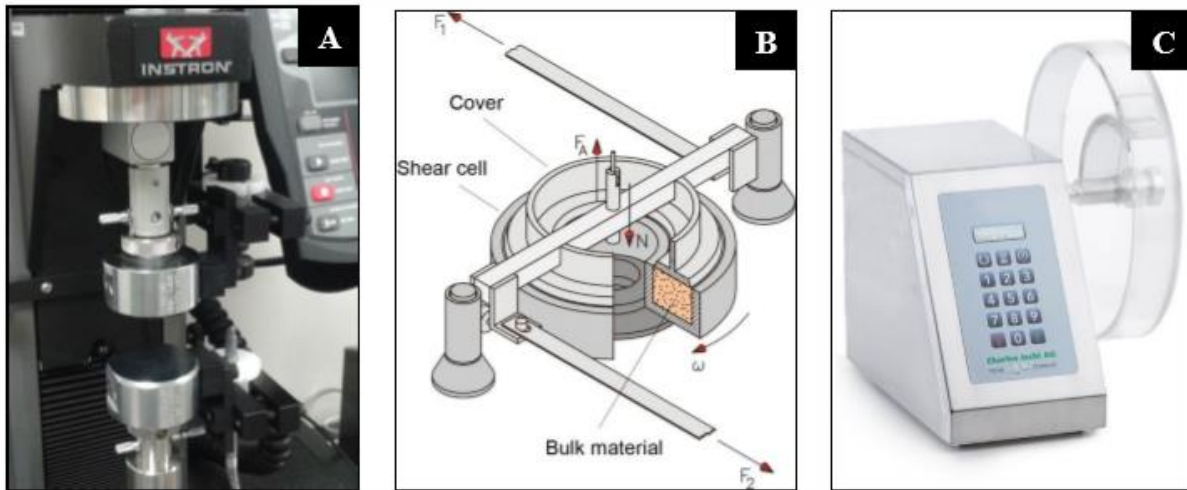


Figure 3-3 Techniques for characterising the mechanical properties of agglomerates (A) Compression Tester (Instron) (B) Ring Shear Tester (Faulhaber) (C) Friabilator(Charles Ischi AG).

Sieving is another convenient method to measure the extent of agglomeration and determine agglomerates' strength (Birch and Marziano, 2013; Papageorgiou *et al.*, 2016). The initial mass of the product is placed on a test sieve and reduces during a sequence of cycles of sieving by recording the mass loss from the test sieve after each cycle, plotting this against the sieve cycle. Then, using the power-law curve, it is possible to calculate an agglomerate brittleness index (ABI index). Figure 3-4 shows sieving data and the fitted curve for a model compound (Simurda, 2017).

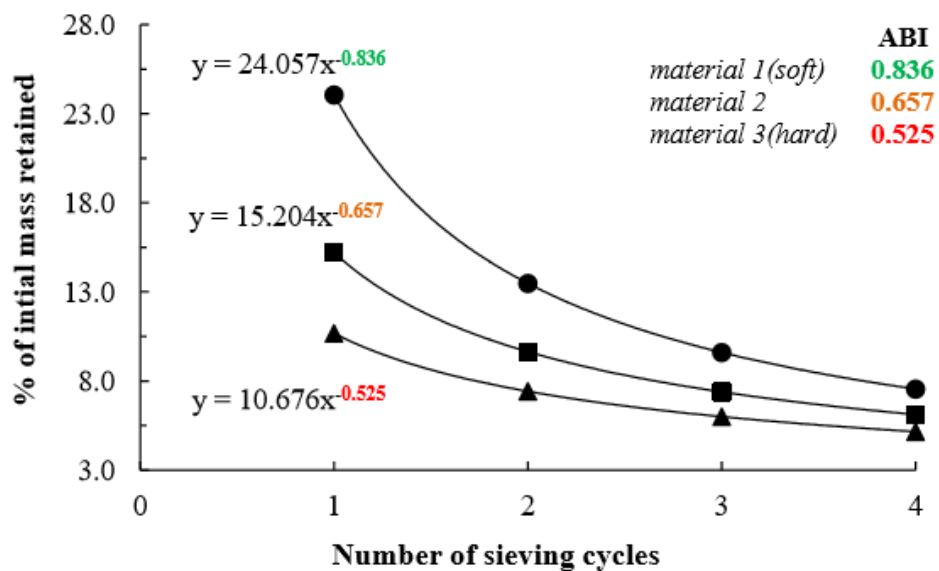


Figure 3-4 ABI calculation of a model compound. (Simurda, 2017)

3.3 Attrition

A key challenge in manufacturing active pharmaceutical ingredients (APIs) is maintaining the particle properties during drying, which is the last step of isolation (filtration, washing, and drying) which follows crystallization (Kemp, 2017). Control of particle properties during drying is not usually investigated during the early developmental stages and it is challenging to make comparison with breakage occurring in larger scale equipment in the later stages of development due to the problems that arise due to scale up (Adamson *et al.*, 2016) or transfer of the isolation process to a different equipment train (Lamberto *et al.*, 2011). The impact of drying on particle properties is less well understood than for crystallization. This is significant because particle properties modified by drying are often linked to critical quality attributes, a particular problem is that particle breakage is not readily controlled (Edward W. Conder *et al.*, 2017). This is partly due to the lack of analytical methods to examine and understand the real-time process, and proper scale-down models, which allow drying to be studied on a lab scale with modest material requirements allowing investigation when API is only available in limited quantities (Zhang and Lamberto, 2014a).

However, Schlünder and Mollekopf (1984), Forbert and Heimann (1989), and Tsotsas and Schlünder (1990) successfully modelled the drying process by using empirical equations and process parameters. Moreover, interparticle and particle-solvent interactions are now being calculated with the help of computational models using discrete element models (Kwapinska, Saage, and Tsotsas, 2006, 2008). Despite these works, the physical process that occurs throughout the drying process and the effect on particle properties are still not completely understood (Hamilton *et al.*, 2011).

In pharmaceutical manufacturing, dryer selection mainly depends upon the characteristics of the material to be dried (Pakowski and Mujumdar, 2014). Commonly used dryers in pharmaceutical manufacturing include vertical agitated dryers, conical dryers, and filter dryers, all of which involve agitation to reduce drying time with the heat supplied through heated jackets by conduction (Kemp, 2017). The impeller can induce shear stress within the material, leading to the attrition of the particles (Goh, 2019). Attrition of the particles in agitated drying could be either impact breakage due to particle-particle collision and collision with other mechanical parts of dryers (Am Ende *et al.*, 2013) or shear deformation (Neil and Bridgwater, 1994).

3.3.1 Particle attrition due to shear deformation

Paramanathan and Bridgwater (1983) first introduced an annular shear cell to study particle attrition due to shear deformation. In the shear cell, the packed bed of particles is forced to slide under the effect of normal stress (Neil and Bridgwater, 1994; Hare and Ghadiri, 2015; Hare *et al.*, 2018). The shear cell is helpful in the investigation of coarse particles under stress. However, shear cells cannot be used to investigate the attrition of fine particles, which is its major drawback in pharmaceutical isolation (Papadopoulos, 1998).

The most common method to evaluate particle attrition in earlier literature used indices based on particle shape, size distribution, surface area, and flowability (Bemrose and Bridgwater, 1987). Gwyn (1969) proposed an equation (Equation 1) with an attrition index based on the fraction of mass lost with respect to time to describe the attrition of catalysts.

$$W = K_p t^m \quad \text{Equation 3-1}$$

Where,

W is the fraction of mass lost,

K_p is the attrition constant depending upon the initial size of the particle,

m is also attrition constant, and

t is time.

Neil and Bridgwater (1994) used an annular shear cell developed by Paramanathan and Bridgwater (1983) to evaluate the Gwyn equation. They used many materials with different properties and structures and found that the index of t in the Gwyn equation is a material property and varies less with applied stress. However, the value of K_p increases by increasing stress. They concluded that applied stress also contributes to particle attrition in addition to material properties. Jørgensen, Bach, and Jensen (2005) also showed in their work that particle attrition increases by increasing normal stress. Ghadiri *et al.* (2000) tested different attrition models by evaluating the attrition under shear effect on porous silica beads. Their work showed that the model proposed by Neil and Bridgwater (1994) provided a best fit only for fine debris due to surface damage. It did not correlate well if attrition results in larger fragments due to fragmentation (Goh, 2019).

3.3.2 Particle attrition due to impact breakage

Impact breakage in agitated drying is due to interparticle collisions and particle collisions with the mechanical parts of the dryer (Goh, 2019). To better understand particle breakage, detailed information on material properties and the mode of applied stress are required (Papadopoulos, 1998). Material properties like Young's modulus (E), hardness (H), and fracture toughness (K_{IC}) are related to crack propagation and elastic and plastic deformation, which leads to the breakage of the particle (Lawn and Marshall, 1979). Depending upon material properties and the mode of applied stress, the particle breakage can then be classified into three distinct types of failure (Papadopoulos, 1998):

- Brittle failure
- Semibrittle failure
- Ductile failure

3.3.2.1 Brittle failure

In brittle failure, the material breaks without plastic deformation. This failure occurs when a less sharp or rounded indenter is loaded on a flat hard surface or when the area between contacting particles is large. The cracks in this failure initiate because of pre-existing flaws. If pre-existing flaws are not present, the material is strong and can only fail when shear deformation initiates the cracks (Papadopoulos, 1998). However, if the size, position, and the number of these flaws are unknown, then the only possible way to evaluate this failure is using empirical models (Goh, 2019). The most common empirical approach for this type of failure is Weibull statistics (Weibull, 1951) which is based on the principle of the weakest link in the chain or, in general, for particle breakage in solids.

$$S = 1 - \exp[-z \left(\frac{\sigma}{\sigma_s}\right)^m] \quad \text{Equation 3-2}$$

Where

S is the probability of breakage of a chain consisting of z particles with strength σ_s ,

σ is the applied load or stress, and m is the Weibull parameter of the probability distribution (Vogel and Peukert, 2005).

Vogel and Peukert (2004, 2005) further introduce the material parameters to the above

equation to investigate the effect of material properties in attrition.

3.3.2.2 Semi brittle failure

If the material undergoes a limited but measurable plastic deformation before breakage, the failure is termed a semi-brittle failure. This failure occurs when a sharp or conical indenter is loaded on a flat hard surface or when the area between contacting particles is small. The cracks in this failure initiate because of a plastic zone. Suppose the stress is applied to a small contacting area, for example, at the corner of the particle. In that case, the stress developed due to collision becomes more significant than the yield stress of the material, which can cause breakage of the particle. A crack propagates when the plastic zone reaches a critical value (Papadopoulos, 1998).

3.3.2.3 Ductile failure

In ductile failure, the material eventually breaks because of the domination of extensive plastic flow in the damaged zone. Rupture occurs when the plastic deformation under the contact area exceeds the particles' physical boundaries. Usually, the breakage of metals and soft polymers occurs due to this type of failure. This failure occurs when a hard material hits the surface of the soft material at a certain angle (Papadopoulos, 1998).

3.3.3 Mode's particle breakage

Modes of particle attrition can be classified as chipping, fragmentation, and disintegration (Ghadiri *et al.*, 2000; Ghadiri and Zhang, 2002; Zhang and Ghadiri, 2002; Grof, Kohout and Štěpánek, 2007; Grof *et al.*, 2011; Goh, 2019). Chipping occurs when the fine particles break from the parent particle due to the impact, while in fragmentation, the particles break into two or more smaller fractions (Hamilton, 2011). To analyze attrition, it is necessary to identify the breakage pattern. Papadopoulos (1998) studied the change in particle size distribution by applying different breakage patterns. It has been found that the cumulative distribution of undersized particles as a function of normalized particles is different for different breakage modes (Goh, 2019).

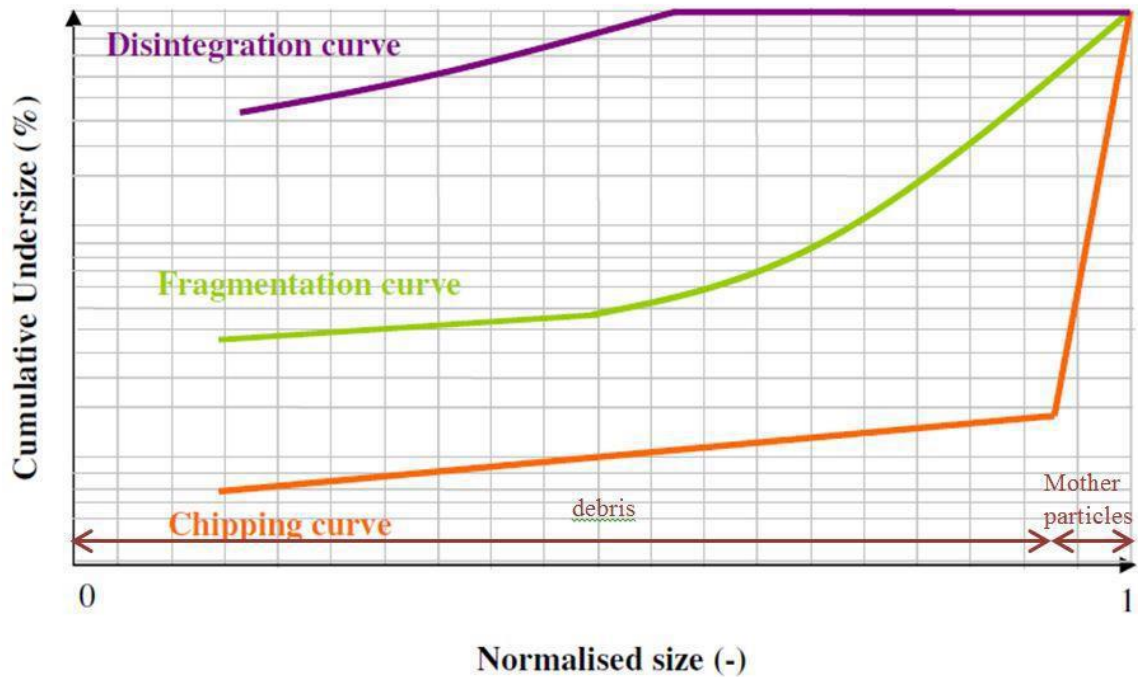


Figure 3-5 Cumulative distribution of undersize particles as a function of normal size particles for chipping, fragmentation, and disintegration (Goh, 2019)

Single-particle attrition can either be due to fragmentation or surface wear. As mentioned above, fragmentation occurs when a particle breaks into several smaller parts due to radial and median crack propagation that starts from areas of the particle subject to high stress (Evans and Wilshaw, 1977). While wearing is the damage to the surface of the particle due to abrasion or erosion. Abrasion wear occurs when particles in a system roll or slide over each other. In contrast, particle collisions cause erosion wear. During wear attrition, the chipping effect exposes a new sub-surface (Shipway and Hutchings, 1993).

3.3.4 Parameters affecting particle attrition

In agitated drying, particle attrition occurs when a force is exerted on the particle due to an impact as a result of the collision with

- Other particles in the dryer
- Agitator blade
- Walls of the dryer (Am Ende *et al.*, 2013).

Many other factors like material properties, operating parameters equipment configuration also affect the extent of attrition of the particles. *Figure 3-6* lists various parameters affecting particle attrition.

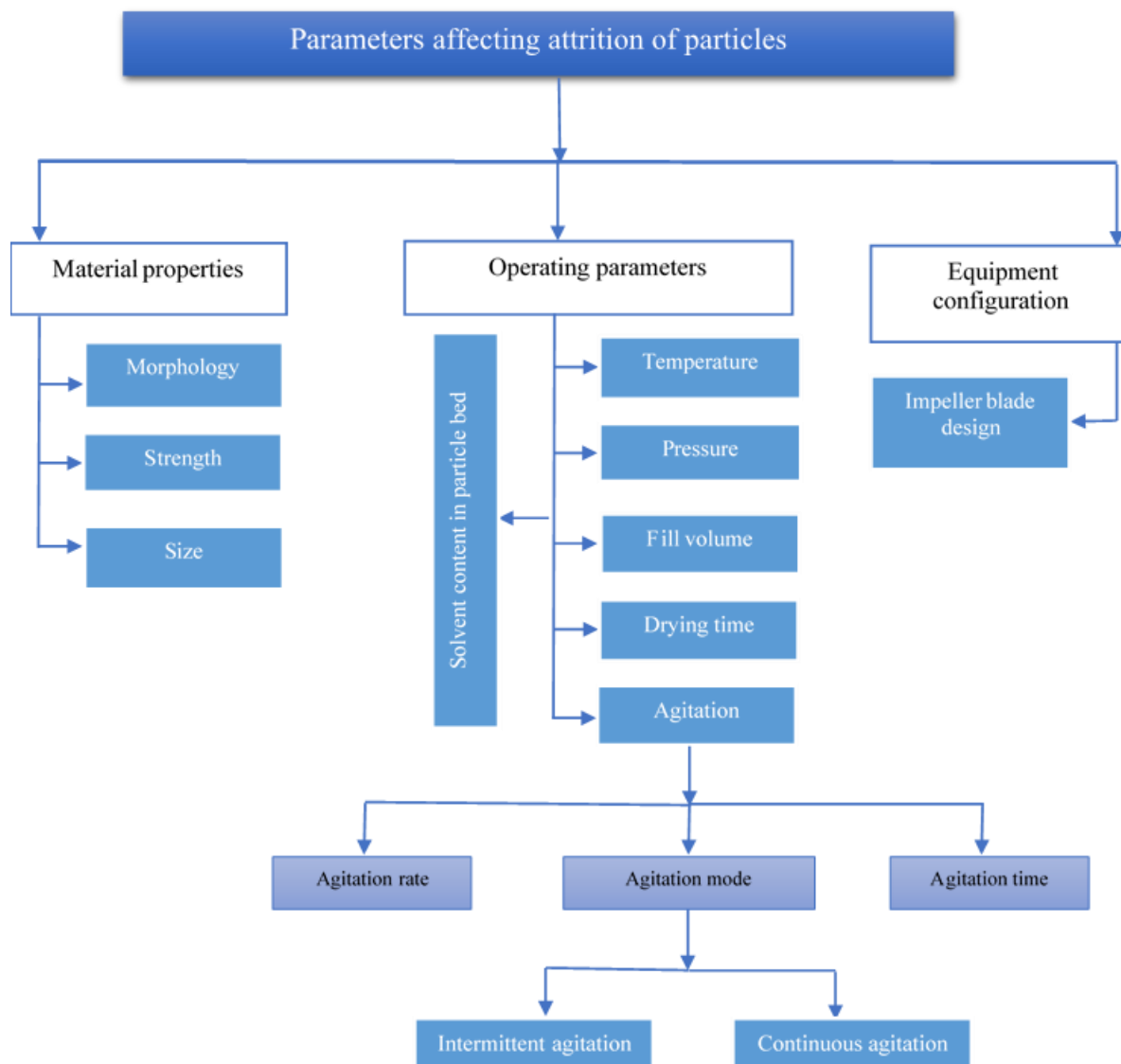


Figure 3-6 Parameters affecting particle attrition

3.3.4.1 Material Properties

Lekhal *et al.* (2003, 2004) studied the effect of two different materials with different crystal habits, Potassium chloride (KCl) and L-threonine, and they showed that long needle-shaped crystals of l-threonine are more prone to attrition via breakage than cubical crystals. Moreover, in the case of compact cubical crystals like KCl, attrition occurred mainly by chipping of the edges (Ghadiri and Zhang, 2002). The temperature can also affect the strength of the material during drying. Ghadiri and Zhang (2002) & Zhang and Ghadiri (2002) showed that by increasing the temperature, the fracture toughness of material decreases, increasing the extent of attrition.

3.3.4.2 Operating parameters

Agitation during the initial period of drying cause limited or no attrition due to the presence of residual solvent forming liquid bridges between the particles acting as a lubricant and reducing frictional force (Goh, 2019). As the drying proceeds and the moisture content reduces to a critical moisture level, i.e., 1.5 – 2 %, then the agitation cause attrition of the particles due to an increase in the intensity of collisions of the particles (Lekhal *et al.*, 2003, 2004). However, by increasing the drying temperature and reducing the pressure, drying time is reduced. When material dries in a shorter time the duration of exposure to the shearing effect of the impeller blade is less hence reducing the attrition of the particles (Lekhal *et al.*, 2003, 2004; Lim, Hapgood and Haig, 2016).

Sahni, Bogner, and Chaudhuri (2013) investigate the effect of fill volume or bed depth on the attrition of particles. They showed that lower bed depth or less fill volume increases the number of collisions between the particles due to increased exposure of fewer particles to the impeller blade, which increases particle attrition. Similar results were reported by Lim, Hapgood, and Haig (2016). Another operating parameter that can cause particle attrition is agitation speed. Increasing agitation speed increases the impeller blade's shear effect, increasing particle attrition (Iveson *et al.*, 2001; Kougoulos, Chadwick, and Ticehurst, 2011; Sahni, Bogner, and Chaudhuri, 2013).

3.3.5 Models for analyzing attrition of particles

Considerable effort has been made to develop a model to predict particle breakage involving the interaction of particles. Broadbent and Gallgot (1956) presented a population balance model based on the concept of breakage function (Broadbent *et al.*, 1956). Subsequently, this model has been applied to analyze several other attrition processes, such as attrition in shear cells (Neil and Bridgwater, 1994).

Ghadiri & Zhang (2002) developed a model to evaluate impact attrition due to chipping of particulate solids based on the indentation fracture mechanism and impact damage. They developed an attrition propensity parameter, which relates the breakage extent with material properties and conditions of impact (Equation 6-3) (Ghadiri and Zhang, 2002; Zhang and Ghadiri, 2002).

$$\eta = \frac{\rho v^2 l H}{k_c^2} \quad \text{Equation 3-3}$$

where,

η is the attrition propensity parameter,

ρ is the particle density,

v is the impact velocity,

l is characteristic particle size,

H is the hardness and

K_c is the fracture toughness.

Remy *et al.* (2015) investigated the attrition phenomena from a macroscopic point of view, using a laboratory agitation device to design a workflow procedure to simulate attrition obtained in larger dryers. In seeking to develop a scale-up procedure for agitated dryers, the main problem is to get the same particle size in lab scale equipment matching outcomes in larger industrial dryers. The main cause of this lack of agreement is the extent of attrition and agglomeration at different scales (Am Ende *et al.*, 2013).

Traditional laboratory drying devices cannot mimic the attrition achieved during process scale drying. This problem is believed to be mainly due to the lower stress applied to the particles due to the different compressive normal stress contributions transferred into the shearing direction. In laboratory devices, cake height is much lower than in larger dryers: as reported by the Coulomb-Mohr equation, lower bed heights imply lower shear stress. For the first time, Lamberto *et al.* (2011) proposed a laboratory device that mimics the normal pressure obtained in larger dryers.

$$\sigma_{yy} = \frac{F}{A} = \rho g V = \frac{mg}{A} \quad \text{Equation 3-4}$$

Where,

F is the normal load applied on the particles bed,

A is the area of the load applied,

ρ is the particles bed density,

g is the gravity acceleration and

V is the volume material applied to get the normal pressure.

Their setup was made up of a small cylinder where particles were maintained under agitation beneath weights that mimic the compressive normal stress contribution given by higher beds in larger dryers. This tool was used to attempt to generate a standardized protocol to define attrition risk level classification. Other similar devices were then proposed to mimic normal pressure in agitated drying by Conder *et al.* (2017), Ghadiri and Zhang (2002), and Zhang and Ghadiri (2002). The torque generated during agitation in the presence of normal pressure was measured to correlate with the amount of shear stress applied to particles and to determine a degree of attrition (Equation 6-5) (Knight *et al.*, 2001 Darelius *et al.*, 2007).

$$\tau_{\theta r} = \frac{T}{2\pi HR_{cyl}} \quad \text{Equation 3-5}$$

Where,

$\tau_{\theta r}$ is the average shear stress generated during mixing,

T is the torque,

H is the height of the powder bed, and

R_{cyl} is the radius of the particle bed container. Sara Ottoboni used the approach proposed by Remy *et al.* (2015) to design a workflow procedure to scale-down agitated dryers to achieve comparable attrition in laboratory-scale agitation devices as in larger dryers. During this work, the evaluation of possible scale-up approaches and the design of an analytical procedure to mimic particle attrition achieved in pilot / large-scale dryers on laboratory scale units were investigated by considering the normal pressure generated in commercial dryers on the powder bed (Unpublished work Ottoboni University of Strathclyde) (Ottoboni, 2013).

Ottoboni analyzed the pre-existing analytical approaches to investigate the comparison of the final product made in the laboratory drying unit with the large pilot plant dryers to get comparable particle size and PSD. In parallel, two different experimental techniques were investigated to mimic the attrition achieved during an agitated drying process in large units: a modified Freeman Technology FT4 cell method using the aerated setup and a bespoke agitation

cell developed in collaboration with a major pharmaceutical company. The two analytical approaches were compared using paracetamol as a test compound to evaluate the achievable final PSD and aspect ratio (AR) variation using a series of mixing conditions. In addition, the material properties gathered with the shear cell method were used to determine yield loci parameters.

So far, attrition has been addressed empirically, without a complete understanding of the effect of material properties and loading conditions. MacLeod and Muller (2012) investigated the attrition of needle-shaped particles to study the effect of particle morphology on attrition. They developed a fracture model to evaluate two different breakage mechanisms: the attrition of the edges of the particles generating small fragments and the fracture of particles into two pieces.

They developed a small-scale test in which they dispersed the particles with pressure, and the reduction in particle size was taken as particle fragility. The developed model relates the maximum stress within a particle with true and bulk density and dimensions of the particle and the applied pressure.

$$\sigma_{max} \approx 6\Delta P \left(\frac{\rho_t}{\rho_b}\right) \left(\frac{l_p}{h}\right)^{0.5} \left(\frac{h}{b}\right)^{0.2} \quad \text{Equation 3-6}$$

Where,

b is the breadth of particle,

h height of particle,

l_p length of particle,

ρ_b bulk density,

ρ_t true density, and

σ_{max} maximum stress developed in a particle.

The above equation shows that by increasing the particle length, the maximum stress developed in the particle increases, increasing the chance of attrition. However, the maximum stress in the particle does not correlate with the extent of breakage because each particle has different

intrinsic strength. Therefore, other material properties are also required, along with the dimensions of the particle, to predict how much the extent of breakage (MacLeod and Muller, 2012).

3.4 Effect of Drying on Physical properties

The solid form of a pharmaceutical material can significantly influence the drying process during pharmaceutical manufacturing. Drying is a critical unit operation in pharmaceutical processing to remove moisture or solvents from the product, ensuring stability, efficacy, and quality. Different solid forms can impact the drying process in several ways:

Surface Area and Particle Size: The surface area exposed to the drying medium (air or hot gases) plays a crucial role in the drying rate. Finely divided pharmaceutical powders with smaller particle sizes have a higher surface area and tend to dry more rapidly compared to larger particles or aggregates.

Crystalline vs. Amorphous Forms: Crystalline and amorphous forms of pharmaceutical compounds have different moisture absorption and desorption characteristics. Amorphous materials are generally more hygroscopic, absorbing moisture from the environment more readily, and may require specific drying conditions to prevent recrystallization during drying.

Polymorphism: Many pharmaceutical compounds exist in different polymorphic forms, each with distinct physical properties. Different polymorphs can have different water contents, and their drying rates may vary significantly due to variations in crystal structures and intermolecular forces.

Hygroscopicity: Some pharmaceutical compounds are highly hygroscopic, meaning they have a strong affinity for water. Such materials can readily adsorb moisture during processing, leading to the formation of hydrates or increased drying times.

Drying Temperature: The solid form of the pharmaceutical material can influence the temperature at which drying occurs. For instance, some amorphous forms may require lower drying temperatures to prevent crystallization, while others may require higher temperatures to achieve sufficient moisture removal.

Drying Method Selection: The choice of drying method can be influenced by the solid form of the pharmaceutical material. For example, fluidized bed dryers or spray drying might be more suitable for powders, while freeze-drying may be preferred for temperature-sensitive compounds.

Moisture Distribution: The initial distribution of moisture within the pharmaceutical material can impact the drying process. If moisture is more concentrated on the surface, drying may start quickly but slow down as moisture needs to migrate from the interior to the surface.

Stability and Quality: The drying process can affect the stability and quality of the final pharmaceutical product. Different solid forms may exhibit variations in chemical reactivity, degradation kinetics, and physical properties, which can influence the overall product stability.

It's crucial for pharmaceutical manufacturers to understand the solid form of their materials and tailor the drying process accordingly. Proper process design and optimization based on the specific solid form can ensure efficient drying, maintain product quality, and comply with regulatory requirements. Thorough solid form characterisation and analysis can help pharmaceutical manufacturers make informed decisions during formulation and processing to achieve desired drying outcomes.

3.4.1 PCM solid forms

Paracetamol exists in five different polymorphic forms denoted as I, II, III, IV, and V. Among these forms, Form I is the most stable one from a thermodynamic perspective. Form II, although not as stable as Form I, is still similar enough in stability to be isolated and thoroughly researched. Forms IV and V, on the other hand, can only be obtained under high-pressure conditions (Agnew *et al.*, 2016).

Form III has been recrystallized under a microscope, but its crystal structure is extremely unstable, making it challenging to conduct any experimental analysis on it.

Form I, known as the monoclinic form, represents the thermodynamically stable structure of paracetamol. On the contrary, Form II, which has an orthorhombic structure, is considered a

metastable form at room temperature (Di Martino *et al.*, 1997). Form I exhibit a herringbone lattice arrangement, leading to difficulties in compaction and tablet formation. This complicates the tableting process and can result in problems during the compression of tablets.

Form II, however, has an advantageous crystal structure that improves physical properties like compressibility and solubility, making it more suitable for tablet production (Heng and Williams, 2006a). Despite this, due to its greater stability at room temperature, Form I is the more commonly used form in practical applications.

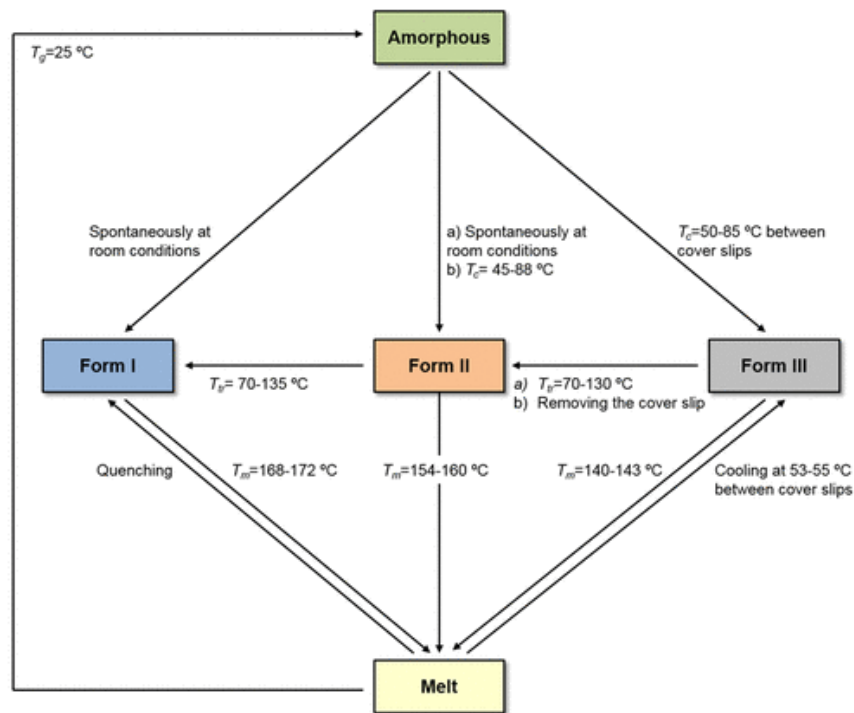


Figure 3-7 Paracetamol phase transitions. T_c is the temperature of crystallization, T_m is the temperature of melting, T_g is the temperature of glass transition, and T_{tr} is the temperature of polymorphic transition. (Cruz, Rocha and Ferreira, 2019)

In this study, Crystalline Form 1 was utilized, and all the samples were subjected to room temperature drying. The phase transition map indicates that the drying process at room temperature had no impact on the solid form transition.

3.5 Summary

The chapter focuses on providing a comprehensive overview of the Agitated Filter Dryer (AFD). The chapter acknowledges two major challenges encountered during agitated drying: agglomeration and attrition. Agglomeration refers to the formation of larger particle clusters, while attrition involves the breakage of particles. The chapter explores various parameters that impact these phenomena during the agitated drying process and provides an in-depth discussion of previous studies related to agglomeration and attrition, shedding light on the factors that

contribute to their occurrence.

Agglomeration in AFD can be influenced by several factors, including the design of the crystallization process, drying operating conditions, properties of the wash solvent, shape and size of the washed crystals, solid-liquid interactions, presence of impurities and residual solvent, dripping of condensed solvent from dryer surfaces, and particle size distribution. One of the main factors contributing to agglomeration is the binding and sticky behavior of particles, resulting from particle-particle and particle-wall interactions. Cohesion and adhesion phenomena can lead to agglomerates forming internally and particles sticking to the surfaces of the drying equipment, respectively. Agglomeration can occur through various binding mechanisms, such as solid bridges formed by sintering, chemical reactions, partial melting, hardening binders, recrystallization of dissolved substances, and deposition of suspended particles. Interfacial and capillary forces, as well as attraction forces between solid particles (e.g., van der Waals forces) and interlocking bonds, can also contribute to agglomeration. The solubility of the main product in the wash solvent and the solvent's properties, such as polarity, surface tension, and viscosity, can affect agglomeration. Operating conditions during drying, including temperature, agitation speed, drying kinetics, pressure, bed height, and residual moisture content, can influence agglomeration. The size and shape of particles also play a role, with needle or plate-like crystals tending to produce weaker agglomerates compared to combining them with spherical crystals. To mitigate agglomeration, controlling operating conditions such as agitation speed and temperature, modifying the composition of the wash solvent, and selecting solvents with lower solubility can be employed.

In pharmaceutical manufacturing, maintaining the particle properties of active pharmaceutical ingredients (APIs) during the drying process is a key challenge. Drying is the final step following crystallization, but its impact on particle properties is not as well understood compared to crystallization. The difficulty in making comparisons with larger-scale equipment or when transferring the process to different equipment, scale-up issues, and limited availability of APIs in early developmental stages make it challenging to investigate particle properties during drying. Empirical equations, process parameters, and computational models have been used to model the drying process and understand particle-solvent interactions, but a complete understanding of the physical process and its effect on particle properties is still lacking.

Particle attrition during drying can occur through shear deformation or impact breakage. Shear deformation involves the sliding of particles under normal stress, while impact breakage is

caused by collisions between particles or between particles and the dryer's mechanical parts. Particle attrition can result in different modes of breakage, including chipping, fragmentation, and disintegration. Factors such as material properties (crystal habits, temperature, fracture toughness), operating parameters (agitation speed, drying temperature, fill volume), and equipment

In summary, maintaining particle properties during drying in pharmaceutical manufacturing is a challenge that requires a better understanding of the drying process and its impact on particle properties. Studying particle attrition, both due to shear deformation and impact breakage, is crucial for optimizing drying conditions and minimizing undesirable effects on API quality. Further research and the development of analytical methods and scale-down models are needed to enhance our understanding of particle behavior during drying and facilitate process optimization.

3.6 References

- Adamson, J. *et al.* (2016) ‘Development of Suitable Plant-Scale Drying Conditions That Prevent’. doi: 10.1021/acs.oprd.5b00327.
- Agnew, L. R. *et al.* (2016) ‘Controlled production of the elusive metastable form II of acetaminophen (paracetamol): A fully scalable templating approach in a cooling environment’, *Chemical Communications*, 52(46). doi: 10.1039/c6cc01032f.
- Am Ende, D. *et al.* (2013) ‘Development and Application of Laboratory Tools To Predict Particle Properties upon Scale-Up in Agitated Filter-Dryers’, *Organic Process Research & Development*, 17(10), pp. 1345–1358. doi: 10.1021/op400080x.
- Bemrose, C. R. and Bridgwater, J. (1987) ‘A review of attrition and attrition test methods’, *Powder Technology*, 49(2), pp. 97–126. doi: 10.1016/0032-5910(87)80054-2.
- Birch, M. and Marziano, I. (2013) ‘Understanding and Avoidance of Agglomeration During Drying Processes: A Case Study’. doi: 10.1021/op4000972.
- Broadbent, S. R. *et al.* (1956) ‘A matrix analysis of processes involving particle assemblies’, *Philosophical Transactions of the Royal Society of London. Series A, Mathematical and Physical Sciences*, 249(960), pp. 99–123. doi: 10.1098/rsta.1956.0016.
- Conder, E. W. *et al.* (2017) ‘The Pharmaceutical Drying Unit Operation: An Industry Perspective on Advancing the Science and Development Approach for Scale-Up and Technology Transfer’, *Organic Process Research and Development*, 21(3), pp. 420–429. doi: 10.1021/acs.oprd.6b00406.
- Cruz, P. C., Rocha, F. A. and Ferreira, A. M. (2019) ‘Application of Selective Crystallization Methods to Isolate the Metastable Polymorphs of Paracetamol: A Review’, *Organic Process Research and Development*, 23(12). doi: 10.1021/acs.oprd.9b00322.
- Darelius, A. *et al.* (2007) ‘Measurement of the velocity field and frictional properties of wet masses in a high shear mixer’, 62, pp. 2366–2374. doi: 10.1016/j.ces.2007.01.033.
- Ende, D. J. *am.* (2010) *Chemical engineering in the pharmaceutical industry : R & D to manufacturing*. Wiley. Available at: https://www.academia.edu/14905402/CHEMICAL_ENGINEERING_IN_THE_PHARMACEUTICAL_INDUSTRY (Accessed: 10 May 2019).
- Evans, A. G. and Wilshaw, T. R. (1977) ‘Dynamic solid particle damage in brittle materials: an appraisal’, *Journal of Materials Science*, 12(1), pp. 97–116. doi: 10.1007/BF00738475.
- Forbert, R. and Heimann, F. (1989) ‘Vacuum contact drying of mechanically agitated, coarse, hygroscopic bulk material’, *Chemical Engineering and Processing*, 26(3), pp. 225–235. doi:

10.1016/0255-2701(89)80021-2.

Ghadiri, M. *et al.* (2000) 'Attrition of granular solids in a shear cell', *Chemical Engineering Science*, 55(22), pp. 5445–5456. doi: 10.1016/S0009-2509(00)00168-8.

Ghadiri, M. and Zhang, Z. (2002) 'Impact attrition of particulate solids. Part 1: A theoretical model of chipping', *Chemical Engineering Science*, 57(17), pp. 3659–3669. doi: 10.1016/S0009-2509(02)00240-3.

Goh, W. P. (2019) 'Attrition and Phase Changes during Agitated Filter Bed Drying'.

Grof, Z. *et al.* (2011) 'Computational and experimental investigation of needle-shaped crystal breakage', *International Journal of Pharmaceutics*, 407(1–2), pp. 12–20. doi: 10.1016/J.IJPHARM.2010.12.031.

Grof, Z., Kohout, M. and Štěpánek, F. (2007) 'Multi-scale simulation of needle-shaped particle breakage under uniaxial compaction', *Chemical Engineering Science*, 62(5), pp. 1418–1429. doi: 10.1016/J.CES.2006.11.033.

Gwyn, J. E. (1969) 'On the particle size distribution function and the attrition of cracking catalysts', *AIChE Journal*, 15(1), pp. 35–39. doi: 10.1002/AIC.690150112.

Hamilton, P. (2011) 'Investigation of a drying process of needle-shaped particles using particle size analysis techniques and non-invasive Raman spectrometry'. doi: 10.48730/ZVV6-A488.

Hamilton, P. *et al.* (2011) 'Studies of particle drying using non-invasive Raman spectrometry and particle size analysis †', pp. 2168–2174. doi: 10.1039/c0an00893a.

Hamilton, P. *et al.* (2013) 'Investigation of factors affecting isolation of needle-shaped particles in a vacuum-agitated filter drier through non-invasive measurements by Raman spectrometry', *Chemical Engineering Science*, 101, pp. 878–885. doi: 10.1016/j.ces.2013.05.035.

Hare, C. *et al.* (2018) 'Impact breakage of pharmaceutical tablets', *International Journal of Pharmaceutics*, 536(1), pp. 370–376. doi: 10.1016/j.ijpharm.2017.11.066.

Hare, C. and Ghadiri, M. (2015) 'Attrition of paracetamol and aspirin under bulk shear deformation', *Chemical Engineering Science*, 125, pp. 13–19. doi: 10.1016/J.CES.2014.10.027.

Heng, J. Y. Y. and Williams, D. R. (2006) 'Wettability of paracetamol polymorphic forms I and II', *Langmuir*, 22(16), pp. 6905–6909. doi: 10.1021/LA060596P/ASSET/IMAGES/MEDIUM/LA060596PE00004.GIF.

Hsu, T.-C. and Chiou, J.-S. (2011) 'Vacuum Drying for Ultrafine Alumina Powders', *Drying Technology*, 29(5), pp. 566–572. doi: 10.1080/07373937.2010.508855.

Iveson, S. M. *et al.* (2001a) 'Nucleation, growth and breakage phenomena in agitated wet granulation processes: a review', *Powder Technology*, 117(1–2), pp. 3–39. doi:

10.1016/S0032-5910(01)00313-8.

Iveson, S. M. *et al.* (2001b) 'Nucleation, growth and breakage phenomena in agitated wet granulation processes: A review', *Powder Technology*. Elsevier, pp. 3–39. doi: 10.1016/S0032-5910(01)00313-8.

Jørgensen, K., Bach, P. and Jensen, A. D. (2005) 'Impact and attrition shear breakage of enzyme granules and placebo particles-application to particle design and formulation', *Powder Technology*, 149(2–3), pp. 157–167. doi: 10.1016/J.POWTEC.2004.11.018.

Kemp, I. C. (2017) 'Drying of pharmaceuticals in theory and practice', *Drying Technology*, 35(8), pp. 918–924. doi: 10.1080/07373937.2016.1222539.

Knight, P. C. *et al.* (2001) 'Prediction of impeller torque in high shear powder mixers', 56, pp. 4457–4471.

Kougoulos, E., Chadwick, C. E. and Ticehurst, M. D. (2011) 'Impact of agitated drying on the powder properties of an active pharmaceutical ingredient', *Powder Technology*, 210(3), pp. 308–314. doi: 10.1016/j.powtec.2011.03.041.

Kudra, T. and Mujumdar, A. S. (2009) *Advanced drying technologies*. CRC Press/Taylor & Francis. Available at: https://www.academia.edu/25013702/Advanced_Drying_Technologies (Accessed: 9 May 2019).

Kwapinska, M., Saage, G. and Tsotsas, E. (2006) 'Mixing of particles in rotary drums: A comparison of discrete element simulations with experimental results and penetration models for thermal processes', *Powder Technology*, 161(1), pp. 69–78. doi: 10.1016/J.POWTEC.2005.08.038.

Kwapinska, M., Saage, G. and Tsotsas, E. (2008) 'Continuous versus discrete modelling of heat transfer to agitated beds', *Powder Technology*, 181(3), pp. 331–342. doi: 10.1016/J.POWTEC.2007.05.025.

Lamberto, D. J. *et al.* (2011) 'Laboratory methods for assessing API sensitivity to mechanical stress during agitated drying', *Chemical Engineering Science*, 66(17), pp. 3868–3875. doi: 10.1016/j.ces.2011.05.016.

LAWN, B. R. and MARSHALL, D. B. (1979) 'Hardness, Toughness, and Brittleness: An Indentation Analysis', *Journal of the American Ceramic Society*, 62(7–8), pp. 347–350. doi: 10.1111/J.1151-2916.1979.TB19075.X.

Lee, H. L., Lin, H. Y. and Lee, T. (2014) 'The impact of reaction and crystallization of acetaminophen (Paracetamol) on filtration and drying through in-process controls', *Particle Technology Forum 2014 - Core Programming Area at the 2014 AIChE Annual Meeting*, pp. 275–286.

- Lekhal, A. *et al.* (2003) ‘Impact of agitated drying on crystal morphology: KCl – water system’, 132, pp. 119–130. doi: 10.1016/S0032-5910(03)00056-1.
- Lekhal, A. *et al.* (2004) ‘The effect of agitated drying on the morphology of l -threonine (needle-like) crystals’, 270, pp. 263–277. doi: 10.1016/j.ijpharm.2003.10.022.
- Lim, H. L., Hapgood, K. P. and Haig, B. (2016) ‘Understanding and preventing agglomeration in a filter drying process’, *Powder Technology*, 300, pp. 146–156. doi: 10.1016/j.powtec.2016.03.003.
- MacLeod, C. S. and Muller, F. L. (2012) ‘On the Fracture of Pharmaceutical Needle-Shaped Crystals during Pressure Filtration: Case Studies and Mechanistic Understanding’, *Organic Process Research & Development*, 16(3), pp. 425–434. doi: 10.1021/op200279m.
- Di Martino, P. *et al.* (1999) ‘Improved dissolution behavior of fenbufen by spherical crystallization’, *Drug Development and Industrial Pharmacy*, 25(10), pp. 1073–1081. doi: 10.1081/DDC-100102272.
- Mitarai, N. and Nori, F. (2007) ‘Wet granular materials’, <https://doi.org/10.1080/00018730600626065>, 55(1–2), pp. 1–45. doi: 10.1080/00018730600626065.
- Neil, A. U. and Bridgwater, J. (1994) ‘Attrition of particulate solids under shear’, *Powder Technology*, 80(3), pp. 207–219. doi: 10.1016/0032-5910(94)02849-4.
- Newitt, D. M. and Conway-Jones, J. M. (1958) ‘A contribution to the theory and practice of granulation’, *Transactions Institute Chemical Engineers*, 36, pp. 422–441.
- Ottoboni, S. (2013) ‘Workflow procedure to predict attrition in agitated dryers Introduction and aims’, pp. 6–8.
- Ottoboni, S. (2018) *Developing strategies and equipment for continuous isolation of active pharmaceutical ingredients (APIs) by filtration , washing and drying Declaration of Author ’ s Rights*. University of Strathclyde.
- Pakowski, Z. and Mujumdar, A. (2014) ‘Drying of Pharmaceutical Products’, *Handbook of Industrial Drying, Fourth Edition*, (January), pp. 681–701. doi: 10.1201/b17208-37.
- Papadakis, S. E. and Bahu, R. E. (1992) ‘The sticky issues of drying’, *Drying Technology*. doi: 10.1080/07373939208916484.
- Papadopoulos, D. G. (1998) ‘IMPACT BREAKAGE OF PARTICULATE SOLIDS’.
- Papageorgiou, C. D. *et al.* (2016) ‘Development of Screening Methodology for the Assessment of the Agglomeration Potential of APIs’, *Organic Process Research and Development*, 20(8), pp. 1500–1508. doi: 10.1021/acs.oprd.6b00201.
- Paramanathan, B. K. and Bridgwater, J. (1983) ‘Attribution of solids—I: Cell Development’,

- Chemical Engineering Science*, 38(2), pp. 197–206. doi: 10.1016/0009-2509(83)85002-7.
- Pietsch, W. (1997) ‘Size Enlargement by Agglomeration’, in *Handbook of Powder Science & Technology*. Springer US, pp. 202–377. doi: 10.1007/978-1-4615-6373-0_6.
- Remy, B. *et al.* (2015) ‘Scale-Up of Agitated Drying : Effect of Shear Stress and Hydrostatic Pressure on Active Pharmaceutical Ingredient Powder Properties’, 61(2), pp. 407–418. doi: 10.1002/aic.
- Rumpf, H. (no date) *H. Rumpf, “The Strength of Granules and Agglomeration,” In W. A. Knepper, Ed., Agglomeration, John Wiley, New York, 1962, pp. 379-418. - References - Scientific Research Publishing. Available at: [https://www.scirp.org/\(S\(351jmbntvnsjt1aadkposzje\)\)/reference/ReferencesPapers.aspx?ReferenceID=664420](https://www.scirp.org/(S(351jmbntvnsjt1aadkposzje))/reference/ReferencesPapers.aspx?ReferenceID=664420) (Accessed: 24 July 2020).*
- Sahni, E. K., Bogner, R. H. and Chaudhuri, B. (2013) ‘Systematic Investigation of Parameters Affecting The Performance of an Agitated Filter-Dryer’, *Journal of Pharmaceutical Sciences*, 102(7), pp. 2198–2213. doi: 10.1002/jps.23572.
- Schæfer, T. *et al.* (1993) ‘Melt pelletization in a high shear mixer. V. Effects of apparatus variables’, *European Journal of Pharmaceutical Sciences*, 1(3), pp. 133–141. doi: 10.1016/0928-0987(93)90003-S.
- Schæfer, T. (1996) ‘Melt pelletization in a high shear mixer. X. Agglomeration of binary mixtures’, *International Journal of Pharmaceutics*, 139(1–2), pp. 149–159. doi: 10.1016/0378-5173(96)04615-7.
- Schæfer, T. and Mathiesen, C. (1996) ‘Melt pelletization in a high shear mixer. VIII. Effects of binder viscosity’, *International Journal of Pharmaceutics*, 139(1–2), pp. 125–138. doi: 10.1016/0378-5173(96)04549-8.
- Schlünder, E. U. and Mollekopf, N. (1984) ‘Vacuum contact drying of free flowing mechanically agitated particulate material’, *Chemical Engineering and Processing*, 18(2), pp. 93–111. doi: 10.1016/0255-2701(84)85012-6.
- Seader, J. D. and Henley, E. J. (2006) *Separation process principles*. Wiley. Available at: https://www.academia.edu/34393321/Separation_Process_Principles_3rd_Edition-J._D._Seader_Ernest_J._Henley_D._Keith_Roper-04704_tupeg.ir_.pdf (Accessed: 9 May 2019).
- Sharma, P. K., Murugesan, S. and Tabora, J. E. (2019) ‘DESIGN OF FILTRATION AND DRYING OPERATIONS’, in *Chemical Engineering in the Pharmaceutical Industry*. Hoboken, NJ, USA: John Wiley & Sons, Inc., pp. 799–831. doi: 10.1002/9781119600800.ch35.

- Shipway, P. H. and Hutchings, I. M. (1993) 'Attrition of brittle spheres by fracture under compression and impact loading', *Powder Technology*, 76(1), pp. 23–30. doi: 10.1016/0032-5910(93)80037-B.
- Simurda, M. (2017) *SOLVENT SELECTION FOR ISOLATION OF PHARMACEUTICAL PRODUCTS*. University of Chemistry and Technology Prague.
- Tamrakar, A., Gunadi, A., Piccione, Patrick M, *et al.* (2016) 'Dynamic agglomeration profiling during the drying phase in an agitated filter dryer : Parametric investigation and regime map studies', *Powder Technology*, 303, pp. 109–123. doi: 10.1016/j.powtec.2016.09.012.
- Tsotsas, E. and Schlünder, E. U. (1990) 'Heat transfer in packed beds with fluid flow: remarks on the meaning and the calculation of a heat transfer coefficient at the wall', *Chemical Engineering Science*, 45(4), pp. 819–837. doi: 10.1016/0009-2509(90)85005-X.
- Vogel, L. and Peukert, W. (2004) 'Determination of material properties relevant to grinding by practicable lab-scale milling tests', *International Journal of Mineral Processing*, 74(SUPPL.), pp. S329–S338. doi: 10.1016/J.MINPRO.2004.07.018.
- Vogel, L. and Peukert, W. (2005) 'From single particle impact behaviour to modelling of impact mills', *Chemical Engineering Science*, 60(18), pp. 5164–5176. doi: 10.1016/J.CES.2005.03.064.
- Wallack, D. A. and King, C. J. (1988) 'Sticking and Agglomeration of Hygroscopic, Amorphous Carbohydrate and Food Powders', *Biotechnology Progress*, 4(1), pp. 31–35. doi: 10.1002/btpr.5420040106.
- Weibull, W. (no date) 'A Statistical Distribution Function of Wide Applicability'. Available at: <https://hal.archives-ouvertes.fr/hal-03112318> (Accessed: 23 September 2022).
- Yalkowsky, S. H. and Bolton, S. (1990) 'Particle Size and Content Uniformity', *Pharmaceutical Research*, 07(9), pp. 962–966. doi: 10.1023/A:1015958209643.
- Zhang, S. and Lamberto, D. J. (2014a) 'Development of New Laboratory Tools for Assessment of Granulation Behavior During Bulk Active Pharmaceutical Ingredient Drying', pp. 152–160. doi: 10.1002/jps.23762.
- Zhang, S. and Lamberto, D. J. (2014b) 'Development of New Laboratory Tools for Assessment of Granulation Behavior During Bulk Active Pharmaceutical Ingredient Drying', *Journal of Pharmaceutical Sciences*, 103(1), pp. 152–160. doi: 10.1002/jps.23762.
- Zhang, Z. and Ghadiri, M. (2002) 'Impact attrition of particulate solids. Part 2: Experimental work', *Chemical Engineering Science*, 57(17), pp. 3671–3686. doi: 10.1016/S0009-2509(02)00241-5.

Chapter 4: Materials and Methodology

This chapter describes the materials being studied and a detailed description of sample preparation and methodology development.

4.1 Raw Materials

4.1.1 Substrates

Substrates were the base material on which the drop of binding agent (solute/API) and the solvent solution were added to create a lump, which was then analysed to quantify the granule formation as a function of solubility of solute/API in the residual solvent, transport mechanism during drying and investigation of alternative techniques for agglomerates quantification.

4.1.1.1 Glass Beads

Glass beads of different sizes, Table 1, from VWR International Limited, were selected as a substrate to investigate the effect of particle size on lump formation and transport mechanism. Glass beads are commonly used as a model compound for method development in various scientific research. Here are a few reasons why glass beads are favoured for this purpose:

- **Physical Properties:** Glass beads possess certain physical properties that make them suitable for method development. They are typically spherical, allowing for uniform packing and flow characteristics. Their size and density can be controlled, providing versatility in experimental design.
- **Chemical Inertness:** Glass beads are chemically inert, meaning they do not react with most substances. This inertness ensures that the beads do not interfere with the analyte or the method being developed. It helps to isolate the effects of other factors under investigation.
- **Reproducibility:** Glass beads are manufactured with high precision, resulting in consistent size and shape. This uniformity allows for reliable and reproducible results during method development.

- **Availability and Cost:** Glass beads are readily available from commercial suppliers in various sizes and quantities. They are relatively inexpensive compared to other materials, making them a cost-effective choice for method development studies.
- **Compatibility:** Glass beads are compatible with a wide range of analytical techniques and methodologies. Their compatibility allows easy evaluation and optimization across different applications.
- **Safety:** Glass beads are generally safe to handle and use in the laboratory. They do not pose significant health or environmental risks, reducing potential hazards during method development experiments.

Table 4-1 List of sizes of glass beads

Glass beads	Size (microns)
GB 1	40-70
GB 2	90-150
GB 3	150-250
GB 4	300-400
GB 5	400-600

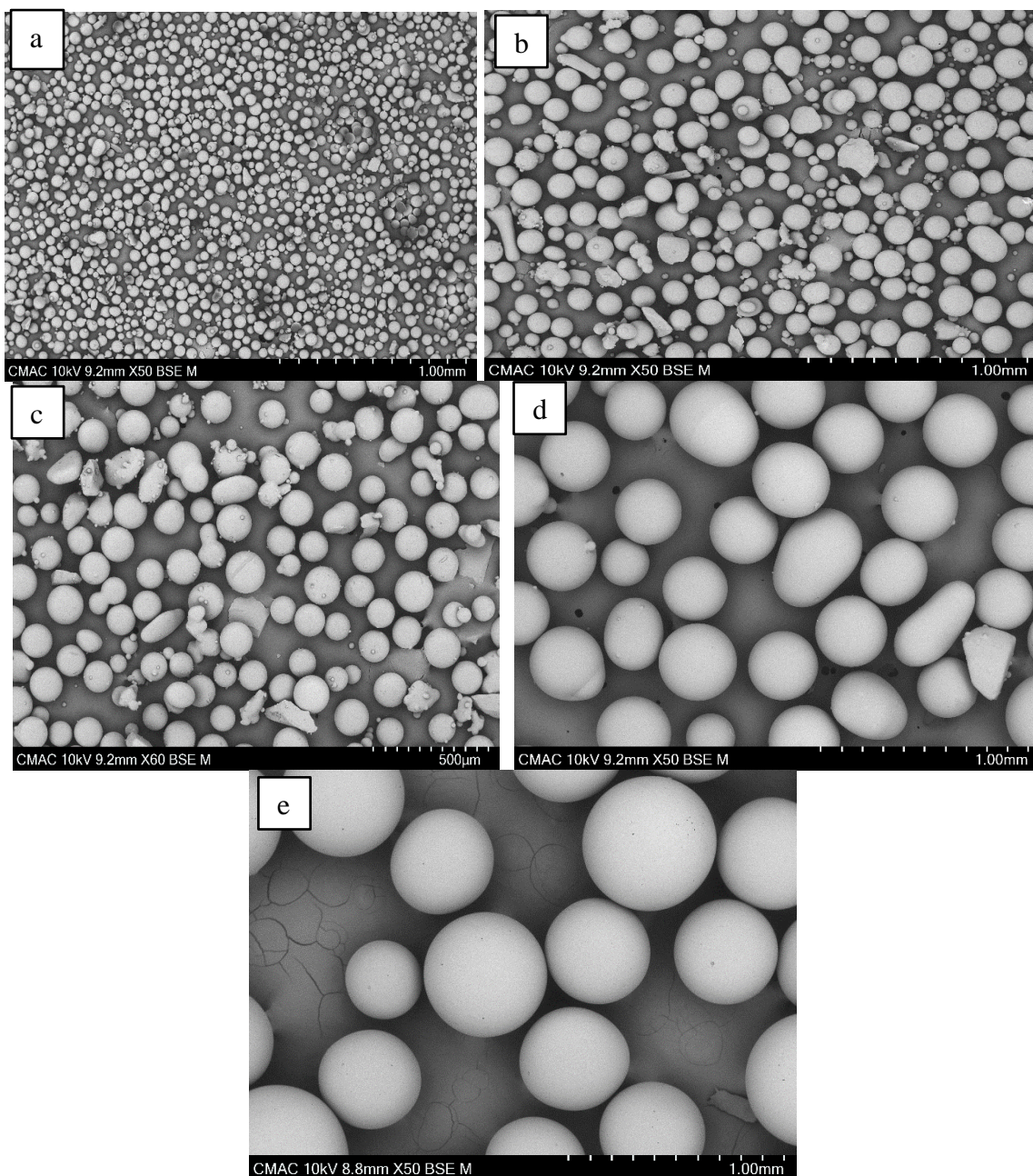


Figure 4-1 SEM of Glass beads (a) 40-70 μm (b) 90-150 μm (c) 150-250 μm (d) 300-400 μm (e) 400-500 μm

4.1.1.2 Paracetamol (PCM)

After developing methodology with glass beads to different grades of PCM i.e., Powdered PCM (purchased from Sigma-Aldrich, batch number MKCJ5427) and special granular as pharmaceutical grade PCM (supplied by Mallinckrodt Inc., Raleigh, N.C., USA, batch number 161713 J561) were selected as the substrate. Powdered PCM was then sieved to get the different size fractions to cover an approximately similar range of particle sizes as of the glass beads.

Paracetamol was selected as a model substrate because:

- It is a simple molecule with a well-understood structure. This makes it easier to study the interactions of paracetamol with other molecules and with biological systems.
- It is a relatively safe drug. This means that it can be used in research studies without putting the participants at undue risk.
- It is widely available. This makes it easy for researchers to obtain and use.
- It has been extensively studied. There is a wealth of information available about the properties and mechanisms of action of paracetamol, which can be used to inform research studies.

Table 4-2 Size analysis of Powdered and Granular Paracetamol

Material	X ₁₀ (µm)	X ₅₀ (µm)	X ₉₀ (µm)
Granular PCM	273.91	363.58	462.26
Powder PCM	29.71	100.57	288.76

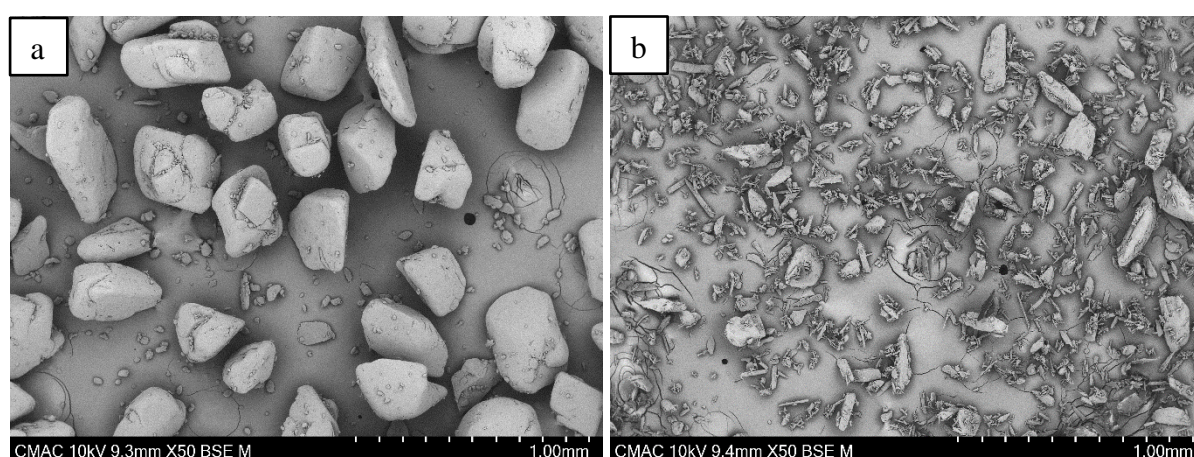


Figure 4-2 SEM of different grades of Paracetamol (a) granular PCM (b) Powdered PCM

4.1.1.3 Spherical agglomerates of Benzoic acid

Spherical agglomerates of benzoic acid (synthesized by Vishal Raval of the University of Strathclyde during his PhD research) were selected as a substrate because of their shape similarity with the glass spheres.

Table 4-3 Size analysis of spherical agglomerates (performed with Morphology G3) (Raval et al., 2022)

Material	$D_{[n,0.1]}$ (um)	$D_{[n,0.5]}$ (um)	$D_{[n,0.9]}$ (um)
J	6.8	41.79	776.04
N2	6.86	33.91	301.69
N15	7.45	47.55	108.20

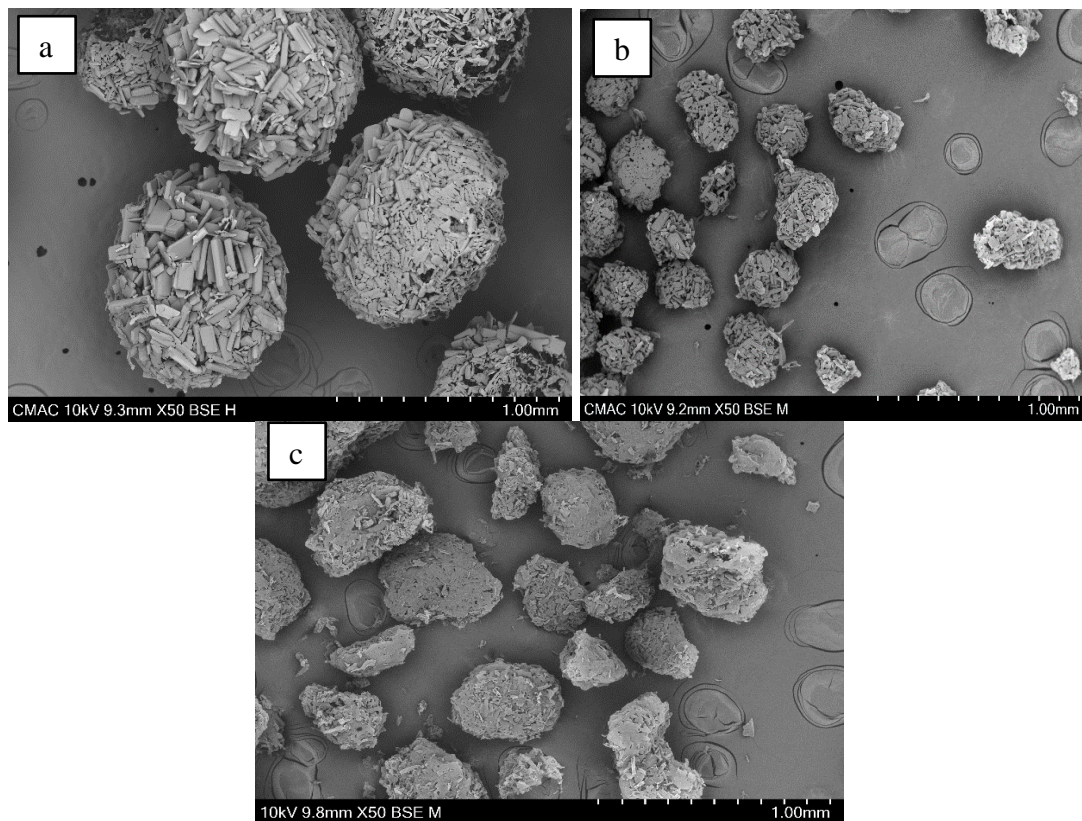


Figure 4-3 SEM of Spherical agglomerates (a) J (b) N2 (c) N15 (Raval et al., 2022)

4.1.2 Solvent

Water and methanol are the most commonly used crystallization solvents because:

- **Solvent Polarity:** Both water and methanol are polar solvents. Many compounds, especially organic molecules, exhibit polar characteristics and are more soluble in polar solvents. The polarity of water and methanol allows them to dissolve a wide range of compounds, making them versatile crystallization solvents.
- **Solvent Miscibility:** Water and methanol are highly miscible with many other solvents, including each other. This property allows them to be used in various solvent mixtures, expanding their applicability in crystallization processes.
- **Solvent Availability and Cost:** Water is the most abundant and widely available solvent on Earth. It is inexpensive and easily accessible, making it a convenient choice for many laboratory applications. Similarly, methanol is a readily available and relatively low-cost solvent.
- **Stability:** Both water and methanol are relatively stable solvents under typical laboratory conditions. They do not readily react with most compounds, ensuring that the solvent itself does not interfere with the crystallization process or react with the solute.
- **Temperature Range:** Water and methanol have relatively wide liquid temperature ranges, allowing for crystallization under a variety of temperature conditions. For example, water is commonly used in cooling crystallization processes due to its high heat capacity and the availability of cooling methods.
- **Safety:** Water and methanol are considered relatively safe solvents to handle in the laboratory compared to highly volatile or toxic solvents. Their low toxicity and non-flammability make them preferable choices in terms of safety.
- **Solvent Properties:** Water has a high dielectric constant, which enables it to dissolve ionic compounds and promote the formation of hydrated crystals. Methanol, on the other hand, has a lower dielectric constant but still exhibits good solvent properties for a wide range of organic and inorganic compounds.

As the aim of this research was to investigate the effect of residual solvent/mother liquor/crystallization solvent Methanol (purchased from VWR (purity 99.9%)) and water (produced using a Millipore Water Deioniser) were selected as solvents for the experiments with glass beads as a substrate.

When Paracetamol and spherical agglomerates of benzoic acid were used as a substrate a binary mixture of n-heptane (anti-solvent) and ethanol(solvent) was used to reliably control the quantity of solvent which on evaporation would deposit the dissolved solute material. This binary mixture was used to achieve a range of concentrations similar to the ones used in the experiments with the glass sphere without dissolving the substrate.

4.1.3 Binding agent (solute)

4.1.3.1 Carbohydrates

Initially, some experiments were performed to determine the capability of glass beads to form lumps. For these experiments, carbohydrates, Lactose (α -D-Lactose monohydrate, crystalline), and Fructose (D- fructose, 99%), purchased from Alfa Aesar (now Thermo Scientific Chemicals UK), were used. Carbohydrates are generally chemically stable and do not undergo significant degradation or reaction during drying processes. Carbohydrates like lactose and fructose are readily available and relatively inexpensive compared to other solutes. This accessibility makes them convenient choices for conducting preliminary experiments and feasibility studies on drying processes before applying the findings to more complex systems.

Table 4-4 Solubility of carbohydrates in water and methanol (Granberg, Ke and Rasmuson, 1999)

Solvent	Fructose (g/mL)	Lactose (g/mL)
Water	3.750	0.195
Methanol	0.1420	0.0096

4.1.3.2 Paracetamol

After developing the required methodology and relevant factors using carbohydrates as a

solute, with glass beads as substrate, the next set of experiments was performed using Micronized PCM as a solute supplied by Mallinckrodt Inc., Raleigh, N.C., USA.

Table 4-5 Solubility of PCM in water and methanol (Montañ, Olano and Ibáñez, 2007)

Solvent	PCM (g/mL)
Water	0.0128
Methanol	0.2978

Micronized PCM (supplied by Mallinckrodt Inc., Raleigh, N.C., USA, batch number 042213E407) was used to prepare solutions along with Ethanol (absolute, purity $\geq 99.8\%$, purchased from Sigma-Aldrich) and n-Heptane (purity 99.9%, purchased from Sigma-Aldrich) for the experiments with PCM as substrate.

Table 4-6 Solubility of PCM in pure solvents and binary mixtures of heptane and ethanol (Shahid et al., 2021)

Heptane: Ethanol	PCM solubility (g/g solvent)
0: 100	0.226
25: 75	0.164
50:50	0.086
60:40	0.065
70: 30	0.046
80:20	0.034

90: 10	0.033
100: 00	0.020

4.1.3.3 Benzoic acid

Benzoic acid (purchased from VWR, batch number 20D064128) was used to prepare solutions which mimic the residual solution remaining at the end of filtration and washing for the experiments with spherical agglomerates of benzoic acid as substrate. Ethanol and n-Heptane were used to prepare binary solutions.

The same material was used to perform solubility measurements of benzoic acid in pure solvents and binary mixtures.

4.1.4 DYE

Two dyes, Patent V Blue and Oil Red EGN were selected to investigate and improve visualization of the transport mechanism of residual moisture through the bed of substrate during drying, depending upon the solubility of the dye in different solvents (Patent Blue V in polar solvents and aqueous mixtures and Oil red EGN (Sigma Aldrich) in less polar organic solvents).

4.2 Methodology

4.2.1 Sample preparation (lump formation)

An agglomerate or lump was produced with a known concentration and its quantification was performed to study the effect of residual moisture on agglomeration during drying.

To produce an agglomerate a solution of known concentration in the selected solvents was prepared to mimic the residual solvent. Then a drop of a known volume of that solution was added carefully to the top of a bed of glass beads of known mass held in a glass sample vial (25 ml, dia 2 mm). The sample was then placed in a fume hood for a specific period until it was completely dry. The residual solvent in the dried sample was determined by calculating loss on drying (LOD). This was done by comparing the mass of the wet sample with the sample

placed in a fume hood for 24 hours, so the amount of evaporated solvent could be calculated from the weight loss over 24 hours. After complete drying, the material was characterised by evaluating the extent and strength of agglomeration. Figure 4-4 shows the experimental sequence and equipment used.

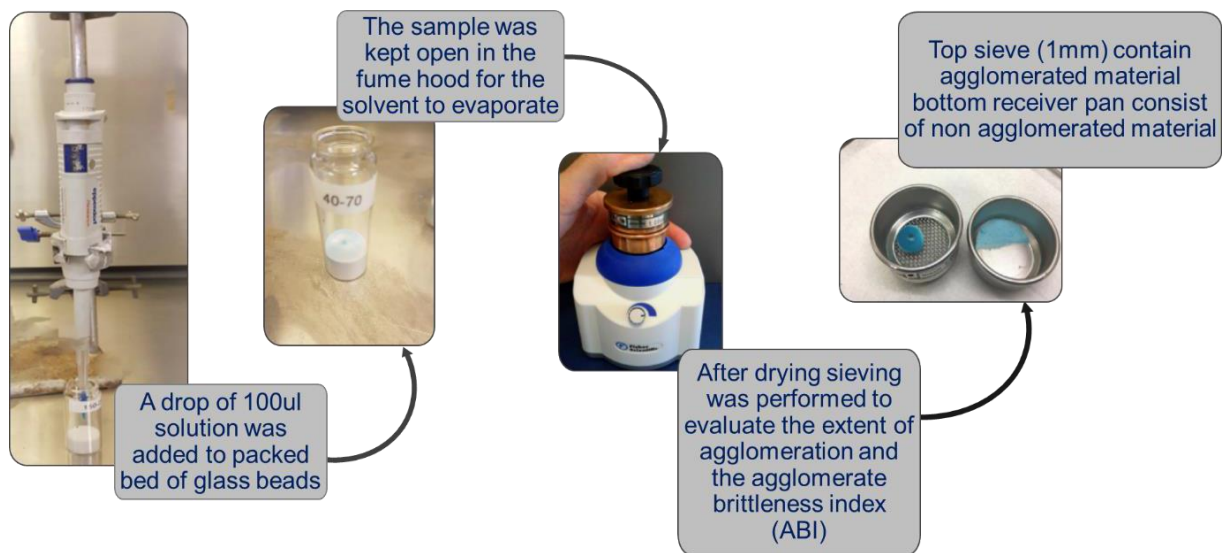


Figure 4-4 Experimental sequence and equipment to create and characterize agglomerates.

4.2.2 Characterization of dried samples

4.2.2.1 Loss on drying

The wet sample was placed in the fume hood for drying. To determine that the sample is completely dried, the loss on drying (LOD) was calculated as in Equation 2-3.

4.2.2.2 Agglomerate brittleness index (ABI) and extent of agglomeration

Birch & Marziano (2013) arbitrarily defined agglomerates as particle aggregates retained by a 1mm sieve. The extent of agglomeration is taken as the mass of agglomerates retained on a 1mm sieve over the total sample mass (Equation 4-2).

$$\text{Extent of agglomeration} = \frac{\text{mass of agglomerate retained above 1 mm seive}}{\text{total mass of the cake}} \quad \text{Equation 4-1}$$

Birch and Marziano (2013) also developed a qualitative approach for calculating an arbitrary Agglomerate Brittleness Index (ABI). In this work, the same approach has been taken. A 1mm stainless steel sieve (Figure 4-5, Endecott's Ltd, London) was used to separate particles at the

1mm size boundary.



Figure 4-5 Sieving Assembly for glass beads.

The sieves were shaken gently for 5-10 seconds by hand to minimise the breakage of particles. The material retained on the 1mm sieve was quantified by weighing and then shaken on the same sieve using a Variable Speed Mini Vortex Mixer (Fisherbrand™) at 2800 rpm for 1 minute. The cycle was repeated four times for each sample investigated, and after every sieving cycle, the masses were recorded. The mass loss of the upper retained fraction was recorded and plotted using a power-law curve. The power of the fitted curve is then taken as a descriptor of the mechanical properties of the agglomerated material and indicates the agglomerate brittleness. The higher the index, the softer the agglomerates.

4.3 References

Granberg, R. A., Ke, A. ° and Rasmuson, C. (1999) ‘Solubility of Paracetamol in Pure Solvents’. doi: 10.1021/je990124v.

Montañ, F., Olano, A. and Ibáñez, E. (2007) ‘Modeling Solubilities of Sugars in Alcohols Based on Original Experimental Data’, *American Institute of Chemical Engineers AIChE J*, 53, pp. 2411–2418. doi: 10.1002/aic.11258.

Raval, V. *et al.* (2022) ‘Particle engineering-size controlled spherical agglomeration of benzoic acid’. doi: 10.17868/STRATH.00081904.

Shahid, M. *et al.* (2021) ‘Exploring the Role of Anti-solvent Effects during Washing on Active Pharmaceutical Ingredient Purity’, *Organic Process Research and Development*. American Chemical Society, 25(4), pp. 969–981. doi: 10.1021/ACS.OPRD.1C00005/SUPPL_FILE/OP1C00005_SI_001.PDF.

Chapter 5: Quantification of granule formation as a function of solubility in residual solvents

This chapter explains the work done to quantify the correlation between the mass of deposited material and lump formation. To investigate the amount of residual solvent that is needed to cause lump formation, a model system of glass beads representing the primary particles was developed. Paracetamol was dissolved in methanol as the API present in the residual mother liquor/ wash liquor. It is demonstrated that by reducing the concentration of dissolved material in the residual mother liquor, the amount of deposited material reduces and decreases the strength of the resulting agglomerates and the extent of agglomeration.

5.1 Introduction

Drying Active Pharmaceutical Ingredient (API) crystals by removing the residual solvent after filtration and washing can profoundly affect the isolated powder characteristics. Any product dissolved in the residual solvent is deposited when the solvent evaporates, some of this material forms solid bridges between particles leading to agglomeration. Therefore, a set of experiments was performed to quantify granule formation as a function of solubility in residual solvents and to confirm the appropriateness of the method. Following these preliminary experiments, further investigations were carried out with paracetamol.

The main objective of the work presented in this chapter is to quantify the amount of deposited material that can cause robust lump formation., and this has been addressed using glass spheres of different sizes as substrate and paracetamol (PCM) solutions of different concentrations to mimic residual mother liquor/wash solvent mixtures. It was demonstrated that by reducing the concentration of dissolved material in residual mother liquor, the amount of deposited material reduces, decreasing the strength of agglomerates. The effect of varying concentrations on the extent of agglomeration was also investigated.

5.2 Materials and Methodology

5.2.1 Materials

Initially, some experiments were performed to determine the capability of glass beads to form lumps. For these experiments, carbohydrates, Lactose (α -D-Lactose monohydrate,

crystalline), and Fructose (D- fructose, 99%), purchased from Alfa Aesar (now Thermo Scientific Chemicals UK), were used. Methanol (purchased from VWR (purity 99.9%)) and water (produced using a Millipore Water Deioniser) were selected as solvents based on the solubility of respective solutes. Two dyes, Patent V Blue and Oil Red EGN were selected, to help visual observation of the transport mechanism of residual moisture during drying, depending upon the solubility of the dye in different solvents (Patent Blue V in polar solvents and aqueous mixtures and Oil red EGN (Sigma Aldrich) in less polar organic solvents).

Glass beads (GB1, GB2, GB3, GB4, GB5) (section 4.1.1.1), from VWR International Limited, were selected as a substrate to investigate the effect of particle size on lump formation.

After developing the required methodology and relevant factors using carbohydrates as a solute, experiments were performed using Micronized PCM as a solute supplied by Mallinckrodt Inc., Raleigh, N.C., USA. The solvent system was the same as for preliminary investigations.

5.2.2 Methodology

A series of fundamental experiments were performed to investigate the minimum amount of solid deposition, which can cause lump formation during drying. First, glass beads were selected as the substrate to simplify the data analysis. The experiments also enabled the transport of dissolved material through the bed to be investigated (Chapter 6:). Then the effect of decreasing solute concentration on lump formation was investigated. Preliminary experiments were performed by using carbohydrates to test the methodology, and then subsequently, API (Paracetamol) was used as a solute to prepare a realistic residual solution as moisture in the wet filter cake.

Sample Preparation and characterization

Sample was prepared and characterized with the methodology explained in Section 4.2.1.

Table 5-1 shows the parameters and their corresponding ranges selected for different sets of experiments during this work.

Table 5-1 Summary of Experiments performed for Chapter 5

Exp No.	No of samples	Exp description	Substrate	Solvent	Solute/Binder	Substrate mass (g)
1	10	preliminary experiment with Fructose as a binder	GB1, GB2, GB3,GB4, GB5	Water and Methanol	Fructose	10
2	10	preliminary experiment with Lactoses a binder	GB1, GB2, GB3,GB4, GB5	Water and Methanol	Sucrose	
3	10	Decreasing concentration of Lactose	GB2	Water and Methanol	Lactose	
4	12	DOE experiments for screening of factors effecting agglomeration	GB2, GB3, GB4	Water	Lactose	
5	10	Preliminary experiment with Paracetamol as binder	GB1, GB2, GB3,GB4, GB5	Water and Methanol	Paracetamol	
6	10	0.01 g/ml PCM with dye	GB1, GB2, GB3,GB4, GB5	Water and Methanol	Paracetamol	

7	10	0.0075 g/ml PCM with dye	GB1, GB2, GB3,GB4, GB5	Water and Methanol	Paracetamol
8	10	0.005 g/ml PCM with dye	GB1, GB2, GB3,GB4, GB5	Water and Methanol	Paracetamol
9	10	0.0025 g/ml PCM with dye	GB1, GB2, GB3,GB4, GB5	Water and Methanol	Paracetamol
10	10	0.01 g/ml PCM without dye	GB1, GB2, GB3,GB4, GB5	Water and Methanol	Paracetamol
11	10	0.0075 g/ml PCM without dye	GB1, GB2, GB3,GB4, GB5	Water and Methanol	Paracetamol
12	10	0.005 g/ml PCM without dye	GB1, GB2, GB3,GB4, GB5	Water and Methanol	Paracetamol
13	10	0.0025 g/ml PCM without dye	GB1, GB2, GB3,GB4, GB5	Water and Methanol	Paracetamol

14	20	<p>Experiment was performed to check the role of blue dye in agglomeration. Samples were prepared by adding a solution of blue dye in methanol. Dilution factor of 10%,100%, and 1000% was also applied to solution.</p>	<p>GB1, GB2, GB3,GB4, GB5</p>	<p>Methanol</p>	<p>Blue dye</p>	
----	----	--	-------------------------------	-----------------	-----------------	--

5.2.2.1 Design of experiment

A multivariate design of experiments approach was used to optimize the experiments by investigating the effects of different parameters on the extent of agglomeration and the ABI Index. MODDE Pro V11.0.1, developed by MKS Umetrics (*MODDE® - Design of Experiments Software / Sartorius*), was selected as a design of experiment software.

Design of experiments (DOE) is a systematic, efficient method to study the relationship between multiple input variables (factors) and key output variables (responses). This structured approach enables the user to determine whether a factor, or a collection of factors, has an effect on the response; to determine whether factors interact in their effect on that response. It also enables the user to model the behaviour of a given response as a function of the factors and so to adjust the parameters to optimize the response.

MODDE is designed to plan, execute, and analyze experiments efficiently. It allows to design experiments, collect data, and perform statistical analyses to identify critical process

parameters, optimize conditions, and make informed decisions based on the results. MODDE provides tools for creating experimental designs, generating statistical models, and visualizing data trends. It is often used in research, development, and manufacturing environments to improve processes, reduce costs, and enhance product quality by systematically exploring the effects of various factors and their interactions.

This methodology simultaneously plans experiments while varying relevant factors over a set of experiments to extract the maximum amount of information from the collected data in the presence of noise. It connects the results using a mathematical model which is then used for interpretation, predictions, and optimization. The objectives are to determine how the factors influence the responses and determine the best values of the variables to achieve optimal conditions to obtain the best performance of the process. The software MOODE was used to create a design of experiments.

The screening was the first step of the investigation. The objective of screening was to identify the essential factors. An essential factor is a factor that causes substantial changes (effects) in the response when it is varied. Simple models, like linear models, are used during screening. Factors with the most significant results are chosen to run the fewest possible experiments to determine the overall response. After screening, an investigation is carried out to approximate the responses by a model to understand how the factors influence the responses. Optimization aims to compare the responses by a mathematical model and find the best conditions. Robustness tests are then used to evaluate whether a process performs satisfactorily even when some influential factors vary.

The main aim of using the DOE approach in this work was to identify the parameters that significantly affect the extent of agglomeration and the ABI index. This approach provided a basis to develop a methodology for the quantification of agglomerate formation.



5.3 Results and discussion

5.3.1 Experiments for Method Development

Preliminary experiments were performed to develop a methodology for the estimation of the minimum amount of dissolved material present in residual moisture, which can cause lump formation during drying, and check the lump's robustness formed by the glass beads held together by the deposited carbohydrates left behind when the solvent was evaporated. Table

5-2 summarizes the equipment setup and the procedure for these preliminary experiments. The experiments were repeated three times and the error bars were calculated by standard deviation for all experiments.

Table 5-2 Summary of parameters and procedure for experiments performed for method development.

Exp. No.	No of samples	Material	Procedure	Images
1	10 samples 5 for fructose/water system 5 for Fructose/Methanol system	Fructose as a binder (2.5 g for water and 0.71g for methanol)	Ten grams of glass beads were added to the preweighed vials. Then, 100µL of the solution was added as one drop using an Eppendorf pipette to dispense the solution onto the glass beads, and the sample was left for drying in a fume hood for 24 hours.	
		Glass beads (GB1, GB2, GB3, GB4, GB5)		
		Solvents (5mL)		
		Methanol Water		
2	10 samples 5 for Lactose/water system 5 for Lactose/Methanol system	Lactose as binder (0.9 g)	Ten grams of glass beads were added to the preweighed vials. Then, 250µL solution was dispensed as one drop using an Eppendorf pipette to add the solution to the glass beads, and the sample was left today in a fume hood for three days.	
		Glass beads (GB1, GB2, GB3, GB4, GB5)		
		Water as a solvent (5mL)		

Fructose has higher solubility in methanol than Lactose (Table 5-2) but the issue encountered with fructose was the formation of deformable lumps (fructose bridges are more deformable than those formed with Lactose) as shown in Figure 5-1 (b), Figure 5-2 (b), and Figure 5-3 (b).



Figure 5-1 Fructose/water system (a) Sample after manual tapping (b) sample after four cycles of sieving.

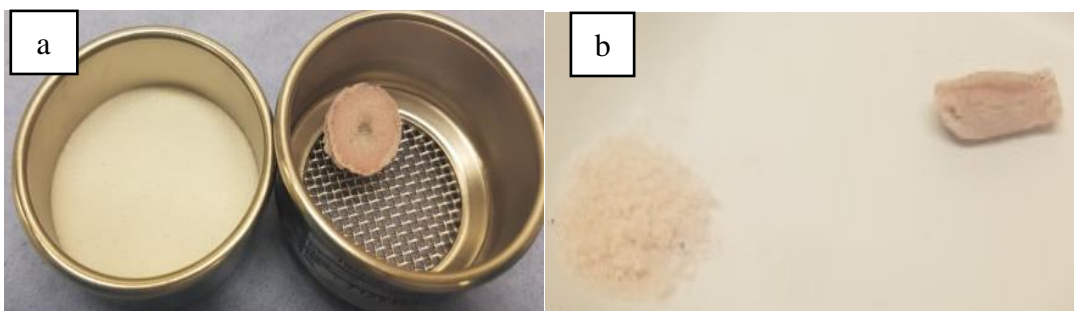


Figure 5-2 Fructose/Methanol system (a) sample after manual tapping (b) sample after four cycles of sieving.

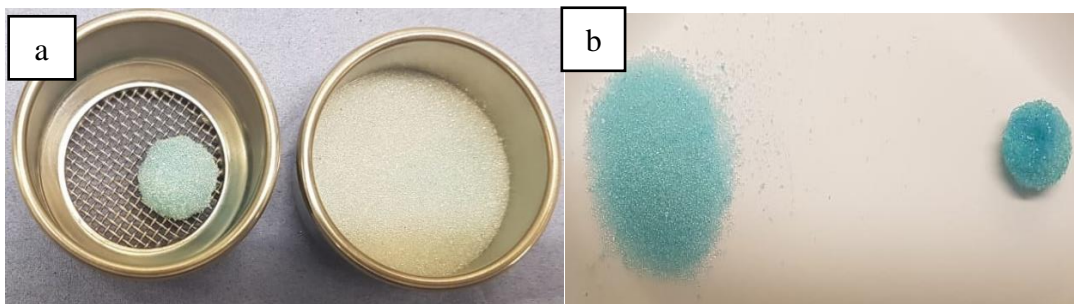


Figure 5-3 Lactose/water system (a) sample after manual tapping (b) sample after four cycles of sieving.

For both lactose/water and fructose/methanol samples, the extent of agglomeration increases by increasing the particle sizes (Figure 5-4 and Figure 5-5), as smaller particles have higher surface area per unit volume and show high resistance to fluid flow (Xue, Guo and Chen, 2020). Thus, the added fluid drop for larger glass spheres can wet a larger volume in the powder bed, forming larger agglomerates. While for the fructose/water system, the extent of agglomeration showed inconsistent results. The extent of agglomeration increased from GB1 to GB3, then decreased for GB4 and then increased for GB5 (Figure 5-5).

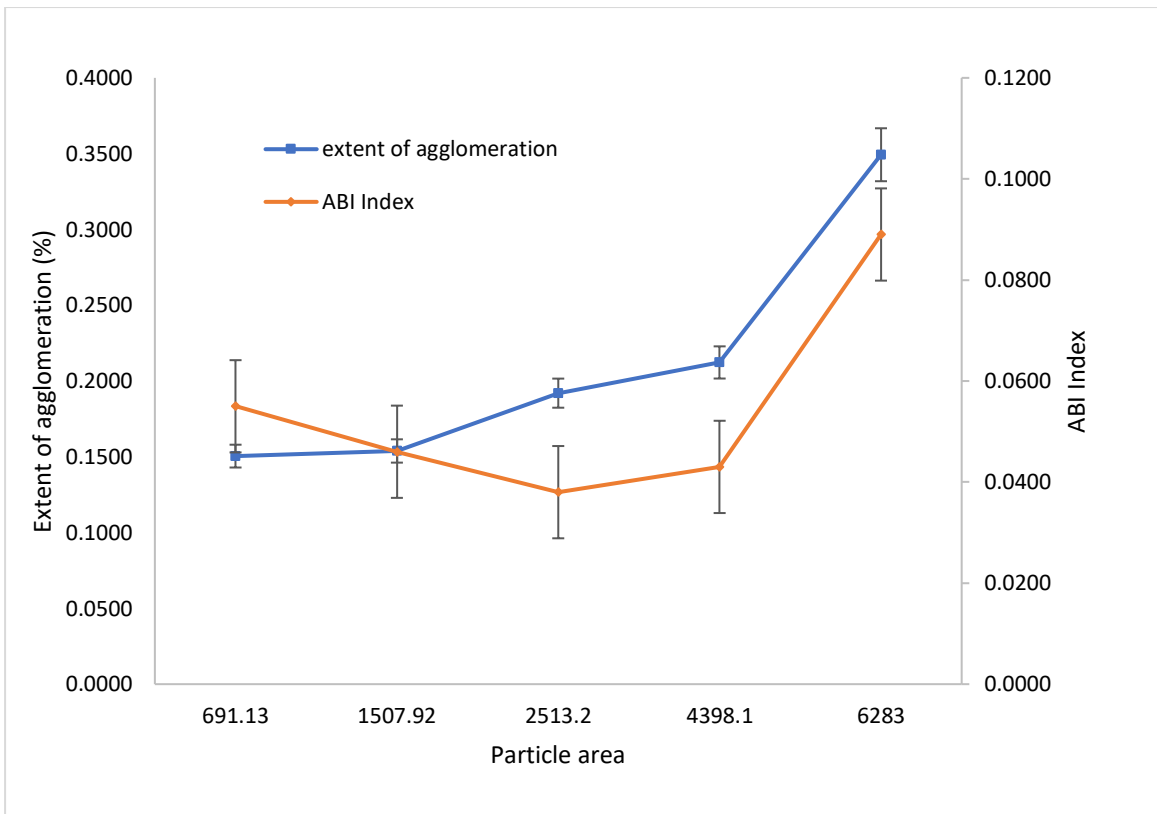


Figure 5-4 Extent of agglomeration and ABI index for Fructose/Methanol system

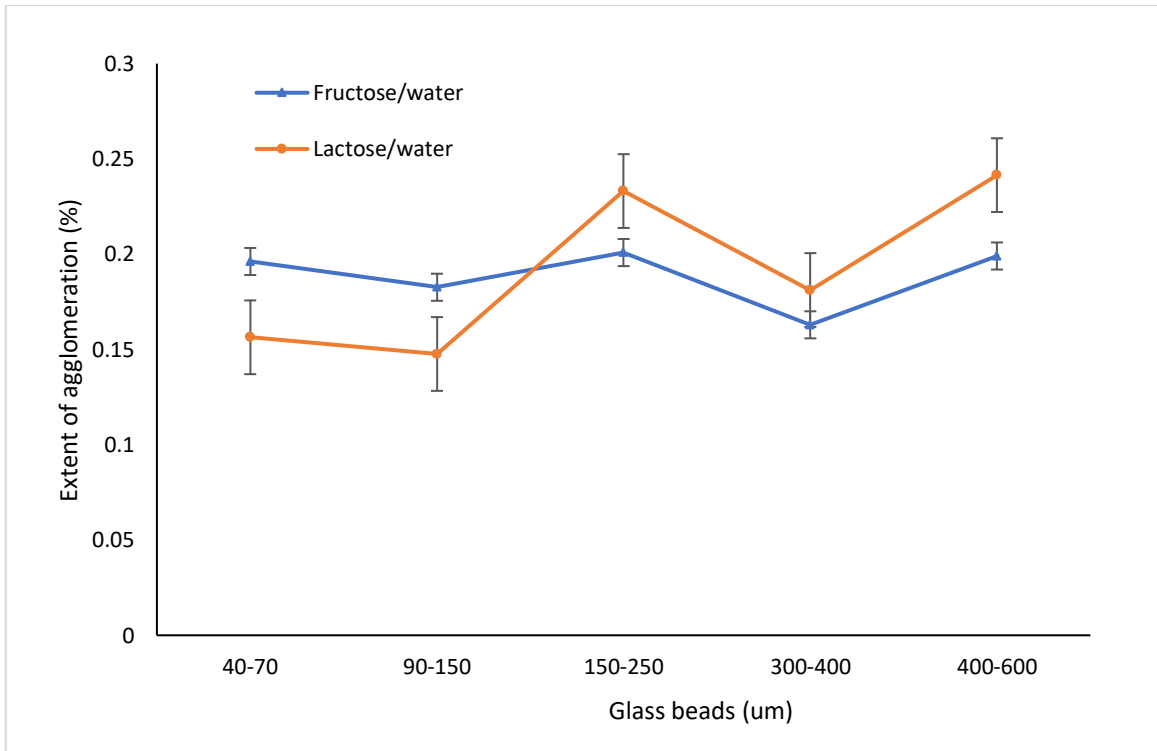


Figure 5-5 Extent of agglomeration for Lactose/water and Fructose/water solutions with glass bead

As mentioned in section 4.2.2.2, higher values of the ABI index indicate soft agglomerates. As

the particle size increases, agglomerates become more fragile for the lactose/water system as they have a high ABI index value (Figure 5-6). Particle size is an important property which significantly affects the behavior of granular material. For smaller particles (diameter of 100 μm), inter-particle forces are higher, thus making their nature more cohesive (Seville, Willett and Knight, 2000). Moreover, Feng *et al.* (2020) in their work show that by increasing particle size void fraction decreases but the addition of wetting liquid increases the void fraction. The effect of liquid is more evident for smaller particles. They also reported that the capillary forces overcome gravitational forces for small particles, making the void impact more obvious. This explains that the number of liquid bridges per unit volume is more for small than big particles. If these liquid bridges contain any dissolved material, their deposition leads to the formation of solid bridges upon drying (Dopfer *et al.*, 2013). Therefore, it is inferred that an increase in particle size leads to the formation of more fragile lumps by reducing the number of solid bridges between the particles, as shown in Figure 5-6 for the lactose/water system.

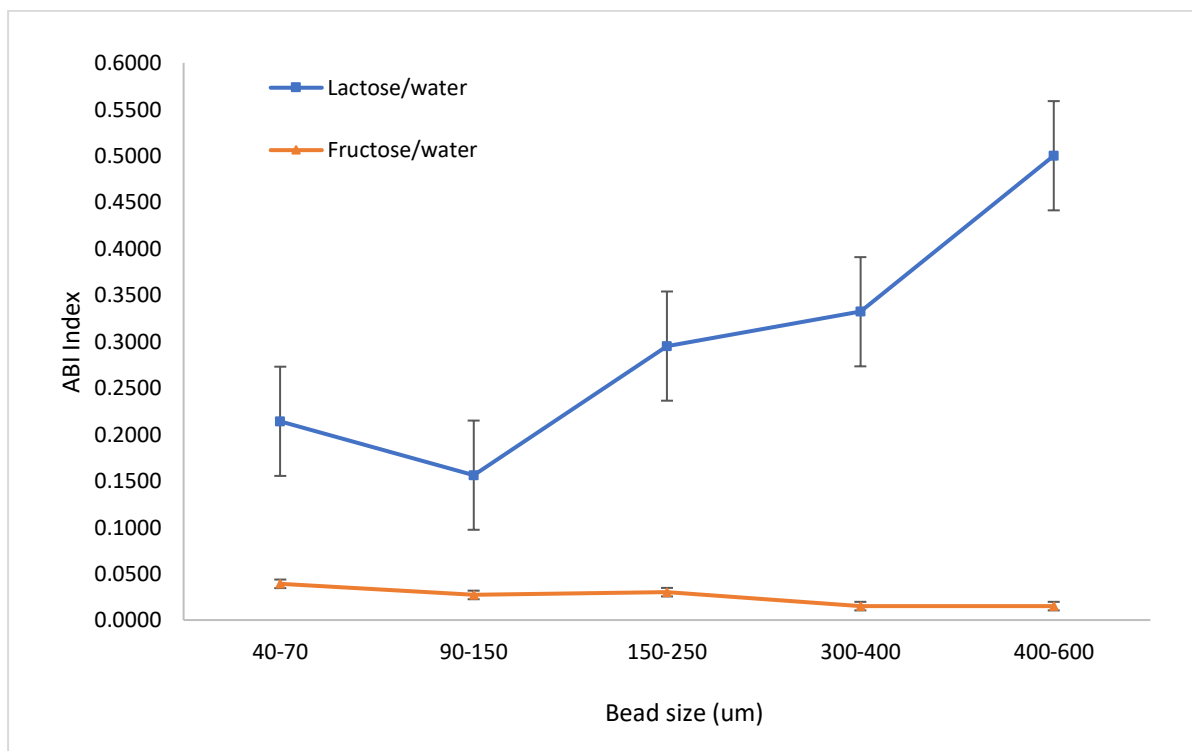


Figure 5-6 ABI index for Lactose/water and Fructose/water solutions with glass beads.

The fructose/methanol system showed inconsistent results for the ABI index (Figure 5-4). In the fructose/water system, the agglomerates showed a very low value of the ABI index (Figure 5-6) because of the viscid nature of the lumps, which deformed instead of breaking (Figure 5-1 and Figure 5-2).

5.3.1.1 Lactose decreasing concentration experiments

Fructose was eliminated from the subsequent investigations due to soft deformable inter-particle crystal bridges. Lactose was used as the bridging agent representing API in the next set of experiments to investigate the effect of minimum and maximum concentration of bridging agent on lump formation and strength. The maximum amount was calculated to prepare saturated solutions using solubility data of Lactose in both solvents (Table 4-4). The drop and bead sizes were kept constant for these experiments. The summary of experimental parameters is shown in Table 5-3.

Table 5-3 Summary of parameters of lactose decreasing concentration experiments.

Beads size (µm)	Solute	Substrate mass (g)	Solute mass (g)	Solvent	Drop volume (µL)
90-150	Lactose	10	0.897	Water (100 ml)	100
			0.620		
			0.347		
			0.156		
			0.0052	Methanol (100 ml)	
			0.0041		
			0.0028		
			0.0010		

The lactose/methanol system generated very brittle agglomerates, breaking after 1 to 2 sieving cycles with decreasing lactose concentration in methanol (Figure 5-7). This was because the solubility of lactose is very low in methanol, and as the solubility decreases, the tendency of the binding agent to form bridges between the particles decreases because of less dissolved material in a solvent (Am Ende *et al.*, 2013; Birch and Marziano, 2013). The results for the lactose/water system were the same by decreasing the concentration of lactose, the value of the ABI index increases, indicating that the lumps became fragile by decreasing concentration. The extent of agglomeration increases for both solvents as the concentration of lactose decreases. This can

be explained by decreasing the concentration of lactose, and the viscosity of the solution decreases (Hidayanto, Tanabe and Kawai, 2010). As the viscosity of the solution decreases, it diffuses to a greater extent leading to larger agglomerates. Table 5-4 summarizes the results for the ABI index and Extent of agglomeration.

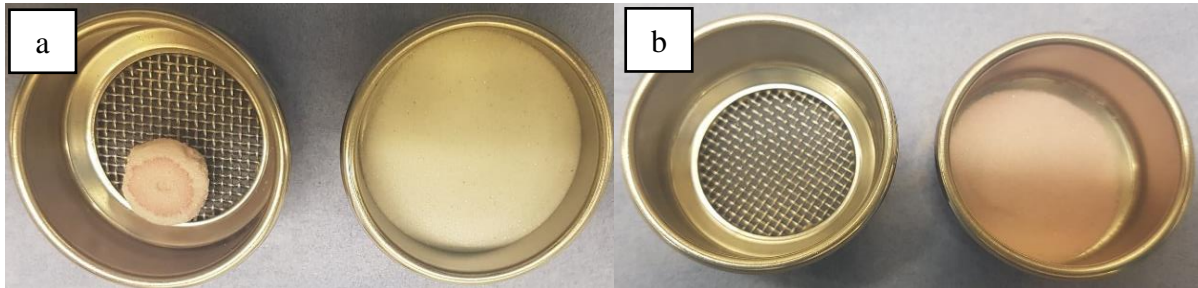


Figure 5-7 Lactose/Methanol system (a) sample after manual tapping (b) sample after two cycles of sieving.

Table 5-4 ABI index and extent of agglomeration for Lactose decreasing concentration experiments.

Solvent	Lactose concentration (g)	ABI index	Extent of agglomeration
Water	0.8970	0.2310	0.0831
	0.6200	0.3660	0.1104
	0.3470	0.2170	0.1706
	0.1560	0.9279	0.1607
Methanol	0.0052	1.398	0.1478
	0.0041	-	0.0231
	0.0028	-	0.1116
	0.0010	-	0.0372

*[Note, the characteristics of the methanol wet samples meant that no ABI index could be obtained for these samples]

5.3.1.2 Lactose DOE Experiments

In previous sections, various parameters have been investigated to develop a methodology for

the quantification of lump formation during drying. To screen the parameters that significantly contribute to lump formation DOE approach was used as described in section 5.2.2.1. The aim was to identify which parameters are more influential in favoring lump formation and determine their appropriate ranges. L9, a 3-level design using a linear model and three center points, was selected for the DOE. Table 5-5 and Table 5-6 summarizes all the factors with their selected ranges and responses for the DOE experiments. Water was used as the only solvent for this set of experiments as the lactose/methanol system could not produce robust agglomerates.

Table 5-5 Factors and responses of DOE for Lactose concentration

Factors (Abbreviation)	Ranges
Lactose concentration (lac)	0.1-0.9 (g in 100mL of solvent)
Volume of solution (dro)	100 – 250 (μ L)
Particle size (par)	90-150, 150-250, 300-400 (μ m)
Responses (abbreviation)	
Extent of agglomeration (ext)	
ABI index (ABI)	

Table 5-6 Summary of Parameters of DOE experiments

Exp No	Exp Name	Lactose concentration (g/ml)	Solution volume (ul)	Particle size (um)	% agglomeration	ABI index
---------------	-----------------	-------------------------------------	-----------------------------	---------------------------	------------------------	------------------

1	N1	0.1	100	90-150	0.310259	0.344
2	N2	0.1	175	150-250	0.312979	0.285
3	N3	0.1	250	300-400	0.264507	0.328
4	N4	0.5	100	150-250	0.322971	0.15
5	N5	0.5	175	300-400	0.234767	0.202
6	N6	0.5	250	90-150	0.365171	0.333
7	N7	0.9	100	300-400	0.165113	0.631
8	N8	0.9	175	90-150	0.271557	0.266
9	N9	0.9	250	150-250	0.264612	0.199
10	N10	0.5	175	90-150	0.240504	0.203
11	N11	0.5	175	90-150	0.234324	0.201
12	N12	0.5	175	90-150	0.211192	0.251

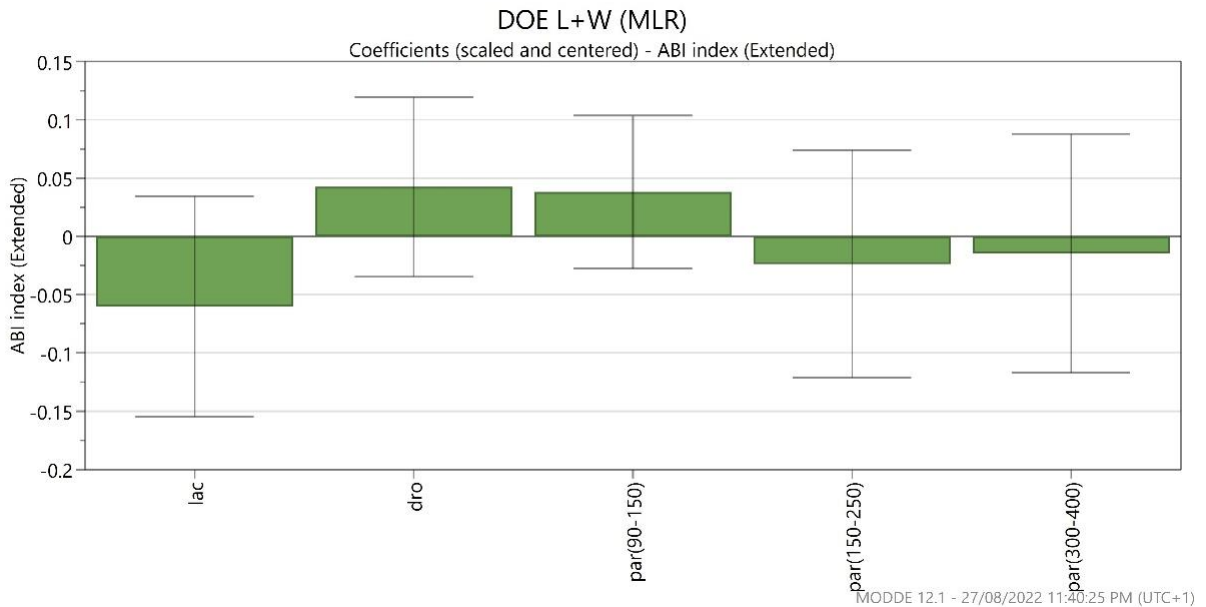


Figure 5-8 DOE factors affect plots on ABI index ($R^2 = 0.59$)

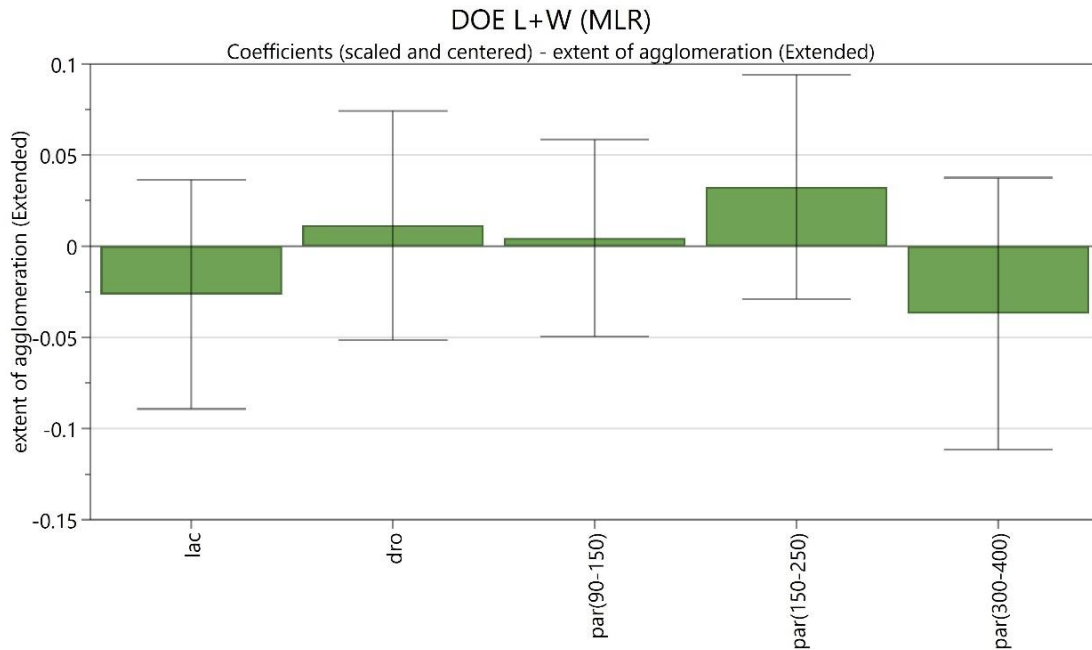


Figure 5-9 DOE factors affect the plot on the extent of agglomeration ($R^2 = 0.28$)

Lactose concentration and drop size are the most significant parameters which affect the ABI index (Figure 5-8). In contrast, for the extent of agglomeration, the most important factors are particle size and lactose concentration (Figure 5-9). The results for this experiment set correspond with the results in previous sections. By increasing lactose concentrations, the ABI index value decreases, and the extent of agglomeration value decreases, thus indicating the formation of small and hard agglomerates. Bigger drop sizes lead to the formation of softer and large agglomerates as the ABI index value increases by increasing drop size, which is not in accordance with the expected results. Adding a bigger drop would be expected to increase the amount of available binding agent within the cake, which would be expected to ultimately increase the number of solid bridges leading to hard agglomerates. However, the results counter this hypothesis. Figure 5-10 and Figure 5-11 summarize results for the ABI index and extent of agglomeration.

This DOE approach concludes that solute concentration and particle size have a significant role in the agglomerate formation. In the next section, the effect of using actual API in place of the glass spheres was investigated using the methodology developed by lactose.

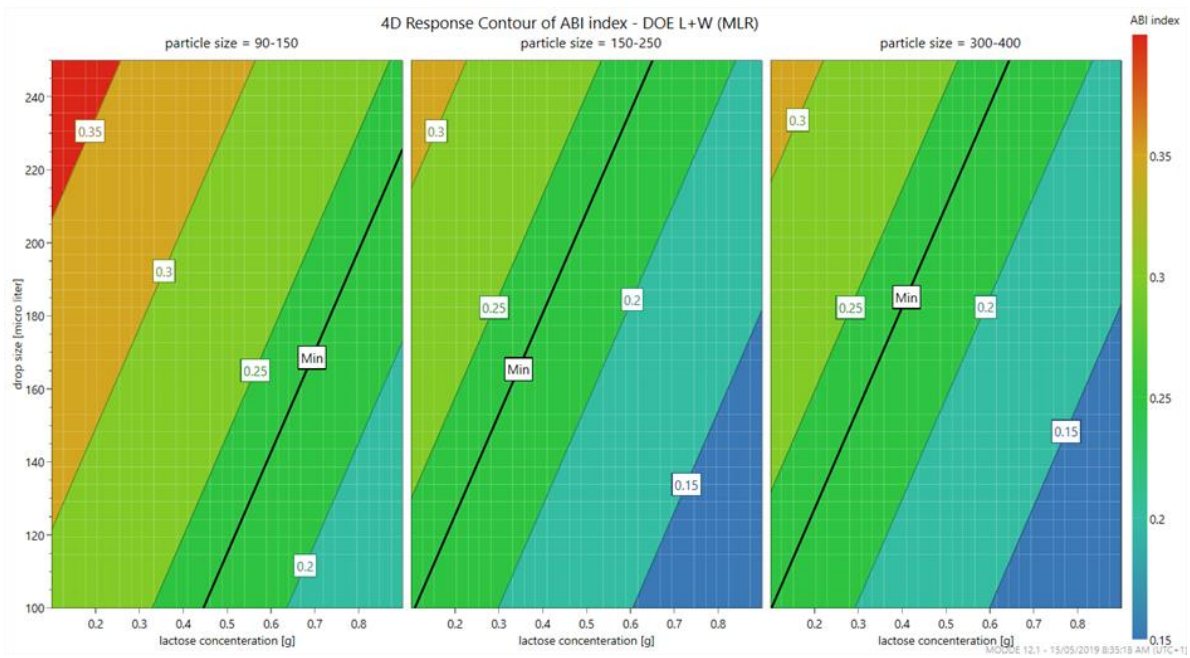


Figure 5-10 Response contour Plot for ABI index

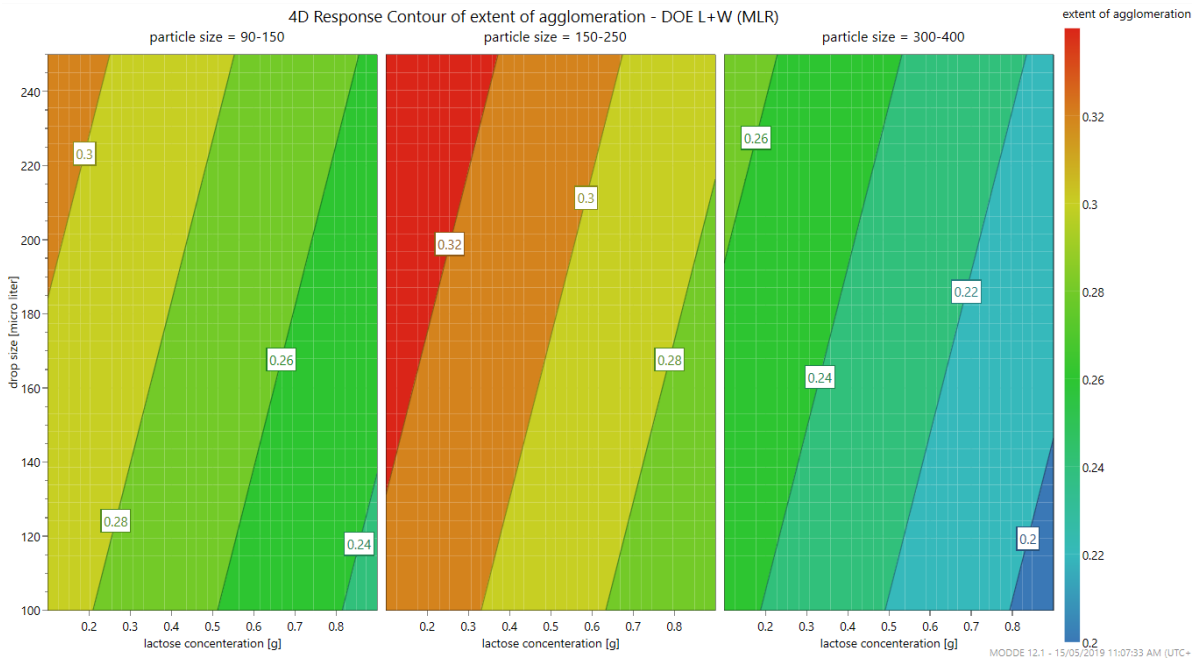


Figure 5-11 Response contour plot for the extent of agglomeration.

5.3.2 Experiments with API

The methodology developed in the previous section by using carbohydrates to quantify the role of residual moisture on agglomeration was then used to investigate the effect of API as a

binding agent with glass beads as the substrate. Paracetamol (PCM) was used as the dissolved compound forming bridges between the glass spheres to evaluate the impact of solution composition on agglomerate strength. Different sets of experiments were conducted to evaluate the propensity of the glass beads to form lumps, to investigate the transport of PCM and dye within the lumps and to detect the effect of decreasing the amount of solvent (drop size) and PCM concentration in solution.

Preliminary experiments were performed to check the robustness of the lumps of PCM formed with both solvents. After checking the robustness of the lumps, the next set of experiments was conducted to investigate the effect of decreasing the concentration of PCM on lump formation whilst keeping the amount of solvent constant. All the experiments in this section were repeated three times and the error bars were calculated by standard deviation.

5.3.2.1 Preliminary experiments

The experiments with carbohydrates allowed the experimental technique to be developed and tested. The next step was to investigate the effect of using an API. PCM was selected as the bridging agent with the aim of gathering data by mimicking the actual situation in pharmaceutical manufacturing. A preliminary test was made to verify the capability of PCM to generate bridges between particles (lump formation). PCM solution with water and methanol was prepared by adding 1 g of PCM to 100 mL of solvent, i.e., 0.01 g/mL.

The main objective was to determine the minimum quantity of crystallizable residue required per particle to form a lump. In a typical crystallization process using 10 mL of solvent per gram of product and achieving a 90% recovery, the API concentration in the mother liquor would be 0.01 g/mL. To prevent agglomeration on drying by this mechanism, we would need to remove at least 90% (Goh, 2019) of the dissolved material during washing, leaving the material wet is predominantly a non-solvent solution to stand a reasonable chance of drying the crystalline product without forming robust agglomerates. This is potentially achievable using washing.

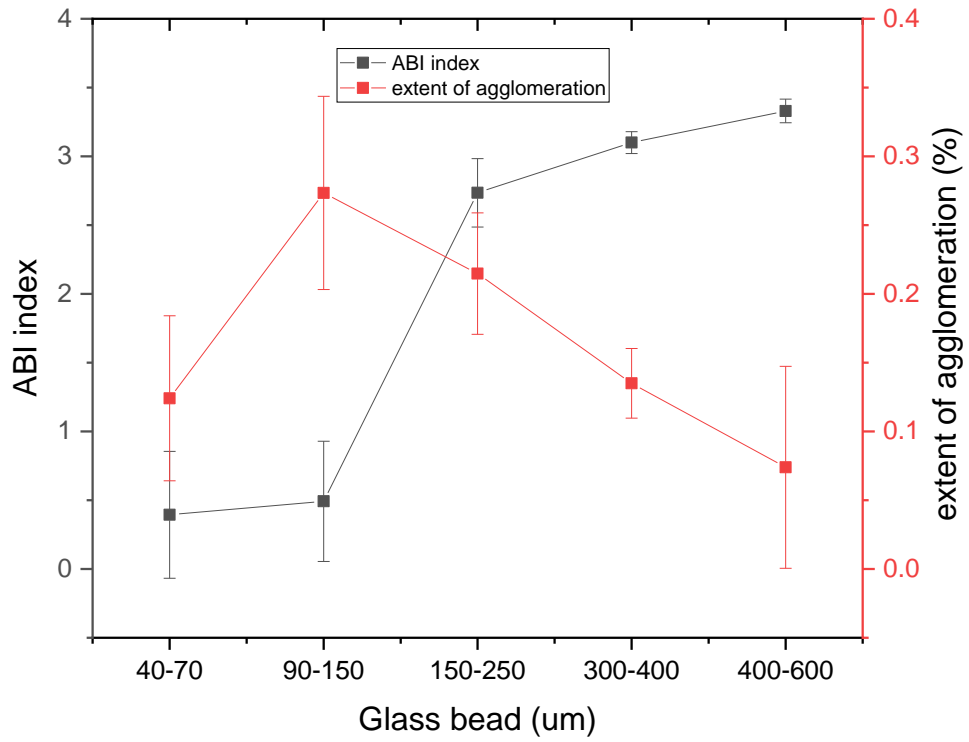


Figure 5-12 Extent of agglomeration and ABI index for PCM/water system.

Extent of agglomeration depends upon the amount of solution added. The size of the lump formed was in accordance with the amount of solution added as explained in section 5.3.3.

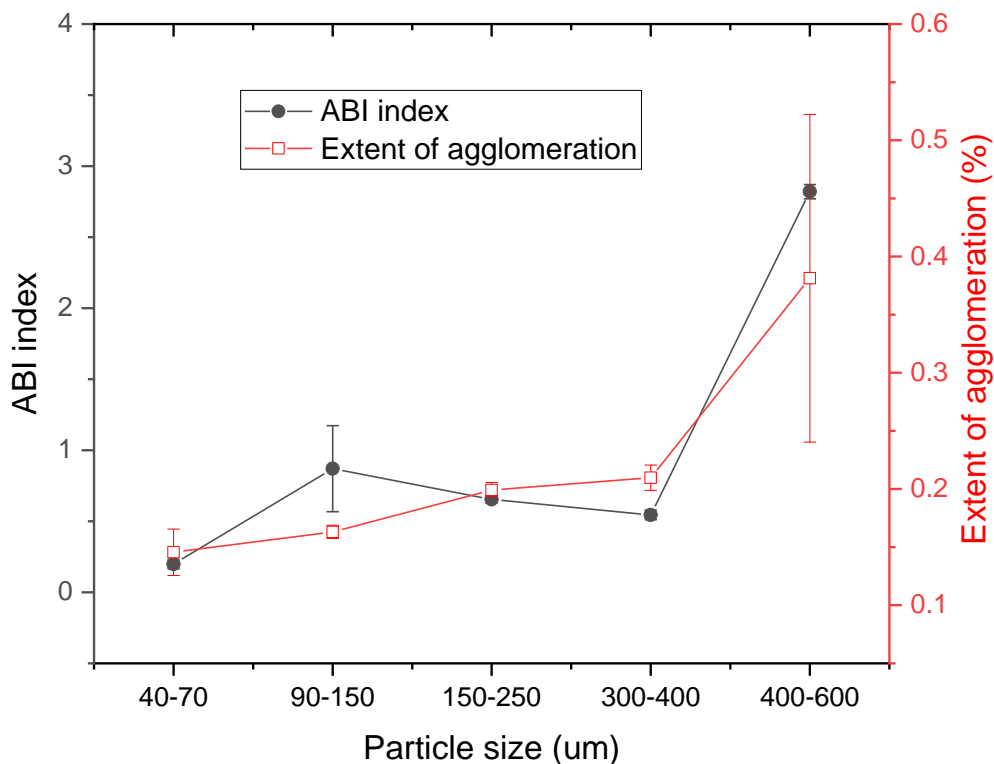


Figure 5-13 Extent of agglomeration and ABI index for PCM/Methanol system.

Results for preliminary experiments with methanol were in accordance with the results in previous sections that by increasing the particle size, the agglomerates become large and soft (Figure 5-13). For water ABI index shows the same results the bigger the particle size, the softer the lump. However, the results for the extent of agglomeration for the water/PCM system controvert those obtained using methanol as solvent. For the water/PCM system, the extent of agglomeration decreases with an increase in particle size (Figure 5-12). This can be linked with the wettability of water with glass beads and PCM (investigated in chapter 4).

5.3.2.2 PCM decreasing concentration experiments

After the preliminary experiments, a subsequent set of experiments was performed to investigate the effect of decreasing PCM concentration (0.01g/mL – 0.0025g/mL) on lump formation.

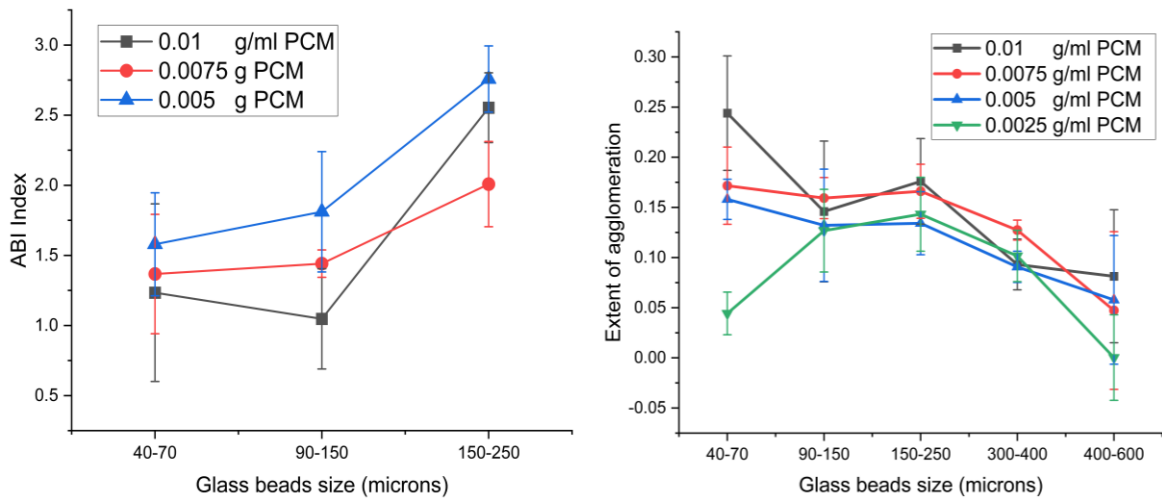


Figure 5-14 ABI index and Extent of agglomeration for decreasing concentration of PCM/water system

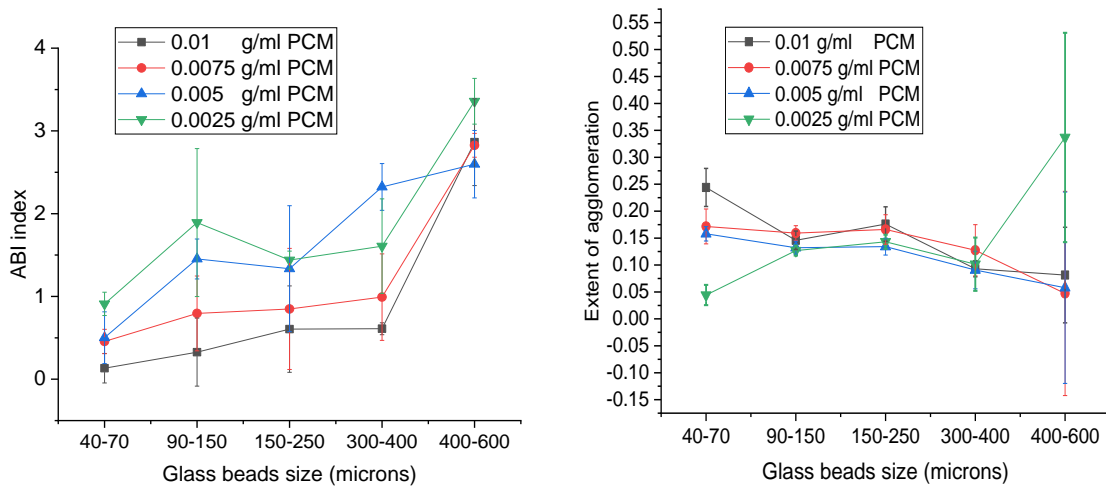


Figure 5-15 ABI index and Extent of agglomeration for decreasing concentration of PCM/methanol system

The decreasing concentration of PCM in water shows the same results as in preliminary experiments that by increasing particle size, the extent of agglomeration decreases. For the ABI index, no robust lumps were formed at PCM concentrations below 0.05 g/mL and as the solubility of PCM is very low in the water. Further reducing the PCM concentration, there was not enough dissolved material available for solid bridging between particles. However, further investigation for quantification of granule formation as a function of solubility of API in the residual solvent system was performed with methanol because of the contradictory results obtained using water to determine the extent of agglomeration. Moreover, the visual observations of moisture transfer for the PCM/water system differed from the PCM/Methanol

system (Figure 6-3), which was further investigated (Chapter 6):

From Figure 5-15, it is possible to observe the effect of solute concentration on the ABI index. By decreasing the PCM concentration, the agglomerates become more fragile as ABI values increase. This is consistent with the hypothesis that the amount of material required for bridging became insufficient to hold the particles together in the lump. However, the decrease in the extent of agglomeration, which occurred by decreasing the API concentration, was unprecedented based on the observed behaviour with decreasing concentration of lactose (section 5.3.1.1 and 5.3.1.2). Moreover, no lumps robust enough to determine an ABI were formed at the lowest concentration investigated, 0.0005g PCM/mL solution.

5.3.2.3 Experiments without dye

After investigating the effect of decreasing concentration, another factor was investigated, and that was the role of dye in agglomerate formation. For this, solutions of PCM decreasing concentration with methanol were prepared without adding dye. Dye was added before to help visual observation of transport of residual moisture throughout the cake during drying.

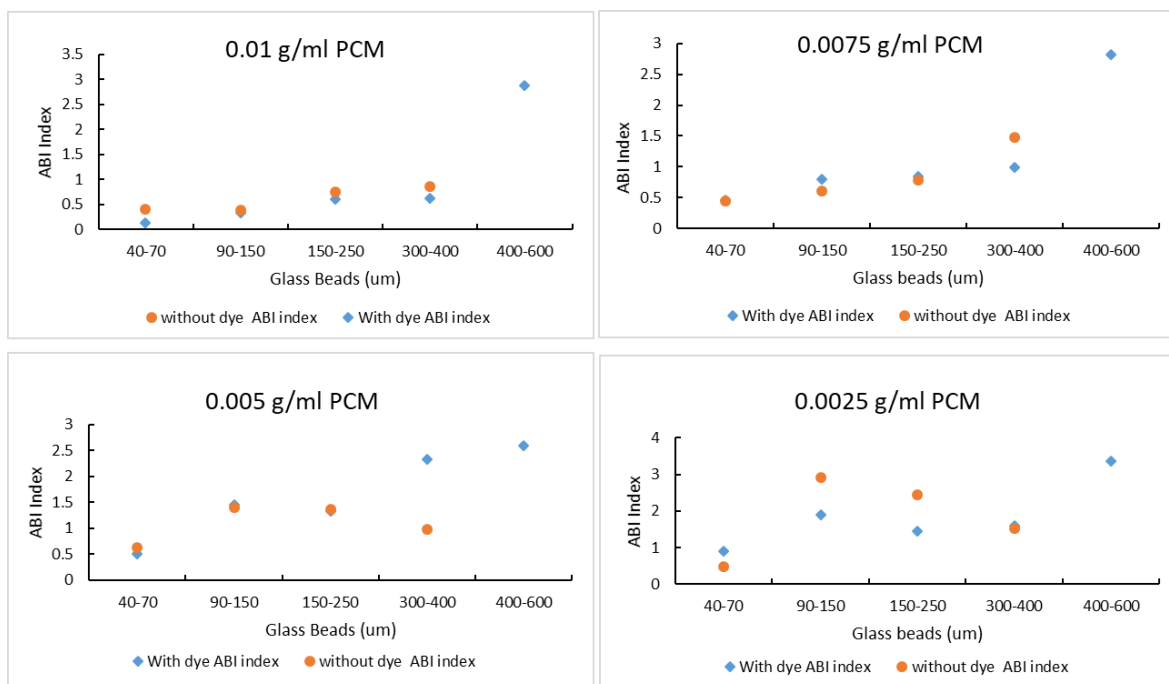


Figure 5-16 Comparison of ABI index for decreasing amount of PCM with Methanol with and without dye

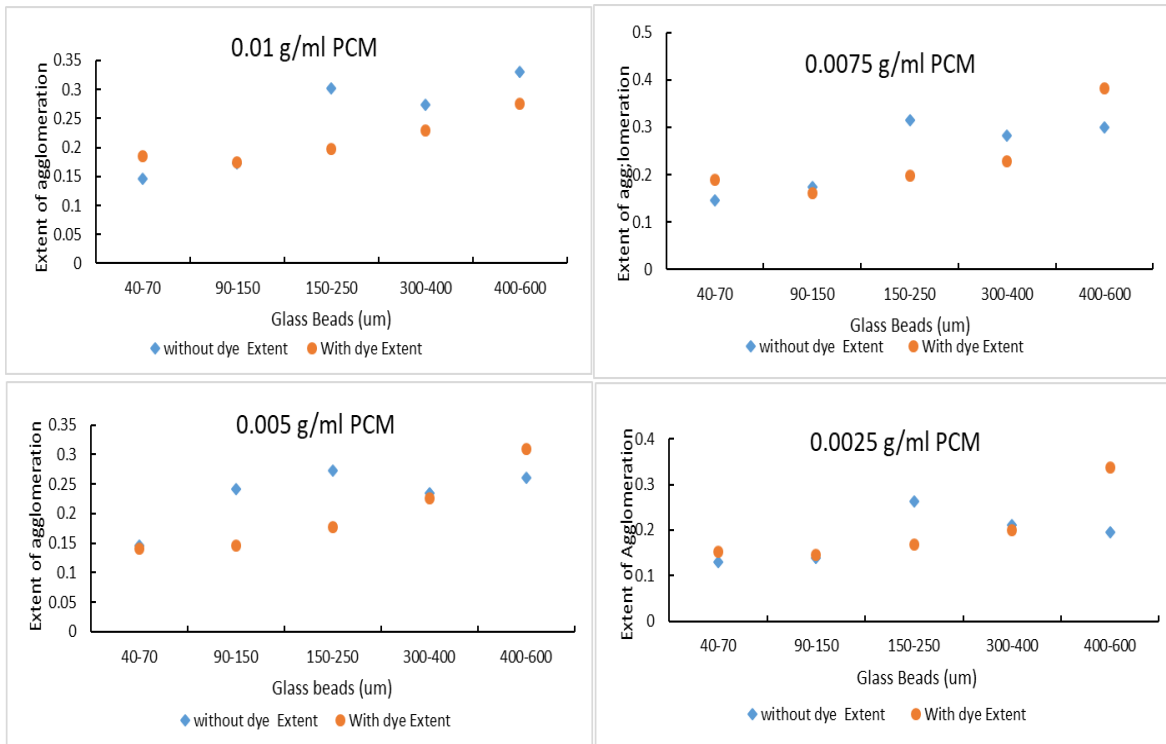


Figure 5-17 Comparison of Extent of agglomeration for decreasing amount of PCM with Methanol with and without dye

The comparison of with and with dye experiment results (Figure 5-16 and Figure 5-17) show that the ABI index and extent of agglomeration for both, i.e. with and without dye, almost follow the same trend. Therefore, it is presumed that dye, which was added to visualize moisture movement through the cake during drying, did not affect agglomeration. Finally, experiments were performed using a dye solution without the dissolved API to investigate whether the dye dissolved in the solvent can affect agglomeration.

The solution was prepared for this set of experiments by adding 0.05 g dye into the solvent (Methanol). No PCM was added to the solution. Experiments with diluted dye solutions up to 10%, 100% and 1000% were also performed. Table 5-7 shows the dilution factor and the results of the experiments which shows that dye had not a significant role in agglomerate formation as most of the lump formed were fragile enough to break during first or second cycle of sieving and even during manual tapping.

Table 5-7 Parameters and results of die dilution experiments

Bead size (um)	Dilution factor	Results
40-70	0	Lump-formed breaks after the first cycle of sieving
90-150		Lump-formed breaks after the first cycle of sieving
150-250		Lump-formed breaks after the first cycle of sieving
300-400		Lump-formed breaks after the first cycle of sieving
400-600		No lump formed
40-70	10	Lump-formed breaks after manual tapping
90-150		Lump-formed breaks after manual tapping
150-250		No lump formed
300-400		No lump formed
400-600		No lump formed
40-70	100	Lump-formed breaks after manual tapping
90-150		No lump formed
150-250		Lump-formed breaks after manual tapping
300-400		No lump formed
400-600		No lump formed

40-70	1000	Lump-formed breaks after manual tapping
90-150		Lump-formed breaks after manual tapping
150-250		No lump formed
300-400		No lump formed
400-600		No lump formed

5.3.3 Filling fraction calculation

The goal was to determine the minimum amount of material needed to hold these spheres together. To determine the minimum amount of material needed to form inter-particle bridges capable of holding the spheres together, the amount of PCM deposited on a single sphere was then estimated by calculating both void volume and filling fraction.

The volume of an agglomerated lump is estimated using its mass and the density of the glass spheres and is then multiplied by 36/64, a typical sphere packing factor, to determine the void volume of the lump. To calculate the fraction of this volume occupied by the added drop of solution (the filling fraction), the volume of the drop is divided by the void volume. The filling fraction is the proportion of the empty space in the powder, which is occupied by the liquid drop used to form the agglomerate.

The number of spheres in the lump was then determined: the lump volume divided by the volume of a single sphere. It was then possible to establish the mass of paracetamol per sphere: the number of spheres in the lump divided by the mass of paracetamol in a drop. The mass of paracetamol was then plotted against the mass of a single sphere, using the data gathered for the different bead sizes and against the size of the beads.

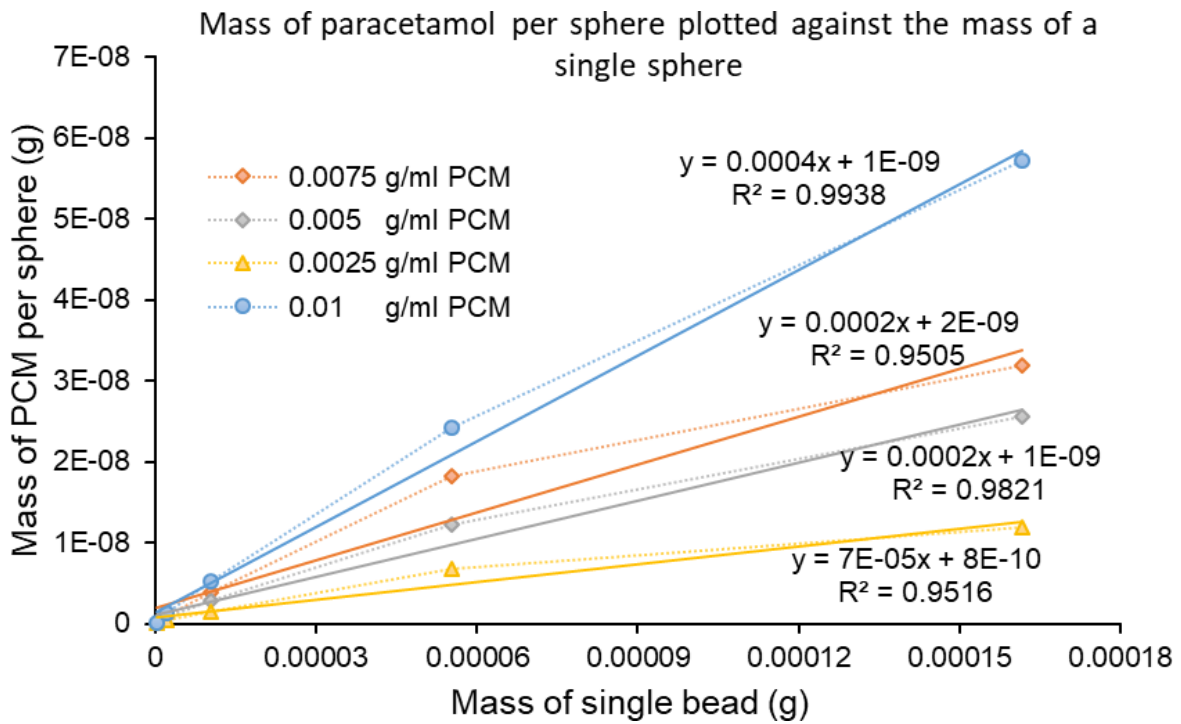


Figure 5-18 Mass of Paracetamol per sphere plotted against the mass of a single sphere

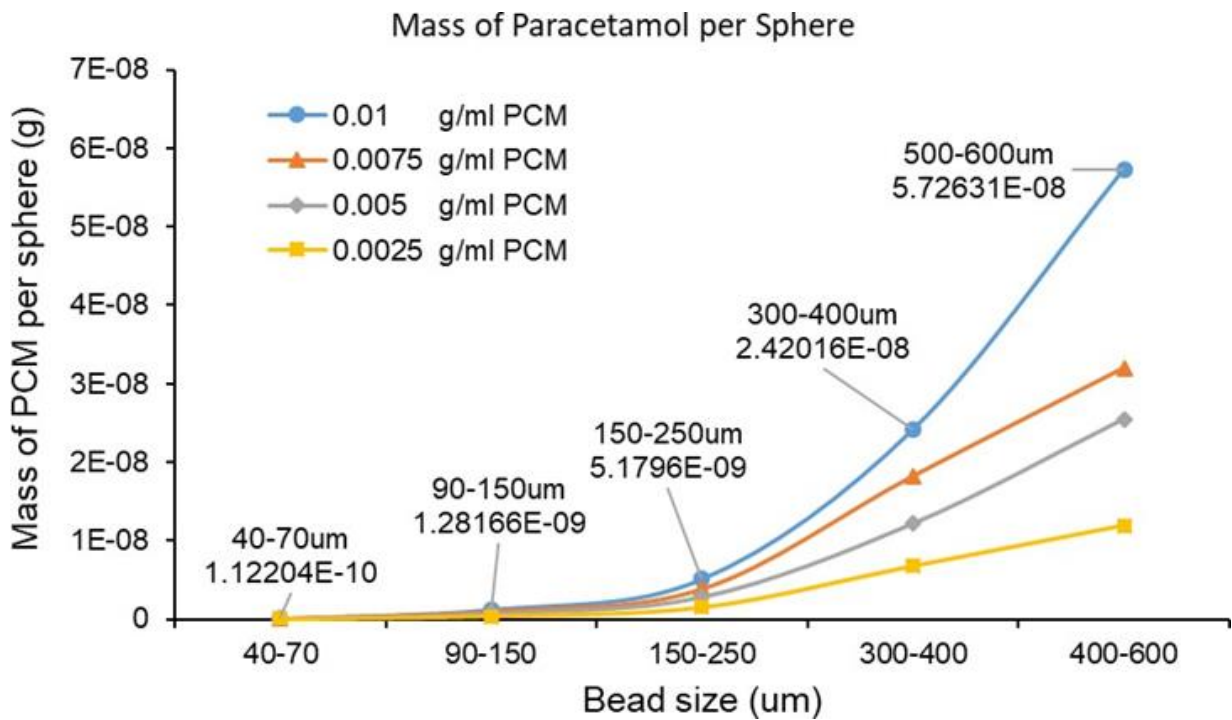


Figure 5-19 Mass of Paracetamol per sphere against the size of the beads

The graph in Figure 5-19 indicates that for a solution of 1 g PCM / 100mL, the mass of paracetamol deposited per sphere is 0.0004 times the mass of a single sphere. Based on a solution concentration of 0.01g PCM/mL, this is equivalent to saying that the solution mass per sphere is 0.04 times the mass of a single sphere. If the density of the paracetamol solution in methanol solution is estimated to be 0.8 g/mL and the density of the glass spheres is 2.5 g/mL, the liquid volume ratio would be 0.08 to 1, leading to 0.1 mL of solution forming a 1.25 cm³ agglomerate. This value is consistent with the size of the agglomerates created, as shown in Figure 5-20.



Figure 5-20 Glass Bead Agglomerate

Presuming the densest packing of uniform spheres, each sphere has 12 contacts and will have a 50 percent share in each bridge of material. Thus, the mass of an individual bridge may be estimated at $0.0004/6$ (i.e., $6.667E-5$) times the sphere mass. However, the glass spheres used during this project have slight variations in diameter and may not pack quite efficiently. Nevertheless, this is a starting point to reflect on the data. Figure 5-19 shows the mass of paracetamol plotted against the size of the beads. This shows how little material is needed to stick particles together, hence the widespread problem of lump formation drying.

5.4 Conclusion

The investigation results in this work indicate that agglomeration is not only affected by the amount of dissolved material in the residual solvent but also by particle size.

Agglomeration and Particle Size: The investigation found that particle size plays a significant role in agglomeration. An increase in particle size can lead to larger agglomerates. However, larger agglomerates are more fragile because they have fewer solid bridges between particles compared to smaller particles.

Inter-Particle and Capillary Forces: Smaller particles tend to form hard agglomerates because inter-particle and capillary forces are more dominant for them. These forces create strong bonds between particles, resulting in smaller and more robust agglomerates.

Effect of Concentration: Agglomerate formation is influenced by the concentration of dissolved material (PCM) in the solvent. Higher PCM and lactose concentrations can lead to more robust agglomerates as there is more dissolved material available to form solid bridges as the solvent evaporates during drying. On the other hand, reducing the PCM concentration can lead to the formation of large agglomerates, especially when the viscosity of the solution decreases due to a decrease in solute concentration. However, there is also evidence that agglomerates become larger by increasing the concentration as in the case of lactose.

The result indicating the minimum mass of paracetamol (i.e 0.0025 g/ml) needed to form an agglomerate is valuable information to support the design of filter cake-washing processes to avoid agglomeration.

5.5 References

Am Ende, D. *et al.* (2013) ‘Development and Application of Laboratory Tools To Predict Particle Properties upon Scale-Up in Agitated Filter-Dryers’, *Organic Process Research & Development*, 17(10), pp. 1345–1358. doi: 10.1021/op400080x.

Birch, M. and Marziano, I. (2013) ‘Understanding and Avoidance of Agglomeration During Drying Processes: A Case Study’. doi: 10.1021/op4000972.

Dopfer, D. *et al.* (2013) ‘Adhesion mechanisms between water soluble particles’, *Powder Technology*. Elsevier, 238, pp. 35–49. doi: 10.1016/J.POWTEC.2012.06.029.

Feng, Q. *et al.* (2020) ‘Effect of particle size and concentration on the migration behavior in porous media by coupling computational fluid dynamics and discrete element method’, *Powder Technology*. Elsevier, 360, pp. 704–714. doi: 10.1016/J.POWTEC.2019.10.011.

Hidayanto, E., Tanabe, T. and Kawai, J. (2010) ‘MEASUREMENT OF VISCOSITY AND SUCROSE CONCENTRATION IN AQUEOUS SOLUTION USING PORTABLE BRUX METER’, *BERKALA FISIKA*. Edited by G. Balint *et al.* Uniwersytet Śląski. Wydział Matematyki, Fizyki i Chemii, 13(2), pp. 23–28. doi: 10.2/JQUERY.MIN.JS.

MODDE® - *Design of Experiments Software / Sartorius* (no date). Available at: <https://www.sartorius.com/en/products/process-analytical-technology/data-analytics-software/doe-software/modde> (Accessed: 26 August 2022).

Seville, J. P. K., Willett, C. D. and Knight, P. C. (2000) ‘Interparticle forces in fluidisation: a review’, *Powder Technology*. Elsevier, 113(3), pp. 261–268. doi: 10.1016/S0032-5910(00)00309-0.

Xue, L., Guo, X. and Chen, H. (2020) ‘Basic theory’, *Fluid Flow in Porous Media*. WORLD SCIENTIFIC, pp. 47–67. doi: 10.1142/9789811219535_0002.

Chapter 6: Transport of residual moisture during drying

This chapter explains the investigation of moisture transport through wet cake during static drying. For this work, a model system of glass beads was selected. The main aim of this work was to investigate the effect of the transport of residual moisture on agglomeration. Transport of different solvent systems (water and methanol) was explored with PCM and blue dye (for visual observation). The results illustrate that for the methanol/PCM system, the dye and the PCM show similar transport behaviours and remain confined in agglomerate. In contrast, the water/PCM system shows contradictory results. Due to this obverse behavior, the effect of the water system with different solute Potassium hydrogen L tartrate (PHL-t) and solvent compositions (methanol-water) was studied. Moreover, the wetting behavior of water with PCM and glass beads was explored.

6.1 Aims and Objectives

The main objective of this work was to analyse the interaction and transport of the residual moisture with API during drying. The work was done to investigate the transport of dissolved API along with a dye, which was added for visual tracking, and their role in the agglomerate formation. The effect of various solvent compositions and the wetting behaviour of solvents with API and glass beads were also studied. The particle surface of glass beads, the wetting behaviour of glass beads, and both solute and solvent effect on moisture transport during drying were explored.

6.2 Materials and Methodology

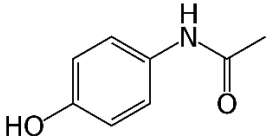
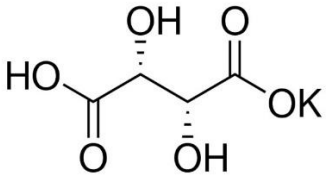
6.2.1 Materials

Materials were the same as described in section 5.2.1. The concentration of PCM and dye in each sieved fraction and the residual lump was measured using high-pressure liquid chromatography (HPLC) and Ultraviolet-visible (UV-VIS) spectroscopy. The eluents for HPLC were water (Ultrapure, HPLC Grade, purchased from Alfa Aesar UK) and methanol (ultrapure, HPLC grade, purity > 99.8%, purchased from Alfa Aesar UK). Laboratory-grade water was also used to wash the sieved fractions and residual lump to prepare the sample for HPLC and UV-Vis analysis.

For investigating the wetting effect relative to the transport mechanism, another solute in

addition to PCM, Potassium hydrogen L tartrate (PHL-t), was selected. The potassium hydrogen L tartrate grade selected was chosen to have a similar particle size distribution compared to powdered PCM, as shown in Table 6-1.

Table 6-1 Particle size distribution of PCM and PHL-t

Material	X ₅₀ (um)	SMD (um)	Molecular structure
Paracetamol	64.03	46.35	
Potassium hydrogen L tartrate	57	41	

*SMD: The Sauter mean diameter (SMD) is defined as the diameter of a sphere that has the same volume/surface area ratio as a particle of interest.

*X₅₀ refer to the particle size at which 50% of the particles are smaller and 50% are larger. It's a metric used to describe the distribution of particle sizes in a sample.

6.2.2 Methodology

The sample preparation methodology was the same as in 4.2.1. HPLC and UV- Vis analysis was performed to evaluate the concentration of PCM and dye in sieved fractions, residual lumps and non-agglomerated beads to investigate the relative transport of PCM and dye with residual solvent. After observing the unexpected wettability behavior of water (Figure 6-3, Figure 6-4, and Figure 6-5), a set of experiments were performed using different solvent mixture compositions of water with methanol and different dissolved solutes. Finally, the wetting behavior of API and dye with water was investigated using the Washburn method.

6.2.2.1 High-pressure liquid chromatography (HPLC)

HPLC is an analysis technique which separates and detects different substances mixed in a solution. (Karger, 1997)(Karger, 1997)(Karger, 1997)(Karger, 1997)(Karger, 1997)(Laux, 2019). The quantity of PCM in each sieved fraction and in the residual lump after sieving was determined using an Agilent 1260 Infinity II system containing a diode array detector was used. The column used was an Agilent Poroshell 120 EC-C18 4.6 x 100mm 4µm operated at 40°C,

with a 1mL/min flow rate. The injection volume was 5 μ L, the absorbance wavelengths were 243 and 230.5 nm, and the mobile phase was 80:20 water and methanol, respectively. The sample preparation for HPLC analysis is explained in section 6.3.2.

6.2.2.2 Ultraviolet-VIS spectroscopy

Patent V Blue dye was used to visualize solvent transport through the powder bed during drying. The amount of dye in each fraction was measured using the same solution samples prepared for HPLC. The wavelength for quantifying the blue dye was fixed at 633 nm, corresponding to the absorbance curve's peak. Based on a simple calibration, each sample's absorbance was then used to calculate the relative amount of dye, the dilution factor was multiplied by the absorbance, and that result was divided by the mass of the glass spheres.

6.2.2.3 Washburn method

Washburn (1921) developed a technique to measure porous material's contact angle and surface energy by penetrating liquid into the solid material. The most common setup for Washburn capillary rise method is to use a glass tube containing filtration frit or any other porous media at the bottom, filled with the material of which the contact angle is to be measured (Figure 6-1). This tube is then immersed in the test liquid. The penetration of the fluid into the solid is due to capillary rise.

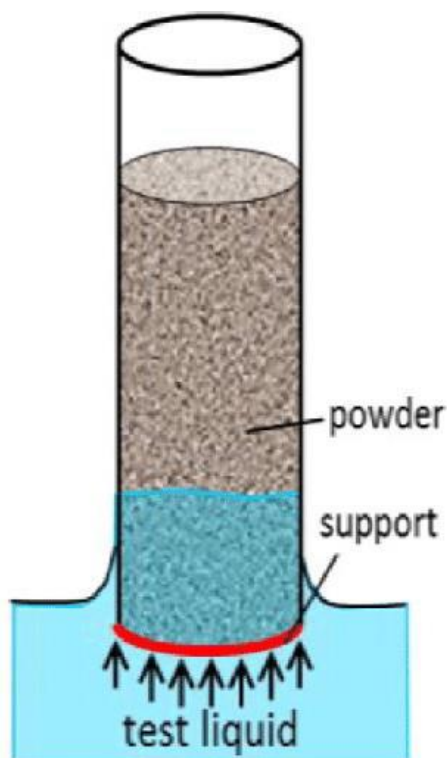


Figure 6-1 Simplified setup for Washburn capillary rise method (Meng et al., 2017)

The contact angle of glass beads with a saturated aqueous solution with solutes was measured using the Washburn technique. Approximately 5 g of glass beads were added to a 5ml borosilicate glass tube with an inner diameter of 0.9 cm. the bottom of the tube was impeded with glass fibre to block the glass beads within the tube and to enhance the laminar flow of the solvent to the glass beads.

For the Washburn setup, a Sartorius Quintix balance (analytical balance YPK03) was connected to a computer and transferred the recorded mass over time to Microsoft Excel software. Then, the sample holder and scaffolding were set up using the Sartorius density measurement kit, YDK01LP, as shown in Figure 6-2. Then, the sample material in the tube was brought into contact with the saturated solution. The increase in the tube mass was recorded every second until the liquid reached the top of the material.

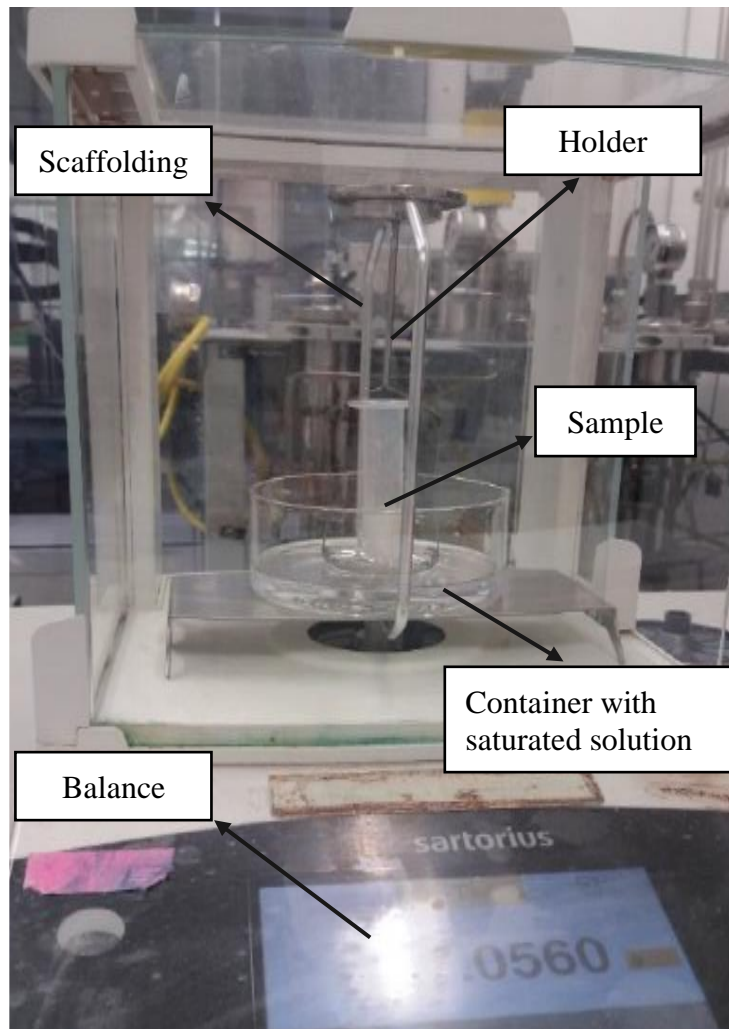


Figure 6-2 Washburn capillary rise setup utilizing Sartorius balance and density measurement kit (Pedussaut, 2018)

6.3 Results and discussions

6.3.1 Investigation of relative transport of PCM and dye during drying

The sample preparation for the quantification of granule formation as a function of solubility in residual lump (section 4.2.1) with different solvents, i.e., water and methanol, showed different behaviour of moisture transport. The methanol/PCM system showed that the PCM and dye were constricted to the lump formed by wetting the glass beads with the solution. However, for the water/PCM system, the dye seems to be dispersed out in the loose beads towards the wall upon wetting (Figure 6-3).

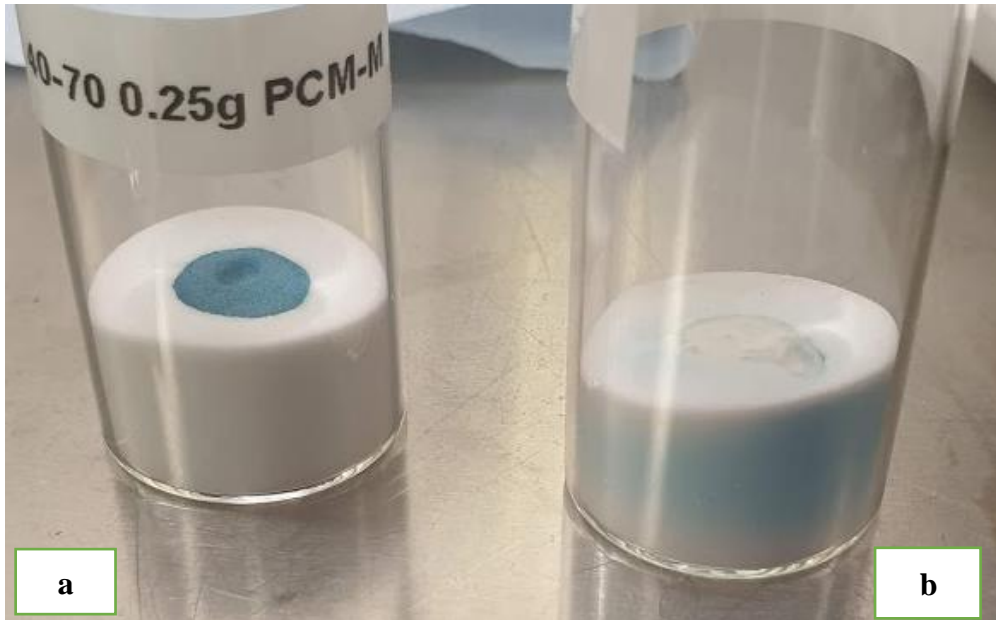


Figure 6-3 (a) PCM/Methanol system (PCM and Dye confined within the lump) (b) PCM/ water system (Dye spread out in the loose beads towards the wall)



Figure 6-4 Dried sample PCM/Water system (a) dye dispersed in the loose beads transporting towards the wall (b) agglomerate formed free from dye

The same behaviour was observed with the carbohydrates by using methanol as a solvent, all the solute and dye concentrated within the lump, while with water, the dye was transported towards the walls as shown in following Figure 6-5 and Figure 6-6.

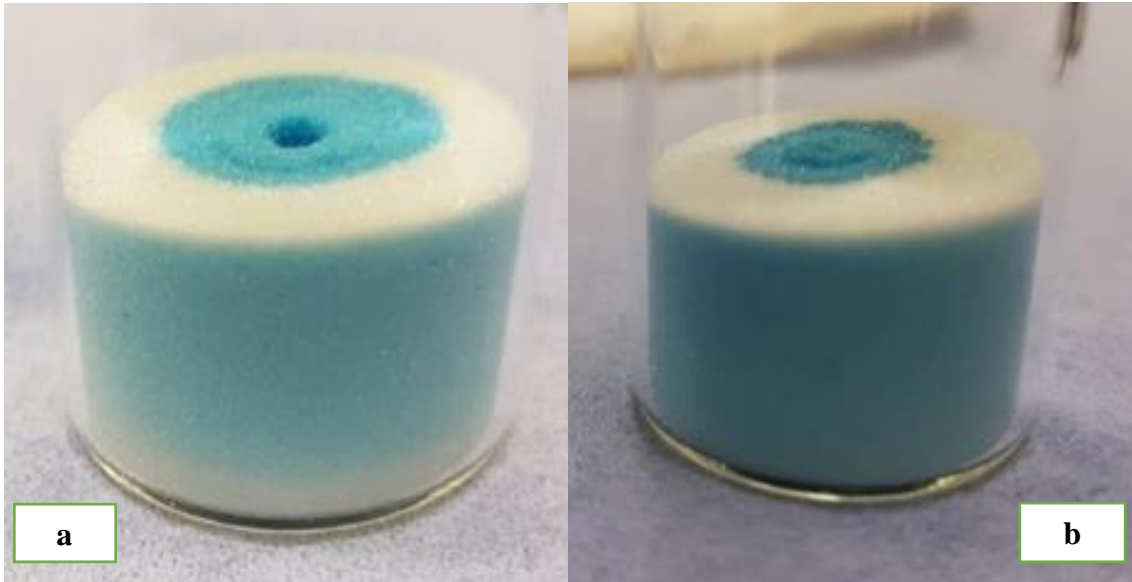


Figure 6-5 (a) Fructose/Water system (b) Lactose/water system

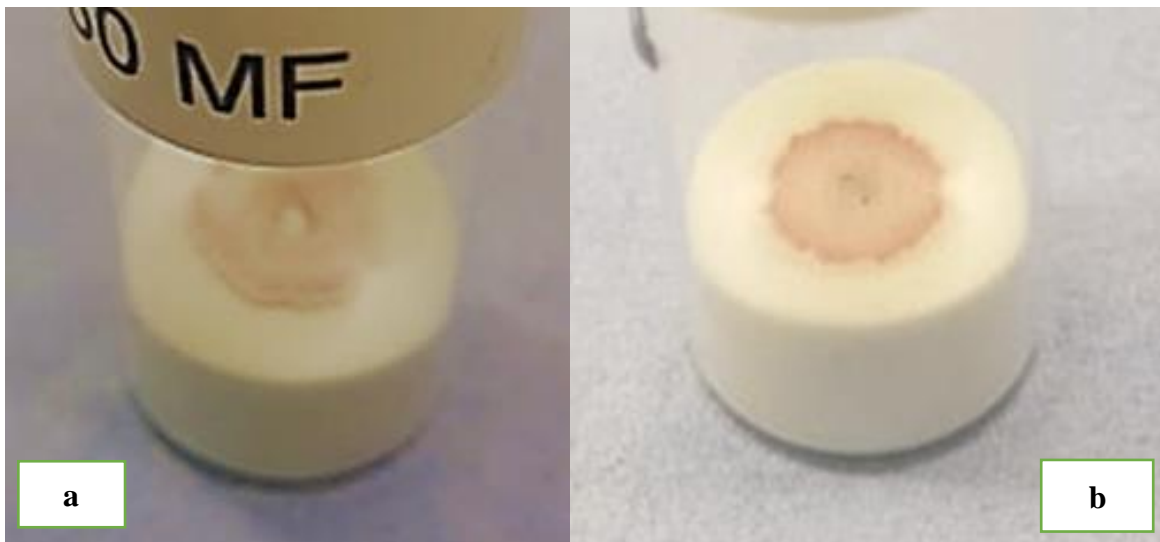


Figure 6-6 (a) Fructose/Methanol system (b) Lactose/Methanol system

To confirm the visual observations that the dissolved PCM and dye in water (Figure 6-3) do not follow the relative transport to each other as in the case of methanol, HPLC and UV-Vis analyses were performed. The concentration of PCM was determined by using HPLC, and the dye concentration was measured by UV-Vis spectroscopy, as HPLC did not detect its peak. The concentration was measured in the loose beads obtained within the bottom pan after hand sieving of the samples, each sieved fraction (as four cycles of sieving were performed for each agglomerate, section 4.2.2.2) and the lump retained after four cycles of sieving.

6.3.2 HPLC analysis

HPLC was used to measure the concentration of paracetamol in the sieved fractions obtained after each cycle of sieving, the loose beads collected in the bottom pan after manual tapping, and the residual lump retained after sieving. HPLC-grade water (Table 6-2) was used to dissolve the deposited paracetamol from each fraction of the collected glass spheres. The resulting solutions were taken from the vial using a syringe and filtered using a PES syringe filter (Fisher brand, CAT No. 15206869. 0.2um pore size, sterile) to prepare samples for HPLC analysis.

Table 6-2 Quantity of water used for HPLC Sample preparation.

Components	Volume of water (mL)
Loose beads after manual tapping	5
Glass beads after each cycle of sieving	2
Residual lump after sieving	2

The calibration curve for paracetamol with the constants of the linear function is shown in the graph in Figure 6-7.

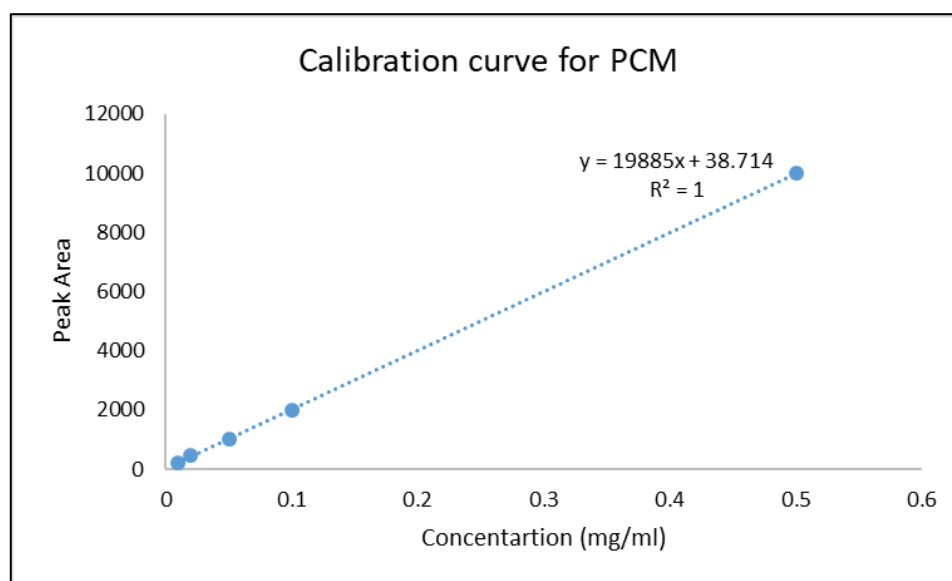


Figure 6-7 Calibration curve of paracetamol

To calculate the concentration with the area, the slope, and the intercept:

$$C = (area + b)/a \quad \text{Equation 6-1}$$

With

a = 19885 and

b = 38.714

Table 6-3 Results of the HPLC analysis for Methanol/PCM samples

Sample	Area (mAU*s)	Measured PCM concentration (mg/ml)
Residual lump (S0)	7832.7	0.3958
Loose beads (S-1)	349.81	0.0195
1 st fraction (S1)	6242.948	0.3159
2 nd fraction (S2)	4251.62	0.2158
3 rd fraction (S3)	3021.96	0.1539
4 th fraction (S4)	2784.52	0.1420

The concentration calculated from HPLC analysis followed the visual observation. The loose beads have the least concentrated amount of paracetamol, which shows that the PCM remained within the lump formed and did not migrate into the loose glass beads as shown in Figure 6-3 a. The concentration is higher for the first cycle for the different samples from the agglomerates gathered after each cycle and keeps decreasing as the sieving goes by. The decrease mainly depends upon the mass of the sieving fraction. The first sieving fraction has a higher mass than the fourth because as the sieving proceeds, the lump becomes hard to break. This was also proved by the highest concentration of PCM in the residual lump. The predicted concentration was multiplied by the amount of solvent used for washing each

fraction and divided by the masses of each fraction to calculate the concentration of PCM in each sample (Figure 6-8).

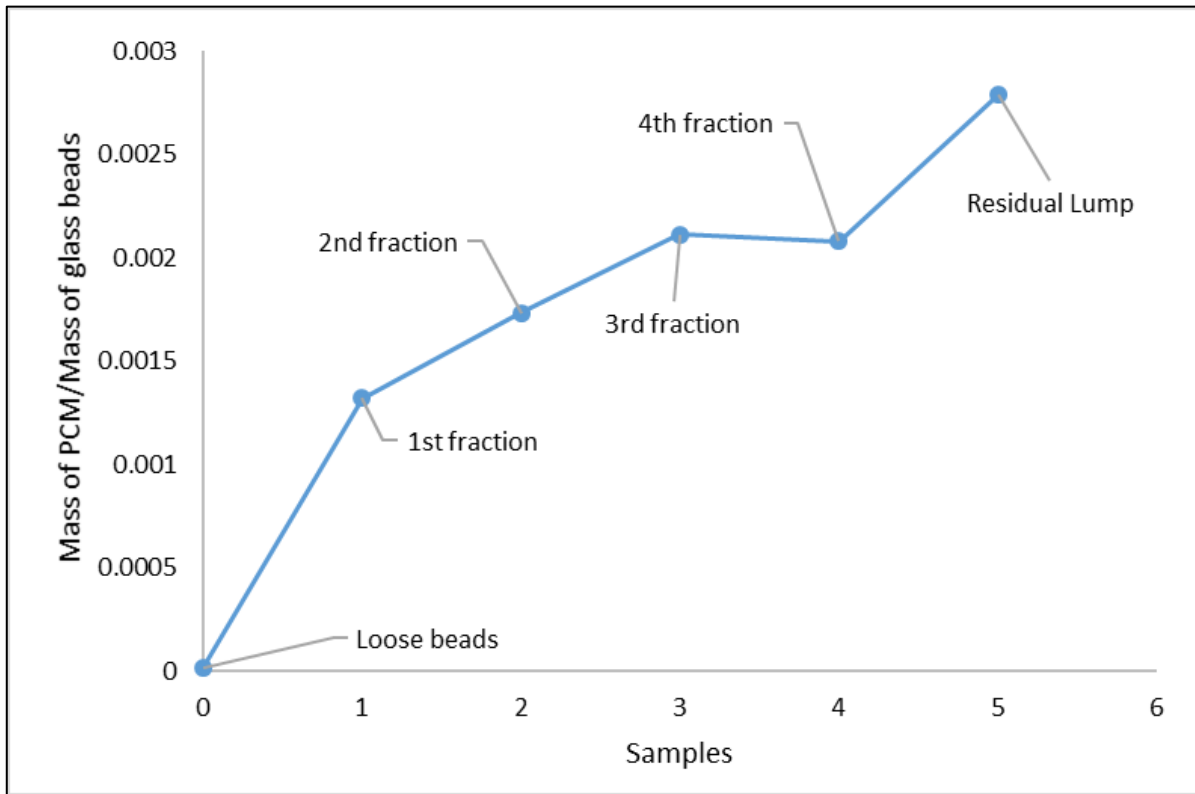


Figure 6-8 Concentration of Paracetamol in sieved fractions of PCM/Methanol Sample

The same procedure was performed for the PCM/water system. For the water system, some PCM was present in the loose beads (Table 6-4). The highest concentration was present in the first fraction of sieving, and the concentration decreased for subsequent sieving fractions. However, the most negligible concentration for the water system was observed in the residual lump, showing the PCM was not confined to the lump formed. Moreover, this relates to the solubility of PCM in water as PCM has low solubility in water, hence lower concentration available for creating solid bridges, making the lump fragile. As discussed in chapter 5 (section 5.3.2.2.), most of the PCM/water system lumps break during sieving cycles; hence, very little material is retained as a residual lump for the 0.01 g/ml solution sample.

Table 6-4 Results of the HPLC analysis for Water/PCM Samples

Sample	Area (mAU*s)	Predicted concentration (mg/ml)
loose beads	3485.08	0.1733
1st fraction	5205.49	0.2598
2nd fraction	877.7	0.0422
3rd fraction	456.83	0.0211
4th fraction	155.72	0.0059
residual lump	110.5	0.0036

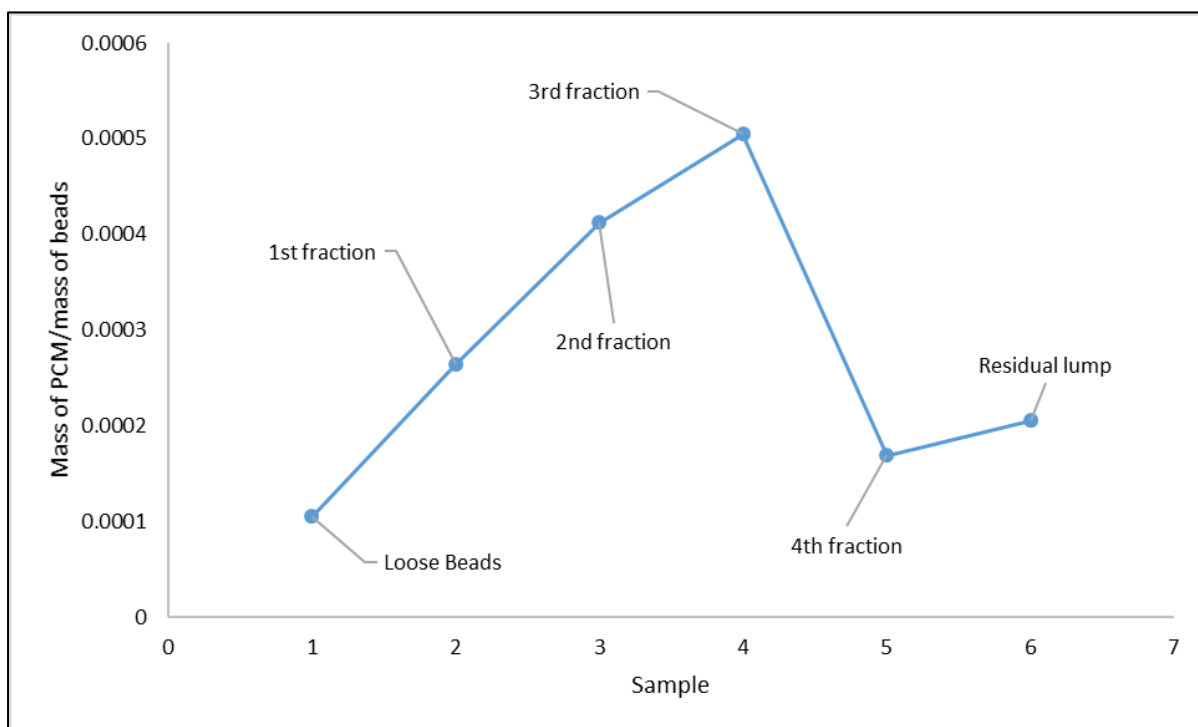


Figure 6-9 Concentration of Paracetamol in sieved fractions of PCM/Water Sample

6.3.3 UV-Vis Spectroscopy

Patent V Blue dye was used to visualize solvent transport through the cake during drying. The amount of dye in each fraction was then measured using UV VIS Spectrometry using the same samples prepared for HPLC.

The wavelength for quantifying the blue dye was fixed at 633 nm, corresponding to the absorbance curve's peak. The absorbance was then used to calculate the relative amount of dye, the dilution factor (amount of solvent used to wash glass beads of each fraction) was multiplied by the absorbance, and that result was divided by the mass of glass spheres to get the relative amount of dye in each fraction.

The calibration curve for the absorbance of blue dye in water with the constant of the linear function is shown in Figure 6-10.

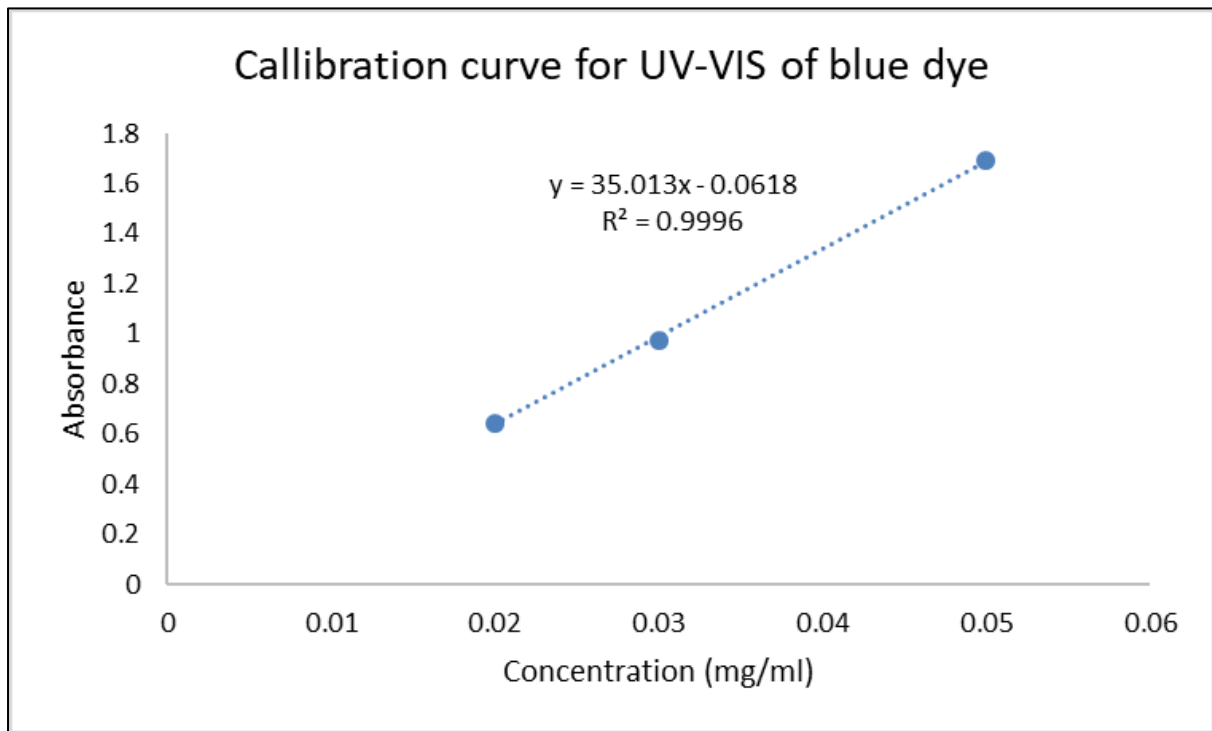


Figure 6-10 Calibration curve for blue dye

The results for the concentration of blue dye in each fraction followed the concentration of PCM (Figure 6-8 and Table 6-3). For the methanol system, the highest concentration was in a residual lump, as in the case of PCM. Similarly, for the water system, the highest concentration is in the first sieved fraction, which was contradictory to the visual observation (Figure 6-4) but follows the results of PCM concentration (Table 6-5 and Figure 6-9).

Table 6-5 Results of UV-VIs Spectroscopy for water and methanol

Sample	Methanol		Water	
	Absorbance	Predicted concentration (mg/ml)	Absorbance	Predicted concentration (mg/ml)
Loose beads	0.059	0.003	0.093	0.004
1 st fraction	0.259	0.009	0.101	0.005
2 nd fraction	0.195	0.007	0.045	0.003
3 rd fraction	0.154	0.006	0.044	0.003
4 th fraction	0.142	0.006	0.042	0.003
5 th fraction	0.327	0.011	0.045	0.003

The relative amount of paracetamol and dye was calculated to estimate the amount of dye and paracetamol in each fraction. Figure 6-11 and Figure 6-12 reports that the PCM and dye as dissolved species are transported together and broadly to the same extent. These are also in line with the graphs shown in Figure 6-8 and Figure 6-9, which confirm that the dye and PCM show relative transport during drying. However, the transport of dye and PCM in the loose beads towards the walls of the vials raised the debate about the wetting behavior of water with PCM and glass beads.

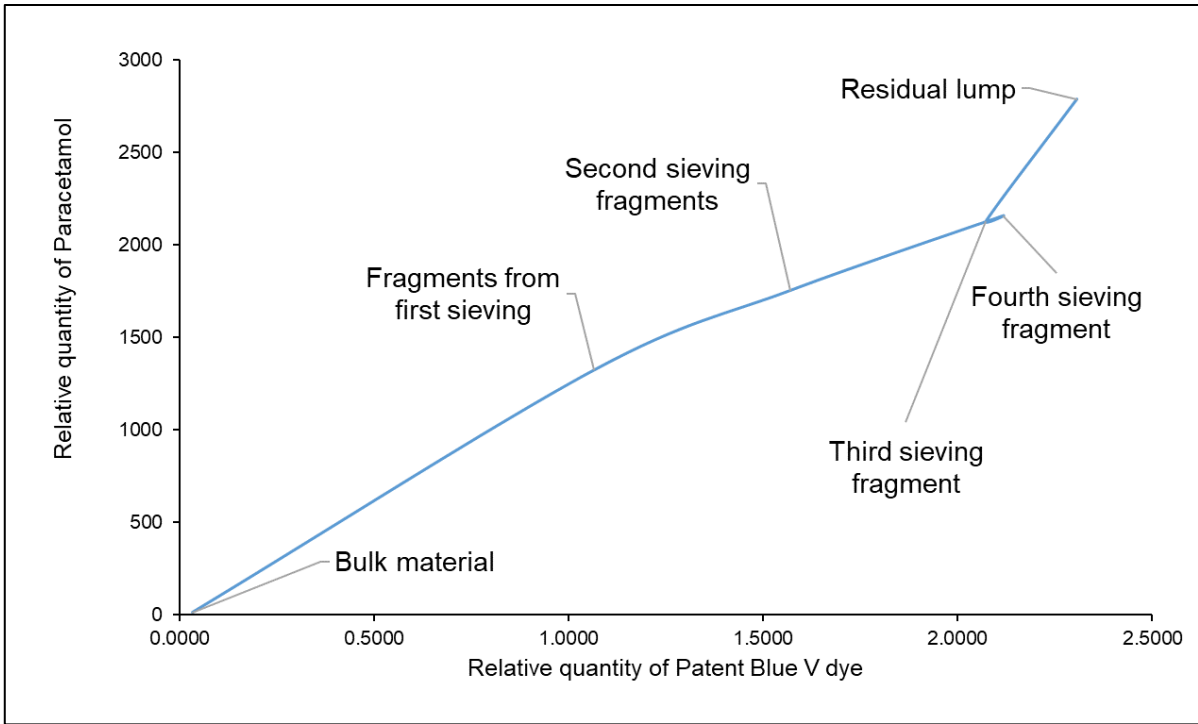


Figure 6-11 Relative amount of paracetamol plotted against the relative amount of dye for the Methanol system

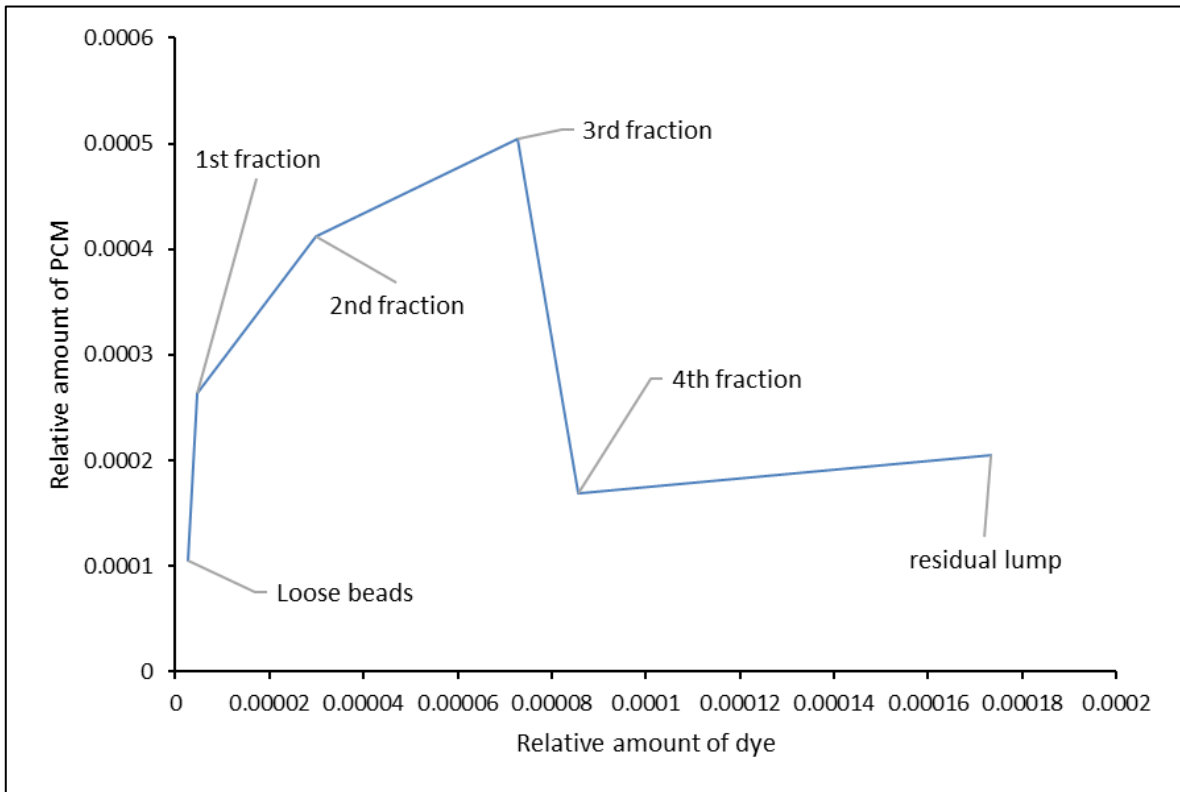


Figure 6-12 Relative amount of paracetamol plotted against the relative amount of dye for the Water system

6.3.4 Investigation of the wetting behaviour of water

Various experiments were performed to investigate the contradicting transport of PCM and dye with water compared to methanol.

6.3.4.1 Rewetting an already-dried sample

In this experiment, the sample was prepared by adding 0.0025 g/mL PCM/Water solution to the glass bead substrate and left for drying for 24 hrs. Figure 6-13 shows the dried sample after 24 hr. After drying, the sample was rewetted with the same solution and left for another 24 hr for drying. The primary purpose of this experiment was to observe whether the dissolved PCM and blue dye followed the same path after rewetting the dried sample. After observing the dried lump and rewetting the dried sample by adding the drop of the solution by following the same procedure as mentioned above (Figure 6-17), it was concluded that dissolved PCM and dye followed the same transport profile, the top of the lump was white, i.e. free of dye, and the dye was transported towards the bottom of the vials. However, it seems that the dye was already transported towards the walls during the first wetting and drying of the sample; after rewetting and drying, the blue dye remains at the bottom of the lump, leaving the upper surface of the lump free of dye (Figure 6-17).

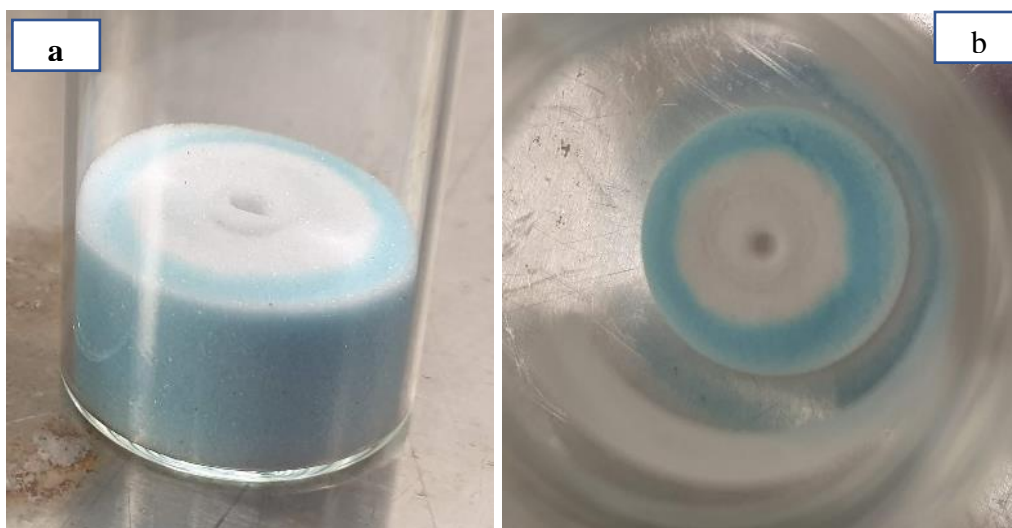


Figure 6-13 Dried samples (90-150 um glass beads) wetted with 0.0025g/ml PCM/Water solution (a) side view (b) top view

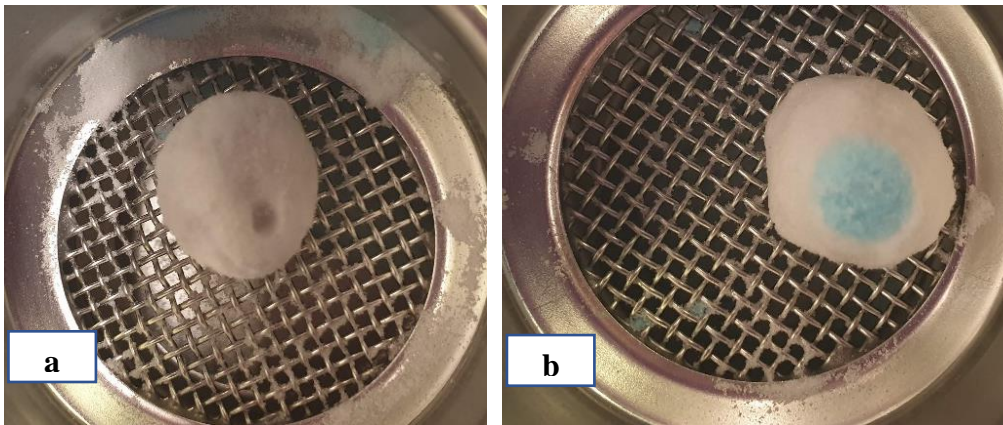


Figure 6-14 Lump created after first wetting (a) the top side of the lump (b) the bottom side of the lump

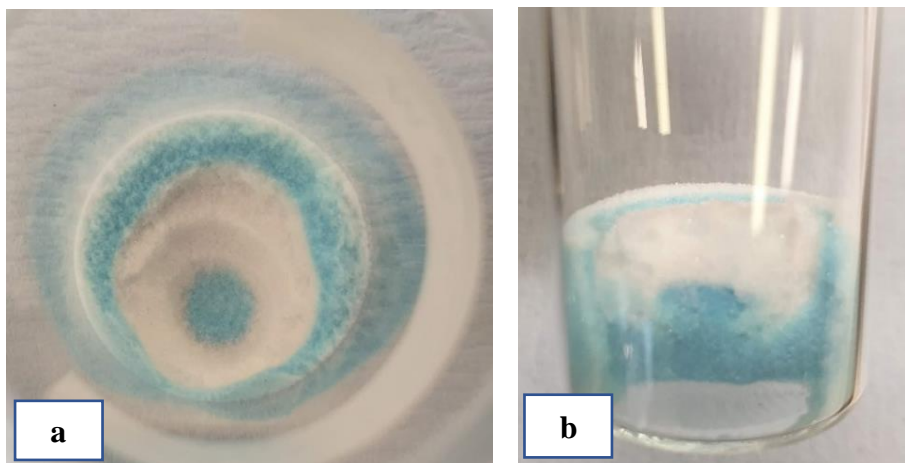


Figure 6-15 Vial with loose beads after removing the lump created by first wetting (a) top view (b) side view with half of the material removed

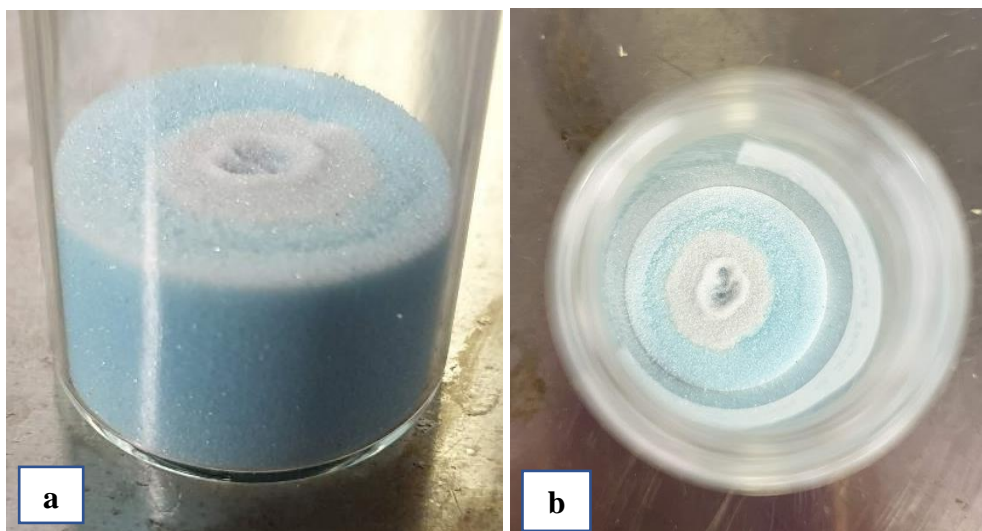


Figure 6-16 Dried samples (90-150 μm glass beads) rewetted with 0.0025 g/ml PCM/water solution (a) side view (b) top view

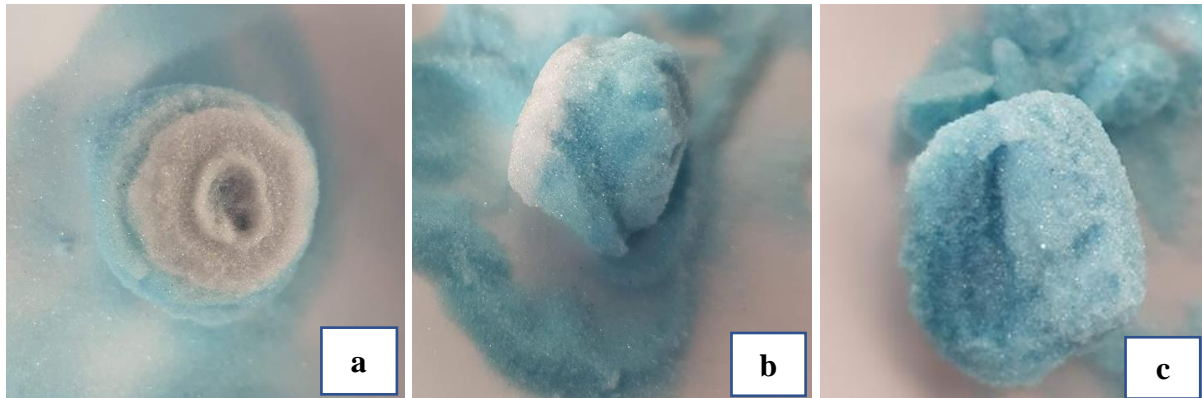


Figure 6-17 Lump created after rewetting (a) top side of lump (b) side view of the lump (c) bottom side of the lump

This transport behaviour of dissolved PCM and dye may be due to the wetting behaviour of PCM with water. Heng and Williams (2006a, 2006b) studied the wettability of PCM with water. Their work shows that the different facets of PCM show different wetting behaviour. Their results showed that different faces of PCM form I have the following hydrophilicity order:

$$(001) > (011) > (201) > (110) > (010)$$

This wetting behaviour depends on the OH group available to form hydrogen bonding. This wetting behaviour of PCM was confirmed by Todorova and Delley (2008). They determined PCM forms I and II hydrophilicity by using the COSMO approach. Their result was similar to Heng et al. according to their results, the hydrophilicity order for PCM form I is:

$$(001) > (201) > (011) > (110) > (010)$$

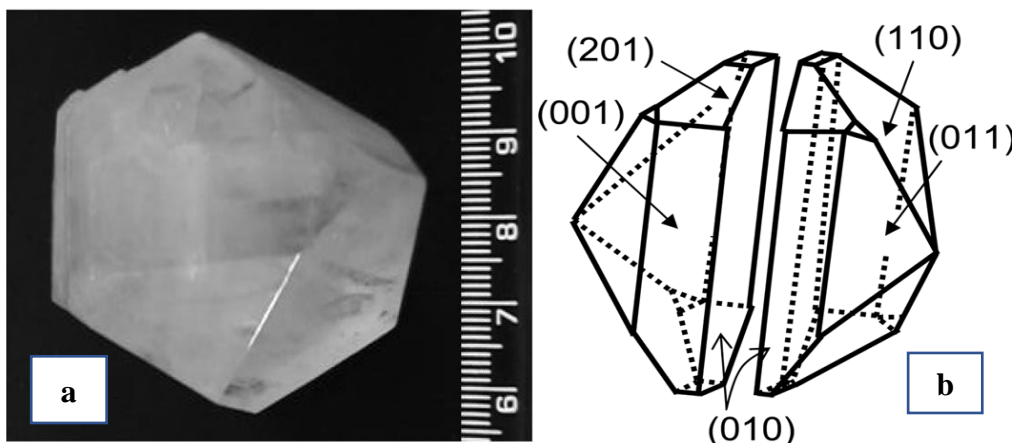


Figure 6-18 (a) Single large crystal of PCM (b) Crystal habit of PCM form 1 (Heng et al., 2006)

From the results of their work, it can be concluded that depending on which facet of PCM

formed a bond with water, some of the PCM stayed in the lump formed, and some were transported along with water. The contact angles of different facets of PCM measured by Heng et al. are listed in Table 6-1Table 6-6.

Table 6-6 Advancing and Receding angle of PCM form I with water

Facets of PCM form I	Advancing angle (θ_A)	Receding angle (θ_R)
(201)	38.1 ± 4.6	22.6 ± 3.6
(001)	15.9 ± 3.1	0
(011)	29.8 ± 5.7	23.7 ± 6.0
(110)	50.8 ± 4.9	17.5 ± 3.0
(010)	67.7 ± 2.5	26.4 ± 4.5

6.3.4.2 PCM and dye transport in binary mixtures of water and Methanol

In this experiment, glass beads were wetted with different compositions of binary mixtures of water and methanol solution containing the same concentration of blue dye (100:0, 75:25, 50:50, 25:75, 0:100, respectively). This experiment's primary purpose was to investigate PCM's transport in binary mixtures and to observe whether the PCM solution transported towards the walls with binary mixtures as in the case with water.



Figure 6-19 Glass beads wetted with different compositions of water & methanol solution (at the start of the Experiment)



Figure 6-20 Dry samples of glass beads wetted with different compositions of water & methanol solution (after completion of the experiment)

From Figure 6-20, it is clear that with the increasing concentration of methanol, the transport of dissolved material is reduced, and when no water is present, the dye is retained within the lump. This behaviour is due to the wetting behaviour of the PCM aqueous solution, as described in section 6.3.4.1. In principle, viscosity may also play a part in the transport of the solutions. In her work, Singh (2022) reported that the viscosity of aqueous PCM solutions is less than the binary mixture of Methanol and water. She also mentioned that as the percentage of methanol increases, the viscosity of the solution increases. In this study, the solutions are relatively dilute, and the role of viscosity is likely to be minor.

6.3.4.3 Experiments with different solutes

The next set of experiments was performed to investigate the wetting behaviour of aqueous solutions with another solute in addition to PCM. For this purpose, Potassium hydrogen-L-tartrate (PHLT) was selected. 40-70 μm glass beads were wetted with decreasing PHLT and PCM solution concentrations in water, starting from 0.01 g/mL to 0 g/mL. Figure 6-21 confirms that the water has a different wetting behaviour for both solutes. From this experiment it was decided to further investigate the contact angle measurement of PCM solution with glass beads. The sample without dissolved solute also shows that water with only blue dye completely wets the glass beads. This confirms that the transport profile observed with PCM/water samples ultimately depends on the wetting behaviour of PCM and water.

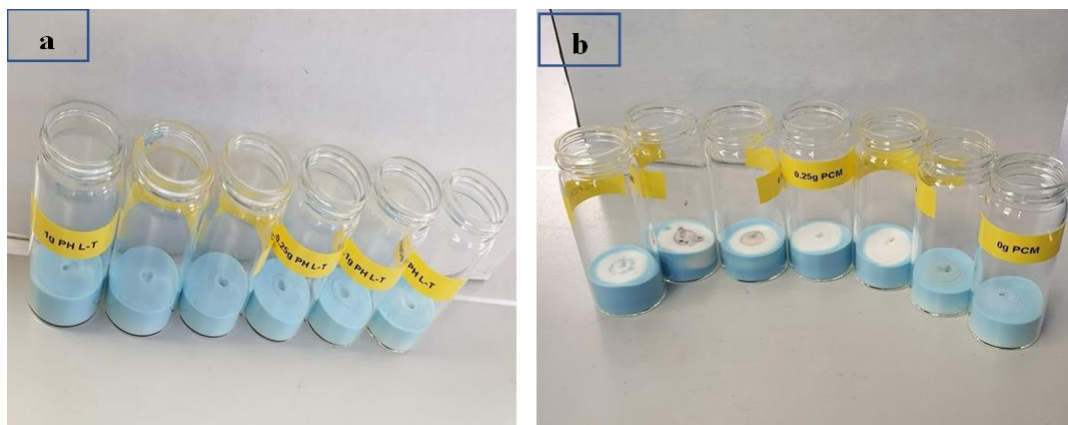


Figure 6-21 (a) Decreasing concentration of PHL-t (b) Decreasing Concentration of PCM

Experiments on microscopic slides

Another experiment was performed to investigate the wetting behaviour of water further. In this experiment, a layer of PCM powder and PHLT powder was formed on a microscopic slide, and a drop of pure solvent (water) was added to the slide to observe the wetting behaviour of the water. Blue dye was added to keep track of moisture transport.

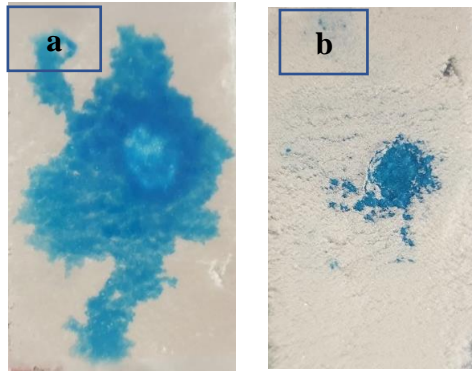


Figure 6-22 Paracetamol powder wetted with water (a) bottom side of the slide (b) top side of the slide

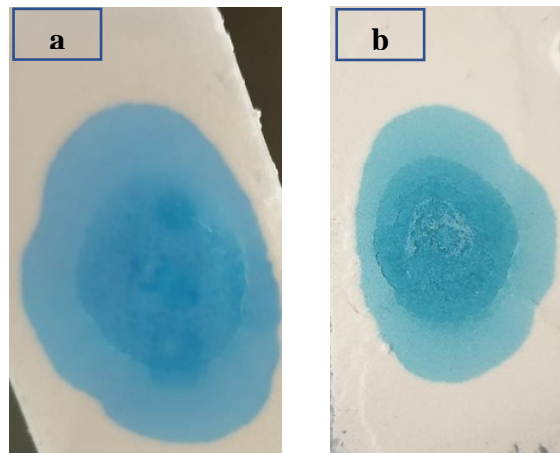


Figure 6-23 PHL-T powder wetted with water (a) bottom side of the slide (b) top side of the slide

From Figure 6-22 (a), it is clear that water tends to wet the glass surface of the slide instead of the Paracetamol powder (Figure 6-22 b). While water completely wets PHL-T powder (Figure 6-23).

6.3.5 Washburn Method

From the discussion in the previous sections, it is concluded that the wetting behaviour significantly influences moisture transport during drying. The contact angle was calculated by using the Washburn method for the materials listed below:

- Powdered PCM
- Granular PCM
- PHL - t
- PCM coated beads
- PHL-t coated beads
- Dried sample beads
- Beads from 1st sieving fraction

Coated beads preparation

For PCM and PHL-t coated beads saturated solutions of respective solutes were prepared with water and then sprayed on the glass beads using a spray bottle and dried. After drying a layer of solid material was coated on the glass beads.

Dried sample beads

To get dried beads, the sample was prepared using glass beads and 0.01g/ml PCM/water solution to create a lump, and then sieving was performed. After completing four cycles of sieving, the separated material was used to perform a Washburn experiment with a water/blue dye solution.

Beads from 1st sieving cycle

The sample was prepared using glass beads and 0.01g/mL PCM/water solution to create a lump, and then sieving was performed. The fraction after the 1st cycle of sieving was collected, and then the Washburn capillary rise method was performed using water and a saturated solution of PCM/water.

The data obtained from the Washburn method is inconsistent, as shown in Figure 6-24. This problem was already addressed in the work of previous students in Prof. Price's research group (Irvine, 2016; Pedussaut, 2018; Setter, 2019). So, the K value for each repeat is calculated, and the range of the K value is given in Table 6-7. (For the graph of each solute, see Appendix B)

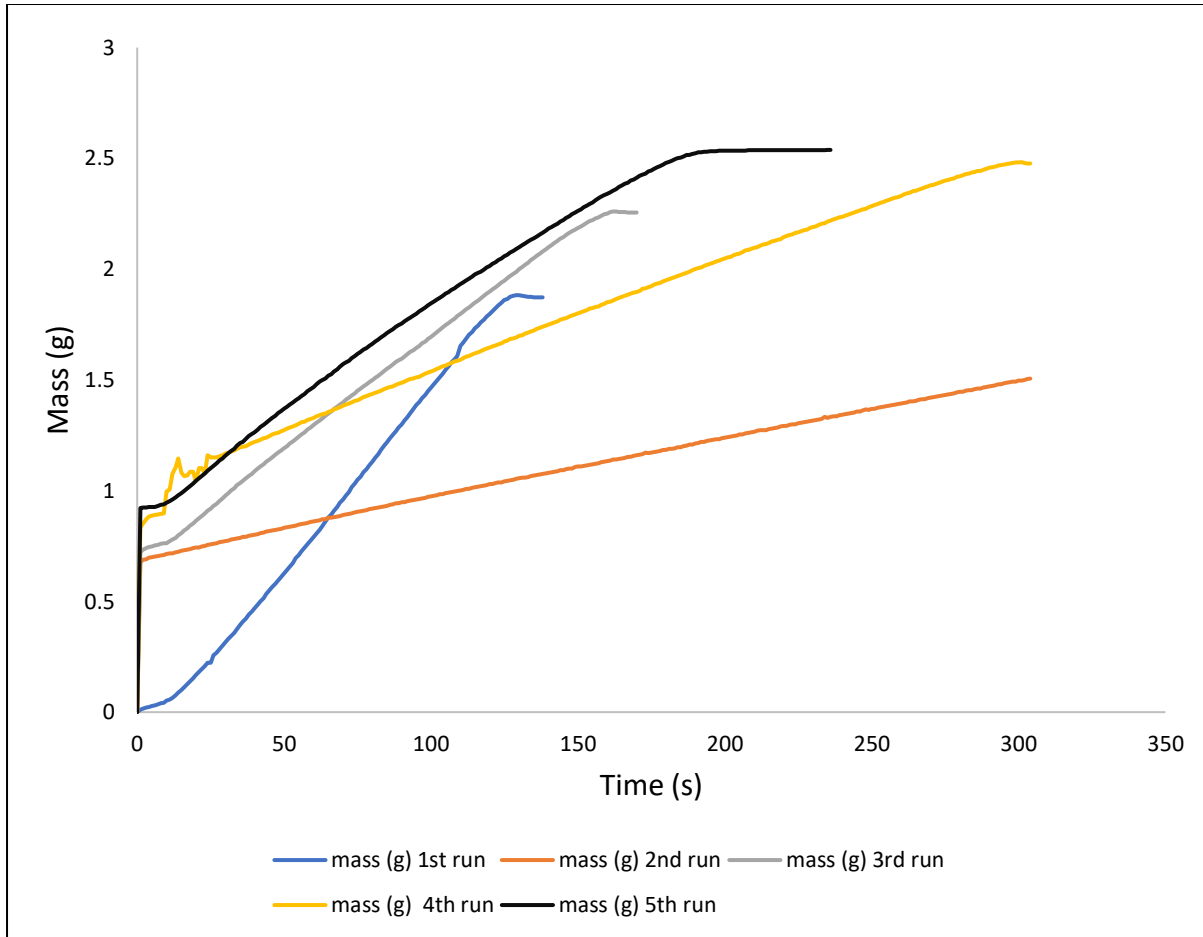


Figure 6-24 The mass vs time interparticle capillary rise of water and dye solution in PCM-coated glass beads compacted by tapping for 100 - 300 seconds

Firstly a geometric factor K needs to be calculated by assuming that the solvent is completely wetting the solute ($\cos \theta = 1$) using Equation 6-6 (Irvine, 2016). K values calculated for all materials are listed in Table 6-7.

$$k = \frac{m^2 \cdot \mu}{\rho^2 \cdot \gamma_L \cdot t} \quad \text{Equation 6-2}$$

Where,

m^2 is the squared mass of the liquid rise in the tube (Kg^2),

t is the time taken by the liquid to rise (sec),

μ is the viscosity ($\text{N}\cdot\text{s}/\text{m}^2$),

ρ is the density of the liquid (kg/m^3),

γ_L is the surface tension of the liquid (N/m).

Table 6-7 K- value Results

Material	K (m ⁵) * 10 ⁻²¹	Average K (m ⁵) * 10 ⁻²¹
Powdered PCM	350 - 40670	41000
Granular PCM	1710 - 2063	37700
PHL-t	13320 - 36620	43900
PCM coated beads	102500 - 2.773	38000
PHL-t coated beads	0.6553 - 2.159	2.81
Dried sample beads	730600 - 741800	14700
1 st sieving fraction beads	0.3637 - 1.244	1.61

After getting the k values, the contact angle is calculated by Equation 6-7, derived from Poiseuille law (Irvine, 2016).

$$m^2 = k \frac{\rho^2 \gamma_l \cos \theta}{\mu} t \quad \text{Equation 6-3}$$

Generally, a single solute is tested against various solvents in the Washburn method. The solvent with the highest K value is selected as the reference for calculating the contact angle. In this study, a single solvent was used to investigate the contact angle of various solutes, so from Table 6-7, the highest K value was for dried sample beads, so the K value of dried beads was used as a reference for the calculation of contact angle of the rest of the solutes.

Table 6-8 Contact angles of different solutes with water/dye solution

Material	Contact angle θ (°)
Powdered PCM	86.81 - 89.97
Granular PCM	73.85 – 84.49
PHL-t	65.22 – 79.65
PCM coated beads	68.05 -81.94
PHL-t coated beads	88.98 - 90
Dried sample beads	0
1 st sieving fraction beads	89.98 - 90

High values of contact angles (Table 6-7) proved that PCM solution was not wetting the glass beads properly. Moreover, the wetting of powdered and granular PCM showed that the solution only penetrated around the walls and did not penetrate the solid (Figure 6-25). This further confirms the wettability behaviour of PCM discussed in section 6.3.4.1.

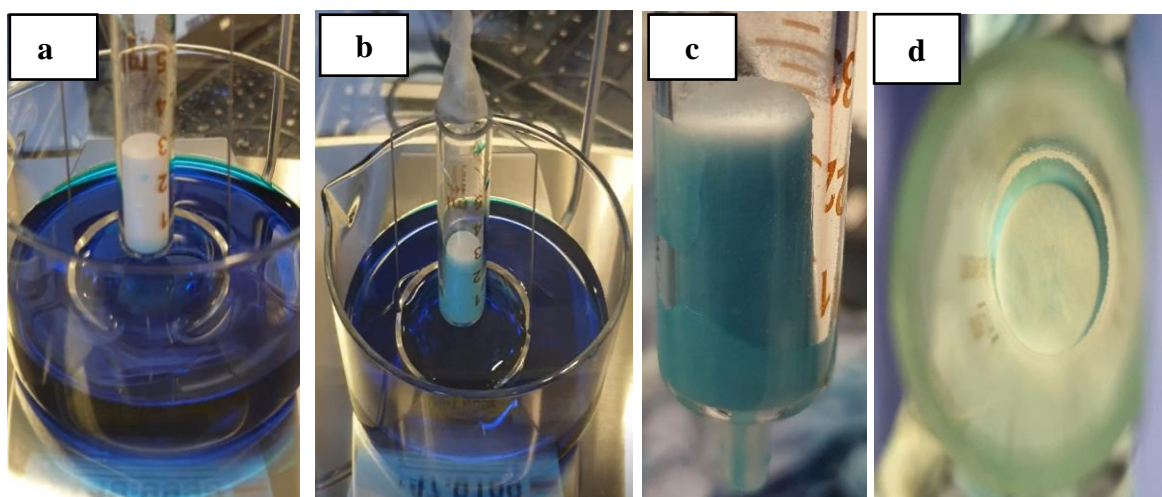


Figure 6-25 Washburn analysis for powdered PCM (a) start of experiment (b) end of experiment (c) top view of wetted sample (d) side view of the wetted sample

6.4 Conclusion

The results presented in this chapter indicate that the dissolved PCM and dye in water and methanol show similar transport behaviours. For the PCM/methanol system, the concentration of dissolved material remains confined within the lump, and the loose beads are free from PCM and dye. However, for the PCM water system, the blue dye tends to transfer towards the loose beads along with some concentration of PCM. This is due to the wetting behaviour of the aqueous PCM solution. Moreover, this phenomenon is likely to be influenced by the system viscosity. The viscosity of the PCM/water system is less than the PCM/Methanol system and binary mixtures of methanol. Due to low viscosity, the solutions tend to diffuse to a more considerable extent.

The wetting behaviour of aqueous PCM solution is influenced by the different levels of hydrophilicity shown by different faces of PCM. Some faces are hydrophilic, and some are hydrophobic; this leads to the idea that the hydrophobic faces displace the water molecules during transport and influence what is retained within the lump. In this case, a reduced concentration was retained within the lump, which was in accordance with the results of chapter 2, in which we concluded that the agglomerates created with the PCM/water system mostly break during the sieving as less material is available to form solid bridges.

Further investigation of water with methanol binary mixtures and different solutes also favors the effect of wetting in the moisture profile.

6.5 References

Heng, J. Y. Y. *et al.* (2006) ‘Anisotropic surface energetics and wettability of macroscopic form I paracetamol crystals’, *Langmuir*. American Chemical Society , 22(6), pp. 2760–2769. doi: 10.1021/LA0532407/ASSET/IMAGES/LARGE/LA0532407F00011.JPEG.

Heng, J. Y. Y. and Williams, D. R. (2006a) ‘Wettability of paracetamol polymorphic forms I and II’, *Langmuir*. American Chemical Society , 22(16), pp. 6905–6909. doi: 10.1021/LA060596P/ASSET/IMAGES/MEDIUM/LA060596PN00001.GIF.

Heng, J. Y. Y. and Williams, D. R. (2006b) ‘Wettability of paracetamol polymorphic forms I and II’, *Langmuir*. American Chemical Society , 22(16), pp. 6905–6909. doi: 10.1021/LA060596P/ASSET/IMAGES/MEDIUM/LA060596PE00004.GIF.

Irvine, A. and Engineering, P. (2016) ‘THE ROLE OF WETTABILITY IN FILTRATION AND WASHING OF MATERIALS’, (August).

Karger, B. L. (1997) ‘HPLC: Early and Recent Perspectives.’, *undefined*. American Chemical Society, 74(1), pp. 45–48. doi: 10.1021/ED074P45.

Laux, A. (2019) ‘PARTICLE AGGLOMERATION AND BREAKAGE DURING DRYING’.

Meng, X. *et al.* (2017) ‘Removal of coke powder from coking wastewater by extraction technology’, *Separation and Purification Technology*, 175. doi: 10.1016/j.seppur.2016.10.015.

Pedussaut, L. (2018) ‘THE ROLE OF CONTACT ANGLE AS A DESCRIPTOR OF WASH PERFORMANCE IN THE ISOLATION OF PHARMACEUTICAL CRYSTALS’, pp. 1–60.

Setter, C. (2019) ‘Investigating the wettability of Aspirin and Lactose using the Washburn Method with different solvents’, (2), pp. 1–13.

Todorova, T. and Delley, B. (2008) ‘Wetting of paracetamol surfaces studied by DMol3-COSMO calculations’, <https://doi.org/10.1080/08927020802235672>. Taylor & Francis Group , 34(10–15), pp. 1013–1017. doi: 10.1080/08927020802235672.

Washburn, E. W. (1921) ‘The dynamics of capillary flow’, *Physical Review*, 17(3). doi: 10.1103/PhysRev.17.273.

Chapter 7: Quantification of granule formation as a function of solubility in Residual solvent (part b)

This chapter explains the work done to implement the methodology developed for quantifying agglomerate formation as a function of the solubility of API within the residual solvent by using glass beads to mimic API crystals. The API crystals were selected to demonstrate application of the approach to the real industrial problem instead of using glass beads as the substrate. The overall findings indicate that the methodology developed using the glass beads was not fully applicable to the API crystals potentially due to differences in particle shape, size, solubility and wetting behavior.

7.1 Aims and objectives

The main aim of the research in this chapter is to implement the methodology developed by using glass spheres in chapter 3 to quantify the amount of deposited material needed to cause lump formation amongst API crystals

7.2 Materials and Methodology

Two different sets of experiments were performed: first with PCM as a substrate and second with spherical agglomerates of benzoic acid as substrate. To reliably control the quantity of solvent which on evaporation would deposit the solute material, a solution of PCM in a binary mixture of heptane and ethanol was used. This binary mixture was used to achieve a range of concentrations similar to the ones used in the experiments with the glass spheres by controlling saturation level by adding antisolvent of the required amount. Moreover, a similar methodology was applied when using spherical agglomerates of benzoic acid in order to compare spherical crystalline particles with glass spheres and for this set of experiment to mimic residual moisture during drying solution of benzoic acid was used in binary mixture of heptane and ethanol.

7.2.1 Materials

7.2.1.1 Material for 1st set: PCM experiments

Sieved fractions of powdered PCM (purchased from Sigma-Aldrich, batch number MKCJ5427) and special granular as pharmaceutical grade PCM (supplied by Mallinckrodt Inc.,

Raleigh, N.C., USA, batch number 161713 J561) were selected as a substrate to cover an approximately similar range of particle sizes as of the glass beads used in the experiments reported in Chapter 3, section 3.3.1. Micronized PCM (supplied by Mallinckrodt Inc., Raleigh, N.C., USA, batch number 042213E407) was used to prepare solutions along with Ethanol (absolute, purity $\geq 99.8\%$, purchased from Sigma-Aldrich) and n-Heptane (purity 99.9%, purchased from Sigma-Aldrich). Glass spheres GB1 (40-70 μm) (as used in Chapter 3, section 3.3.1.) were also used to investigate the lump formation with binary solvent mixture solutions of PCM.

7.2.1.2 Material for 1st set: Spherical agglomerate experiments

Spherical agglomerates of benzoic acid (synthesized by Vishal Raval of the University of Strathclyde during his Ph.D. research) were selected as a substrate because of their shape similarity with the glass spheres used in chapter 3, section 3.3.1. Benzoic acid (purchased from VWR, batch number 20D064128) was used to perform solubility measurements and to prepare solutions which mimic the residual solution remaining at the end of filtration and washing. Ethanol (absolute, purity $\geq 99.8\%$, purchased from Sigma-Aldrich) and n-Heptane (purity 99.9%, purchased from Sigma-Aldrich) were used to prepare solutions and for solubility measurements. Glass beads GB1 (40-70 μm) was also used to investigate the lump formation with binary solvent mixture solutions of benzoic acid.

7.2.2 Methodology

7.2.2.1 Sample Preparation

Sample was prepared by using same methodology as explained in Chapter 4 section 4.2.1.

7.2.2.2 Sieving of Paracetamol

Sieving was performed to segregate PCM crystals into different size fractions. A vibratory sieve shaker (Analysette 3 Pro) was used for this purpose. This sieve shaker is different from the one used for characterization of agglomerates and much bigger in size and was only used for sieving of powdered PCM to get different fractions of PCM crystals. Sieve shakers are commonly used to analyze particle size distributions by segregating materials into a series of particular size classes. A series of test sieves, with the smallest mesh size at the bottom and largest at the top, were stacked on each other to form a sieve nest. A receiver pan was placed at the bottom of the sieve nest to collect the material passing through the finest mesh size, and

a lid prevents the material from being lost from the nest during sieving. This whole assembly was then placed on the sieve shaker shown in Figure 7-1. PCM sieving was performed using two sets of sieving nests with an amplitude of 1.0 mm. The duration of sieving for each sample was 5 minutes. The 10 grams of material were added to 20cm diameter sieve and 5 grams of material was added to 10 cm diameter sieve for each sieving cycle. In order to segregate larger masses of materials in each sub fraction more rapidly sieving with higher sample masses than recommended in British Standards Institution (1989)(BS1796) was performed. However, excess material clogged the aperture of the mesh, causing the blockages in the sieves. Consequently, many sieving runs needed to take place to separate sufficient material for the experiments which were planned.



Figure 7-1 Sieve shaker assembly with sieve nest

Table 7-1 Sieve diameters and mesh sizes

Sieve diameter (cm)	Mesh size (um)
20	500, 212, 75

10	425, 250, 150, 75
----	-------------------

7.2.2.3 Size Analysis

The size distribution of the sieved fractions was then measured using a Sympatec QIC/PIC particle analyzer (Figure 7-2). QICPIC is an offline dynamic particle sizing and image analysis instrument. For dry particle analysis, QICPIC has two dispersion units (*QICPIC*):

- RODOS is used for fine particles < 200 μm
- GRADIS is used for coarse particles > 200 μm



Figure 7-2 QICPIC setup

For dynamic image analysis, particles flow continuously through a camera-controlled volume measurement. The free random movement of the particles allows the measurement of the shape and size of the particle to take place (*RODOS*). The basic concept combines well-established dispersing unit *RODOS* and dynamic image analysis to capture a large number of particles per image. Figure 7-3 shows the optical setup of the QICPIC (*Dynamic Image Analysis*). The dispersion of the particles in *RODOS* is achieved using a long, straight dispersion line, which releases the dispersed particles and accelerates them into the sampling zone. The instrument

uses a pulsed light source to freeze the particle motion eliminating motion blur.

The RODOS/L with VIBRI feeder was set up at a feed pressure of 0.5 bar, feed rate of 25%, and 0.5 mm gap width for measuring the size of particles within the sieved fractions.

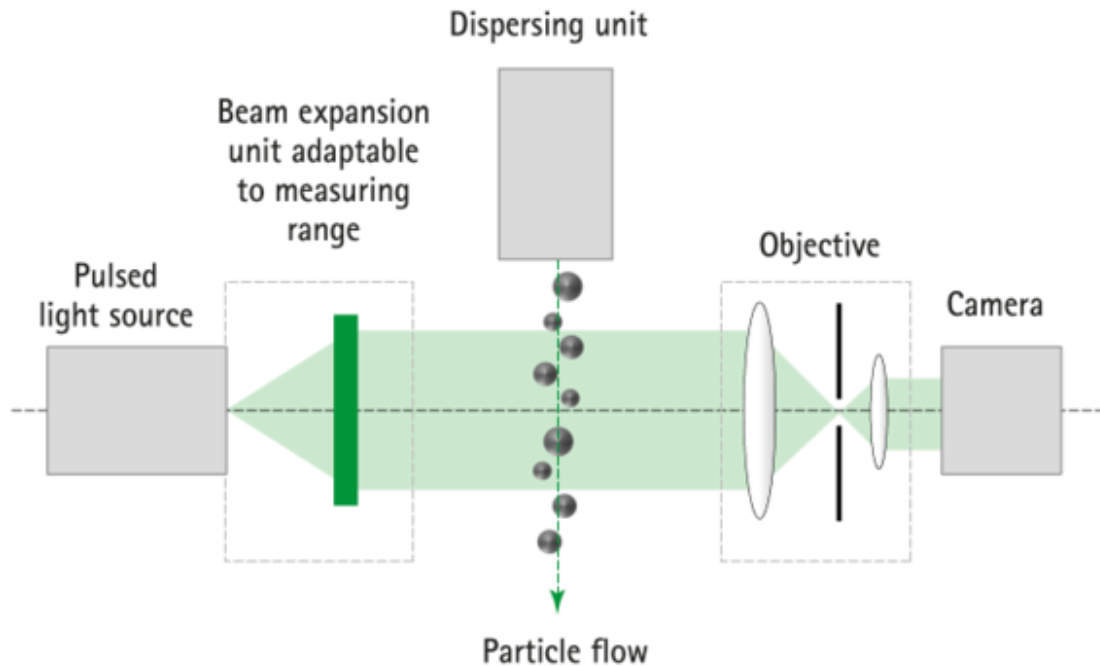


Figure 7-3 Optical setup of QICPIC

Particle size distribution can be evaluated as:

- Cumulative distribution (Q, %): shows the probability that the variable (particle size) is smaller or larger than a value; from this representation the percentile PSD parameters, such median (D50), D10, D90 can be evaluated easily
- Distribution density (q, lg): using a logarithmic scale aids resolution of the particle size across size ranges

Other methods for describing particles size are used:

- Sauter mean diameter (SMD, D[3,2]) is a weighted mean diameter represented by the sum of the cubic equivalent diameters of particles divided by the sum of the square equivalent diameter (Equation 7-1) where n_i is the number of particles at a specific equivalent diameter and D_i is the equivalent diameter

$$SMD = \frac{\sum n_i D_i^3}{\sum n_i D_i^2} \quad \text{Equation 7-1}$$

- Volume mean diameter (VMD, D[4,3])

$$VMD = \frac{\sum n_i D_i^4}{\sum n_i D_i^3} \quad \text{Equation 7-2}$$

7.2.2.4 Solubility Measurement

Solubility measurements of benzoic acid in a binary mixture of heptane and ethanol were performed using a Technobis Crystalline Platform (Figure 7-4) (Technobis Crystallization Systems, Alkmaar, The Netherlands). The Crystalline consists of eight parallel reactors. The Crystalline measures the solubility and metastable zone width (mszw) of APIs using turbidity and particle imaging. Conventionally it operates by cycling through a temperature profile whilst agitating a known mass of crystals suspended in a defined quantity of solvent detecting dissolution and nucleation in order to measure the phase diagram.



Figure 7-4 Crystalline PV

In this case the Crystalline was setup to provide constant temperature (20°C) and stirring rate (700 rpm) to produce a saturated solution. After getting a saturated solution, samples were removed from the crystalline vials using syringes. The solution samples were then filtered using a PES syringe filter (Fisherbrand, Cat No. 15206869, 0.2 µm, sterile) in to a pre-weighed

vial. The vials were then left to evaporate to dryness to determine the quantity of dissolved material.

5.3. Results and discussion

5.3.1. Experiments with PCM

In the methodology developed in Chapter 5, glass spheres were wetted with solutions containing different concentrations of dissolved solute mimicking the residual solution present at the start of drying to evaluate the effect of solid deposition after solvent evaporation. To apply the same methodology delivering the same range of quantities of dissolved material to PCM crystals, a binary mixture of an anti-solvent and a solvent is required to prepare saturated solutions covering a similar range of concentrations as developed in the methodology. For this purpose, an experiment is performed with granular PCM and pure n-heptane. It was presumed that wetting of a PCM sample with n-heptane would produce a free-flowing powder as PCM has very low solubility in PCM (Table 4-6).



Figure 7-5 Dry sample after wetting the granular PCM with heptane



Figure 7-6 Dry sample after transferring to sieving assembly of 1mm sieve and bottom pan

Figure 7-5 and Figure 7-6 shows the dry sample after wetting the granular PCM with heptane with a red dye added to aid the visual observations of the area affected by the solvent. After transferring the dried sample from the vial to the sieve nest comprising a 1mm sieve and a bottom pan, virtually the whole sample passed through the sieve without shaking. This result confirms the hypothesis that wetting the PCM crystals with heptane will not cause agglomeration. The next step was to sieve the crystalline grade of the PCM.

7.2.2.5 Sieving of PCM

The powder grade of PCM was sieved with a sieve shaker as described in Section 7.2.2.2. initially 20 grams of PCM was added to 20 cm sieves with the mesh size 500 μm , 212 μm , and 75 μm and sieved for 30 min. However, with a 20 gram load of PCM, the particles passed through 500 μm sieve but became clogged on the 212 μm sieve. Sieving 10 grams of PCM on the same sieving assembly and sieving for 5 min was more effective. The sieving time was reduced as it was considered that with the higher number of vibrations, the electrostatic charges generated between the particles increased, which contributed to the formation of lumps (Fotovat, Bi, and Grace, 2017).



Figure 7-7 Sieved fractions of PCM with 20 cm diameter (a) 500 um sieve (b) 212um Sieve (c) 75 um sieve (d) bottom pan

Figure 7-7 shows the sieved fractions with 20 cm diameter sieves. A further problem with 20 cm diameter sieves was that sieve shaker was not reliable in holding the sieve assembly tightly and so became very noisy. It was decided to work with 10 cm diameter sieves using 5 gram portions of PCM with mesh sizes of 425 µm, 250 µm, 150 µm, and 75 µm (Figure 7-8) and sieving for 5 minutes. The sieving cycles were repeated multiple times to collect 10 grams of PCM from the 150 µm sieve, 75 µm sieve, and the bottom pan. However, the problem of small particles sticking together and blinding the sieves persisted, and it was not possible to get large quantities of single crystals; it was therefore decided to do the experiments with these 10 grams material, and if the experiments were successful, then to continue the sieving process to obtain more segregated material.

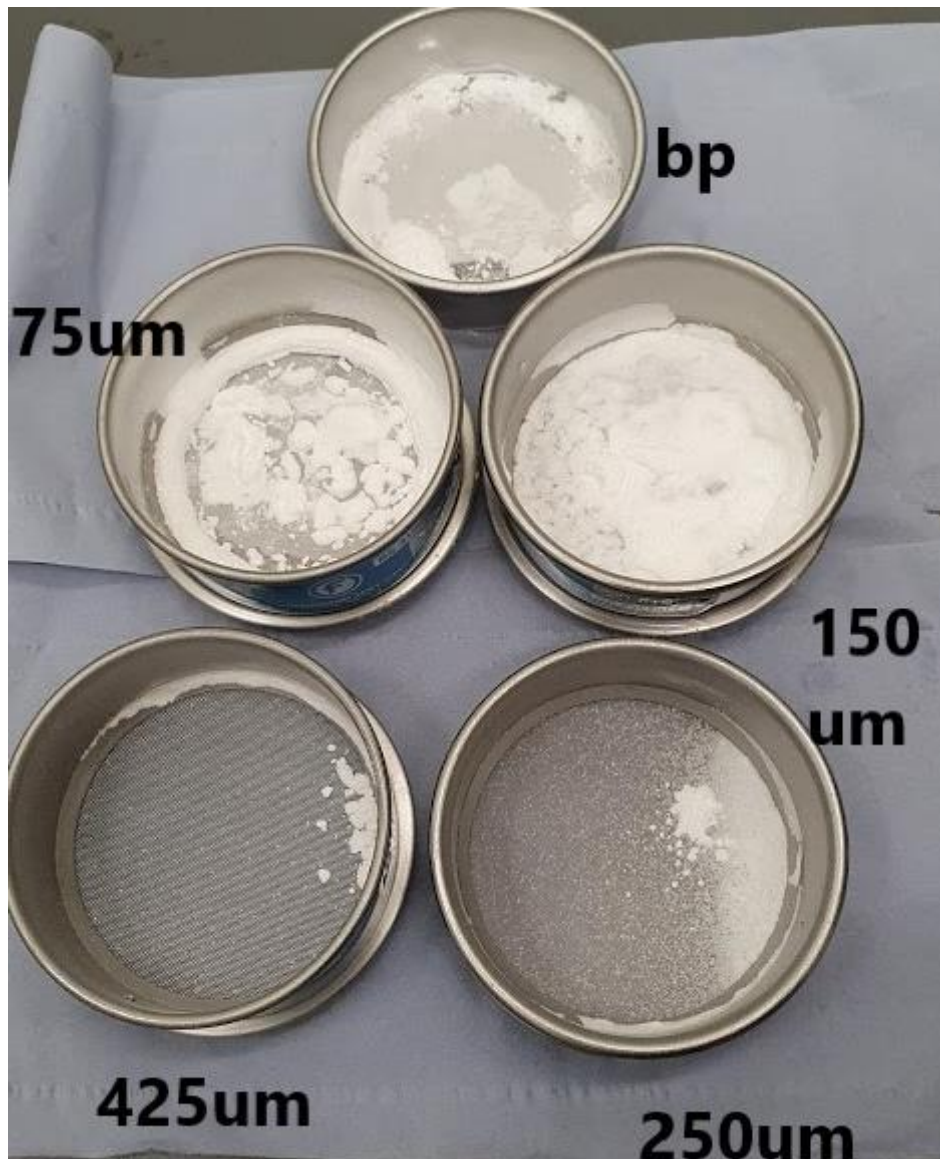


Figure 7-8 Sieved fractions of PCM with 10 cm diameter sieves

Table 7-2 gives x_{10} , x_{50} , x_{90} , Sauter mean diameter (SMD) and volume mean diameter (VMD) of granular and powdered PCM and the fractions of the powdered PCM after sieving measured with QICPIC as described in section 7.2.2.2. Microscope images of each fraction were also taken to further verify the sizes obtained from various sieves are in accordance with the sieve size (Figure 7-9).

Table 7-2 Particle size analysis of Granular and powdered PCM and sieved fractions of powdered PCM by QICPIC

Material	X_{10} (um)	X_{50} (um)	X_{90} (um)	SMD (um)	VMD (um)
Granular PCM	273.91	363.58	462.26	299.30	360.03

Powder PCM	29.71	100.57	288.76	59.76	135.53
250 μm sieve fraction	29.60	111.28	305.01	66.49	160.76
150 μm sieve fraction	27.30	58.32	84.12	42.82	57.24
75 μm sieve fraction	24.04	52.93	100.20	41.48	57.79
Bottom pan	17.43	40.42	67.03	31.22	41.85

The data for the size analysis of sieved material is not in accordance with the sieve sizes, which may be possible because of two possible reasons, firstly the particles which stay together as a cluster on the sieve are dispersed during particle sizing or that the load on the sieve is such that the particles are not presented to the sieve screen optimally to fall through, or possibly a mixture of both effects.

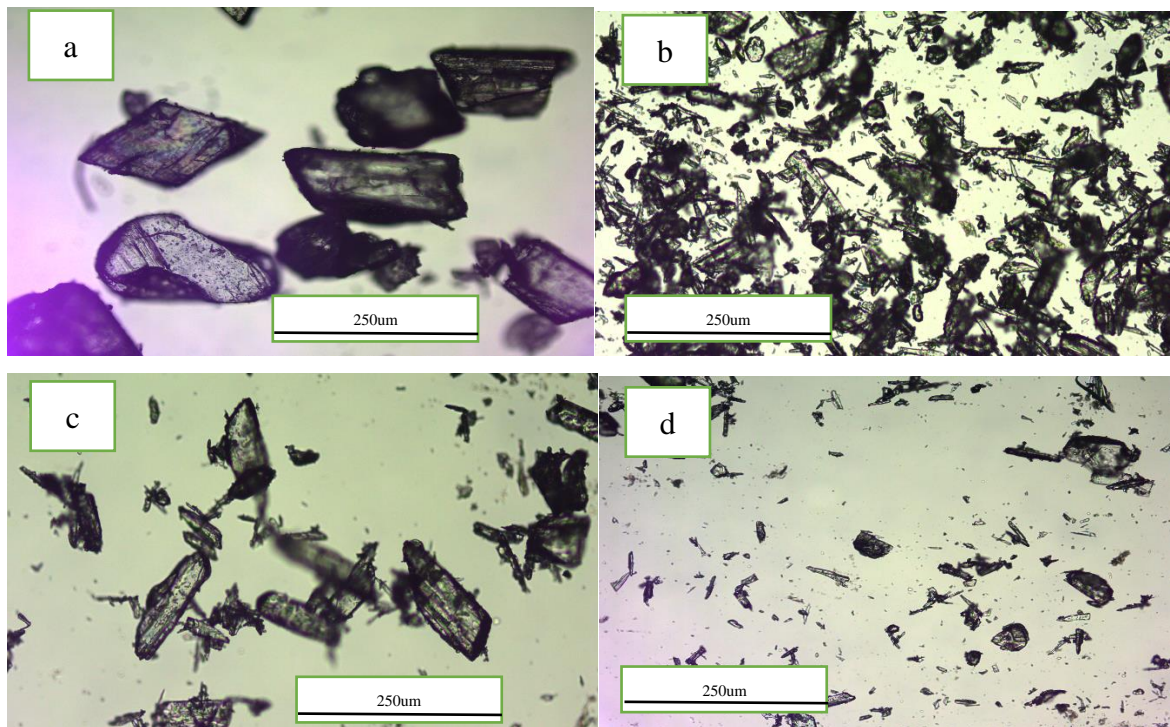


Figure 7-9 Microscopic images of the sieved fractions (a) 250 μm (b) 150 μm (c) 75 μm (d) bottom pan with 10x objective lens

7.2.2.6 PCM agglomeration experiment

Three different sets of experiments were performed to investigate the agglomeration by the deposition of solid material after evaporation of the solvent. In the first experiment, powdered PCM 75 μm sieve fraction was taken as a substrate. In the second experiment, granular PCM was the substrate, and the third experiment was performed with glass beads as substrate. The methodology for preparing the sample was the same as in chapter 4 (section 4.2.1). Table 7-3 lists the parameters of all three sets of experiments. The solvent composition was selected based on solubility data (Table 4-6) to deposit a similar amount of PCM as was deposited in the earlier glass bead experiments (chapter 5).

Table 7-3 Parameters of PCM agglomeration experiment with binary mixtures

Exp. #	Substrate	Substrate mass (g)	Solvent (ml)		Solute (g)
			Heptane (mL)	Ethanol (mL)	
1	75 μm sieved fraction	3	90	10	2.2736
2	Granular PCM	5	90	10	2.2736
			100	0	1.3562
3	Glass beads	10	90	10	2.2736
	GB1 (40-70 μm)		100	0	1.3562

7.2.2.7 Experiment with 75 μm sieved fraction.

The sample was prepared by adding three grams of 75 μm sieved fraction of powdered PCM into the vials, and a drop of 100 μL of solution was added to the substrate. The resulting sample was then placed in the fume hood for drying. After complete drying, the sample was transferred to the sieving assembly (1mm sieve and bottom pan) to separate the lump which formed from non-agglomerated crystals.

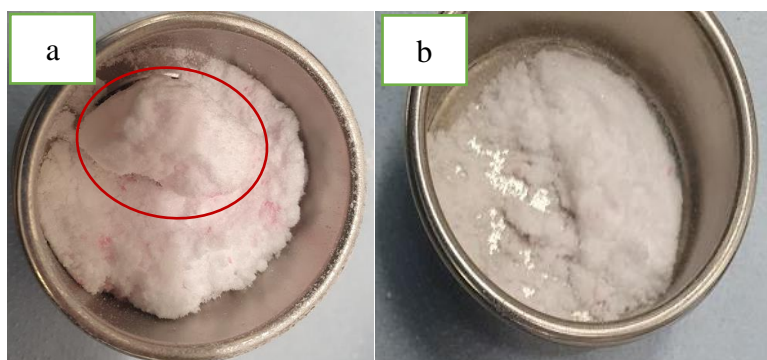


Figure 7-10 75 μm sieved fraction dried sample after transferring to the sieving assembly (a) 1mm sieve (b) bottom pan.

Figure 7-10 shows the sample after transferring to the sieving assembly. It is clear from the picture that the lumpiness of the powdered PCM fraction made it difficult to sieve the dried sample to separate the agglomerate formed by evaporation of the added solution. The lump formed was then separated with the spatula from non-agglomerated material and sieved by Variable Speed Mini Vortex Mixer (Fisherbrand™) at 2800 rpm. However, after 1st cycle of sieving, PCM clogged the mesh and blocked sieve mesh (Figure 7-11). Moreover, the agglomerate formed was fragile and almost broke after the first cycle of sieving. Due to these issues with the powdered PCM fractions, it was decided to stop working with powdered PCM.



Figure 7-11 Sieving assembly after the first cycle of sieving of 75 μm fraction sample

7.2.2.8 Experiment with granular PCM and glass beads

After observing the issues with the powdered PCM, the next set of experiments was performed with granular PCM. The first experiment was performed with heptane/PCM solution, and the agglomerates formed broke after manual tapping. The second experiment was performed with the PCM solution in a binary mixture of heptane and ethanol with a 90:10 ratio. However, the

agglomerate formed with this solution concentration was also very fragile, breaking completely after manual tapping.

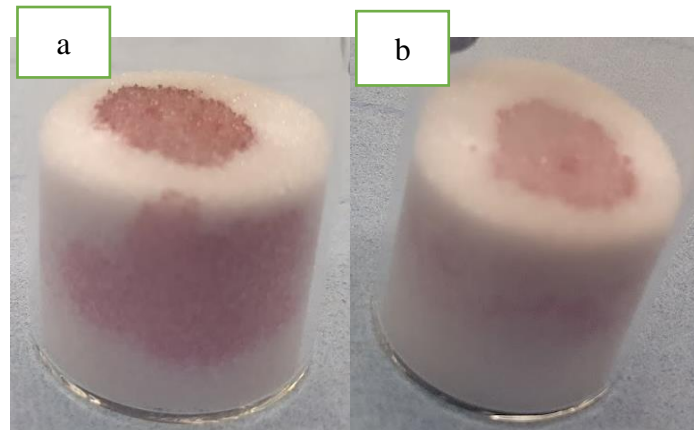


Figure 7-12 Dried sample of granular PCM (a) experiment with heptane/PCM solution (b) experiment with 90:10 heptane: Ethanol/PCM solution

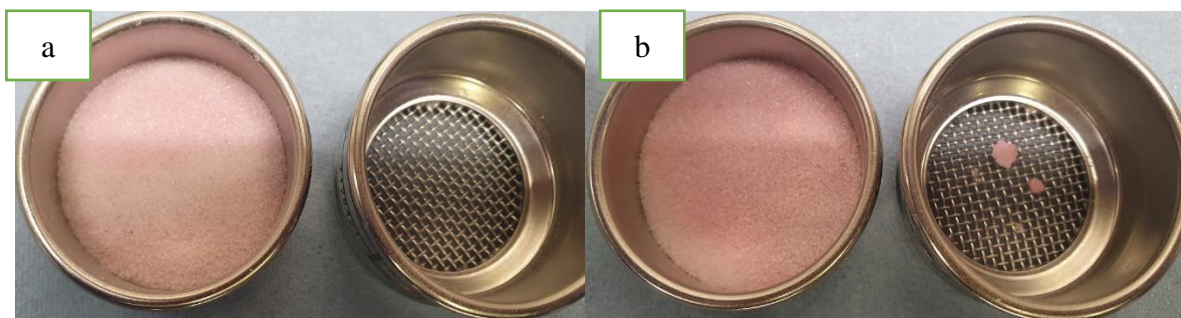


Figure 7-13 Granular PCM (a) experiment with heptane/PCM solution after manual tapping (b) experiment with 90:10 heptane: Ethanol/PCM solution after manual tapping

The experiments with granular PCM were performed twice, and similar results were obtained. So, the following experiment was performed on glass beads to investigate whether this PCM solution concentration formed robust agglomerates using the glass beads. GB1 (40-70 μm) glass beads were selected, and the experiment was performed with the same solution concentrations. The agglomerate formed with heptane PCM solution was fragile and broke after manual tapping. In contrast, a solid agglomerate was obtained from PCM solution in a binary mixture of heptane and ethanol.

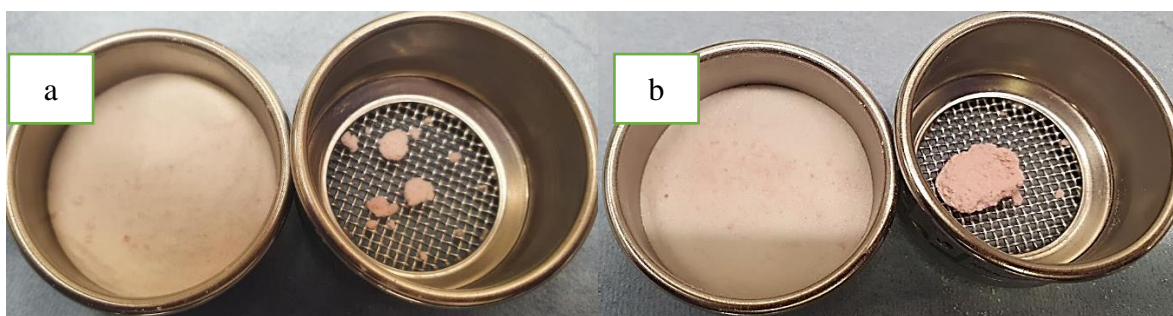


Figure 7-14 GB1 (40-70 um) glass beads (a) experiment with heptane/PCM solution after manual tapping (b) experiment with 90:10 heptane: Ethanol/PCM solution after manual tapping

After comparing the results of the granular PCM and glass bead experiment, it was presumed that the solid deposition mechanism is different for API crystals and glass beads. The most likely explanation is that for API crystals, the solution wets the surface of the crystals forming a thin liquid film and as the solvent evaporates the dissolved API is deposited across the surface of the crystals rather than being deposited mostly at the contact points between crystals. In contrast, for glass beads, while the solution is presumed initially to wet the entire surface there is initially a nucleation barrier to deposition on surfaces such that more solvent needs to evaporate before sufficient supersaturation is generated for the dissolved PCM to be deposited.

A further factor which may contribute to this is the difference in surface texture and surface area of the substrates, the glass spheres being smoother and possibly having a lower surface area per unit mass than the PCM crystals. Microscopic analysis of granular PCM and glass beads samples (Figure 7-15 and Figure 7-16) supports this point. As the images of the glass spheres seems to show a broken point of contact, many small point deposits of crystalline material and the obvious accumulation of material at points of contact. In contrast the PCM sample seems to support the argument that the material is deposited uniformly across the crystal surfaces there being no evidence of accumulation and points of contact.

According to Papadakis and Bahu (1992), when a viscous binder forms a thin layer on the surface of the particle, then immobile liquid bridges form between the particles and cause agglomeration. When the liquid bridge formed between the particles is made up of a solvent in which the product has some solubility the dissolved material is deposited when the solvent evaporates. Thus during drying these liquid bridges become bridges of crystalline material deposited at points of contact holding the particles together in an agglomerate (Dopfer et al., 2013). The strength of these bonds depends not only upon the amount of dissolved material but also on the crystal properties and structure (Papadakis and Bahu, 1992). Papadakis and

Bahu also describe the granulation process when a viscous binder forms a thin layer on the surface of the particle, then immobile liquid bridges form between the particles.

As the glass beads are of defined shape and remain intact when wetted with the solution the liquid bridges between glass spheres upon drying turns into solid bridges at contact points with the glass beads. While for the API crystals interact with the solvent and effect agglomeration. In case of PCM the binary mixture of ethanol and heptane was used and heptane act as an antisolvent for PCM and inhibits the formation of strong bond between crystals (Shahid et al., 2021).

However, further investigation on solution transport and solute deposition on PCM crystals was not performed due to time limitations arising from the COVID pandemic. However, the approach was tested further using spherical agglomerates of benzoic acid.

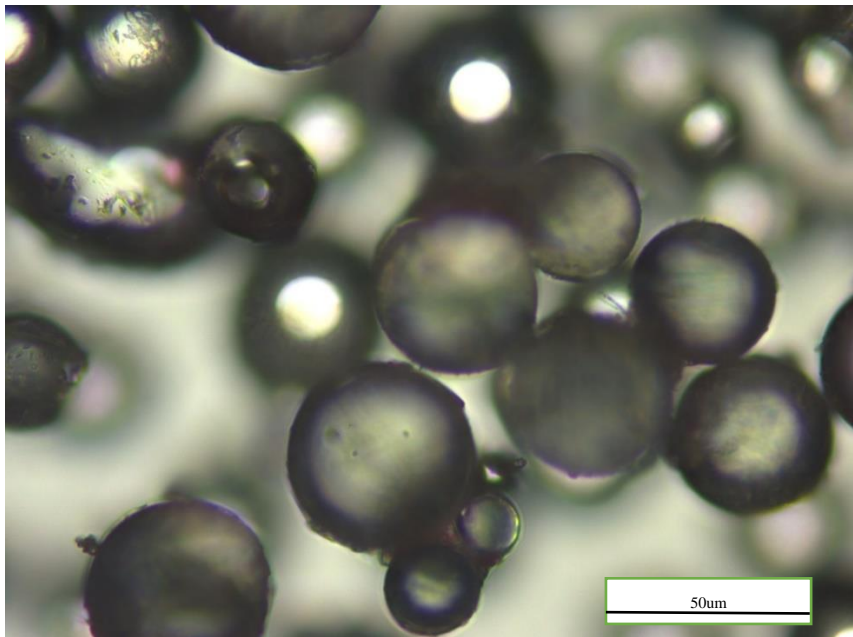


Figure 7-15 Sieved fraction of glass beads sample with 90:10 heptane: Ethanol/PCM solution

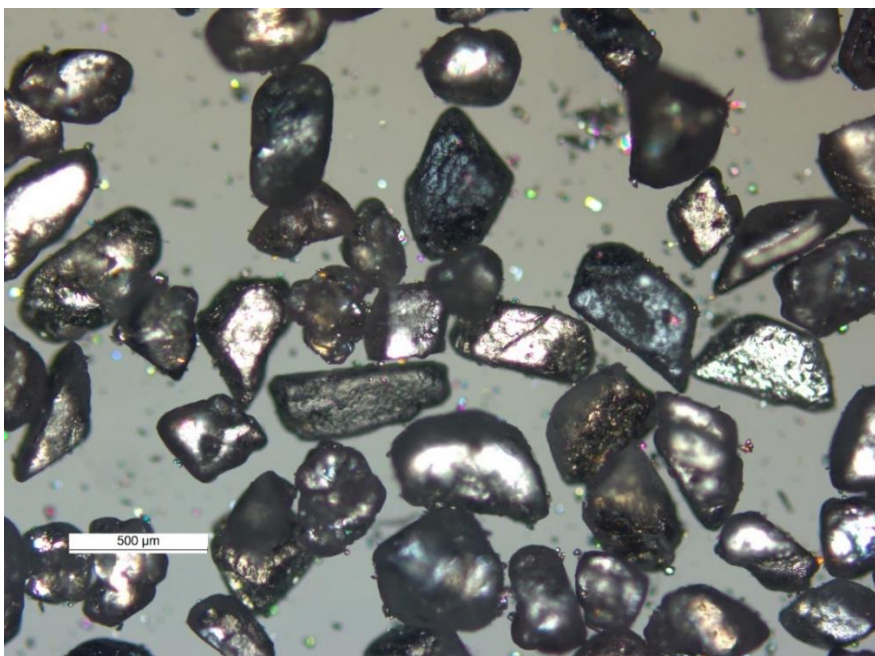


Figure 7-16 Granular PCM sample with 90:10 heptane: Ethanol/PCM solution after manual tapping

7.2.3 Experiments with spherical agglomerates of benzoic acid

In this set of experiments, the methodology developed using the glass beads (chapter 5) was implemented on spherical agglomerates of benzoic acid. The spherical agglomerates were selected because of their resemblance in shape to the glass beads. To implement the methodology for spherical agglomerates, the first step was to conduct solubility measurements of benzoic acid in binary mixtures of heptane and ethanol to enable preparation of solutions of benzoic acid that mimic the likely residual solution composition anticipated in washed wet filter cakes. Benzoic acid has a high solubility in ethanol and low in heptane. By increasing the concentration of heptane in the binary mixture of ethanol and heptane, the solubility of benzoic acid decreases (Thati, Nordström, and Rasmuson, 2010). Hence by measuring the solubilities of benzoic acid in a binary mixture of heptane and ethanol, it was possible to identify a range of saturated solution compositions to deposit similar amounts of benzoic acid on spherical agglomerates as achieved in the methodology developed for glass beads.

7.2.3.1 Solubility measurement

To measure the solubility of benzoic acid in pure solvents and binary mixtures, the samples were prepared in the Crystalline as described in section 7.2.2.4. Five grams of solvent / solvent mixture were added to crystalline vials along with a magnetic stirrer. Then weighed amounts

of solute was added to the solvent at short intervals until saturation of the solution. The temperature and agitation in the crystalline reactors were kept constant at 20 °C and 700 rpm, respectively. After saturating the solution, the crystalline vials were removed from the platform, and the solution was removed from the vials using syringes. The solution was then filtered using a PES syringe filter (Fisherbrand, Cat No. 15206869, 0.2 µm, sterile) into a pre-weighed vial. The vials were then left for the solvents to evaporate until the sample as dry to determine the quantity of the dissolved benzoic acid remaining after the evaporation of the solution.

Table 7-4 Solubility of benzoic acid in pure solvents and binary mixtures of heptane and ethanol

Solvent Heptane: Ethanol	Solubility (g/g)
0: 100	0.5214
30: 70	0.4274
80:20	0.1535
85:15	0.1266
90:10	0.0993
95:05	0.0761
100: 0	0.0121

7.2.3.2 Agglomeration experiment with spherical agglomerates and glass beads

For this set of experiments, spherical agglomerates of benzoic acid were selected as the substrate. Three different sizes of spherical agglomerates were chosen to have relevance to the sizes of glass beads used in earlier work. Dr. Vishal Raval produced these spherical agglomerates in his Ph.D. work. Table 4-3 gives the size analysis of spherical agglomerates.

To investigate the amount of deposited material that can cause lump formation after drying with spherical agglomeration, a solution of benzoic acid with a binary mixture of heptane and ethanol in a 95:05 ratio was prepared (Table 7-5). Three grams of spherical agglomerates were added to the pre-weighed vials. Then a 100 µL drop of solution was added, and the sample was left in the fume hood to dry. The dried sample was then sieved to quantify the extent and strength of agglomerates formed.

Table 7-5 Parameters of agglomeration experiment with spherical agglomerates using binary mixtures

Exp. #	Substrate	Substrate mass (g)	Solvent (g)		Solute (benzoic acid) (g)
			Heptane	Ethanol	
1	Spherical agglomerate (J, N2, and N15)	3	4.77	0.3512	0.3908
2	GB1 (40-70 um)	10	4.77	0.3512	0.3908

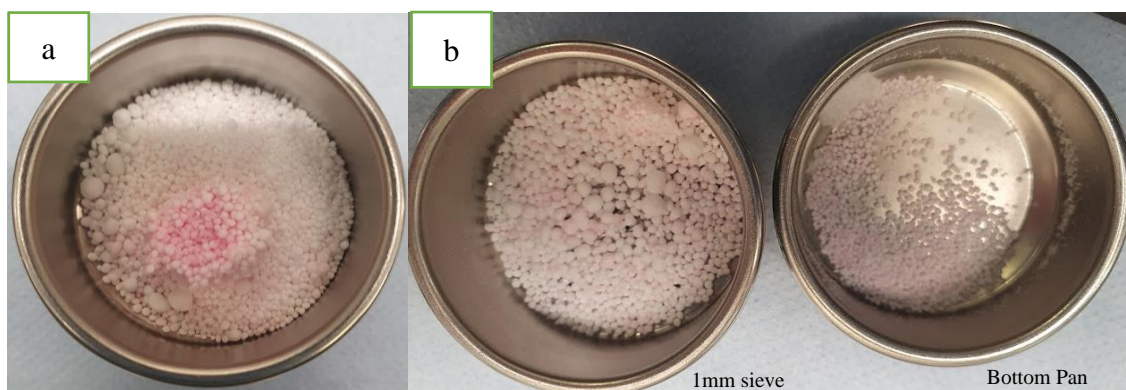


Figure 7-17 Dried sample J (a) after transferring from the vial (b) after first cycle of sieving

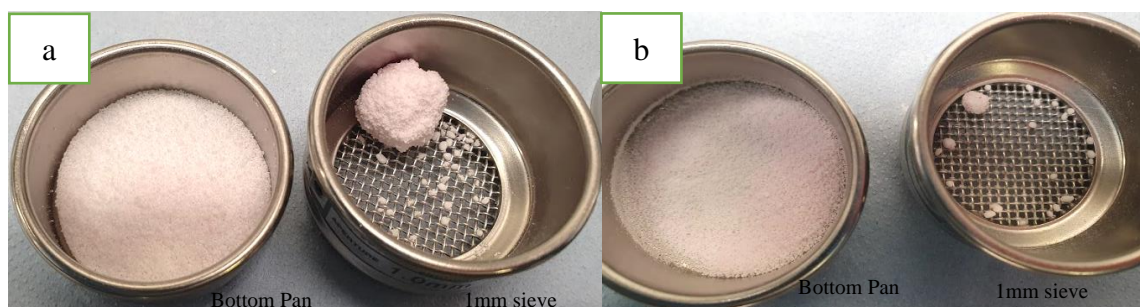


Figure 7-18 Dried sample N2 (a) after manual tapping (b) after second cycle of sieving.

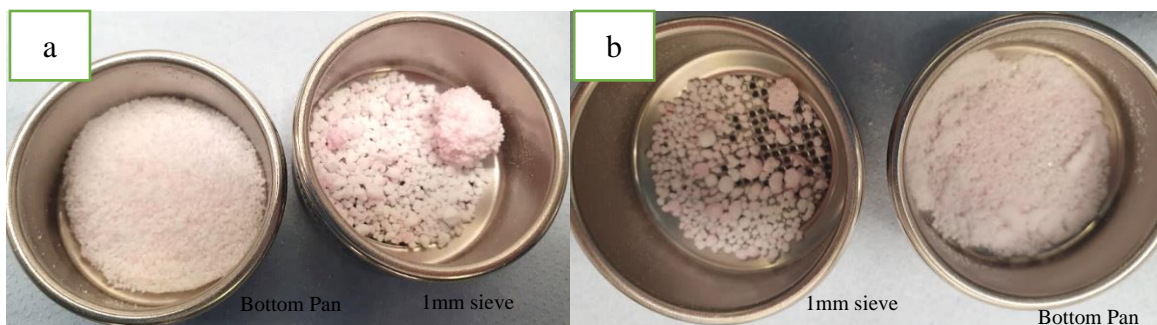


Figure 7-19 Dried sample N15 (a) after manual tapping (b) after second cycle of sieving.

Figure 7-17, Figure 7-18, and Figure 7-19 show the dried sample before and after sieving. The agglomerates formed were fragile and broke almost completely after the first or second cycle of sieving. It was also clear from the images that the solution was transported throughout the whole sample and caused formation of many small spherical agglomerates in addition to the larger lump which was formed in the case of sample N2. This can be related to the properties of spherical agglomerates and the wetting behavior of the solution. However, the results of the experiments were not as predicted, i.e., the anticipated hard lump was not formed. The effect of the same solution concentration of benzoic was investigated by experimenting with glass beads.



Figure 7-20 Glass beads (GB1) dried sample with the benzoic acid solution in binary mixture of heptane and ethanol (95:05)

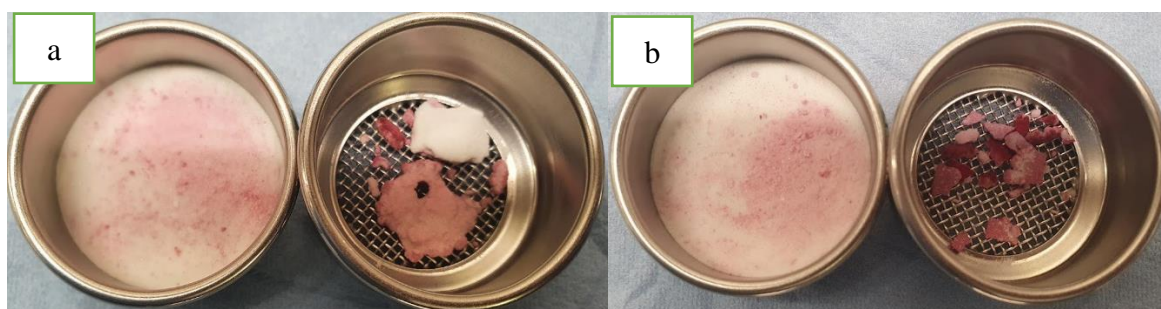


Figure 7-21 Dried sample of glass beads (GB1) (a) after transferring the material from the vial (b) after manual tapping.

The evaporation of the benzoic acid solution did not result in any agglomerate formation with the glass beads, a layer of deposited material was formed on the surface of the glass beads beds rather than depositing at the points of contact. These results may be related to the wetting behavior of benzoic acid on the glass beads. However, further investigation of the wetting properties of the benzoic acid solution on both spherical agglomerates of benzoic acid and glass beads with the solution due to time limitations arising from the COVID19 pandemic.

7.3 Conclusion

In this chapter, work was done to investigate the implementation of the methodology developed with glass beads (chapter 3) to quantify the minimum amount of deposited material that can cause lump formation during drying of API crystals wet with a solution representing the likely composition of the residual solution following classical filtration and washing.

The initial approach was to sieve powdered PCM to get isolate single crystal fractions with size ranges corresponding to the glass spheres used to develop the methodology. This was unsuccessful because of the behavior of the paracetamol crystals on the sieves which may be linked to the electrostatic properties of paracetamol powder. The vibration applied during sieving is likely to increase the electrostatic charge between particles causing promoting clogging of the sieves.

- Then the methodology was implemented on granular PCM and spherical agglomerates of benzoic acid, however it was not as successful as the work on glass spheres, reasons which contribute to this lack of success include: The shape and size of the PCM and spherical agglomerates.
- Material properties of substrates
- Wetting behavior of the solutions on the substrate particles
- The transport of the simulated wash solution during drying

7.4 References

British Standards Institution. (1989) ‘Method for test sieving. Part 1. Methods using test sieves of woven wire cloth and perforated metal plate.’ British Standards Institution, p. 13.

Dynamic Image Analysis (no date). Available at: <https://www.sympatec.com/en/particle-measurement/sensors/dynamic-image-analysis/> (Accessed: 8 September 2022).

Fotovát, F., Bi, X. T. and Grace, J. R. (2017) ‘Electrostatics in gas-solid fluidized beds: A review’, *Chemical Engineering Science*. Pergamon, 173, pp. 303–334. doi: 10.1016/J.CES.2017.08.001.

QICPIC (no date). Available at: <https://www.sympatec.com/en/particle-measurement/sensors/dynamic-image-analysis/qicpic/> (Accessed: 8 September 2022).

RODOS (no date). Available at: <https://www.sympatec.com/en/particle-measurement/dispersing-units/rodos/> (Accessed: 8 September 2022).

Thati, J., Nordström, F. L. and Rasmuson, Å. C. (2010) ‘Solubility of benzoic acid in pure solvents and binary mixtures’, *Journal of Chemical and Engineering Data*. American Chemical Society, 55(11), pp. 5124–5127. doi: 10.1021/JE100675R/ASSET/IMAGES/JE-2010-00675R_M002.GIF.

Chapter 8: Refining Agglomeration brittleness Index Method

This chapter investigates different approaches to developing convenient methods for quantifying agglomerate brittleness. For this work, a model system of glass beads was selected. The main aim of this work was to refine the existing technique to quantify agglomeration strength by exploring various graphical analyses and data fittings. The work was performed on multiple sieving frequencies, and the data were analysed by plotting various factors seeking to obtain straight-line curves for linear fitting. In addition a hardness testing technique was also analysed to find the hardness of the agglomerates.

8.1 Introduction

Free-flowing APIs with uniform PSD are highly preferred as they require less intense secondary processing during formulation. Unfortunately, the formation of agglomerates during drying is quite an abundant phenomenon which cannot be effectively avoided in many cases. To achieve desired product PSD, extra particle size reduction operation (e.g. milling) has to be incorporated into the manufacturing process, resulting in increased production time due to long milling cycles additional analysis and laborious sanitation.

It is anticipated that process parameters during cake filtration, cake washing and drying contribute to the variable propensity of particles to agglomerate and their final mechanical properties. The diverse spectrum of solid lumps can then be analysed to provide a rough understanding of their hardness/brittleness to eliminate the worst-case scenarios and optimise the process with the most promising parameters.

Currently, no precise technique is used to measure agglomerate's mechanical properties. Birch and Marziano (2013) were the first to publish a valid approach to test agglomerate hardness. Based on this method, the % of the initial mass retained on the sieve is recorded after four shaking cycles and then plotted against the number of cycles. By fitting a power law equation to the experimental data points, the ABI factor is obtained from the power value b . The larger this value is, the softer the agglomerated material and vice versa (Figure 3-4).

Although this method provides satisfactory data, there are cases where the results are questionable. One of the pitfalls in measuring the agglomerate brittleness index is the significant deviation between individual agglomerates within the same sample. Since clusters are formed in different cake parts, this feature is inevitable and reflected in the sample's average

agglomerate hardness. There are experiments where the majority of the agglomerates are shattered at the beginning of the analysis, in which case only a small percentage defines the average brittleness index of the material since the b value is independent of the initial amount of agglomerates hence indicating the lump hard and challenging to break as shown in Figure 8-1.



Figure 8-1 0.01 g/ml PCM/Methanol dried sample (a) after manual tapping (b) after 1st sieving cycle (c) after 2nd sieving cycle (d) after 3rd cycle of sieving (e) after 4th cycle of sieving

8.2 Previous work in the group

Despite limited generalised methodologies to determine agglomerates' properties (hardness/brittleness), Simurda (2017) explored some techniques developed by modifying previous methods to test the tablets' hardness. He tried to find the mechanical properties of agglomerates by using Instron, a direct compression instrument and a Friabilator, an impact breakage test. Moreover, some work was also done on evaluating different data fitting approaches to develop a convenient method to quantify agglomerates' brittleness. Georgia Sanxaridou (unpublished work) worked on exponential decay fitting and compared the results with the power law fitting approach developed by Birch and Marziano (2013).

8.2.1 Friability Analyser

The Friability Tester or Friabilator (Figure 8-2) consists of a static platform connecting a rotating drum with a baffle. As the drum spins, the material is exposed to a series of impacts from a constant height as a specially shaped baffle periodically lifts and drops the tablets. When the tumbling stops, the samples are removed from the drum and reweighed. The difference between the mass before and after the cycle is defined as friability. Simurda (2017) used the same approach for testing agglomerates; however, he disqualified this method based on several

factors. One of the reasons for disqualifying the technique was the forces that hold particles in agglomerates together are much weaker than in tablets; thus, tumbling was too aggressive. Agglomerates also relatively quickly release fine dust that builds-up electrostatic charge while in contact with moving plastic surfaces. Due to the dimensions of the spinning drum, rather large amounts of the sample (~10-15 grams) have to be used.



Figure 8-2 Friability tester or Friabilator (Charles Ischi AG – Testing Technology)

8.2.2 Compression tester

Simurda (2017) also used a compression tester (developed by Instron) to crush agglomerates and got information on their hardness and breakage profiles. This instrument consists of two main components (Figure 8-3) static base plate and a moving anvil.



Figure 8-3 Compression Tester (Instron : Materials Testing Machines for Tensile, Fatigue, Impact, Rheology and Structural Testing)

The sample is placed in the centre of the base plate (Figure 8-4 a), and the upper anvil slowly begins to move downwards. As the anvil touches the sample, the software starts plotting the extension's real-time profile against compressive load. He showed for some samples, the agglomerates cannot withstand the applied stress and break apart (Figure 8-4 b), and a distinctive peak in the graph is recorded (Figure 8-5), reflecting maximum compressive load in the weakest spot (Simurda, 2017).



Figure 8-4 Fragmentation of particle agglomerate during compression test (Simurda, 2017)

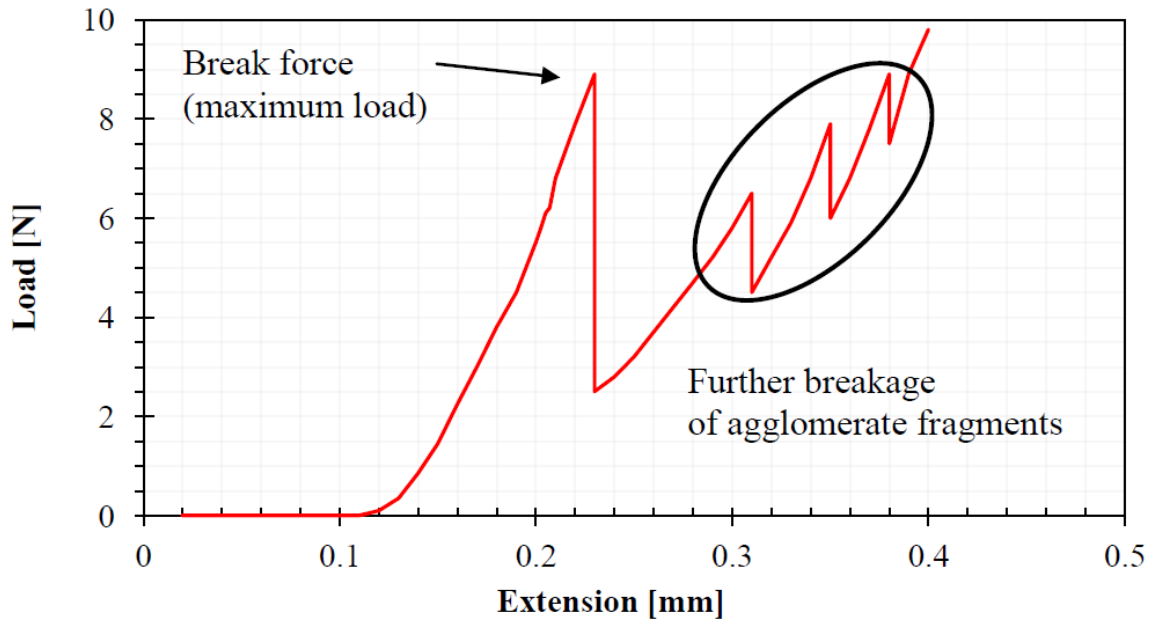


Figure 8-5 Breakage point of model agglomerate using Instron (Simurda, 2017)

He concluded that this method was also unsuitable for studying agglomerates' mechanical properties because the crushing force needed to break agglomerates was much lower in magnitude than for tablets hence was at the bottom of the measurement range of the instrument. He also found that as agglomerates typically have very random textures, the crushing force was not distributed evenly throughout the agglomerate's entire volume but through several contact points (Figure 8-7). Generally, it is almost impossible to produce agglomerates with uniform particle size and shape (Simurda, 2017).

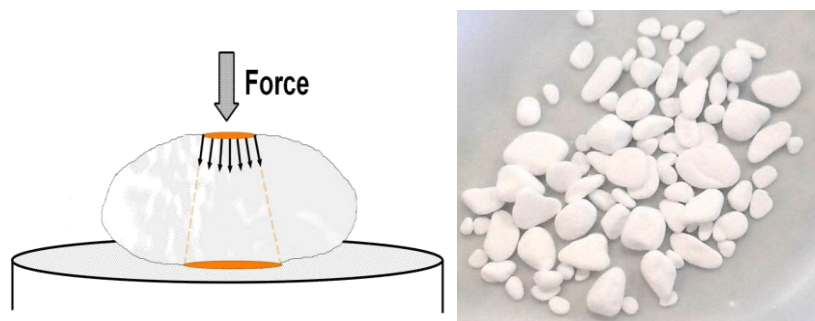


Figure 8-6 Distribution of force on smooth-edged particles

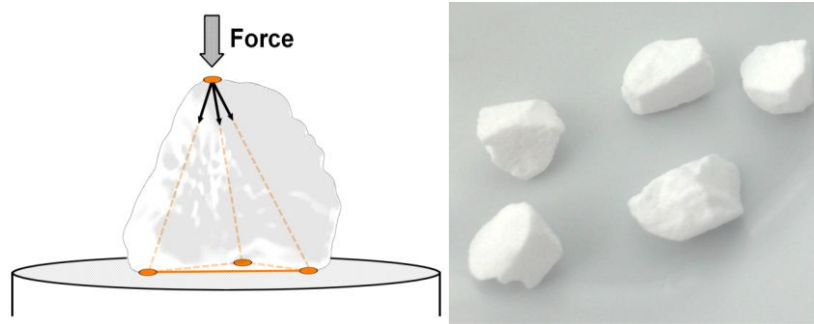


Figure 8-7 Distribution of force on sharp-edged particles

8.2.3 Exponential Decay fitting

Sanxaridou (unpublished work) worked on an alternative approach to data fitting by using an exponential decay equation. Exponential decay describes a process where the initial amount a is reduced by a decay factor b over time x . In her work, the factor b was the average percentage rate at which the original agglomerates decreased during four identical cycles.

$$y = a \cdot (1 - b)^x \quad \text{Equation 8-1}$$

She compared the two equations, the power law and the exponential decay equation, for the sieving data. The latter results in more reliable ABI data and, in most cases, has similar or greater R^2 values. Furthermore, by ranking the b values for the same experiments from higher to lower, there are significant differences in the agglomerate softness based on the equation used. However, the exponential decay model didn't fit all of her ABI index data. This could be due to the considerable variation in the brittleness of individual agglomerates within the same sample, leading to inconsistent measurements.

8.3 Aims and objectives.

This work aimed to refine the ABI index method that Birch and Marziano developed and a more convenient methodology. In this work, a series of experiments were performed by varying the frequencies and duration of sieving cycles. The data was analysed by plotting various parameters to get the straight-line curves for linear fitting. Moreover, work has also been done to investigate the mechanical properties of the agglomerates by using a hardness tester.

8.4 Materials and Methodology

8.4.1 Material

Glass beads (GB1-GB5), from VWR International Limited, were selected as a substrate. Micronized PCM as a solute supplied by Mallinckrodt Inc., Raleigh, N.C., USA. Methanol, purchased from VWR (purity 99.9%) was used as a solvent.

8.4.2 Methodology

Sample was prepared with the same methodology as explained in Chapter 4.

The agglomerated material was characterized in the same by measuring extent of agglomeration and ABI index as explained in chapter 4. For these set of experiments the RPM number of sieving cycle, and sieving cycle time were not constant. Table 8-1 Experimental parameters for refining of ABI index method provides summary all the parameters.

Table 8-1 Experimental parameters for refining of ABI index method

Parameters	Range	
	Minimum	Maximum
RPM	500	2800
Cycle time (sec)	30	60
No of sieving cycles	Until the lump breaks completely	
The concentration of PCM (g) in 100 mL solvent	0.2	1
Glass beads (μm)	GB1, GB2, GB3, GB4, GB5	

8.4.2.1 Hardness testing

A tablet hardness tester is a method used to measure a tablet's hardness or breaking point.

During hardness testing, the tablets are placed between two jaws, one of which is attached to the load cell and is immobilized and the other is connected to a motor that provides the mechanical drive. The motorised jaw compresses the tablet against the stationary jaw until the tablet cracks. As soon as the tablet cracks, the motorised jaw retracts. The force generated to break the tablet gives the hardness value (Tablet Hardness tester: The complete guide, 2020). Similarly, in this work, the same hardness testing technique was applied to measure the hardness of the agglomerates. Kreamer Elektronik hardness tester (Figure 8-8) was used with a load cell of 50 N. This hardness tester also measured the length/diameter of the agglomerates.

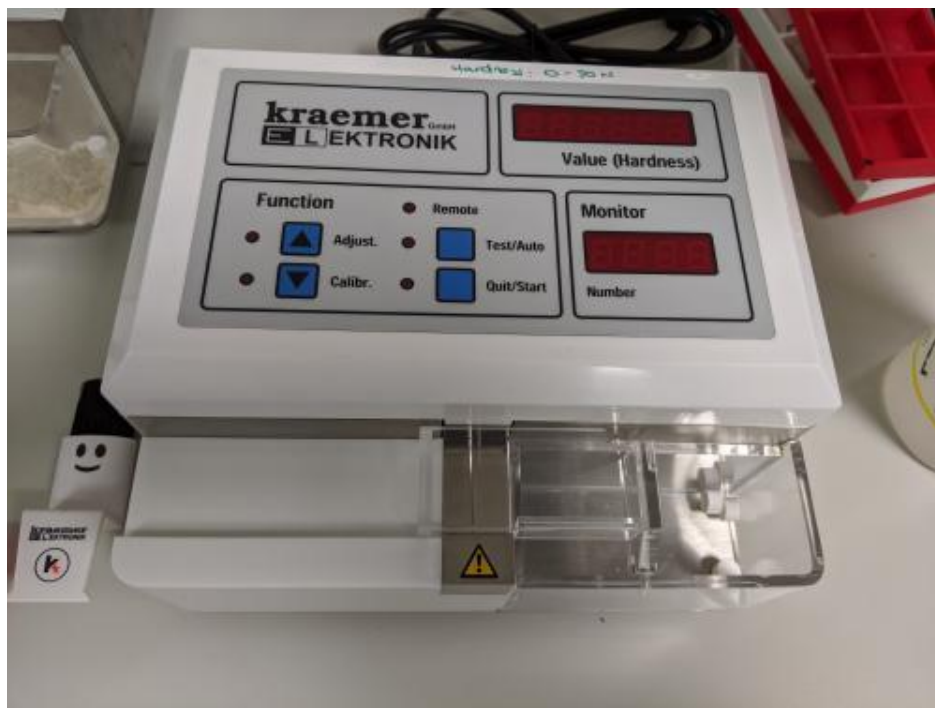


Figure 8-8 Hardness tester

8.5 Results and discussion

A series of experiments were performed to develop a more convenient plot fitting technique to evaluate the mechanical strength of agglomerates. The work was done by varying the frequency of the mini vortex mixer used for sieving the samples generated with different solution concentrations. The aim was to obtain a straight line curve for linear fitting, which can relate linear decay with time by involving the initial amount of agglomerate in data fitting. Moreover, the effect of varying the breakage pattern of agglomerates was also analysed.

8.5.1 Linear fitting

8.5.1.1 Experiment with minimum and maximum concentration sample

In this experiment set, samples were prepared using maximum concentration, i.e., 1 g PCM in 100 mL of solvent, and the minimum concentration, i.e., 0.2 g of PCM in 100 mL of solvent, by using GB1 and GB5 as a substrate. Dried samples were sieved at 500,700, 1400, 1600, and 2800 rpm. The lumps were sieved up to the number of cycles or until they broke completely. The maximum number of cycles for harder lumps was 20.

Table 8-2 Results for the extent of agglomeration for minimum and maximum concentration solution samples with smallest and largest bead size

PCM concentration (g/ml)	Glass beads (um)	RPM	Extent of agglomeration (%)
0.01	40-70	500	0.1303
		700	0.1460
		1400	0.1635
		1600	0.1180
		2800	0.1512
0.01	400-600	500	0.1303
		700	0.1460
		1400	0.1635
		1600	0.1180
		2800	0.1512
0.002	40-70	500	0.1287
		700	0.1086

		1400	0.1647
		1600	0.1611
		2800	0.1155
0.002	400-600	500	0.1666
		700	0.1216
		1400	0.1046
		1600	0.0845
		2800	0.1356

The mass retained on the top sieve after each cycle was recorded and plotted against different sets of parameters as listed;

- Frequency into number of cycles
- Frequency into number of cycles divided by solution concentration.

Frequency into number of cycles

The power law fitting graphs in Birch and Marziano's work was plotted for mass retained on the top sieve against cycle time. Those plots were not straight line graphs, so in this work, the mass retained on the top sieve was plotted against the product of frequency used to sieve that particular sample and the number of cycles of sieving till agglomerates break entirely. Figure 8-9 and Figure 8-10 represent the results. However, this didn't lead to straight-line curves.

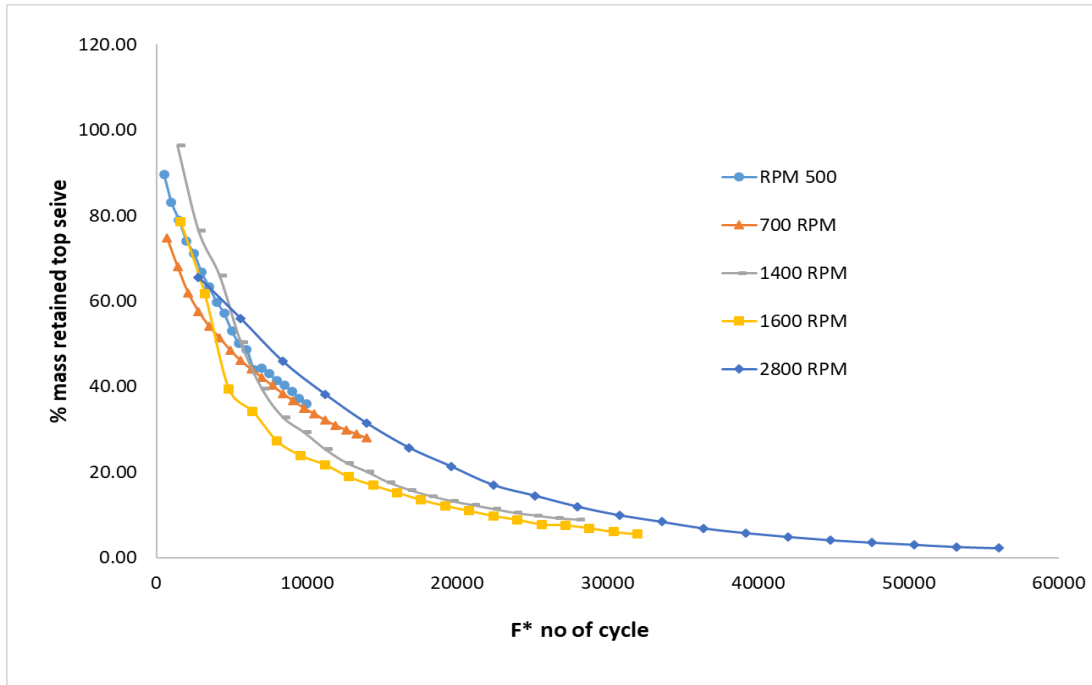


Figure 8-9 Percentage of mass retained on top sieve V/s Frequency*no of cycles for 1 g PCM/100ml methanol 40-70 μm beads

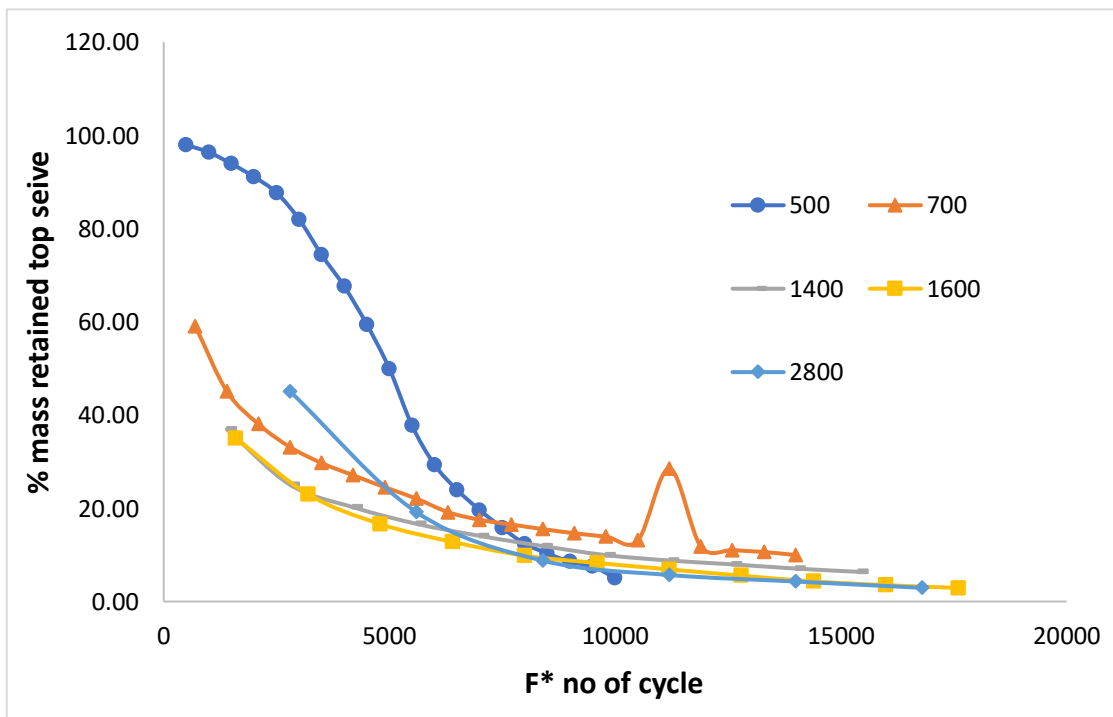


Figure 8-10 Percentage of mass retained on top sieve V/s Frequency*no of cycles for 0.2 g PCM/100ml methanol 40-70 μm beads

Frequency into number of cycles into solution concentration

After not getting the straight line curves by using frequency as a plotting parameter, in the next step, the product of frequency and number of cycles was divided by solution concentration and

plotted against the percentage of mass retained on the top sieve.

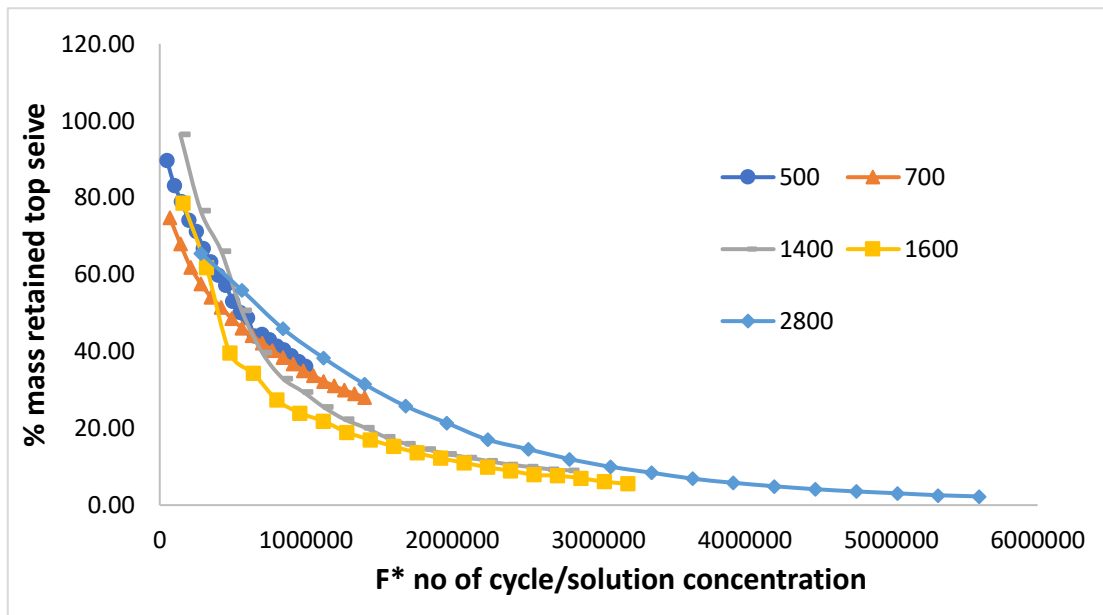


Figure 8-11 Percentage of mass retained on top sieve V/s Frequency*no of cycles/solution concentration for 1 g PCM/100ml methanol 40-70 μm beads

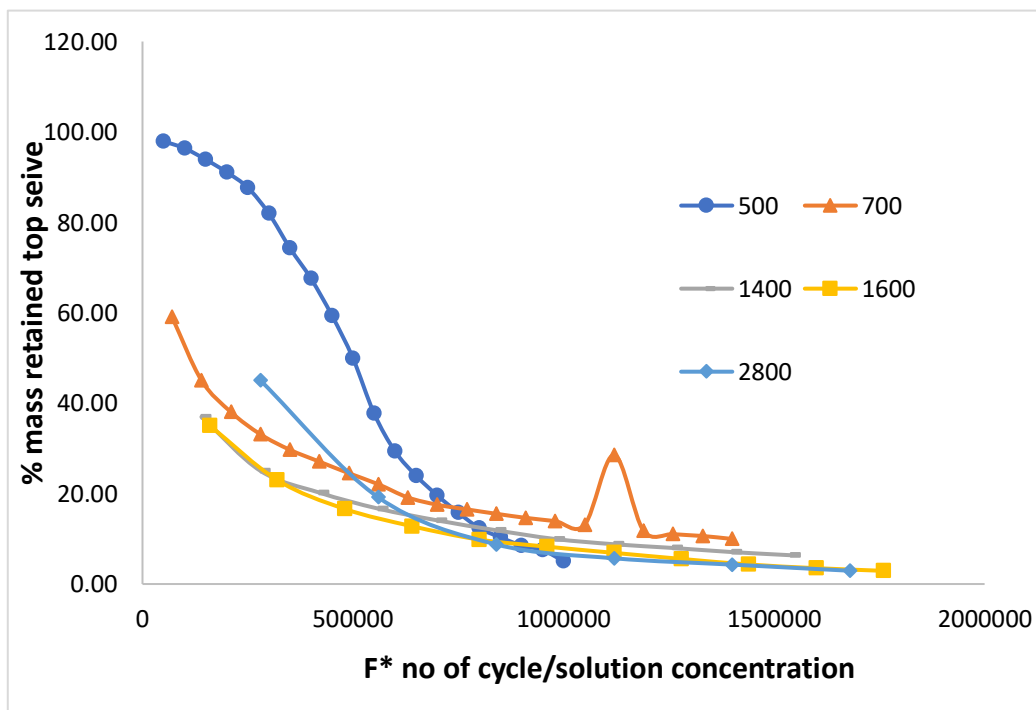


Figure 8-12 Percentage of mass retained on top sieve V/s Frequency*no of cycles/solution concentration for 1 g PCM/100ml methanol 40-70 μm beads

The resulting graphs (Figure 8-11 and Figure 8-12) were almost similar to the previous ones and were not a straight line. Moreover, some other parameters, like the mass of the solute used, was plotted against the percentage of mass retained on the top sieve, but the result was the

same, there was no ready path to get straight line curves for linear fitting.

8.5.2 Breakage analysis

Different breakage patterns of agglomerates were observed depending on varying frequencies during sieving cycles. For lower frequency, the breakage pattern was more like sanding. The effect was more evident for smaller bead sizes. Even for agglomerates with larger bead sizes, the agglomerates didn't flip upside down; however, the lump chipped off from the sides along with the sanding movement.

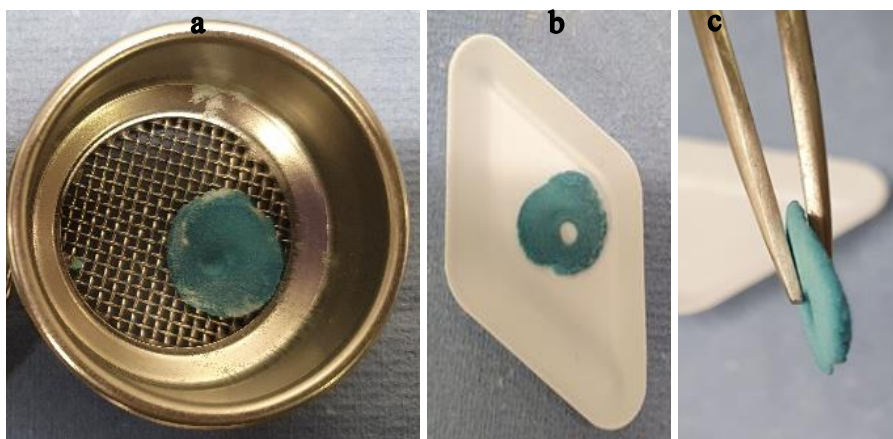


Figure 8-13 0.01g/ml PCM methanol 40-70 μm beads agglomerate sieved at 500 rpm (a) Agglomerate after manual tapping (b) and (c) agglomerate after 8 cycles of sieving

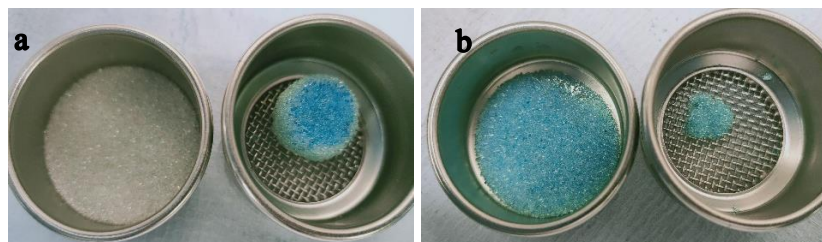


Figure 8-14 0.01g/ml PCM methanol 400 – 600 μm beads agglomerate sieved at 500 rpm (a) agglomerate after manual tapping (b) agglomerate after 8 cycles of sieving

Another observation for the breakage pattern at low frequency was the difference in the mass loss after each cycle of sieving depending on the initial placement of agglomerates, as agglomerates didn't flip during sieving cycles at low frequency. The top side of the agglomerate formed is hard, while the bottom is soft. If the bottom side of the agglomerate is towards the sieve, the mass loss is more rapid than the top side.

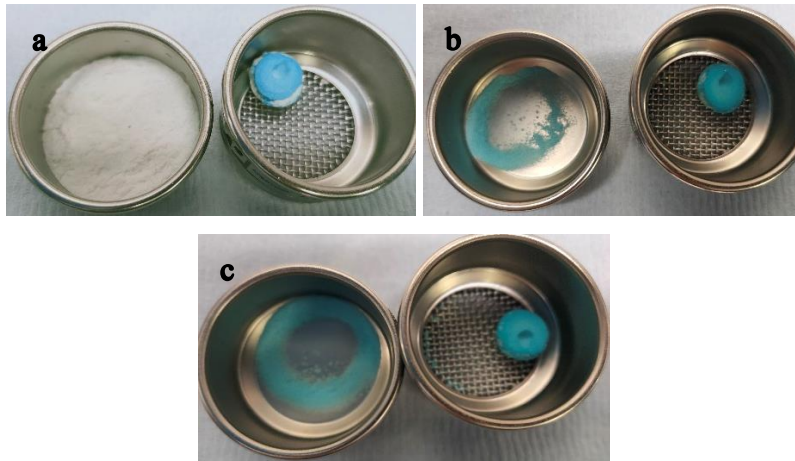


Figure 8-15 0.01g/ml PCM methanol 400 – 600 μm beads agglomerate sieved at 500 rpm with the top side towards sieve
 (a) agglomerate after manual tapping (b) after 4 cycles of sieving (c) after 8 cycles of sieving

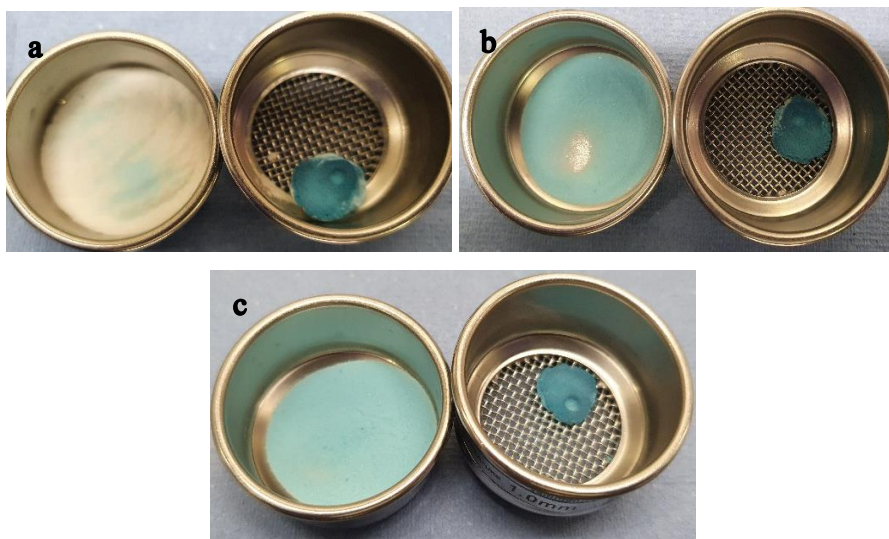


Figure 8-16 0.01g/ml PCM methanol 400 – 600 μm beads agglomerate sieved at 500 rpm with the bottom side towards sieve
 (a) agglomerate after manual tapping (b) after 4 cycles of sieving (c) after 8 cycles of sieving

The agglomerates vigorously move around the sieves for higher frequencies, and the breakage occurs from all sides of the agglomerates. Moreover, the percentage of mass loss for each cycle is higher for higher frequencies than for the cycles at low frequencies.

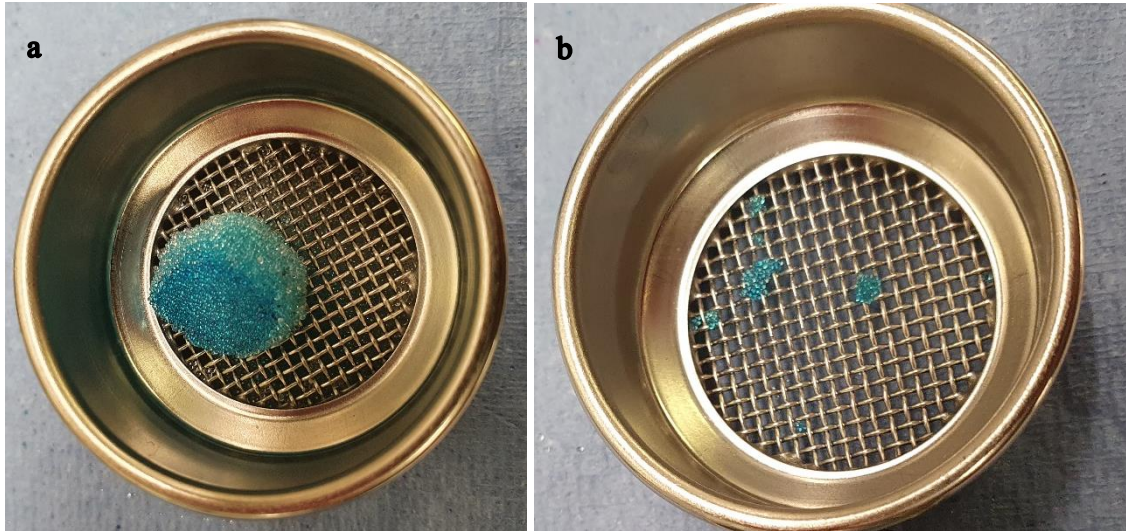


Figure 8-17 0.01g/ml PCM methanol 400 – 600 μm beads agglomerate sieved at 2800 rpm (a) agglomerate after manual tapping (b) agglomerate after 4 cycles of sieving

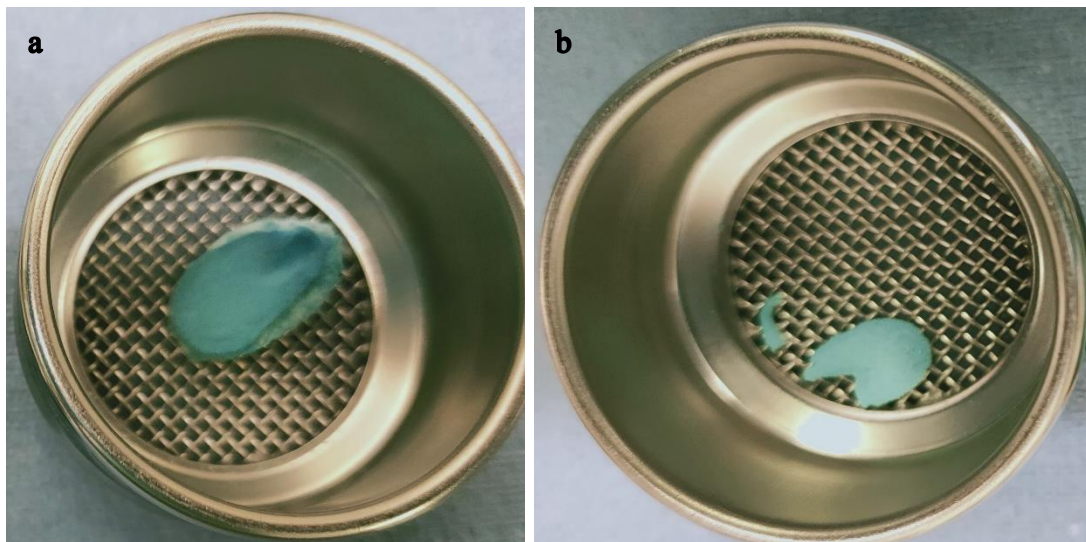


Figure 8-18 0.01g/ml PCM methanol 40 – 70 μm beads agglomerate sieved at 2800 rpm (a) agglomerate after manual tapping (b) agglomerate after 8 cycles of sieving

8.5.3 Hardness testing

Hardness testing was performed by using Kreamer Electronic 50 N load cell. This methodology was rejected for hardness testing of agglomerates after some initial experiments due to various issues. The agglomerates formed were oval and triangular (Figure 8-19) from the bottom side, due to which the distribution of force was not uniform, and the crack didn't propagate throughout the lump; instead, some sides got chipped off, hence not providing the accurate hardness of the lump. Due to shape, the agglomerate also flipped to the side as the plate exerted force on the lump (Figure 8-20 b). Moreover, the agglomerates formed with a lower

concentration of PCM got entirely crushed by applying force (Figure 8-20 a).



Figure 8-19 Pointed oval-shaped agglomerate.

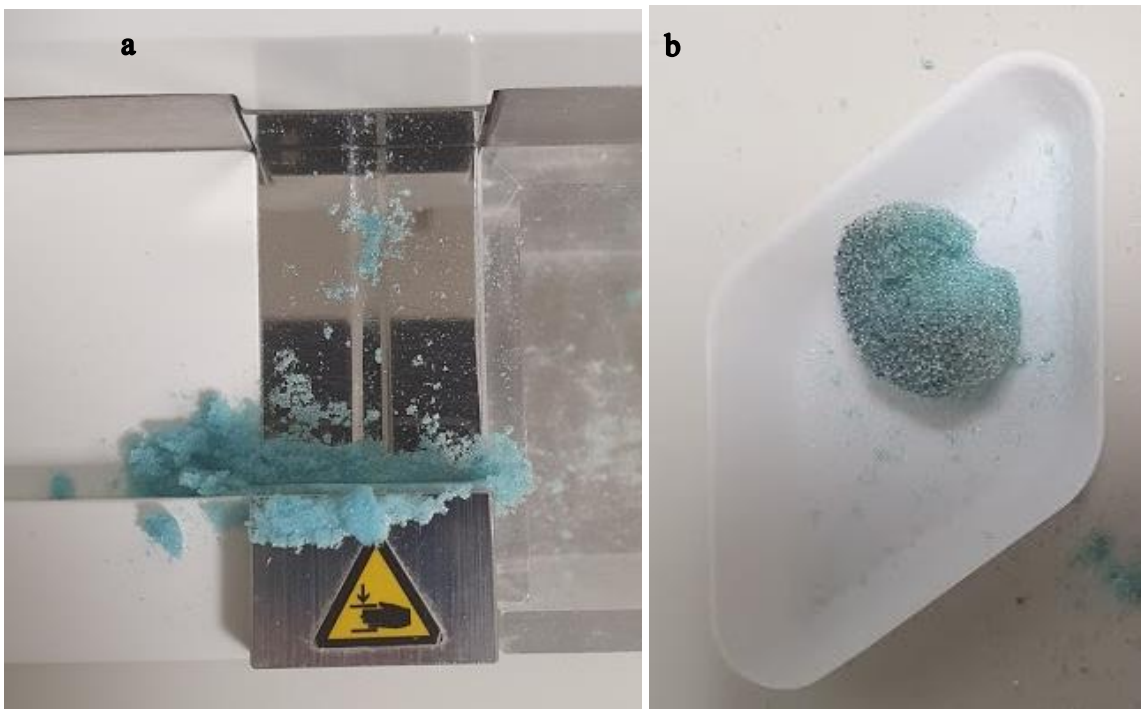


Figure 8-20 (a) agglomerate completely crushed after applying force on hardness tester (b) agglomerate chipped off from one side due to unequal force distribution from hardness tester

8.6 Conclusion

The objective of the study was to explore an alternative data fitting method to facilitate a more convenient analysis for determining agglomerate strength. Unfortunately, the results and graphs obtained from this attempt did not lend themselves well to linear fitting. The initial approach involved incorporating initial masses into the plots and fitting the curve linearly, aiming to establish a connection between the initial and final mass after sieving. The purpose was to investigate whether the decay in mass during sieving follows a linear pattern.

The decision to incorporate initial mass in the analysis arose from the observation that some lumps were exceedingly fragile and broke apart during the first few cycles of sieving, while others remained intact due to their hardness. This resulted in very low ABI (Agglomerate Breakage Index) values when applying power law fitting without accounting for the initial mass, indicating that the lumps were perceived as extremely hard. However, by including the initial mass in the ABI index calculation, it became apparent that a significant portion of the lump's mass was lost during the initial sieving cycles, thereby supporting the assertion that the lump is indeed fragile.

Furthermore, an attempt was made to employ a hardness tester as an alternative technique to assess agglomerate strength in addition to sieving. However, this approach proved ineffective due to the unique nature of the bonds between the particles of the agglomerates, which could not be accurately evaluated using the hardness tester.

In summary, the search for an alternative data fitting method to analyze agglomerate strength did not yield the desired results, and attempts to use a hardness tester as an additional evaluation technique were unsuccessful, primarily due to the complexities of the agglomerate particle bonds.

8.7 References

Birch, M. and Marziano, I. (2013) 'Understanding and Avoidance of Agglomeration During Drying Processes: A Case Study. Doi: 10.1021/op4000972.

Charles Ischi AG – Testing Technology (no date). Available at: <https://www.ischi.ch/> (Accessed: 19 May 2019).

Instron : Materials Testing Machines for Tensile, Fatigue, Impact, Rheology and Structural Testing - Instron (no date). Available at: <https://www.instron.co.uk/en-gb> (Accessed: 19 May 2019).

Simurda, M. (2017) *SOLVENT SELECTION FOR ISOLATION OF PHARMACEUTICAL PRODUCTS*. University of Chemistry and Technology Prague.

Tablet Hardness tester: The complete guide (2020) *Tablet Hardness Tester: The Complete Guide - SaintyTec*. Available at: <https://www.saintytec.com/tablet-hardness-tester/> (Accessed: 9 December 2022).

Chapter 9: Investigation of lab scale equipment for particle breakage

This chapter presents the work done to investigate alternative crystal breakage assessment tests to provide a scaled-down apparatus for mimicking particle breakage encountered in agitated dryers at various scales. The main objective was to develop a small-scale test to predict likely particle breakage behaviour in process scale equipment. Three approaches were considered. The first used a tapped bulk density measurement instrument to evaluate the changes in particle packing behaviour and the extent of crystal breakage by applying different normal pressures linked to varying the tapping procedure. Particle breakage was also evaluated using a Freeman FT4 powder rheometer (Freeman Technology Tewkesbury UK.) and a bespoke agitated drying test rig developed for the University of Strathclyde by Alconbury Weston Ltd. (Part of the DEC Group Ecublens Switzerland). A comparison was made by performing a size analysis of the crystalline powder and measuring the normal stresses applied to the powder.

9.1 Aims and objectives

Figure 9-1 sets out to provide a “big picture” regime map for particle breakage and describes the importance of applying a combination of techniques to achieve the project objective of developing a strategy and small-scale tests to predict likely particle breakage behavior in process scale equipment. The figure indicates the utility of combining single crystal characterization experiments (A) to investigate individual particle propensity to break with investigations of small populations for crystals, (B), i.e., small lab scale tests suitable for deployment early in the process development cycle and linking this with suitable bulk powder characterization, (C), i.e., particle size analysis.

“Particle breakage Big Picture”

Aim to deploy a combination of (A) (B) & (C)

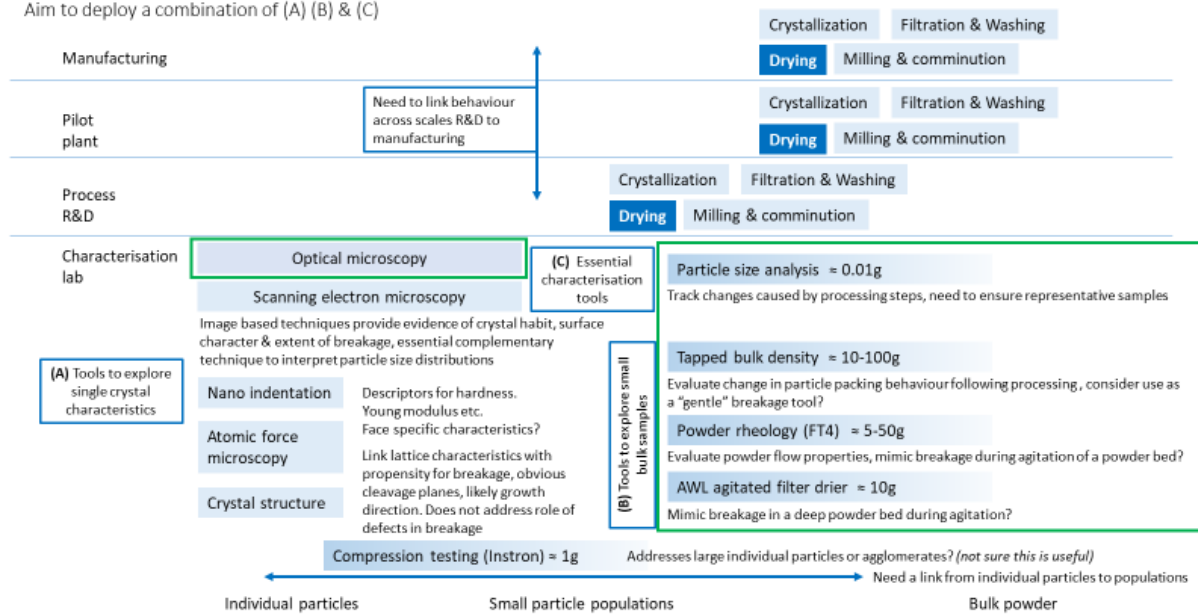


Figure 9-1 Overview of potential approaches to characterizing particle breakage behaviors

This research project was planned to develop a semi-empirical approach based on the correlation of material properties and breakage assessment tests to provide a scaled-down concept/apparatus for mimicking particle breakage in agitated dryers at various scales. The experimental plan was divided into three components:

1. Single crystal mechanical properties characterization by using an Atomic force microscope (AFM) and nanoindentation.
2. Development of an appropriate small-scale (<10g) particle attrition and breakage test selected from:
 - a. The modified tapped bulk density measurement instrument
 - b. Particle breakage investigation using the Freeman FT4 shear cell method
 - c. Particle breakage investigation by using AWL vacuum agitated dryer
3. Particle size measurement to evaluate the nature and extent of particle breakage arising in the procedures in (2) by using Morphology G3.

However, due to time and travel limitations arising because of Covid-19, the characterization of a single crystal using AFM and nanoindentation was not performed. The main element of the work which was performed was to investigate whether less sophisticated techniques (like a tapped bulk density density measurement cell) can be considered a gentle breakage tool which could correlate with breakage in agitated dryers and to get comparable results correlating shear

stress-normal stress and particle size distribution (PSD) variation by using freeman FT4 shear cell method and the AWL vacuum agitated dryer.

9.2 Materials and Methodology

9.2.1 Material

Powdered PCM (purchased from Sigma-Aldrich, batch number MKCJ5427) was used as a test compound.

9.2.2 Methodology

As mentioned above, three pieces of equipment were selected to investigate particle attrition to provide a potential scaled-down apparatus that can mimic particle breakage in agitated dryers at various scales. Particle size analysis of the material before and after the experiment was performed to observe the extent of breakage.

9.2.2.1 Tap bulk density

A tapped density analyzer (Autotap Anton Paar GmbH Graz Austria) (Figure 9-2) is designed to measure tapped density. The initial concept was to evaluate the potential of the Autotap instrument by mechanically changing the step height (i.e., drop) and investigate attrition by monitoring for changes in particle size distribution. However, the required modification could not be performed easily and instead another approach was applied by placing metallic discs on top of the powder bed and performing the experiments with the unmodified Autotap. In this way the metallic discs applied normal pressure on the powder bed, and particles were expected to break under this pressure. Change in particle size was analyzed to see if this approach could cause attrition of the particles.

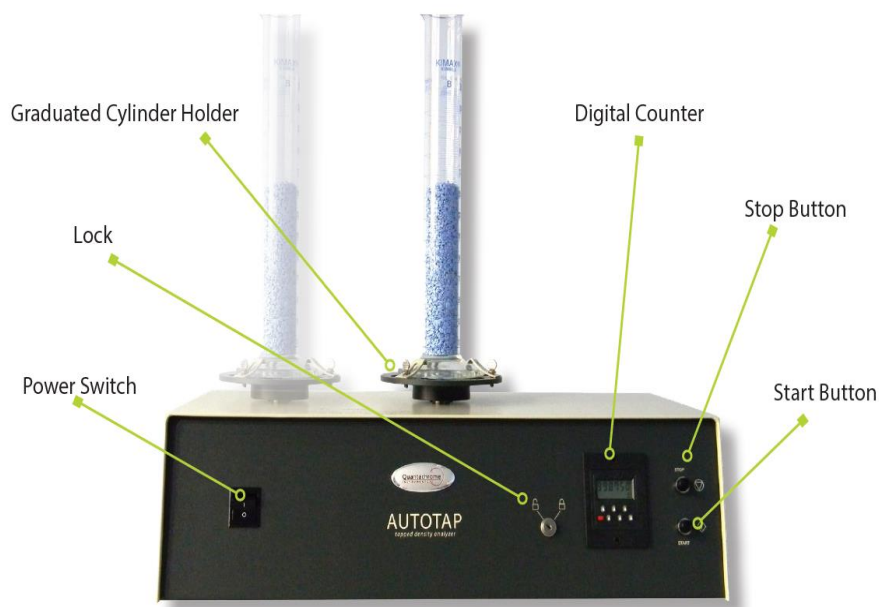


Figure 9-2 Quanta chrome Auto tap Tapped Density Instrument (quantachrome instruments)

Suitable stainless-steel discs were prepared in the departmental workshop. The diameter of the disks was matched to fit the diameter of the glass cylinder used for auto tap (Table 9-1). The thickness of each disc was 5mm.

Table 9-1 Dimensions of measuring cylinder and disks used in modified tap bulk density experiment

Disk number	Glass cylinder volume (ml)	Glass cylinder diameter ($\pm 0.5\text{mm}$)	Discs diameter ($\pm 0.5\text{mm}$)	Disks
1	10	12	10	
2	25	18	16	


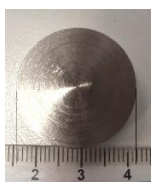
3	100	24	21	
4	250	28	26	

Table 9-2 Parameters of experiments with tapped bulk density equipment

Exp #	Sample name	Cylinder	Sample mass (g)	Weight load (g)	Number of taps
Exp 1	Exp with weight	100 ml	20	15.24	250
	Exp without weight	100 ml	20	15.24	250
Exp 2	Sample 1 & 01	25 ml	5	8.86	150
	Sample 2 & 02	25 ml	5	8.86	250
Exp 3	Sample 1	25 ml	5	0	100
	Sample 2	25 ml	5	13.95	100

	Sample 3	25ml	5	22.65	100
--	----------	------	---	-------	-----

9.2.2.2 Freeman FT4 shear cell method

The Freeman FT4 powder rheometer (Freeman Technology Ltd Tewkesbury UK) is used for the rheological characterization of powders. The instrument is generally used to measure the resistance of the powder to flow while the powder is in motion and, therefore, is appropriate for simulating process conditions. Additionally, the FT4 can measure a powder's shear strength and flow against wall surfaces and bulk properties such as density, compressibility, and permeability. Figure 9-3 shows the general setup of the FT4 powder rheometer. The FT4 standard shear cell method provides flow information for powder at rest which is to shear stress. The rotating shear cell module consists of a vessel containing the powder sample and a shear head to induce both vertical and rotational stresses. The shear head moves downwards, inserting the blades into the powder and induces normal stress as the shear head face contacts the top of the powder. The shear head moves downwards until the required normal stress, σ , is established.

Slow rotation of the shear head then begins, inducing shear stress, τ . A shear plane is established just below the ends of the blades (for more information consult the FT4 instrument documents).

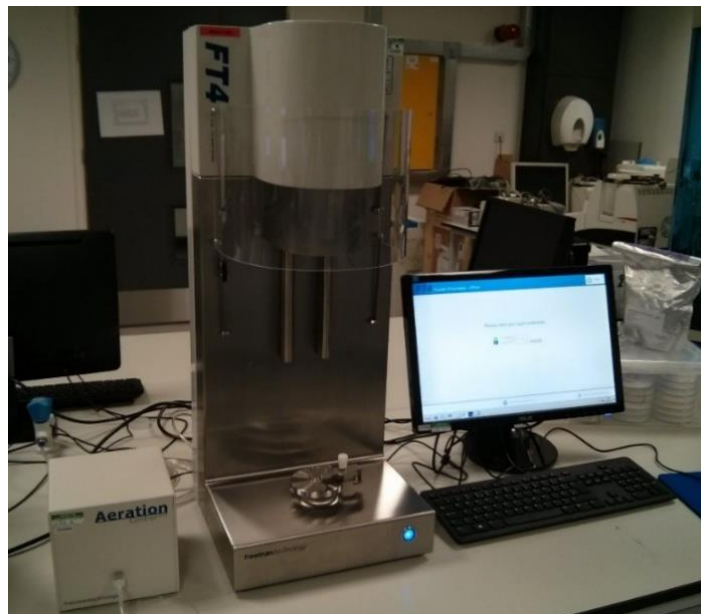


Figure 9-3 Freeman FT4 setup

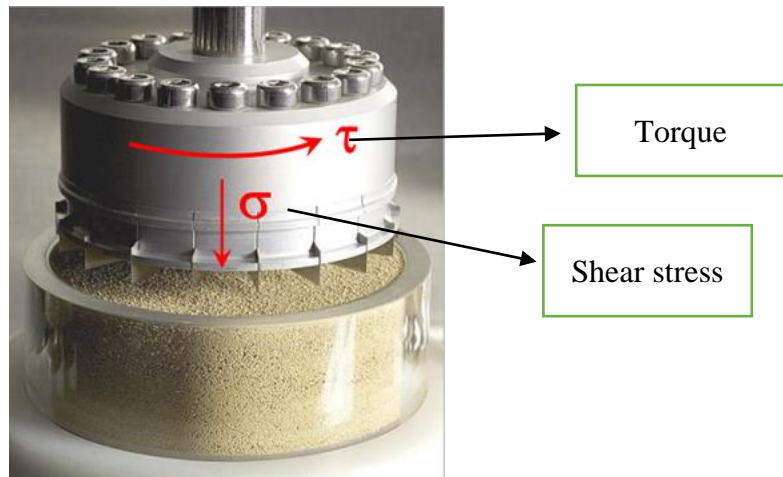


Figure 9-4 FT4 shear cell method (supporting documents)

As the powder bed resists the rotation of the shear head, the shear stress increases until the bed fails or shears, at which time maximum shear stress is measured. The normal stress is maintained constant throughout the shearing step. This maximum shear stress is the point of incipient failure, also called the yield point.

The idea of using an FT4 rheometer in this case study was to use it as a particle breakage analysis tool. The experiment was performed using the 25mm shear cell and applying different normal stresses, i.e., 3 Kpa, 5 kpa, 9 kpa, and 15 kpa, separately on each sample. A 25mm x 10ml split vessel was used for these experiments (Figure 9-5).



Figure 9-5 25mm x 10ml split vessel with bottom assembly (FT4 support document – 25mm Vessel Assemblies – W7021)

The setup was prepared using the plastic bottom with a relative plastic clamp ring, the 25mm glass container, the blade, the plastic funnel, and the clamp screw; the plastic clamp ring was positioned at the right height and locked to the glass cylinder. The plastic bottom was inserted into the glass vessel. The setup was positioned on the instrument table. The vessel was secured by ensuring that the prongs were correctly located in the notches of the clamp ring and tightening the clamp screw. A plastic funnel was placed on top of the glass vessel. The powder was added to the vessel, and mass was recorded.

Initially, the powder was conditioned using a standard FT4 blade to produce a homogenous sample. Then a vented piston was used to consolidate the material. Pre-consolidation allows any entrapped air to escape and ensures that the material is consolidated before applying the shear cell head. This prevents the shear cell head from being surrounded by excess powder, which can adversely affect the application of shear stress to the particle bed.

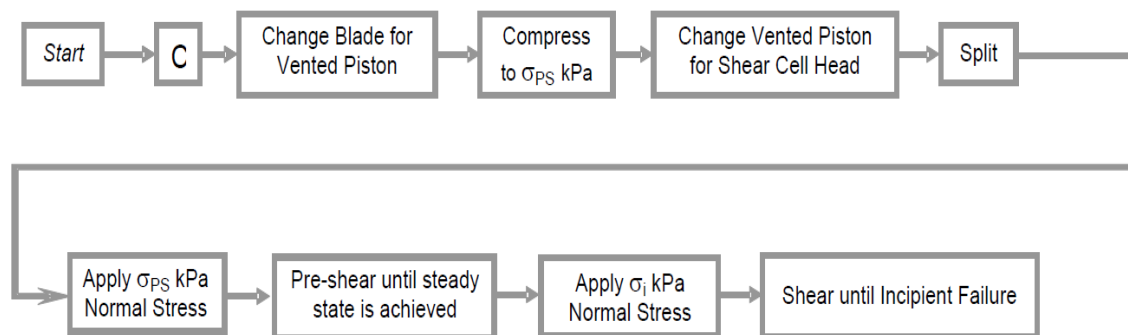


Figure 9-6 Shear cell test sequence (FT4 support document – Shear cell – W7018)

Size analysis of the material was performed before and after each shear cell experiment to measure particle breakage.

9.2.2.3 AWL Vacuum agitated dryer

Alconbury Weston Ltd. (AWL) designed a prototype small-scale drying platform to evaluate the impact of static and agitated drying (Figure 9-7). This drying rig was developed to perform drying investigations with very little material, i.e., 10-15 grams. The drier can be heated by circulating heat transfer medium from a circulator through a coiled copper tubing jacket or by passing air or nitrogen through an AWL heated transfer line before feeding it into the drier by reducing the outlet pressure. The cake temperature is tracked using a thermocouple. Agitation in the drier is provided by a combination of rotation and vertical movement of a stainless steel

agitator, the rotation rate and frequency of vertical movement can be varied independently. The rotation rate ranges from a minimum of 2 rpm to a maximum of 60rpm. The vertical motion in regular operation is limited to 25mm with a frequency range of 4 to 10 cycles per minute. It is possible to change the amplitude of the vertical movement by changing an eccentric cam wheel.

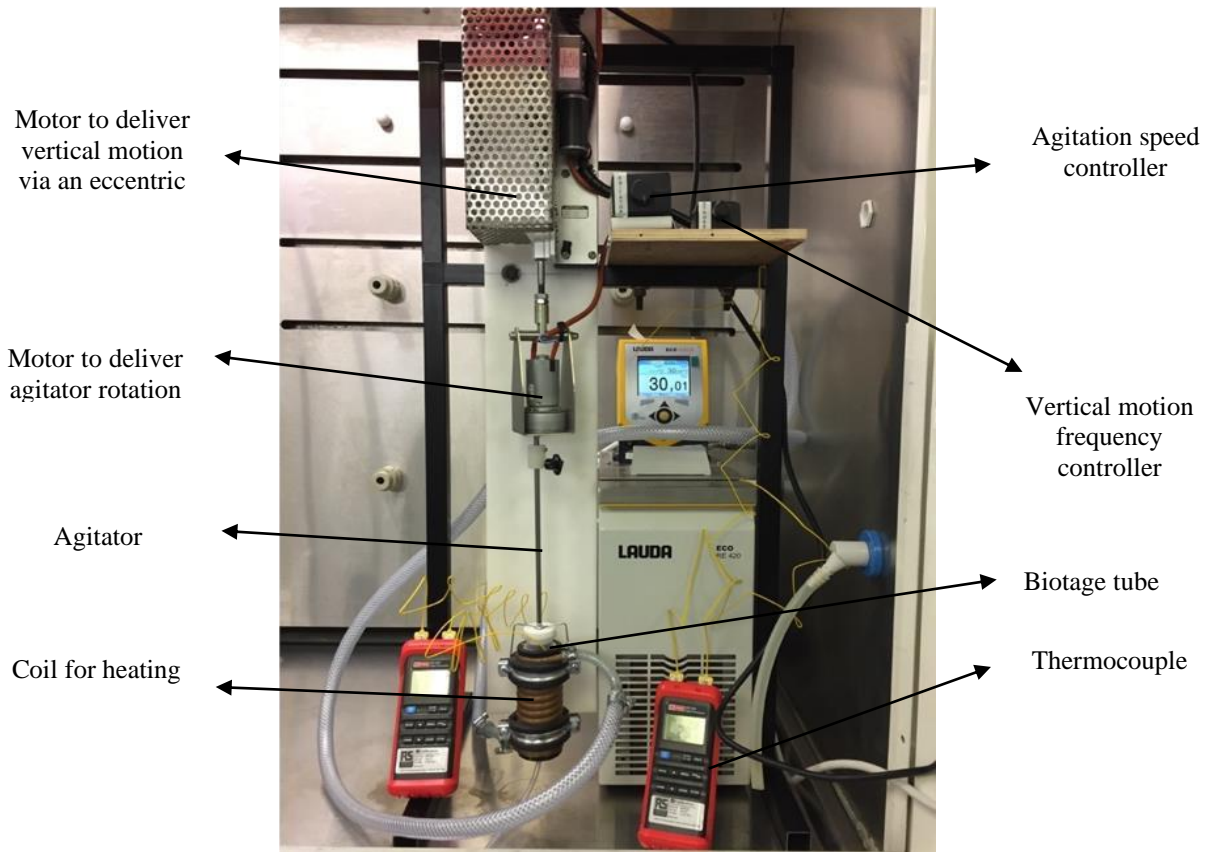


Figure 9-7 AWL agitated vacuum dryer

In this experiment, the aim was to observe the extent of particle attrition by using this agitated dryer by placing different loads on top of the powder bed to apply normal pressure. Ten grams of PCM powder was inserted into the Biotage tube (Biotage, Uppsala, Sweden), and the cake height was measured. The agitator was gently inserted into the powder bed, providing particle conditioning. Then, the weights (tungsten washers - external diameter: $24 \pm 0.5\text{mm}$ and thickness: $2 \pm 0.5\text{mm}$) were gently deposited on the powder bed minimising disturbance of the powder surface. The Biotage tube was lifted and positioned within the dryer, and the agitator was coupled with the drive motors. Agitation speed was maintained at 2 rpm for 20 minutes.

In addition to the evaluation of particle breakage, another aim of this experiment was to

generate a comparison between a vacuum agitated dryer and the FT4 shear cell correlating shear stress with normal stress on particle size distribution (PSD) variation.

Table 9-3 Parameters of experiments with Vacuum agitated dryer

EX P	Raw Material	Filter tube Dia ($\pm 0.5m$ m)	agitator blade dia ($\pm 0.5m$ m)	time (min)	disks weight (g)	bed hight ($\pm 0.5m$ m)	sampl e mass (g)	frequen cy of rotation (rpm)	disk dia ($\pm 0.5m$ m)
S1	Paraceta mol	26.56	26.13	20	0	46	10.0192	2	24
S2	Paraceta mol	26.63	26.13	20	57.6553	45	10.0334	2	24
S3	Paraceta mol	26.54	26.13	20	102.6963	48	10.0842	2	24

9.2.2.4 Particle size analysis and breakability index

Particle size and particle size distribution were determined using Sympatec QIC/PIC and Morphology G3 (Malvern).

Morphology G3 (Malvern Panalytical Ltd., Malvern UK) is a fully integrated software-controlled dry powder dispersion system that measures the morphological characteristics, i.e., the size and the shape of the particles. The instrument is a highly sensitive, high-resolution tool that uses image analysis to characterize the sample particles and provides number-based statistics. Hence the results are generated on multiple individual individual particle providing a statically sound description of the whole sample. A key strength of the instrument is the capability to detect the presence of fine particles (Malvern instruments, no date)

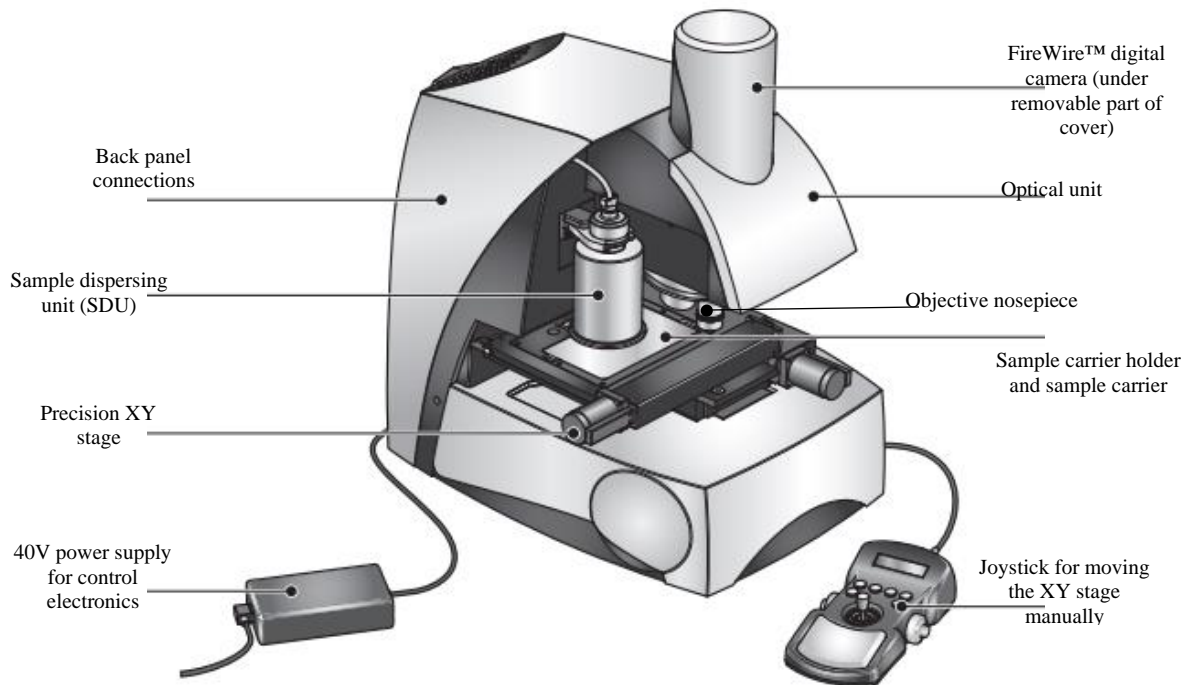


Figure 9-8 Components of Morphology G3 (Malvern instruments)

An SOP was developed for the Morphology G3 analysis to evaluate the particle sizes of the samples generated using each of the potential breakage characterization tools (tapped bulk density, Freeman FT4, AWL Vaccum agitated dryer). The particle size measurements were made using a 0.5 bar injection pressure and 20 ms injection time. An episcopic light source was used in brightfield mode, and an objective lens of 5x magnification was used to measure particle size between 6.5 μm to 430 μm . For QICPIC, RODOS/L with VIBRI feeder set up at a feed pressure of 0.5 bar, feed rate setting of 40%, and a 1.5 mm gap width was used.

The extent of particle breakage can be verified by comparing the raw material and the material characterized with the breakage characterization tools. The breakability index is calculated as a normalized x_{50} variation between the untreated and broken samples, as reported in the following equation (Equation 9-1) (Unpublished work Ottoboni University of Strathclyde) (Ottoboni, 2013).

$$\text{Breakability index} = \left(\frac{x_{50 \text{ untreated}} - x_{50 \text{ treated}}}{x_{50 \text{ untreated}}} \right) * 100 \quad \text{Equation 9-1}$$

Where,

Untreated is the raw material, and

Treated is the sample obtained from the breakage characterization tool.

9.3 Results and discussion

9.3.1 Tap bulk density

1st Experiment: Comparison of particle breakage with and without added weight

Preliminary experiments were performed to evaluate the particle breakage in the tapped bulk density (TBD) experiment with and without adding additional weight on the particle bed. Before and after the experiment, the sample size analysis was performed using sympatec QICPIC. The procedure was repeated three times, and the average values of size analysis were taken to calculate the breakability index.

Table 9-4 Particle size analysis and breakability index of preliminary experiment with powdered PCM by QICPIC

Material	X₁₀ (um) (STDV)	X₅₀ (um) (STDV)	X₉₀ (um) (STDV)	Breakability index (%)
Powder PCM	46.48 (5.71)	222.04 (18.23)	288.76 (59.64)	-
Powder PCM after TBD experiment with weight	32.28 (9.72)	105.20 (44.88)	282.01 (118.12)	0.53
Powder PCM after TBD experiment without weight	35.10 (8.44)	136.48 (24.09)	367.42 (103.03)	0.39

There was a significant variance in the repeated size analysis with QICPIC leading to the high standard deviation, especially for x₉₀ (Table 9-4). However, this size analysis indicates that particle breakage is occurring. Calculating the breakability index using equation 6-7 and comparing the values for the experiments with and without weight loads on the particle bed

confirms that the material breakage increased by adding a weight on top of the powder bed.

2nd experiment: Investigation of powder consolidation

The objective of this work was to develop a small-scale methodology for particle breakage investigation. After performing preliminary experiments, the following experiment was performed with a 25mL cylinder and 5 grams of material to which the appropriate metal disk for a 25ml cylinder was added as the weight (Table 9-2). The investigation was performed with 150 (Sample 1, three replicates) and 250 taps (Sample 2, three replicates). After the required number of taps the consolidated material was removed from the glass cylinders and the particle size was determined and is recorded in Table 9-5.

Table 9-5 Particle size analysis and breakability index of 2nd experiment by using 25 ml cylinder with 150 and 250 taps performed by QICPIC

Material	X₁₀ (um) (STDV)	X₅₀ (um) (STDV)	X₉₀ (um) (STDV)	Breakability index (%)
Powder PCM	46.48 (5.71)	222.04 (18.23)	288.76 (59.64)	-
Sample 1	28.06 (5.40)	78.36 (9.45)	196.70 (43.37)	0.6471
Sample 2	28.98 (4.67)	100.20 (24.84)	284.88 (83.88)	0.5487

The results in Table 9-5 indicate unexpectedly that particle breakage decreases by increasing the number of taps, this may be because the compressed material begins to become agglomerated as the number of taps is increased and the material becomes more densely packed. However, the variation between the repeats was high, so it was decided to perform size analysis using the morphology G3 in addition to QICPIC. Moreover, it was observed that the metal disk load rests on the upper part of the particle bed while it is the bottom part of the bed which becomes most consolidated.

Based on this observation of uneven consolidation a further experiment was performed under

the same conditions as the previous one, i.e., 5 grams of material was added to a 25 mL cylinder, the experiment was performed with 150 taps and 250 taps. However, in this experiment the consolidated (A) and unconsolidated (B) material was removed from the cylinder and analyzed separately. It was also observed that the upper unconsolidated material could be removed from the cylinder easily, while the bottom-packed material needed taping to be taken out (Figure 9-9).

Table 9-6 Particle size analysis and breakability index of consolidated and unconsolidated material by using 25 ml cylinder with 150 and 250 taps performed by QICPIC

Material	Morphology G3				QICPIC		
	Dv ₁₀ (μm)	Dv ₅₀ (μm)	Dv ₉₀ (μm)	STDV (μm)	x ₁₀ (μm)	x ₅₀ (μm)	x ₉₀ (μm)
Powder PCM	28.99	99.72	231.70	15.47	46.48 (5.71)	222.04 (18.23)	288.76 (59.64)
Sample 01 A	37.74	114.00	257.10	19.60	43.01 (1.02)	168.29 (84.44)	476.75 (104.79)
Sample 01 B	29.28	81.24	231.70	14.65	26.17 (2.64)	76.86 (12.91)	167.13 (36.34)
Sample 02 A	38.33	110.10	259.60	16.73	41.3067 (4.46)	155.03 (23.90)	417.59 (65.90)
Sample 02 B	31.84	99.91	246.90	15.72	23.04 (4.78)	62.17 (21.00)	167.97 (90.09)

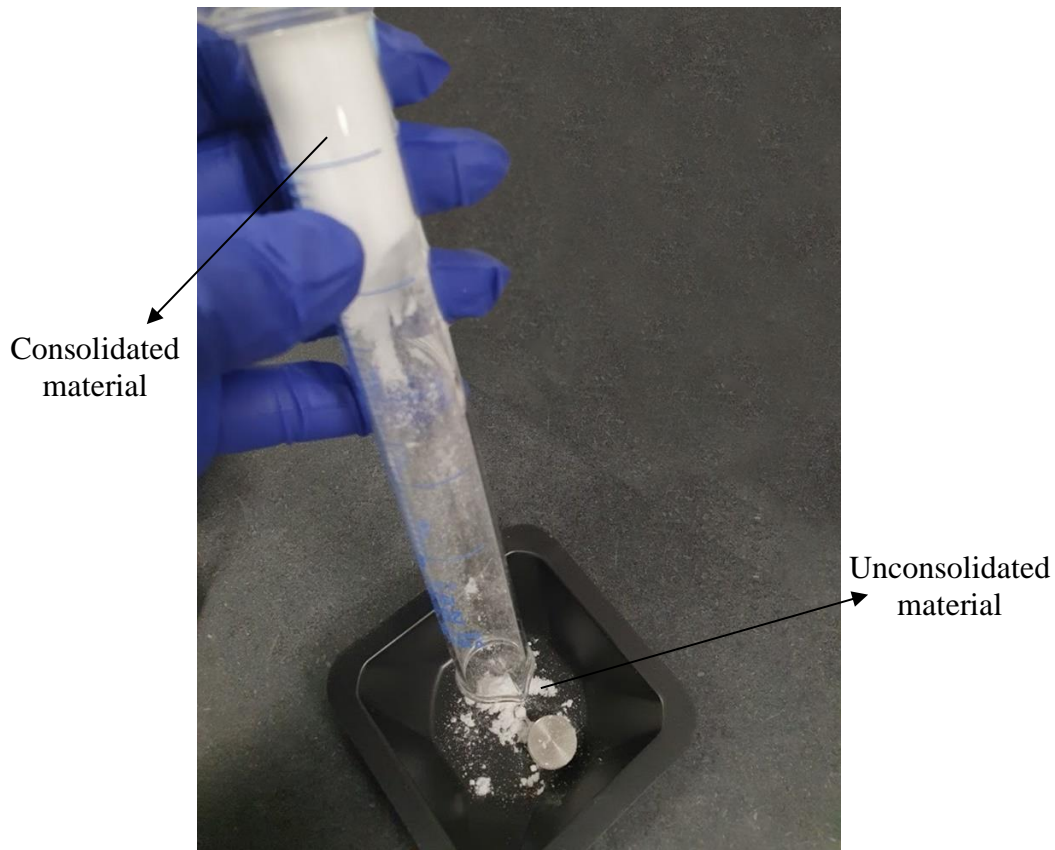


Figure 9-9 Consolidated and Unconsolidated particle bed after tap bulk density experiment with weight loads

The results from Table 9-6 suggest that the particle breakage is greatest in the unconsolidated material, i.e., near the metal disk, while the packed material in the base of the cylinder shows less particle attrition. However, comparing x_{90} and dv_{90} of raw and consolidated material, it can be presumed that material starts agglomerating instead of attrition. Moreover, by comparing the size analysis of sample 01 (150 taps) with sample 02 (250 taps), it appears that by increasing the number of taps attrition of particles reduces, which is a counter intuitive finding.

3rd Experiment: Investigation of the effect of increasing the weight loading

In this experiment, the effect of the increasing weight loads on the attrition of a particle bed subject to tapping was investigated by keeping the sample mass the same for each experiment, i.e., 5 grams. Each experiment was performed using a 25 ml cylinder with increasing weight loads. Size analysis of the samples was performed by morphology G3 and is reported in Figure 9-10.

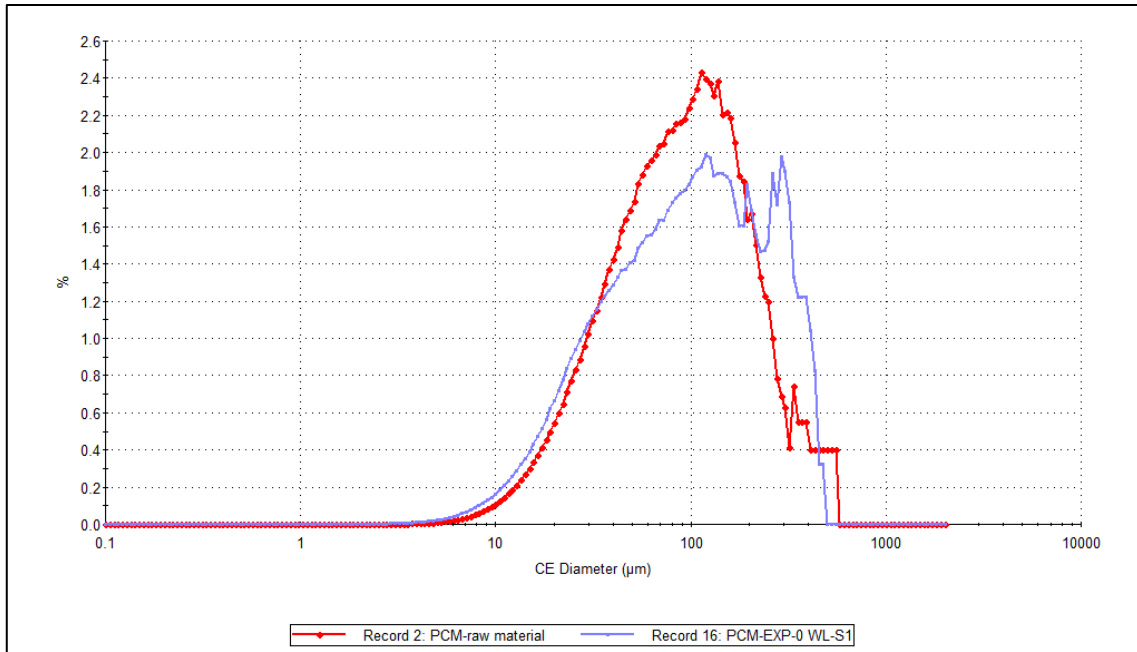


Figure 9-10 Comparison of the particle size distribution of raw material with sample 1 (analysis was performed without adding weight load on particle bed) using tap bulk density by using Morphology G3

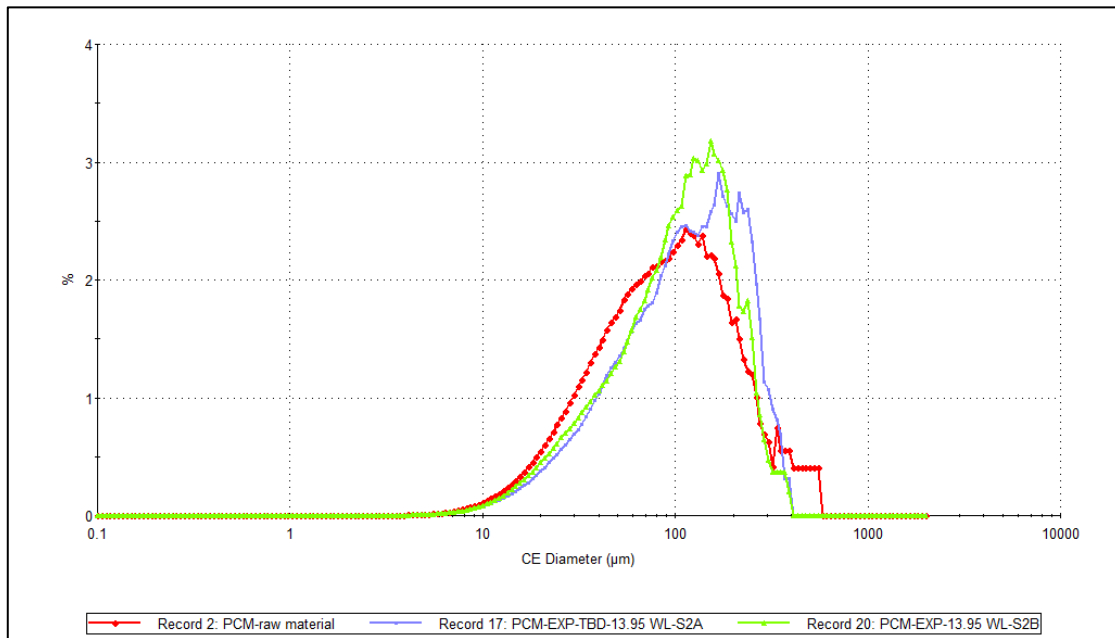


Figure 9-11 Comparison of the particle size distribution of raw material with sample 1 (analysis performed by adding two weight loads on powder bed,) using tap bulk density by using Morphology G3

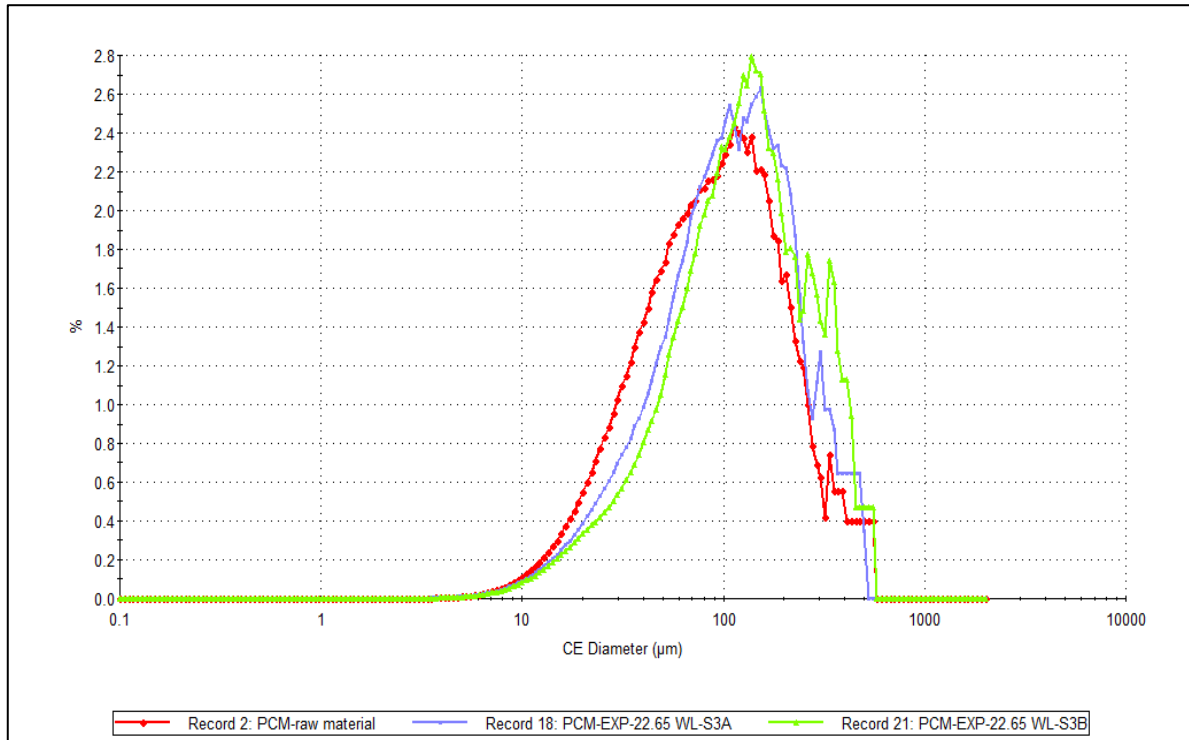


Figure 9-12 Comparison of the particle size distribution of raw material with sample 1 (analysis was performed by adding three weight loads on particle bed) using tap bulk density by using Morphology G3

The results are shown in Figure 9-10, Figure 9-11, and Figure 9-12, indicating that by increasing the weight load on the particle bed, particle attrition appears to decrease. This may be because particles tend to agglomerate under the applied forces as well as breaking. Moreover, the particle size of the material close to the metal disks (unconsolidated, sample b) appears to increase more than for the consolidated material at the bottom of the powder bed. This might conceivably be due to increases in the electrostatic charge in the PCM powder closest to the disks linked to the increased particle motion, as encountered in the case of sieving (chapter 7, section 7.2.2.5) (Fotovat, Bi, and Grace, 2017).

From the results of the experiments using tapped bulk density instrument, it was concluded that this equipment could not be used as a particle breakage characterization tool as by increasing the number of taps and the weight loads on the particle bed, the particle bed tends to form lumps which are not readily dispersed during particle sizing hence leading to an apparent decrease in the particle breakage. Moreover, the data obtained from tapped bulk density instrument was insufficient to correlate the particle breakage with the large-scale dryers. Normal stresses applied by the weight loads could be calculated by using Equation 3-4.

However, the shear stress, which plays an important role in particle breakage, could not be calculated as the disks are moving vertically, and there is no angular rotation to measure torque and shear stress related to that torque. For this reason the tapped bulk density instrument fails to replicate the particle shear stress experienced in an agitated drier.

9.3.2 FT4 shear cell test

Previously, Ottoboni (2013) (by using Am Ende *et al.*, 2013; Remy *et al.*, 2015 methodology) (chapter 3) had investigated particle breakage by using a normal FT4 blade . An advantage of the FT4 instrument is that the force and torque applied to the powder bed during the agitation experiment could be measured. A series of additional bespoke tungsten weights were required to run the experiment with the customized aeration cell and also with higher normal stress (the target 200-300g could not be reached even using a dense metal like tungsten (density:19450 kg/m³) because of the design constraints of the instrument. Consequently, particle breakage with the shear cell test was not investigated.

Therefore, to extend this work to investigate the particle breakage with the FT4 shear cell method, the shear cell test was performed by applying 3, 5, 9, and 15-kPa normal pressure on different samples separately. The idea was to get shear stress data from FT4 that can be compared by the data obtained from AWL vaccum dryer and can be used for down scaling investigations. The experiments were repeated twice. Figure 9-13 shows the values of shear stress generated from applied normal stresses.

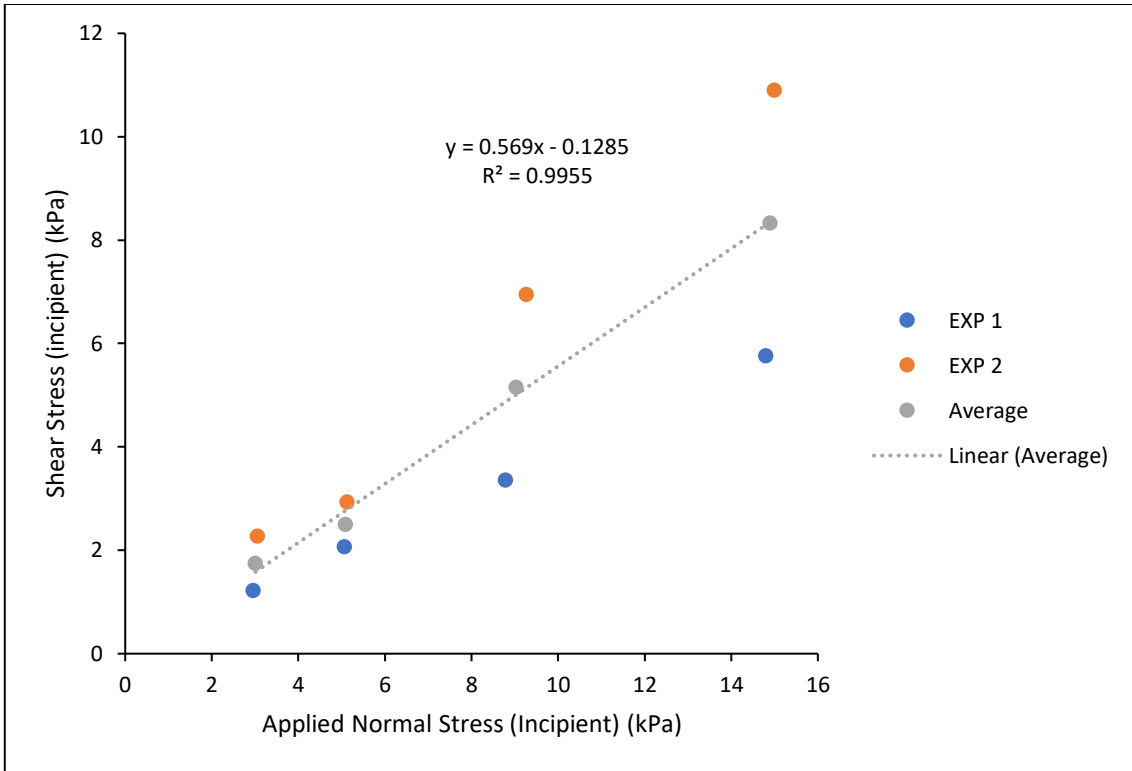


Figure 9-13 Incipient shear stress versus incipient applied normal stress values collected from shear cell test at 3, 5, 9, and 15 kPa

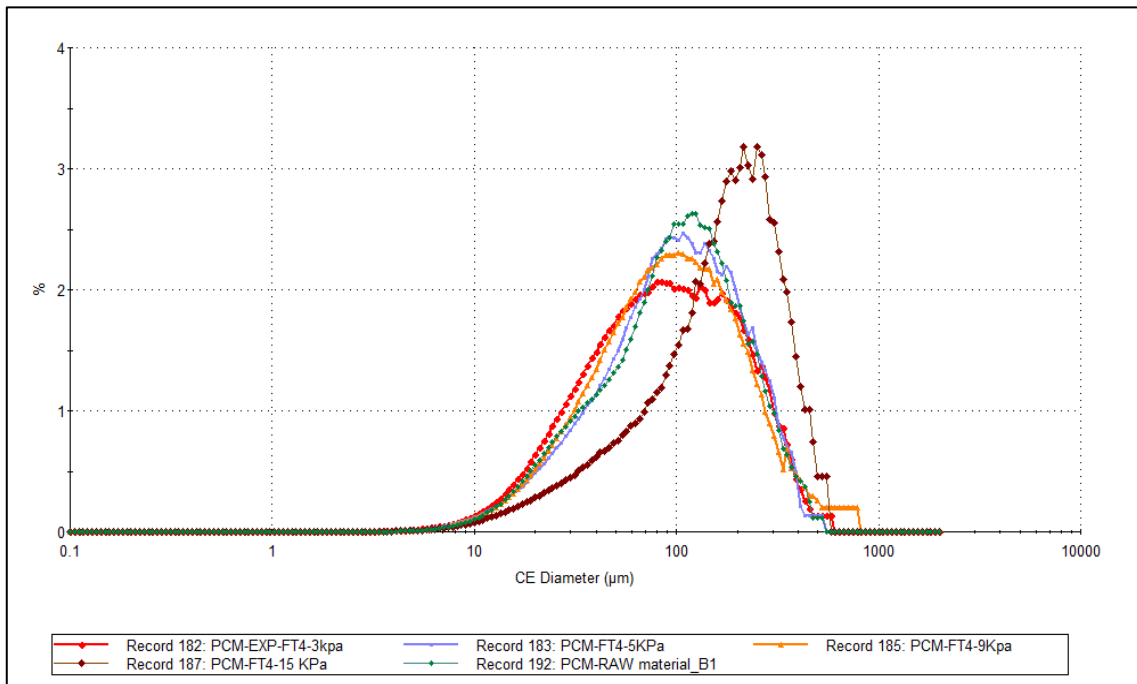


Figure 9-14 Comparison of Raw material and the samples obtained from shear cell test at 3, 5, 9, and 15 kPa

Size analysis of the samples generate in the FT4 shear cell tests was performed using the morphology G3, the data are presented in Figure 9-14. As the applied normal stress increases,

the particle breakage increases. However, for the 15 kPa shear cell test, the particle size increases, indicating that the particle size tends to increase by agglomeration as inferred from the earlier experiemnts. Moreover, the values of the breakability index (Table 9-7) were small, indicating that there was not enough particle breakage for the applied normal stress. However, it was inferred that the FT4 shear cell method is also not an appropriate breakage characterization tool and cannot be used to mimic particle attrition at a large scale, i.e., in industrial dryers.

Table 9-7 Breakability index of FT4 shear cell experiments at 3, 5, 9, and 15 kPa

Material	Breakability index (%)
3 kPa	0.1357
5 kPa	0.0148
9 kPa	0.0852
15 kPa	-

9.3.3 vacuum agitated dryer experiments

This experiment aimed to investigate particle attrition due to the shearing action of the agitator blade and to seek a comparison of the particle breakage in a deeper powder bed in a larger scale experiment by adding weight loads to apply approximately the same normal pressure as in the shear cell test. The parameters of the experiments are listed in **Error! Reference source not found.** Size analysis was performed by Morphology G3 and is listed in .

Sample	Min diameter (um)	x10 (um)	x50 (um)	x90 (um)	Max diameter (um)	STDV diameter (um)	breakability index (%)

Raw material (B2)	2.17	30.41	105.2	239.3	301.21	14.55	
S1	2.17	34.58	108.4	196.8	312.51	14.47	
S2	2.17	27.46	91.26	242.1	359.15	13.78	0.132509506
S3	2.17	29.87	86.36	207.7	331.84	14.11	0.179087452

The results of the size analysis reported in **Error! Reference source not found.** indicate that the D_{10} and D_{50} of the sample of the experiment without adding weight loads increases while D_{90} decreases. However, as the weight loads increase, particle breakage increases, but the breakage is minimal, as indicated by the values of breakability indexes, even by adding 100 grams of weight load. Hence this approach is unsuccessful in mimicing the particle breakage occurring in large-scale pilot plants or industrial dryers with this small-scale agitator dryer. After size analysis, the next step was calculating applied normal stress and the generated shear stresses. Applied normal stresses were calculated using Equation 3-4 and listed in Table 9-8.

Table 9-8 Applied normal stress calculated for tungsten washers used in Vacuum agitated dryer experiment

Number of disks	Disks weight (g)	Applied normal stress (kPa)
4	57.6553	1.7693
7	102.6963	3.1516

The calculation of shear stress by using torque was not possible with this dryer. The complex agitation combining both vertical and rotational motion meant that the motor selected was not equipped to measure the torque generated during the experiment (a further complication being that some torque would have been associated with the mounting of the agitator system which

delivered the complex motion). Never the less an attempt was made to estimate the torque based on the specification sheet provided by the motor supplier (DMN37 Motor). The motor used was Nidec DC geared brushed motor (DMN37 series, 24V, 9.2W).

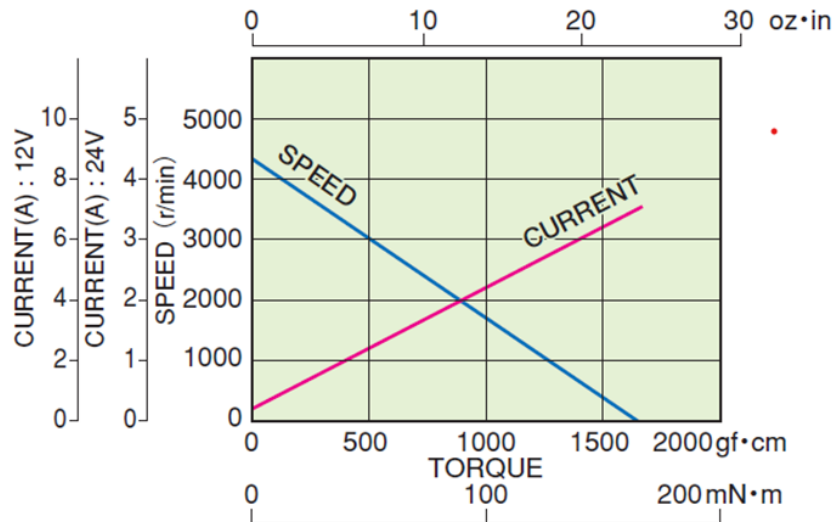


Figure 9-15 Current Speed and torque curve for the motor used to provide rotational motion of agitator used in dryer provided by the supplier.

The graph in Figure 9-15 indicates that the estimated torque for 2 rpm rotation is 0.16 Nm. Using this torque value in Equation 3-5, the shear stress was calculated to be 2.045E-06 Pa. However, this shear stress was not fully representative of the applied normal stress. So, it was not possible to compare the impact of normal and shear stress on particle breakage using the shear cell method and the vacuum agitated dryer.

9.4 Conclusion

The work reported in this chapter aimed to investigate various lab scale equipment; a tapped bulk density instrument, the FT4 shear cell test, and a bespoke vacuum agitated dryer as tools to characterize particle breakage.

The proposed modification of the Tapped bulk density equipment was not possible, so to apply normal stress on the particle bed, different weight loads were added to the particle bed. However, the equipment was not considered an alternative to characterize particle breakage as by increasing the weight load on the particle and the number of taps, particle size increased unexpectedly, suggesting the formation of agglomerates accompanied the anticipated particle breakage. Moreover, the parameters required to scale up/down the attrition occurring in large-

scale industrial dryers, i.e., torque and shear stress, were impossible to calculate in this equipment.

The FT4 shear cell test calculated the torque and shear stress generated from applied normal stress, but the particle breakage observed by applying normal pressure was limited. Moreover, for the increased value of normal stress, i.e., 15 kPa material tends to form lumps, increasing the particle size.

The small vacuum agitated filter dryer is a simple tool in which minimal particle attrition was observed by applying an average load on the powder bed. A further drawback was that the motor where the blade is connected could not be used to monitor torque during experiments.

9.5 References

Am Ende, D. *et al.* (2013) ‘Development and Application of Laboratory Tools To Predict Particle Properties upon Scale-Up in Agitated Filter-Dryers’, *Organic Process Research & Development*, 17(10), pp. 1345–1358. doi: 10.1021/op400080x.

DMN37Motor (no date) ‘DMN37 Motor’, p. 53.

Fotovat, F., Bi, X. T. and Grace, J. R. (2017) ‘Electrostatics in gas-solid fluidized beds: A review’, *Chemical Engineering Science*. Pergamon, 173, pp. 303–334. doi: 10.1016/J.CES.2017.08.001.

Malvern (no date) *Morphologi G3 particle size and particle shape image analyzer | Product support | Malvern Panalytical*. Available at: <https://www.malvernpanalytical.com/en/support/product-support/morphologi-range/morphologi-g3> (Accessed: 18 September 2022).

Malvern instruments (no date) ‘Manual: Morphologi G3 User manual (Man0410-5.0)’. Available at: www.malvern.com (Accessed: 30 September 2022).

Ottoboni, S. (2013) ‘Workflow procedure to predict attrition in agitated dryers Introduction and aims’, pp. 6–8.

quantachrome instruments (no date) ‘automated tap density analyzers’.

Remy, B. *et al.* (2015) ‘Scale-Up of Agitated Drying : Effect of Shear Stress and Hydrostatic Pressure on Active Pharmaceutical Ingredient Powder Properties’, 61(2), pp. 407–418. doi: 10.1002/aic.

Chapter 10: Overall conclusion and future work

This chapter provides an overview of the main conclusions drawn from this study and recommendations for future work.

10.1 Overall conclusion

In pharmaceutical manufacturing, the drug substance, i.e. the active pharmaceutical compound (API), must maintain its physio-chemical properties like purity, particle shape and solid-state form to ensure that the manufactured drug product is safe to use and remains stable with time.

Pharmaceutical manufacturing starts with API molecule synthesis. To make the API suitable for the formulation, purification is required. The most widely used purification process in the pharmaceutical industry is crystallisation. The crystallisation process is followed by filtration, washing and drying to isolate and recover pure API crystals. Drying is the last step in isolating and purifying API crystals, which removes the residual solvent after filtration and washing.

The efficiency of the drying process affects the quality attributes of final drug product. The optimisation of the drying process to obtain free-flowing particles with desired shape and properties is very difficult and poorly understood as it requires an in-depth understanding of the physical and chemical stability of the compound, the drying kinetics and physical control of particle properties. Usually, aggressive drying conditions are adopted during industrial manufacturing to reduce drying time and increase productivity, which can adversely affect particle properties, such approaches may not be suitable for pharmaceutical compounds.

Many physical and chemical changes can occur to the drug product during drying; however, agglomeration and attrition are the two most intractable problems. Agglomeration is undesirable as it can increase the drying cycle time and cause problems in tableting and compaction. After drying, it may be necessary to introduce an additional milling step to have free-flowing non-agglomerated particles. Attrition can also adversely affect the flowability of dried products. Hence, both can affect the particle shape and size distribution, negatively and so impact drug formulation.

Many factors that can cause agglomeration during drying including the selection of wash solvent through different properties of wash solvents like; polarity, viscosity, surface tension, etc., the solubility of API in wash solvent, residual moisture and other processing parameters.

Another factor known to cause agglomeration is the deposition of previously dissolved material at the contact points between particles when the solvent evaporates on drying. When API dissolves in the residual solvent during drying, it creates "sticky" points at the contacts between particles, increasing the formation of solid bridges.

The main objective of this work was to quantify the amount of deposited material that can cause lump formation (Chapter 3). Glass beads were selected as the substrate to simplify the data analysis. The glass spheres have controlled and narrow size distributions, are insoluble and have a defined shape that is simple to model. The investigation of the minimum amount of solid deposition that can cause lump formation during drying shows that:

- As the concentration of dissolved material (PCM) increases, the lump becomes stronger as the strength of the solid bridges increases by increasing the mass of material which is deposited.
- No hard lumps were obtained for solute concentrations below 0.0025 g/mL PCM in methanol and water, which indicates the solute concentration threshold required to prevent agglomerates formation during drying.
- The lumps obtained at PCM concentrations below 0.001 g/mL break completely during manual tapping as the strength of bonds between glass beads reduces by decreasing the concentration of dissolved material.
- The extent of agglomeration decreases by decreasing the concentration of dissolved PCM, but this decrease is very slight.
- Lump size increases as we move from smaller glass beads to bigger ones.
- The agglomerates formed with bigger glass beads are more fragile as the bigger beads have fewer contact points per unit mass than small size glass beads.

The information obtained from this work can help to improve the blowdown and washing stages to remove the residual solvent and hence dissolved solute down to the threshold limit. After developing the methodology with the glass beads, the investigation was performed with the API crystals i.e. PCM and spherical agglomerate of benzoic acid (Chapter 5). It was concluded that due to changes in shape, size, material properties and wetting behaviour of the substrate, the agglomeration behaviour changes, and so the threshold limit of residual solvent to prevent agglomeration also changes (increases).

Any dissolved product or impurities in the solvent remaining in the filter cake following

washing may be re-precipitated, retained, and deposited during drying, reducing the product's purity. Therefore, it is essential to understand the impurity transport during isolation (washing and drying) to maintain product purity.

In this study, work was also done to evaluate the relative transport of dissolved API (PCM) and impurities (blue dye, patent blue V) along with residual solvent during static drying (Chapter 4). For this, a solution of known concentration of PCM was used, to which blue dye was added as an impurity to track the transport of residual moisture through the cake.

It was demonstrated that different solutes and solvents show different transport behaviours depending on wettability and volatility. In the case of methanol as the solvent, the highest concentration of PCM and the blue dye remains within the lump formed at the point where the blue dye was added to the powder bed, but for water, some of the PCM remains concentrated in the lump formed at the point of addition, although some migrated along with the blue dye away from the lump. Experiments were performed using solvent mixture compositions and different solutes to investigate the transport behaviour difference between water and methanol. The Washburn method was used to evaluate wettability and contact angle with the different solute systems. The wetting behaviour of aqueous PCM solution is influenced by the different levels of hydrophilicity shown by different faces of PCM. Some faces are hydrophilic, and some are hydrophobic; this leads to the idea that the hydrophobic faces displace the water molecules during transport and influence what is retained within the lump.

Finally, some work was done to investigate existing and new lab-scale devices to characterise agglomerate strength (Chapter 7) and particle breakage due to dryer loading (Chapter 6).

A tablet hardness tester was utilised as an alternative technique to characterise the mechanical strength of agglomerates which didn't work for various reasons including the irregular shape of the agglomerate, which was the problem for the exertion of proper forces. Moreover, the strength of the bonds between agglomerates particles was much less than in tablets. The equipment is designed for the hardness testing of tablets, making it unsuitable for evaluating agglomerate's strength.

Lab-scale equipment like a tapped bulk density, FT4 shear cell and a bespoke Vaccum agitated dryer was analysed to characterise particle breakage. However, these devices didn't

work as an alternative tool due to many reasons:

- The parameters required to scale up/down the attrition occurring in large-scale industrial dryers, i.e., torque and shear stress, were impossible to calculate for tapped bulk density and the vacuum agitated dryer.
- The applied load in the FT4 shear cell was insufficient to replicate the dryer loading and for particle attrition.

10.2 Future work

The research conducted to quantify agglomerates based on the solubility of API in the residual solvent for API crystals as the substrate has yielded intriguing results. The deposition of the material on all faces of the API crystals rather than just at contact points suggests that further investigation into the surface properties of the material would be beneficial.

Additionally, exploring the wetting behavior of API using various methods, along with the Washburn method, would provide valuable insights into the transport mechanism and agglomeration process.

To effectively utilize the findings from this study and optimize the washing stage to achieve a threshold limit of residual moisture within the wet cake, a comprehensive isolation experiment with filtration washing stages needs to be undertaken.

Furthermore, as the focus of this work has mainly been on static drying, it would be essential to investigate the impact of agitating drying on agglomeration concerning solubility in the residual solvent.

Due to time constraints, the investigations intended to develop a semi-empirical approach for predicting attrition at the lab scale were not fully completed. As proposed in Chapter 6, exploring material properties and correlating them with particle breakage within the dryer could lead to the development of a valuable semi-empirical approach.

In conclusion, the research has provided valuable insights into agglomeration and drying processes, and further investigations into surface properties, wetting behavior, agitating drying, and semi-empirical approaches will contribute significantly to the understanding and optimization of these processes.

Appendix A

Quantification of agglomerate formation as a function of solubility in residual solvent

Table A-1 Calculation of the Extent of agglomeration

Weight of empty sieve 1 mm (g)	Weight of empty bottom	Solvent	Beads size (microns)	Mass on top sieve (g)	mass in bottom (g)	a (mass of lump) (g)	b (mass of lose beads) (g)	Extent of agglomeration
25.8816	12.7342	Methanol	40-70	27.3936	21.6063	1.5120	8.8721	0.1456

Table A-2 Calculation of ABI Index

Solvent	Methanol		
Bead size (micron)	40-70		
Friability			
Mass of solid tested (g)	1.5120		
Sieve	1 mm	Bottom	Sum of cake mass
	25.8816	12.7325	
1st cycle (1min) of shaking			
Mass sieve + cake (g)	27.2805	12.8468	
Mass cake (g)	1.3989	0.1143	1.5132
% Mass cake	92.4465	7.5535	0.0012
2nd cycle (1min) of shaking			
Mass sieve + cake (g)	27.1630	12.9641	
Mass cake (g)	1.2814	0.2316	1.5130

% Mass cake	84.6927	15.3073	0.0010
3rd cycle (1min) of shaking			
Mass sieve + cake (g)	27.0884	13.0385	
Mass cake (g)	1.2068	0.3060	1.5128
% Mass cake	79.7726	20.2274	0.0008
4th cycle (1min) of shaking			
Mass sieve + cake (g)	26.9163	13.2104	
Mass cake (g)	1.0347	0.4779	1.5126
% Mass cake	68.4054	31.5946	0.0006

Cycle	% mass cake top sieve
1	92.45
2	84.6927
3	79.7726
4	68.4054

Friability index	0.1980
-------------------------	---------------

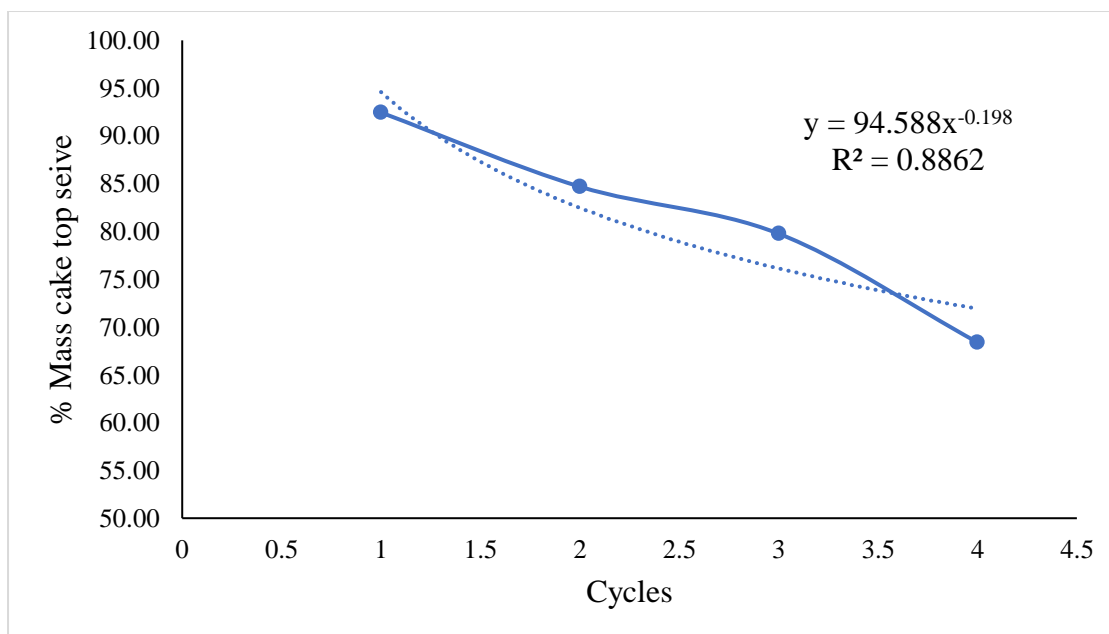


Figure A-1 Power law fitting curve for ABI Index

Table A-3 Parameters for filling fraction calculation

Parameter	Value
Solution (cm ³) (drop size)	0.1
Bed mass (g)	10
Drop size (ul)	100
Density of Paracetamol (g/ml)	1.295
Volume of paracetamol in one drop (ml)	7.72E-04
Density of glass spheres (g/cm ³)	2.47

Table A-4 Filling fraction calculation

Solvent	Paracetamol amount (g/100ml)	Mass of paracetamol in one drop (g)	Bead size (um)	Mass of single sphere (g)	Sphere diameter (cm)	Volume of single sphere (cm ³)	Lump mass (g)	Lump volume (cm ³)	Void volume (cm ³)	Filling fraction	Number of spheres in lump	Mass of paracetamol per sphere (g)	Mass of paracetamol per sphere v/s mass of sphere (g)
methanol	1	0.001	40-70	2.15E-07	5.50E-03	8.71E-08	1.92E+00	7.76E-01	4.36E-01	2.29E-01	8.91E+06	1.12E-10	5.22E-04

0.25	0.5	0.75
0.00025	0.0005	0.00075
40-70	40-70	40-70
2.15E-07	2.15E-07	2.15E-07
5.50E-03	5.50E-03	5.50E-03
8.71E-08	8.71E-08	8.71E-08
1.53E+00	1.41E+00	1.94E+00
6.21E-01	5.73E-01	7.84E-01
3.49E-01	3.22E-01	4.41E-01
2.86E-01	3.10E-01	2.27E-01
7.13E+06	6.58E+06	9.00E+06
3.51E-11	7.60E-11	8.33E-11
1.63E-04	3.53E-04	3.87E-04

Appendix B

Transport of moisture in the residual lump

The following graphs shows the Washburn data for different samples. Every sample measurement was repeated at least three times and plotted in the same graph.

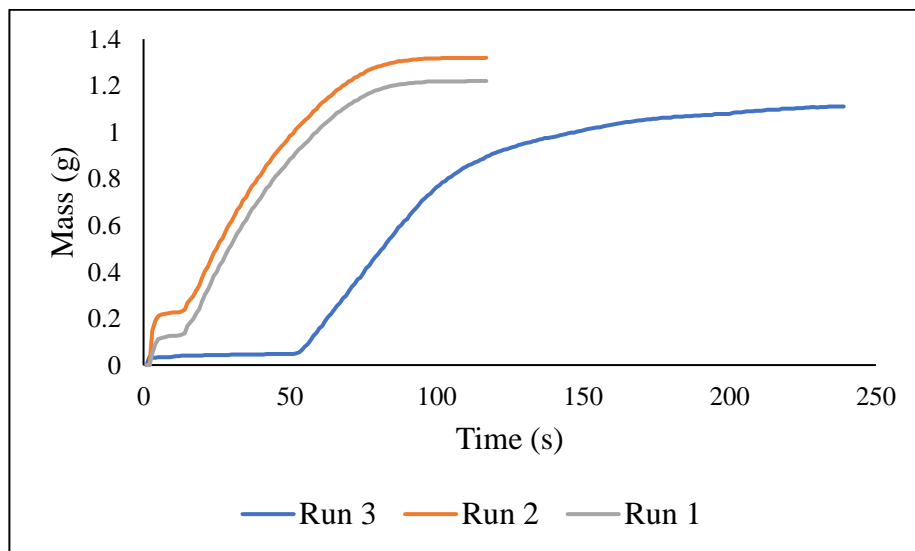


Figure B-1 The mass vs time interparticle capillary rise of water and dye solution in Granular PCM compacted by tapping for 100 - 250 seconds

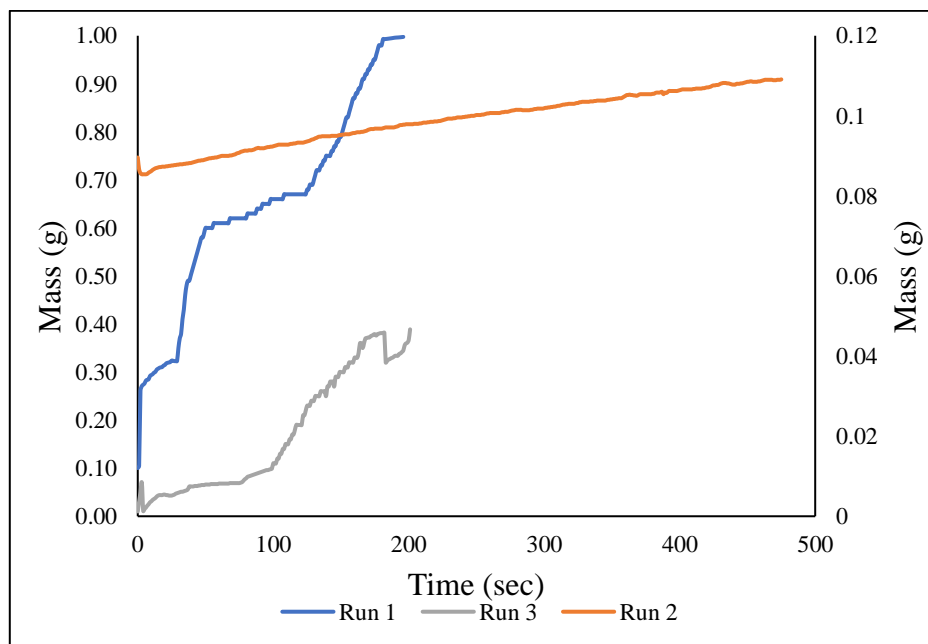


Figure B-2 The mass vs time interparticle capillary rise of water and dye solution in Powdered PCM compacted by tapping for 200 - 450 seconds

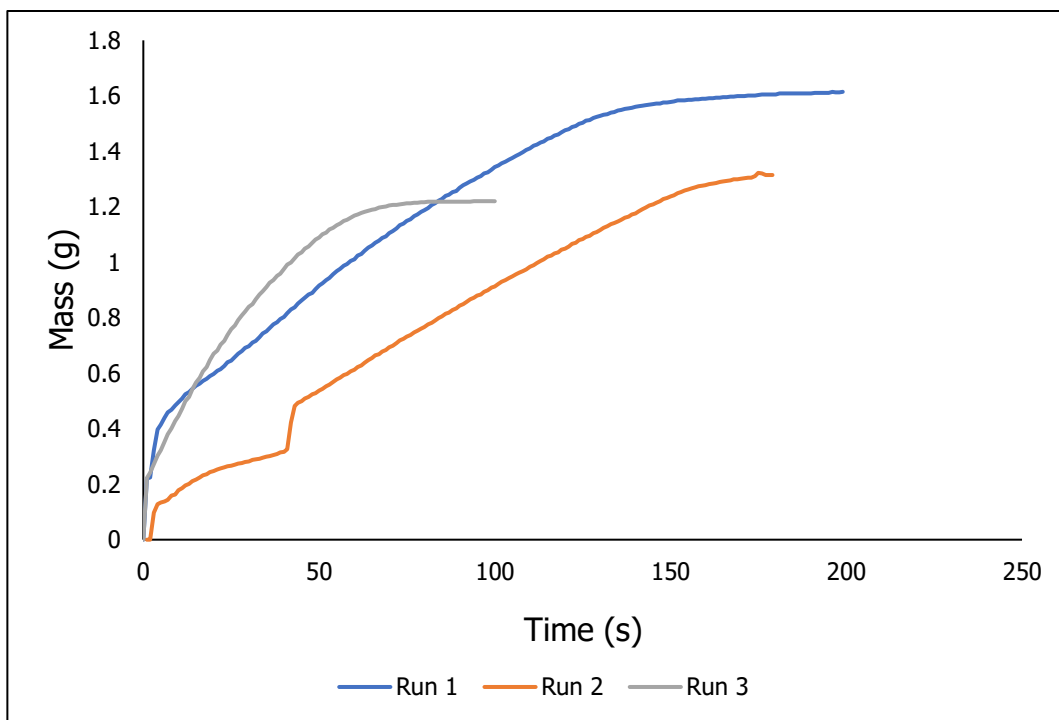


Figure B-3 The mass vs time interparticle capillary rise of water and dye solution in PHL-t compacted by tapping for 100 - 200 seconds

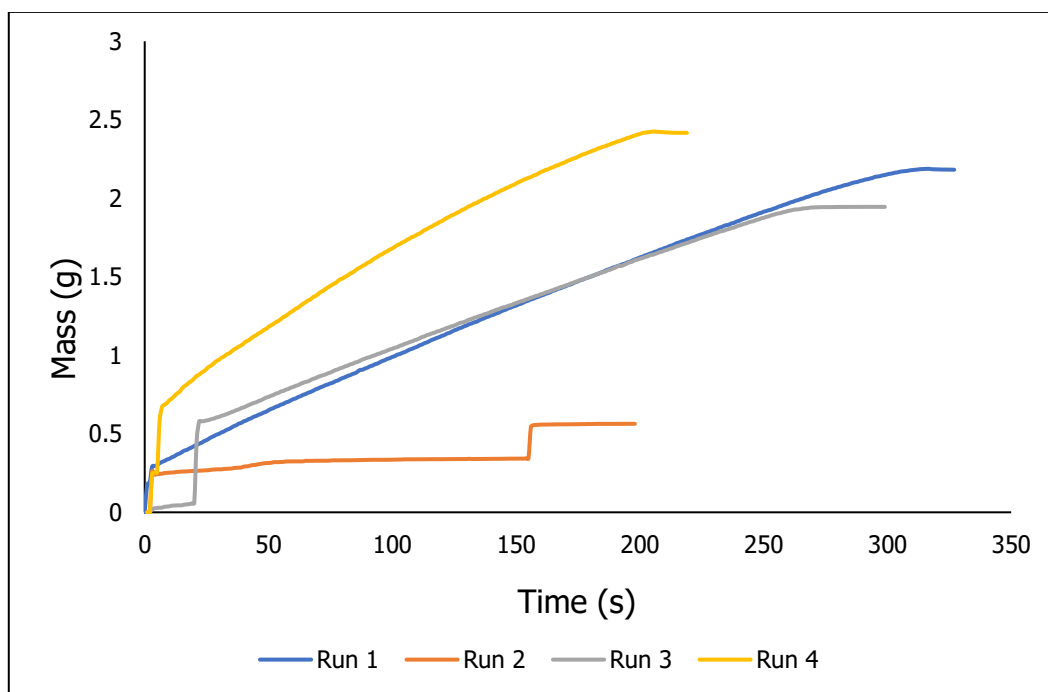


Figure B-4 The mass vs time interparticle capillary rise of water and dye solution in PHL-t coated beads compacted by tapping for 200 - 350 seconds

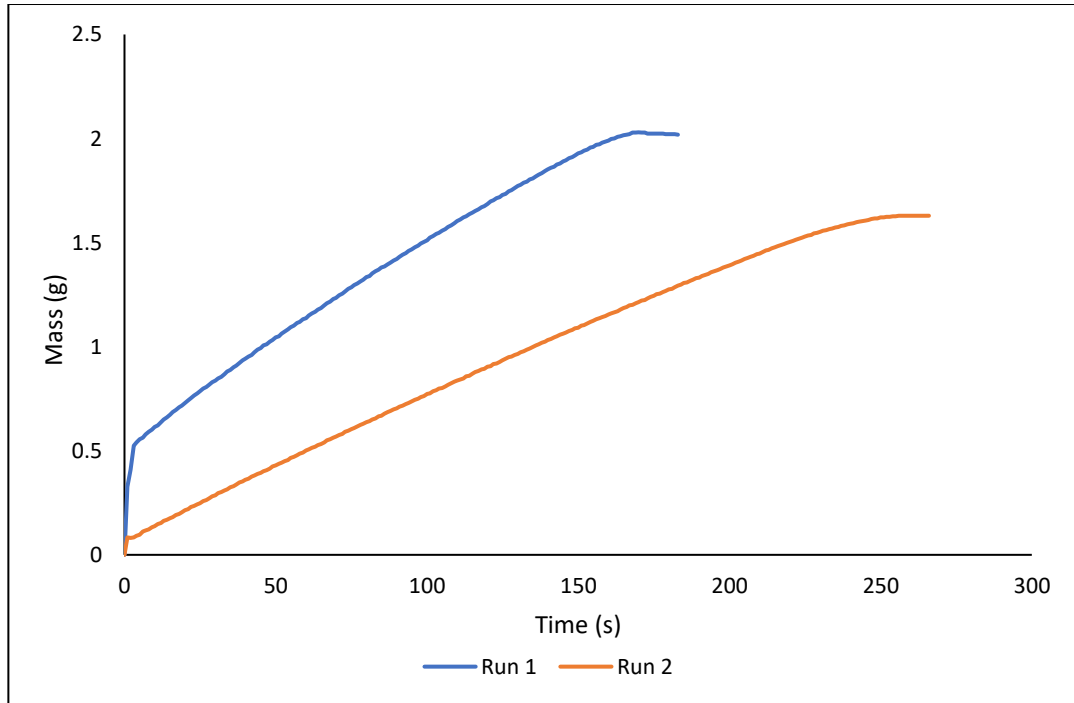


Figure B-5 The mass vs time interparticle capillary rise of water and dye solution in 1st sieving fraction beads compacted by tapping for 200 - 300 seconds

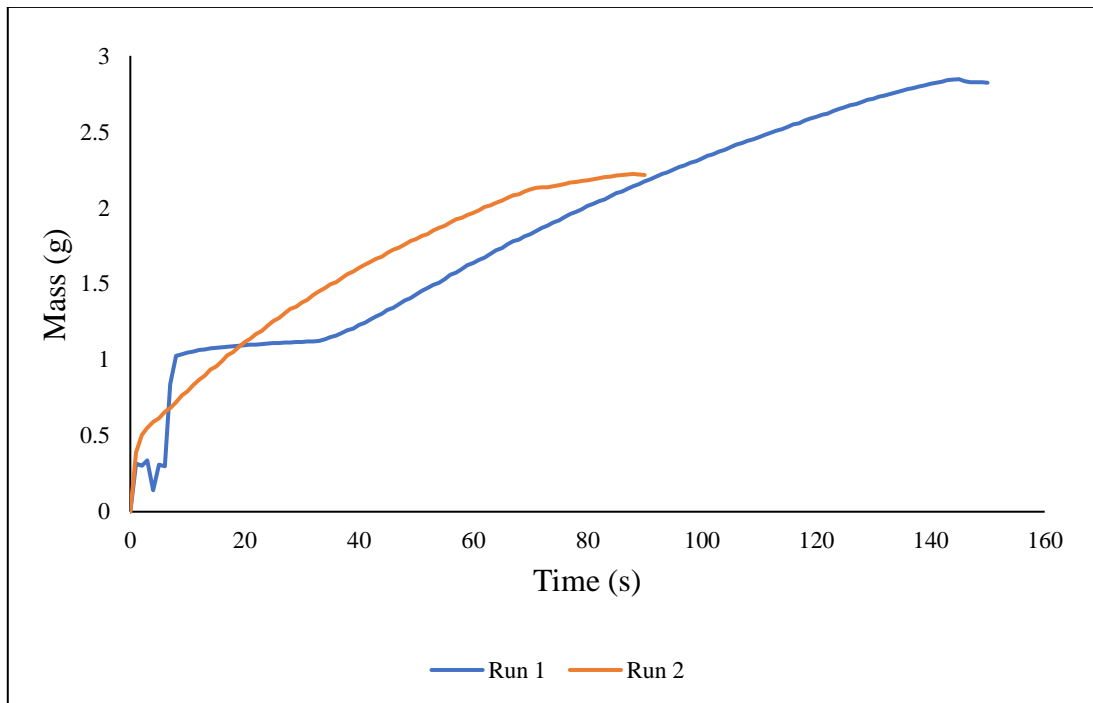


Figure B-6 The mass vs time interparticle capillary rise of water and dye solution in dried sample beads compacted by tapping for 100 - 150 seconds

Appendix C


Refining of agglomeration brittleness index

Table C-1 Sieving data: number of cycles and %mass retained on top sieves for 0.01 g/ml PCM/Methanol system with 40-70 μm glass beads

40-70 μm					
% mass cake top sieve					
RPM \rightarrow	500 RPM	700 RPM	1400 RPM	1600 RPM	2800 RPM
Cycles \downarrow					
1	89.66	74.72	96.48	78.57	65.56
2	83.13	68.01	76.57	61.74	55.94
3	78.93	61.95	66.06	39.50	45.94
4	74.10	57.61	50.58	34.29	38.28
5	71.14	54.15	39.68	27.36	31.46
6	66.73	51.43	32.96	23.94	25.77
7	63.34	48.59	29.46	21.82	21.40
8	59.82	46.12	25.50	18.94	17.05
9	57.15	44.16	22.35	16.99	14.54

10	53.04	42.23	20.19	15.29	11.99
11	50.09	40.30	17.75	13.57	9.97
12	48.66	38.42	15.97	12.18	8.45
13	44.00	36.78	14.54	11.04	6.89
14	44.43	35.03	13.36	9.84	5.81
15	43.02	33.72	12.42	8.94	4.91
16	41.41	32.24	11.51	7.88	4.14
17	40.40	31.04	10.61	7.66	3.56
18	38.88	29.93	9.99	6.97	3.08
19	37.37	28.98	9.36	6.09	2.57
20	36.09	28.00	9.04	5.55	2.27



Table C-2 Sieving data: number of cycles and %mass retained on top sieves for 0.01 g/ml PCM/Methanol system with 400-600 μm glass beads

400-600 μm					
% mass cake top sieve					
RPM 	500 RPM	700 RPM	1400 RPM	1600 RPM	2800 RPM

Cycles ↓					
1	81.11	16.77	6.50	4.43	1.67
2	20.98	12.82	4.22	3.67	1.24
3	12.44	11.29	3.13	2.89	1.01
4	9.17	9.71	2.70	2.06	0.84
5	8.36	9.09	1.89	1.65	
6	8.03	8.23	1.12		
7	7.44	7.34			
8	7.34	6.88			
9	7.01	6.55			
10	7.05	6.05			
11	6.79	5.51			
12	6.58	5.40			
13	6.43				
14	6.50				
15	6.04				



16	5.71				
17	5.35				
18	5.51				
19	5.42				
20	5.27				

Table C-3 Sieving data: number of cycles and %mass retained on top sieves for 0.002 g/ml PCM/Methanol system with 40-70 μm glass beads

40-70 μm					
% mass cake top sieve					
RPM 	500 RPM	700 RPM	1400 RPM	1600 RPM	2800 RPM
Cycles 					
1	97.94	59.10	36.98	35.05	45.05
2	96.37	45.08	25.04	23.00	19.18
3	93.91	38.05	20.22	16.62	8.76
4	91.10	33.12	16.67	12.79	5.69
5	87.69	29.69	14.08	9.83	4.30

6	81.97	27.08	11.89	8.27	2.94
7	74.34	24.50	9.96	6.89	
8	67.58	22.07	8.80	5.55	
9	59.39	19.16	7.98	4.31	
10	49.91	17.54	7.07	3.51	
11	37.75	16.51	6.37	2.92	
12	29.32	15.54			
13	23.94	14.64			
14	19.61	13.92			
15	15.79	13.11			
16	12.37	12.54			
17	10.33	11.75			
18	8.53	11.04			
19	7.51	10.63			
20	5.08	9.97			

Table C-4 Sieving data: number of cycles and %mass retained on top sieves for 0.002 g/ml PCM/Methanol system with 400-600 μ m glass beads

400-600 μm				
% mass cake top sieve				
RPM 	500 RPM	700 RPM	1400 RPM	1600 RPM
Cycles 				
1	26.67	23.26	9.70	5.93
2	21.34	11.25	4.13	
3	20.05	7.63		
4	18.43	5.35		
5	17.34	4.82		
6	14.54	4.12		
7	13.87	3.61		
8	13.65	3.29		
9	13.08			
10	12.22			
11	11.96			

12	10.68			
13	10.36			
14	9.90			
15	9.83			
16	9.16			
17	8.74			
18	8.15			
19	7.63			
20	6.90			